2009

Dynamics and Rheology of Biaxial Liquid Crystal Polymers

Sarthok K. Sircar
University of South Carolina

Dynamics and Rheology of Biaxial Liquid Crystal Polymers

By

Sarthok K Sircar

Bachelor of Science
Indian Institute of Technology, Kanpur, India 2004

Master of Science
Florida State University, Tallahassee, Florida 2006

Submitted in Partial Fulfillment of the Requirements

for the Degree of Doctor of Philosophy in

Mathematics

College of Arts and Sciences

University of South Carolina

2009

Accepted by:

Qi Wang, Major Professor

Hong Wang, Committee Member

Peter Binev, Committee Member

Lili Ju, Committee Member

Andreas Heyden, Committee Member

James Buggy, Interim Dean of the Graduate School

Dedication

To my family and close friends...

Acknowledgments

First and foremost I wish to thank my advisor Professor Qi Wang, for leading me into the field of liquid crystal polymers. As a serious researcher, he showed me how to maintain high academic standards by using critical judgement of one's own work. This experience will be treasured throughout my career. I could not have successfully completed this work without his constant guidance, encouragement and support.

Next, I wish to thank Dr. Hong Wang, Dr. Peter Binev, Dr. Lili Ju and Dr. Andreas Hayden for their willingness to serve on my doctorate committee. I also wish to thank Professor Gregory Forest (Univ. of North Carolina at Chapel Hill) and Professor Ruhai Zhou (Old Dominion University, Old Dominion, VA) for helpful discussions and professional help.

I would also like to thank all my friends who gave me help and encouragement during my stay at FSU. I would also acknowledge my family for their love and support and for their tolerance with my total commitment towards this work.

Finally, I would like to acknowledge the financial support by AFOSR and NSF through grant DMS-0204245

Abstract

In this thesis we derive a hydrodynamical kinetic theory to study the orientational response of a mesoscopic system of nematic liquid crystals in the presence of an external flow field. Various problems have been attempted in this direction. First, we understand the steady-state behavior of uniaxial LCPs under an imposed elongational flow, electric and magnetic field respectively. We show that (1) the Smoluchowski equation can be cast into a generic form, (2) the external field is parallel to one of the eigenvectors of the second moment tensor, and (3) the steady state probability density function is of the Boltzmann type. In the next problem, we study the mono-domain dynamics of rigid rod and platelet suspensions in a linear flow and a steady magnetic field. The flows with a rotational component is mapped to simple shear with rate parameter subject to a transverse magnetic field with strength parameter and the irrotational flows are reduced into a triaxial extensional flow with two extensional rate parameters. For rotational flows, various in-plane and out-of-plane stable steady attractors emerge. For irrotational flows, the biaxial equilibria is characterized generically in terms of an explicit Boltzmann distribution, providing a natural generalization of the analytical results on pure nematic equilibria. Finally, we present the dynamics of a mesoscopic system of biaxial liquid crystal polymers in the presence of a homogenous shear flow. The Smoluchowski equation is derived in the rotating frame and solved using a specially formulated Wigner-Galerkin approximation in selected regions of the material parameter space and a range of accessible shear rates, to investigate the stable mesoscopic states and robust structures.

Contents

List of Figures

Chapter 1

Introduction

In the layman's terms, liquid crystal is a low temperature phase that occur to some anisotropic materials, where the material occurs neither as a liquid nor as a solid (or crystalline) phase. There are two classes of liquid crystal phases: nematic and smectic. In the nematic phase, the molecules acquire orientational order but no positional order, i.e. on average they line up with each other locally but their positions are still random. In smectic phase however, the molecules acquire not only orientational order but also some positional order. There are many different smectic phases depending on the kind of positional order the molecules have. Liquid crystals are fascinating both physically and mathematically for many different reasons:

• Their color is sensitive to small changes in temperature and external fields.

• Their partially liquid, partially solid nature gives rise to peculiar dynamics. [79].

• Liquid crystals often have intricate and beautiful defect structures [84]. In nematic liquid crystals the defects are of topological origin. But in smectic liquid crystals, since a metric is involved in order to describe the positional order, the defects can also be of geometric origin. These defects occur not only in transients, but also in ground states. This means that the variational problems describing the energetics of these liquid crystals have minimizers that contain very intricate singular sets.

• The simultaneous presence of orientational and positional order allows the possibility to explore the difference and similarity between translation and rotation. For example it was suggested that the Janossy effect, an experimental observation, that

the threshold for the optical Frederiks transition is reduced by 2 orders of magnitude after the addition of small percentage of dye molecules to the liquid crystal, which can be explained as an orientational version of the translational ratchets [80], a mechanism that is thought to be responsible for linear momentum transport in biological polymers [83]. However, the permeation process in smectic liquid crystals is a translational version of the angular friction between the molecules and the fluid [84].

• Liquid crystal polymers provide a concrete example for the study of rheology of polymeric liquids.

• In terms of applications, besides the well-known usage in display industry, liquid crystal polymers are often used in industrial processing. Recently smectic liquid crystals have found new interest in the study of biological polymers and cell membranes.

With our focus on the study of a specific class of nematic liquid crystals, we provide an introductory discussion on the latest developments of nematic liquid crystals.

1.1. Nematic Liquid Crystals

There are several different levels of description of the nematic order. The most detailed is the orientation distribution function $f(\mathbf{n})$ which describes the probability density that the molecules lie in the direction $\mathbf{n}$. f can also depend on the position $\mathbf{x}$ and time t. In isotropic phase, $f(\mathbf{n})$ is a constant. In the nematic phase, $f(\mathbf{n})$ is peaked at some preferred direction $\mathbf{n}^*$ in the uniaxial case.

Consider the simplest case of rod-like molecules of thickness b and length L. Let $B(\mathbf{n}, \mathbf{m})$ be the interaction kernel of the two molecules with orientation $\mathbf{n}$ and $\mathbf{m}$. The simplest example is the excluded volume interaction in which case $B(\mathbf{n}, \mathbf{m}) = 2L^2 b|\sin\gamma|$ where γ is the angle between $\mathbf{n}$ and $\mathbf{m}$. Including the entropic effect, the free energy of a system of rod-like molecules can be expressed as

$$F(f) = k_B T \int \int_{S^2 S^2} \{f(\mathbf{n}) \log f(\mathbf{n}) + \frac{c}{2} B(\mathbf{n}, \mathbf{m}) f(\mathbf{n}) f(\mathbf{m})\} dn dm \tag{1}$$

where S^2 denotes the unit sphere, c is the total concentration of the rods, and $c \ll 1$. Minimizing F subject to the constraint $\int_{S^2} f dm = 1$, one finds that at large enough c, there exists an anisotropic minimizer representing the nematic phase. This is the Onsager theory.

There are various ways to coarse-grain this picture. The most popular approach is to use the second moment

$$S = \int_{S^2} \mathbf{n} \otimes \mathbf{n} (f(\mathbf{n}) - \frac{1}{4\pi}) dn \tag{2}$$

S is a symmetric traceless tensor. It vanishes at the isotropic phase. To describe the isotropic-nematic phase transition, one can use the Landau approach and expand the free energy as

$$F_2(S) = \frac{1}{2}\alpha(T) Tr(S^2) + \frac{1}{3}\beta(T) Tr(S^3) + \frac{1}{4}\gamma(T) Tr(S^2)^2 \tag{3}$$

This is the Landau-de Gennes free energy [84]. The distinguished or preferred directions are now the directions of the eigenvectors of S. The symmetry of the system depends on the eigenvalues of S, denoted by $\lambda_1, \lambda_2, \lambda_3$ which obey the relation $\lambda_1 + \lambda_2 + \lambda_3 = 0$. If two of the eigenvalues coincide, the system has uniaxial symmetry.

The dynamics of isotropic-nematic transition is often modeled by a gradient flow of the free energy:

$$S_t = -\frac{\delta F_2}{\delta S} \tag{4}$$

An interesting result of Forest [82] shows that the uniaxial systems are invariant under the dynamics Eq.(4). For uniaxial materials, S is replaced by $\mathbf{n}$, the direction of alignment, and s, the degree of alignment. Away from the phase transition when fluctuations in the degree of order are negligible, it is only important to keep track of the direction of alignment, which we again denote by $\mathbf{n}$. $\mathbf{n}$ is called the director field.

The full hydrodynamics of a uniaxial nematic liquid crystal is described by the well -known Ericksen-Leslie equations [84].

The Ericksen-Leslie equations have one important drawback: it does not allow the existence of line defects which are commonly observed in liquid crystals. This is especially important for liquid crystal polymers where defects are abundant. To overcome this difficulty, Ericksen put back the degree of alignment s and extended the Ericksen-Leslie equations to incorporate this additional dynamic variable [81]. Unfortunately, the resulting system is so complicated with so many undetermined coefficients that there is little hope to make quantitative comparison with experimental data.

1.2. Biaxial nematic liquid crystals [122]

Liquid Crystals are playing a major role in revolutionising electro-optic display devices which range from the simple alpha-numeric displays to the extremely sophisticated flat panel screens used as television monitors [1]. The obvious success of displays based on nematic crystals has ensured that analogous applications have been explored for essentially every other liquid crystal phase. Indeed, it seems that no sooner has a new phase been discovered than an electro-optic application has been found for it. In fact, often before a phase has been found, applications have invariably been proposed. One important example of this phenomenon relates to the prediction that there should be another type of nematic liquid crystal phase: the biaxial nematic phase [102].

The majority of mesogenic molecules are rod-like as exemplified by the elegant molecules created by assembling phenyl and ethyne groups in a linear array [2] and shown in Figure 1.1a. Given the elongated appearance of such molecules it is natural to take them to be cylindrically symmetric and to represent them as, for example, ellipsoids of revolution (Figure 1.1b), with a single director, $\hat{n}$, which is defined as the direction along which the symmetry axes of the molecules tend to point. At a macroscopic

level, properties of the nematic phase, such as the dielectric constant and the refractive index, have cylindrical symmetry. There are two unique principle components of the property which for the general case of a second rank tensor are denoted by $\tilde{Q}_{\parallel}$ and $\tilde{Q}_{\perp}$. The phase is, referred to as a uniaxial nematic although the term properly implies that the system possesses a single axis along which a plane polarised light beam can travel without the state of polarisation being changed.

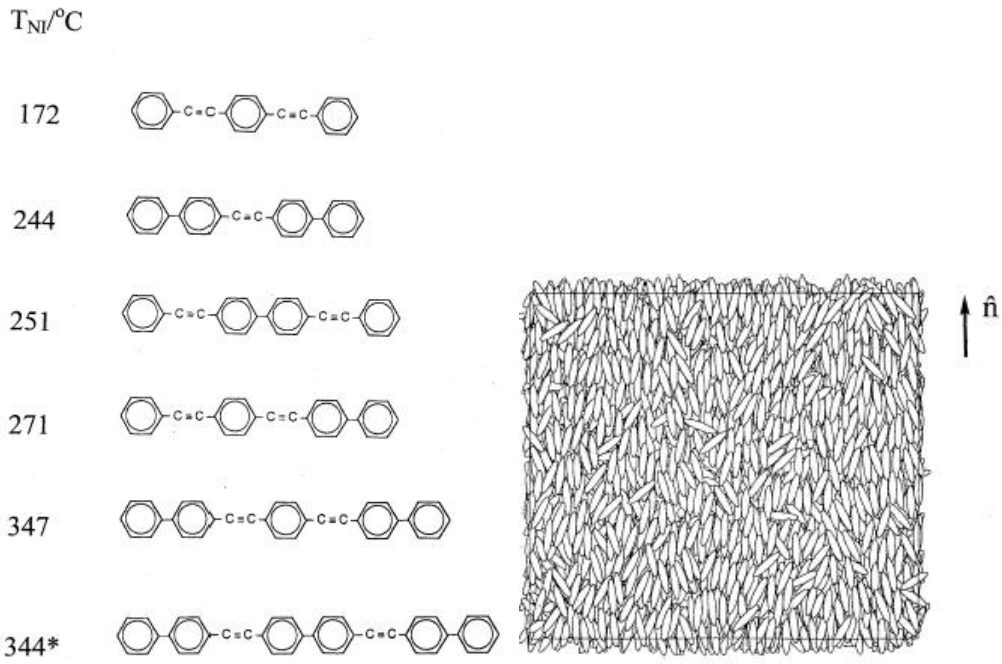

FIGURE 1.1. (a) Structures of linear molecules which seem to approach the cylindrical symmetry often assumed for mesogenic molecules. (b) Molecular organization in a uniaxial nematic phase composed of ellipsoids of revolution.

A closer examination of the molecules forming liquid crystals shows that they deviate from cylindrical symmetry, usually being board-like in structure (see Figure 1.1a). The fact that the nematic phases which they form are uniaxial shows that although there is long range orientational order of the molecular long axes this does not extend to the molecular short axes whose orientations are uncorrelated except at short range. Nonetheless, at some state point the symmetry of the phase should reflect that of the constituent molecules and so a biaxial nematic should be formed. Here the term biaxial strictly indicates that there are now two axes along which a plane polarized

beam can travel without the state of polarization being altered. At the macroscopic level the three principal components of the second rank tensor would all be different, it is appropriate to denote them by $\tilde{Q}_{nn}$, $\tilde{Q}_{mm}$ and $\tilde{Q}_{ll}$ where $\hat{l}, \hat{m}$ and $\hat{n}$ define the three directors of a biaxial nematic. These are shown in Figure 1.2a for a system composed of board-shaped molecules. The director $\hat{n}$ corresponds, by convention, to the axis along which the molecular long axes tend to be parallel. The director $\hat{l}$ is the director along which, on average, the molecular short axes are parallel and the director $\hat{m}$ is orthogonal to $\hat{l}$ and $\hat{n}$.

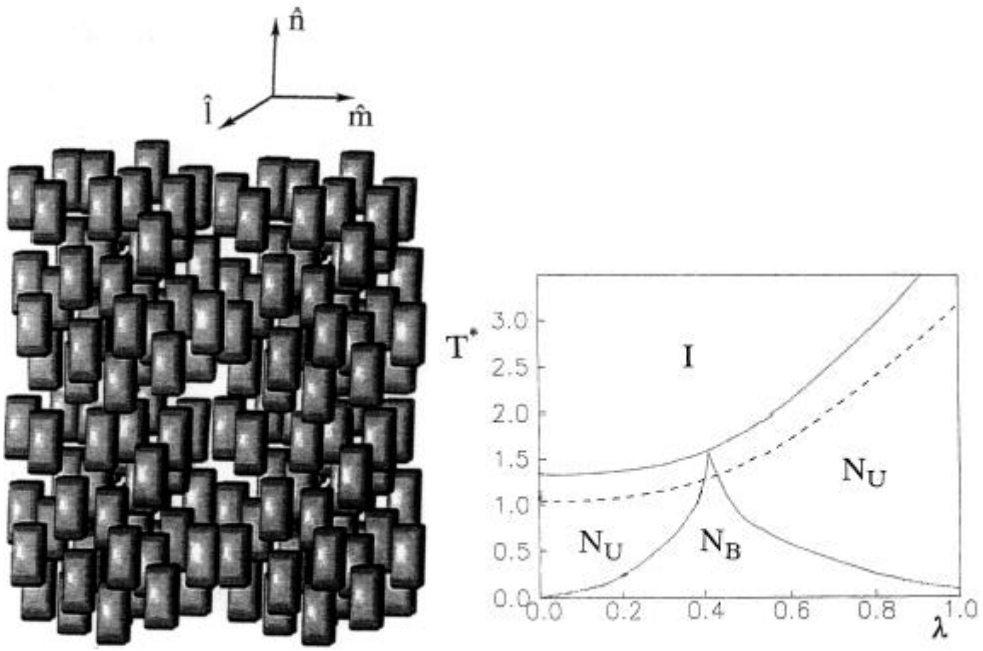

FIGURE 1.2. (a) Molecular organization in a biaxial phase formed from board-like molecules. (b) Phase diagram predicted by the molecular field theory for a system of biaxial molecules as a function of the molecular biaxiality, λ. The dashed line shows the anticipated freezing point of the mesogen at a reduced temperature of 0.8.

A number of applications have already been envisaged for the biaxial nematic phase. For example, it is to be expected that rotation of the minor directors might be relatively rapid and possibly faster than for the director $\hat{n}$. This could produce a display with a fast response and based on in-plane switching. To explore such possibilities as well as the other anticipated unusual properties of the biaxial nematic phase resulting

from its lower symmetry it is clearly necessary to have examples of real systems which form the phase. In Section 1.2.1 we consider how the molecular biaxiality influences the ability to form a biaxial nematic. We shall then describe some materials claimed to form a biaxial nematic and consider how the phase biaxiality can be identified. In Section 1.2.2 we shall discuss how deuterium NMR spectroscopy can be used to determine the symmetry of a nematic phase. The results of applying this powerful technique to a number of materials will then be described. As we shall see the biaxial nematic phase proves to be elusive and so in Section 1.2.3 we consider why this should be and propose new design strategies by which the biaxial nematic could be created. Some ending remarks of this discussion is given in Section 1.2.4.

1.2.1. Molecular biaxiality and phase biaxiality. To explore the relationship between the biaxiality of the constituent molecules and the ability of the material to form the biaxial nematic phase we need first to define a measure of the molecular biaxiality. One but not the only way by which this can be achieved is within the context of the molecular field theory first used to predict the phase behavior of the system [**102**, **101**, **3**]. For the uniaxial nematic phase the potential of mean torque, which describes the energy of a molecule in its anisotropic environment, is given by Luckhurst et al [**88**] as

$$U(\omega) = -\Sigma^{2}_{m=-2} X^{*}_{2m} C_{2m}(\omega) \tag{5}$$

Here ω denotes the spherical polar angles defining the orientation of the director, $\hat{n}$, in the molecular frame and $C_{2m}(\omega)$ is a modified spherical harmonics. This expression describes how the energy changes with the molecular orientation with respect to the director. The magnitude of this change is determined by the strength tensor, X_{2m}, which is related to the molecular anisotropy and the long range orientational order parameters. The molecular biaxiality, λ, is defined by the ratio X_{22}/X_{20} which under certain conditions is determined solely by the molecular anisotropy. Thus, for

a molecule having a cuboidal shape with length, L, width, W and breadth, B, the molecular biaxiality (given by Ferrarini et al. [4]) is

$$\lambda = (3/2)^{1/2} L(B - W)/L(B + W) - 2BW \tag{6}$$

This expression takes certain simple limiting forms; when $B = W$ the molecular cross-section is square and so the molecular biaxiality vanishes and λ is zero. The opposite extreme to this rod-like molecule occurs when $L = B$ and it becomes disc-like; then λ is $\sqrt{(3/2)}$. In between these two extremes, when the molecules are in effect uniaxial, is the most biaxial molecular shape. This occurs when L, B and W are related by the harmonic mean

$$(W^{-1} + L^{-1})/2 = B^{-1} \tag{7}$$

then λ is $1/\sqrt{6}$. Although λ has been estimated here using a model based solely on repulsive forces it is important to note that within the context of the molecular field theory anisotropic attractive forces also contribute to the biaxiality parameter [88].

The phase behaviour predicted by the molecular field theory as the molecular biaxiality is changed is shown in Figure 1.2b. As expected, when λ is zero the system forms only a uniaxial nematic phase which is denoted by N_U. As λ deviates from zero so a biaxial nematic phase is necessarily introduced into the phase diagram. With increasing λ the uniaxial nematic-isotropic transition temperature, $T_{N_U I}$, increases but not as rapidly as that between the biaxial and uniaxial nematic phases, $T_{N_B N_U}$. As a result the two lines meet at a unique point, the Landau point; here the isotropic phase undergoes a transition directly to the biaxial nematic phase. This occurs when λ is $1/\sqrt{6}$, that is, the breadth of the cuboidal molecule is the harmonic mean of the width and length. As λ increases beyond this point so the molecule becomes more uniaxial, in consequence $T_{N_B N_U}$ falls until when λ is $\sqrt{(3/2)}$ only a uniaxial nematic phase is formed by the system of disc-like molecules. The theory also predicts the order of the transitions which can be of importance in identifying the biaxial nematic-uniaxial

nematic phase transition [102, 101, 3]. Thus, the uniaxial nematic-isotropic transition is first-order but as λ increases so the entropy change decreases until it vanishes at the Landau point; that is the biaxial nematic-isotropic transition is predicted to be second-order. In contrast to the uniaxial nematic-isotropic transition the biaxial nematic-uniaxial nematic transition is predicted to be second order irrespective of the magnitude of the molecular biaxiality.

It would appear, therefore, on the basis of molecular field calculations by Freiser [102] and others [101, 3] that any compound composed of biaxial molecules should exhibit a biaxial nematic and that the greater the molecular biaxiality the greater the chance of observing this phase. However, it was not until 16 years after the original prediction that the first claim to have discovered a thermotropic biaxial nematic phase appeared [5]. There then followed, relatively quickly, claims to have found other examples of materials forming a biaxial nematic [6, 7]. A selection of the systems is shown in Figure 1.3 and these structures clearly indicate that the constituent molecules have a high shape biaxiality. It was not surprising, therefore, that they should form a biaxial nematic phase. However, it is important that this phase is correctly identified and in the following section we consider how this might be achieved.

1.2.2. Identifying a biaxial nematic. The defining characteristic of a biaxial nematic phase is the fact that the three principal components of any second tensorial property are different. The refractive index is related to such a property and since small differences in the refractive index can be readily measured this presents a prime quantity, in principle, with which to establish the symmetry of a nematic phase. In this determination it is essential to prepare a monodomain of the nematic. This can achieved by placing a thin film of the nematic between two electrodes and using an electric field to align the $\hat{n}$ director. Surface forces are then employed to align the $\hat{m}$ director for a biaxial nematic phase. The difference in the indices along $\hat{l}$ and $\hat{m}$ can then be determined using conoscopy [8]. These images obtained for uniaxial and

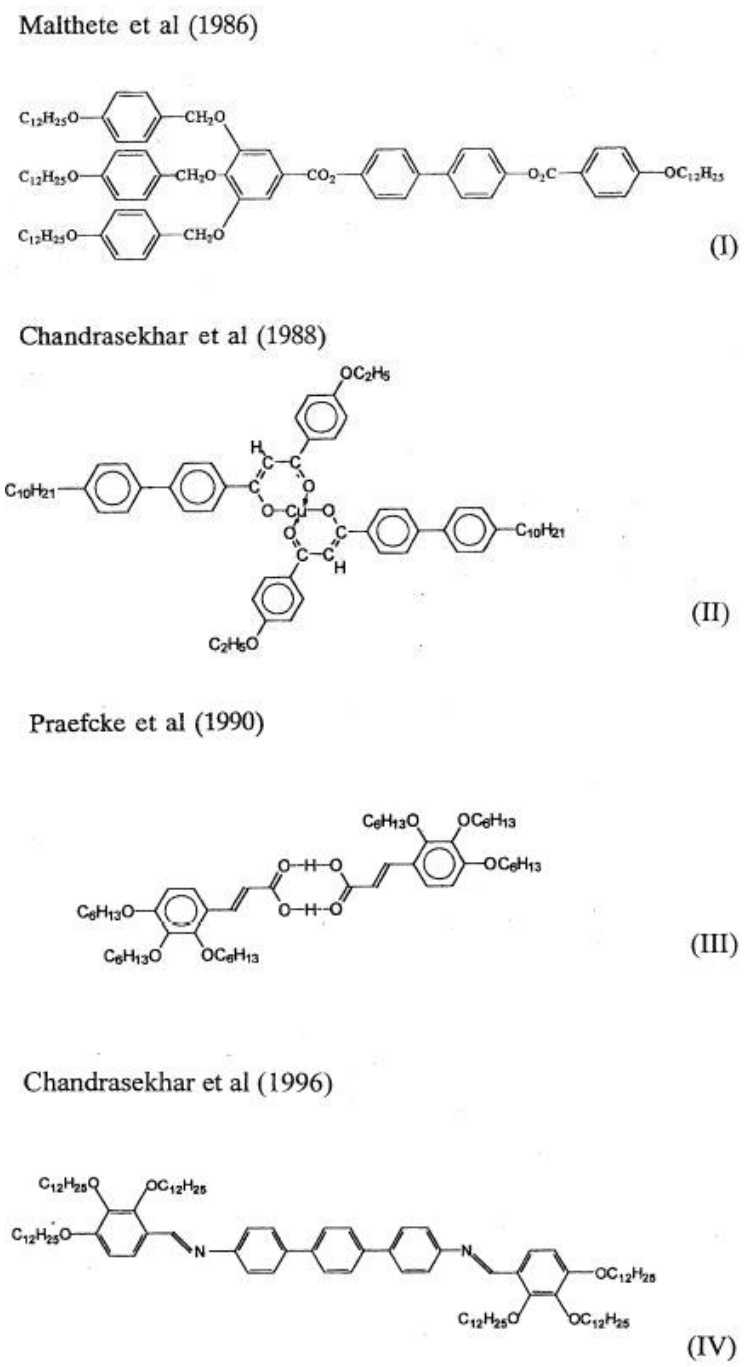

FIGURE 1.3. Molecular structures claimed to form a biaxial nematic phase.

biaxial phases are shown in Figure 1.4a. For a uniaxial nematic there is an interference pattern giving the two dark lines, known as isogyres, which form a cross; however, if the phase is biaxial the isogyres open and so do not cross in the centre of the image.

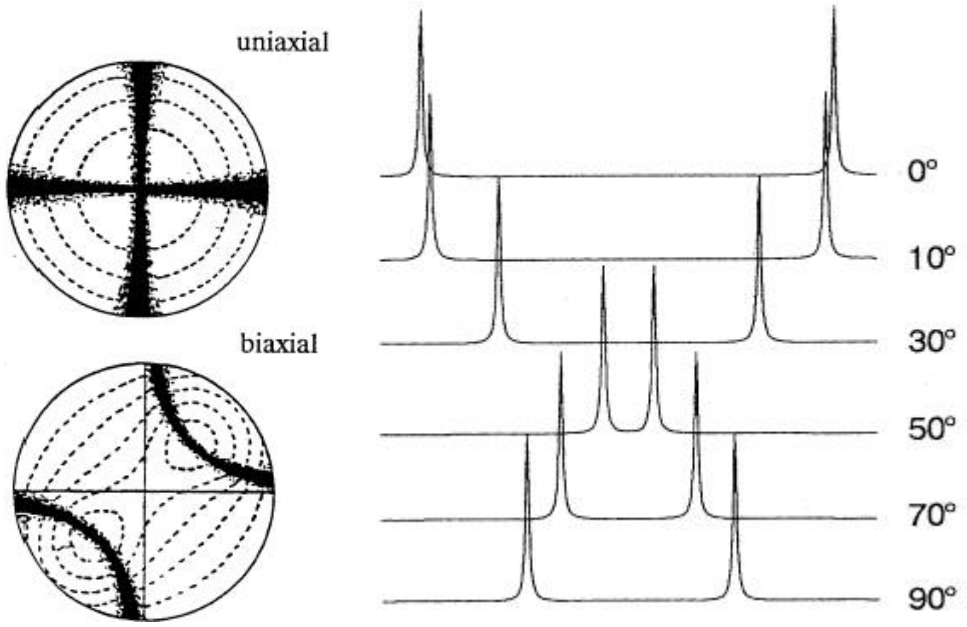

FIGURE 1.4. (a) Conoscopic images expected for monodomain samples of a uniaxial and a biaxial phase.(b) Dependence of the NMR spectrum of a group of equivalent deuterons in a uniaxial phase on the angle, β, between the director, $\hat{n}$, and the magnetic field.

This technique has been used to demonstrate that the nematic phases formed by compounds (II) [6] and (III) [9] in Figure 1.3 are biaxial. However , the extent to which the isogyres are observed to open is rather small which implies that the biaxiality in the refractive index is also small. This presents a problem for the definitive identification of the nematic phase as biaxial since for thin films the surface can induce an optical biaxiality in the sample even if the bulk phase is uniaxial. This is because the director, $\hat{n}$, may be tilted with respect to the surface normal. It would seem, therefore, that an alternative method, free from influence of surface forces on the director orientation, is needed to establish the symmetry of the nematic phase. Deuterium NMR spectroscopy provides such a method and we now outline the essential features of this technique.

In the isotropic phase the NMR spectrum of a sample containing a set of equivalent deuterons contains a single line. However, on entering the liquid crystal phase this is split into a doublet because of the long range orientational order characteristic of the

liquid crystal and the quadrupolar interaction for the deuterons [10]. The magnitude of the splitting depends both on the second rank orientational order parameters for the molecule and the orientation of the director with respect to the magnetic field of the spectrometer. It is this second aspect which is of particular importance here. The variation of the spectrum with the angle, β, between the magnetic field and the director, $\hat{n}$, of a uniaxial nematic is indicated in Figure 1.4b. This shows that the largest quadrupolar splitting occurs when the director is parallel to the field. As the angle between the field and the director increases so the splitting decreases, passes through zero at the magic angle (54.74^o) and then increases again to one-half of its original value. The angular variation of the quadrupolar splitting, $\triangle\tilde{\nu}$, is accurately represented by

$$\triangle\tilde{\nu}(\beta) = \triangle\tilde{\nu}(0)(3\cos^2\beta - 1)/2 \tag{8}$$

Strictly the signs of the quadrupolar splittings when the director is parallel and perpendicular to the magnetic field are opposite, as is apparent from Eq.(8). However, the signs of the splittings cannot be determined from the NMR spectrum and so it is the modulus of the ratio with which we shall be concerned. The important point for the phase symmetry is that for a uniaxial nematic, the modulus of the ratio of the quadrupolar splittings when the field is parallel to the director to that when it is perpendicular is 2:1. In contrast, if the nematic phase is biaxial then the ratio of the splittings when the magnetic field is along $\hat{n}$ to that when it is parallel to $\hat{l}$ or $\hat{m}$ deviates from 2:1. In principle, therefore, it would be necessary to prepare a monodomain sample of the nematic and then change its orientation with respect to the magnetic field to establish the phase symmetry. In practise this can be difficult because one of the directors will always be aligned with the magnetic field of the spectrometer and so a competing electric field would be necessary to change its orientation.

Fortunately, there is an alternative procedure with which to control the director alignment which allows two of the principal components of the quadrupolar splitting to be measured from a single spectrum. To achieve this it is necessary to spin the sample about an axis orthogonal to the magnetic field. Then, provided the diamagnetic anisotropy is positive and the spinning speed is above some critical value, the director is observed to be randomly distributed in a plane perpendicular to the spinning axis [11]. Since the field is in this plane the director will adopt all angles with respect to the magnetic field from 0^o to 90^o. In addition, the NMR spectrum of the system is a sum of spectra coming from each orientation of the director; this is known as a two-dimensional powder pattern. It will then contain spectra from the extreme director orientations from which the associated quadrupolar splittings and hence the phase symmetry can be determined. Simulated spectra illustrating the behavior expected for uniaxial and biaxial nematic phases are shown in Figure 1.5. The static samples with the $\hat{n}$ director aligned parallel to the magnetic field give spectra containing a simple quadrupolar doublet. On spinning the samples above some critical speed the spectra change; in both cases they contain an outer pair of lines associated with the $\hat{n}$ director parallel to the magnetic field in other words with a quadrupolar splitting equal to that found for the static sample. In addition, there is an inner quadrupolar doublet associated with the $\hat{n}$ director orthogonal to the magnetic field. For the uniaxial nematic the outer quadrupolar splitting is just twice the inner one. For the biaxial nematic the ratio of the outer and inner quadrupolar splitting deviates from the value of 2:1; in Figure 1.5 the ratio is larger although it could equally well be smaller [12].

The first thermotropic nematogen for which the NMR technique was used to establish the symmetry of the nematic phase was 2,3,4-trihexyloxycinnamic acid (see III in Figure 1.3 [12]. The nematic phase of this material, formed directly from the isotropic phase, had been identified as biaxial using conoscopic observations [9]. To investigate

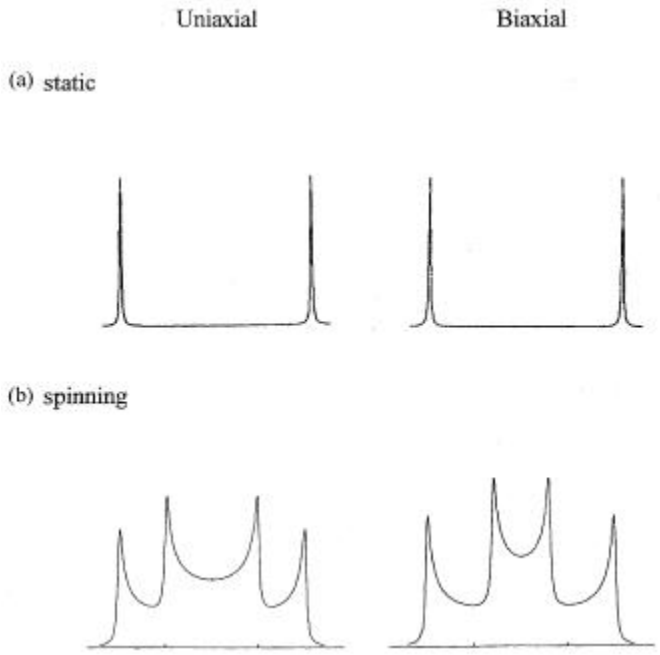

FIGURE 1.5. Simulated deuterium NMR spectra for the uniaxial and biaxial nematic samples for (a) static and (b) spun about an axis perpendicular to the magnetic field of the spectrometer.

the symmetry of this phase using deuterium NMR the compound was specifically deuteriated in one position of the ethylenic bond. The NMR spectrum recorded in the nematic phase is shown in Figure 1.6a. As expected, the spectrum of the static sample contains a single quadrupolar doublet associated with the director parallel to the magnetic field. On spinning the sample about an axis orthogonal to the magnetic field a two-dimensional powder pattern is formed at the relatively low rotational velocity of 2.7 Hz. This low value implies that the rotational viscosity of the nematic is rather large [12]. As predicted (see Figure 1.5) the outer doublet has the same quadrupolar splitting as for the static sample showing that it comes from the director aligned parallel to the magnetic field. The inner doublet has a splitting which is essentially one-half of the major splitting. This suggests that the nematic phase is uniaxial and that this splitting comes from the director being orthogonal to the field. Confirmation of the uniaxial symmetry of the phase is obtained by simulating the NMR spectrum and this simulation is shown as the dashed line in Figure 1.6a; it is

clearly in good agreement with the experimental spectrum. The conclusion that the nematic phase formed by 2,3,4-trihexyloxycinnamic acid is uniaxial and not biaxial as originally claimed is consistent with the observation that there is a large jump in the quadrupolar splitting at the nematic-isotropic transition. This shows that the transition is a first-order and not second-order as predicted for a biaxial nematic-isotropic transition.

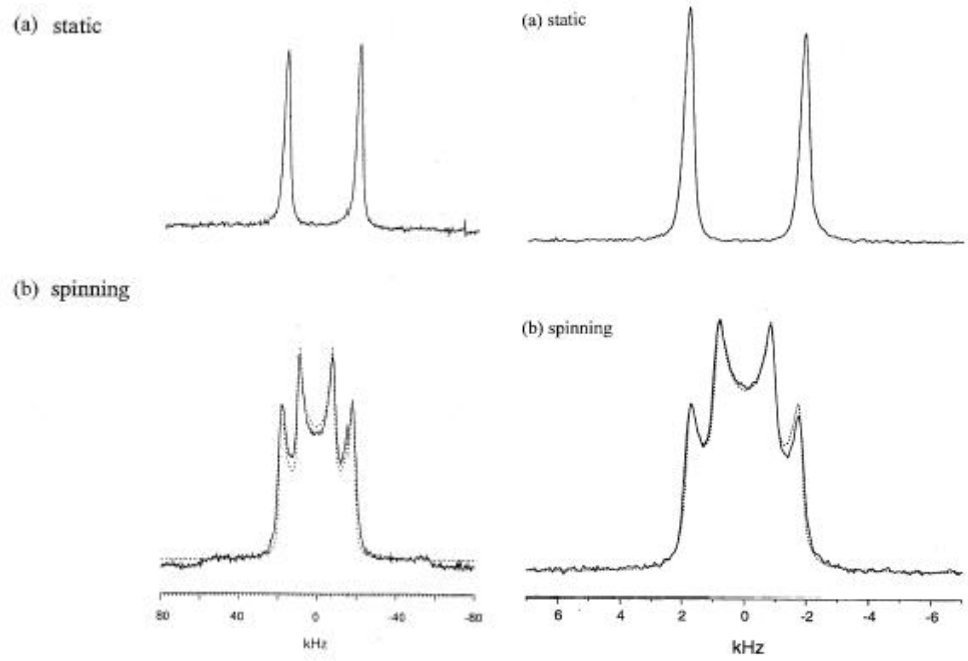

FIGURE 1.6. (a) Deuterium NMR spectrum of mono-deuteriated 2,3,4-tri-hexyloxycinnamic acid (III) in its nematic phase: static and spinning. The simulated spectrum for the spinning sample, assuming a uniaxial nematic phase, is shown as the dashed line. (b) Deuterium NMR spectra of the solute, hexamethylbenzene-d_{18}, dissolved in the nematic phase of the mesogen I for the static and the spinning sample. The two-dimensional powder pattern simulated for a uniaxial nematic phase is shown as the dashed line.

The NMR technique was next used to investigate the symmetry of the nematic phase formed by 4-[3,4,5-tris(4-dodecyloxybenzyloxy)benzoyloxy]-4'-(4-dodecyloxybenzoyloxy)-1',1'-biphenyl (see I in Figure 1.3) which was the first compound claimed to form a biaxial nematic [5] having been identified by its optical texture [8]. To confirm this assignment using NMR spectroscopy the compound was also specifically deuteriated,

now in the three oxymethylene links. This gives a material with two groups of equivalent deuterons that were apparent from the deuterium NMR spectrum of the static nematic phase which exihibited two quadrupolar doublets [13]. On spinning the sample about an axis orthogonal to the magnetic field, again at a relatively low rotational velocity, a two-dimensional powder pattern was observed. This was somewhat more complicated than those shown in Figure 1.5 and Figure 1.6a because there are two quadrupolar doublets, however, simulation of the spectrum [13] revealed that the symmetry of the nematic phase was uniaxial and not biaxial as originally claimed [5].

The specific introduction into a mesogenic molecule can be a difficult and time consuming task. The alternative process of simply adding a deuteriated solute to the mesogenic solvent offers an extremely convenient alternative. The essential point being that the symmetry of the environment experienced by the solute molecules is identical to that experienced by the mesogenic molecules. Offcourse, the addition of a solute may change the phase behavior by changing the transition temperature and possibly the nature of the phase. Such undesirable effects can be minimised by using a low solute concentration which with modern NMR spectrometers is of the order of a few wt.%. This technique for the introduction of deuterium into a mesogenic sample was also used for mesogen I [13]. The solute chosen was predeuteriated hexamethylbenzene$-d_{18}$ for which the 18 deuterons are equivalent. The deuterium NMR spectrum for this solute dissolved in the nematic phase of I therefore contains a single quadrupolar doublet as shown in Figure 1.6b. On spinning the sample a two-dimensional powder pattern was observed and this is apparent from the spectrum shown in Figure 1.6b. The spacing between the outer pair of lines is essentially twice that for the inner pair. This also suggests that the nematic phase is uniaxial, a result confirmed by the spectrum simulated for a uniaxial nematic which is in very good agreement with the experimental powder pattern (see Figure 1.6b). The result obtained with the solute is, therefore, in complete agreement with that found for

the specifically deuteriated mesogen. This is a valuable conclusion since it suggests that the symmetry of nematic phases can be determined without needing to prepare deuteriated mesogens.

More recently, Chandrasekhar and his colleagues [14, 15] have presented apparently convincing evidence that 4,4"(p-terphenyl)-bis[2,3,4-tri(dodecyloxy) benzal]imine (see IV in Figure 1.3) forms a biaxial nematic phase. This evidence included differential scanning calorimetry, optical textures, conoscopy and optical transmittance [15]; all of these observations are consistent with the phase being a biaxial nematic. This appeared, therefore, to be an ideal material with which to demonstrate the NMR methodology. Since a deuteriated sample was not available, deuterium was introduced by the addition of the solute hexamethylbenzene$-d_{18}$. The NMR spectrum of this in the nematic phase, previously identified as biaxial, is shown in Figure 1.7a. As expected the spectrum of the static sample consists of a single quadrupolar doublet and on spinning about an axis orthogonal to the magnetic field a familiar two-dimensional powder pattern was observed was observed [16]. The spacing between the outer and inner pairs of lines is in the ratio of approximately 2:1 and the simulated powder pattern is found to be in very good agreement with experiment. It would seem, therefore, that the phase previously identified by Chandrasekhar and his colleagues as a biaxial nematic is, according to the NMR experiment, uniaxial.

This apparent failure of deuterium NMR spectroscopy to observe the biaxiality of nematic phases when other techniques are apparently able to do is somewhat surprising. It could result, for example, from some flaw in the NMR method whereby the biaxiality in the quadrupolar tensor, $\tilde{q}$, is somewhat averaged to zero. Alternatively, it could be that the biaxiality in $\tilde{q}$ and hence of the phase is too small to be determined with the NMR technique.

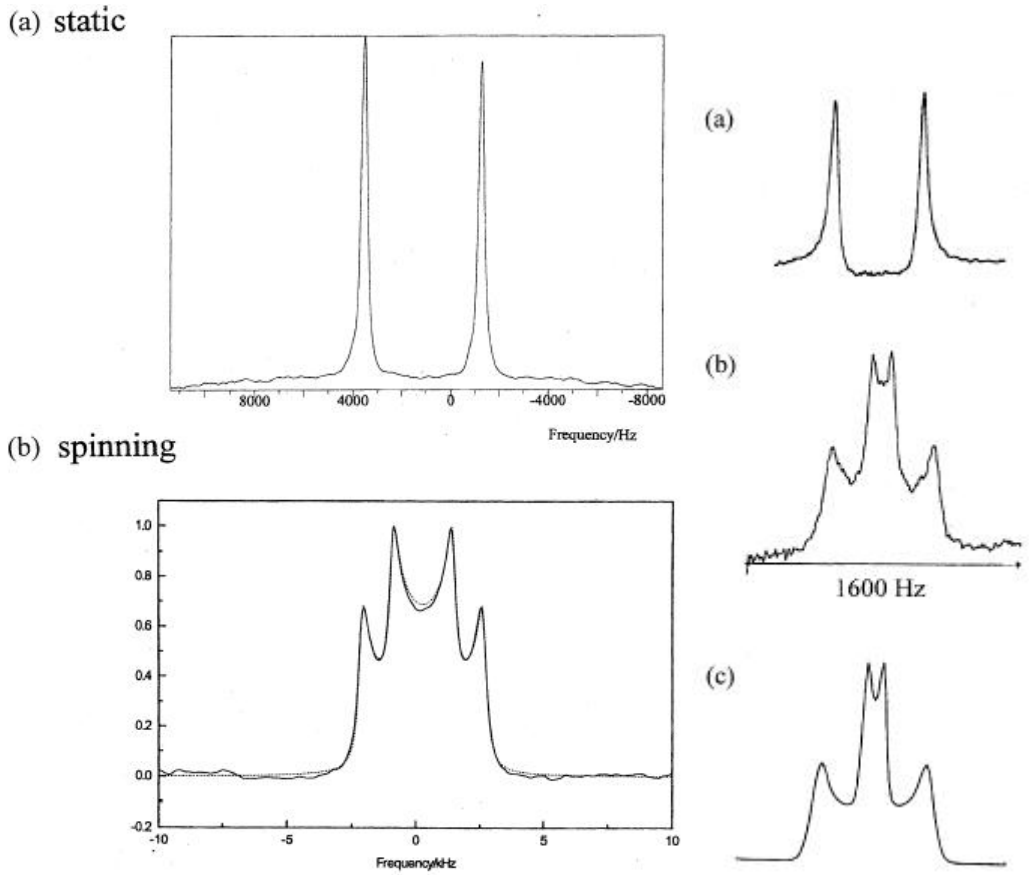

FIGURE 1.7. (a) Deuterium NMR spectra of the solute, hexamethylbenzene-d_{18}, dissolved in the nematic phase of IV for the static and the spinning sample. (b) Deuterium NMR spectrum of D_2O in the biaxial nematic phase formed by the lyotropic mesogen composed of potassium laurate, decylammonium hydrochloride and water: (i) static; (ii) spinning; and (iii) simulated two-dimensional powder pattern with $\tilde{\eta} = 0.68$.

The validity of the method itself to observe the symmetry of a biaxial nematic phase has in fact been demonstrated for such phases formed by lyotropic mesogens. Indeed the first biaxial nematic phase to have been reported was for a lyotropic system composed of potassium laurate, 1-decanol and water [17] although some doubt has been cast on the chemical stability of the phase in this particular system [18]. This chemical instability of the biaxial nematic phase is reduced if the decanol is replaced by decylammonium hydrochloride [19]. Such a system has been studied by deuterium NMR spectroscopy and for this the source of deuterium was obtained by replacing

light (H_2O) with heavy (D_2O) water [20]. The range of the biaxial nematic is now determined not only by temperature but also by the concentrations of the various components in the lyotropic mesogens. The deuterium NMR spectra for one such system in its biaxial nematic phase is shown in Figure 1.7b. The spectrum of the static sample contains a single quadrupolar doublet as expected when one of the directors is aligned parallel to the magnetic field. On spinning the sample about an axis orthogonal to the magnetic field with a rotational velocity of approximately 2 Hz a two-dimensional powder pattern was observed. However, unlike the powder patterns obtained for thermotropic mesogens the spacing between the inner pair offlines is clearly not equal to half that between the outer pair. It is clear, therefore, that the NMR spectrum of a spinning nematic can be used to determine the symmetry of a biaxial nematic phase. Consequently, the failure of the NMR technique to observe the biaxiality in the nematic phase formed by thermotropic mesogens is unlikely to be associated with some flaw in the methodology.

The other possible explanation suggested is that the biaxiality of the nematic phase is too small to be observed by NMR spectroscopy. It is, perhaps, helpful at this stage to see how the biaxiality parameter obtained from the NMR experiments is defined. At a formal level the quadrupolar splittings determined from the NMR spectrum are related to the partially-averaged quadrupolar tensor, $\tilde{q}$. The principal axes for $\tilde{q}$ are simply the symmetry axes of the phase, that is, the three directors and so the principal components are denoted by $\tilde{q}_{ll}$, $\tilde{q}_{mm}$ and $\tilde{q}_{nn}$; two subscripts are used because $\tilde{q}$ is a second rank tensor tensor. The quadrupolar splittings when the magnetic field is aligned parallel to a director is just three halves times the principal components of $\tilde{q}$ for that direction .

Determination of the splittings associated with the field parallel to the directors then gives $\tilde{q}$ and its biaxiality which reflects that of the phase [12, 13] and is defined by

$$\tilde{\eta} = (\tilde{q}_{mm} - \tilde{q}_{ll})/\tilde{q}_{nn}, \tag{9}$$

where the labels n, l and m are assigned such that $|\tilde{q}_{nn}| > |\tilde{q}_{mm}| > |\tilde{q}_{ll}|$. With this assignment, $\tilde{\eta}$ vanishes for the uniaxial nematic while for the biaxial nematic it can take limiting values of ± 1 depending on the signs of the principal components. These limiting values obtain because $\tilde{q}$ is traceless, that is, the sum of the diagonal elements vanishes. The form of the NMR spectrum given in Figure 1.7b shows that for the spinning sample one director is aligned parallel to the spinning axis and the other two are distributed in the plane orthogonal to this. The principal components of $\tilde{q}$ are then readily obtained from the spectrum and give a value for the biaxiality parameter of 0.68; the spectrum simulated with $\tilde{\eta} = 0.68$ is in good agreement with experiment [20] as can be seen from Figure 1.7b. This biaxiality is clearly large although at other temperature the biaxiality parameter is even larger and is found to reach its limiting value of unity [20]. These biaxiality parameters are clearly significant but they are in keeping with molecular field theory predictions for thermotropic biaxial nematics [4]. Detailed analysis of the NMR spectra for the supposed thermotropic biaxial nematic phases reveals that the biaxiality parameter, $\tilde{\eta}$, is certainly less than 0.1 [12, 13, 16] which is significantly smaller than the value expected for a biaxial nematic. It would seem, therefore, that the assignment of the nematic phases claimed to be biaxial as uniaxial nematics is correct and so in the following section we consider why it is so difficult to prepare a compound exhibiting a biaxial nematic phase.

1.2.3. Designing biaxial nematogens. To understand the inherent difficulty in designing materials to form a biaxial nematic phase it is useful to return to the predicted phase diagram shown in Fig. Figure 1.2b. Here we see that as soon as the constituent molecules deviate from cylindrical symmetry the mesogen should exihibit a biaxial nematic phase following the uniaxial nematic. However, in practise the uniaxial nematic does not usually form a biaxial nematic because another phase

intervenes. That is, the uniaxial nematic may simply crystalize or undergo a transition to a smectic phase. To see how this will influence the value of the molecular biaxiality parameter needed to give an enantiotropic biaxial nematic it is necessary to make an assumption about the nematic range. Typically real nematogens freeze at a reduced temperature, T/T_{NI}, of approximately 0.9 and certainly by a reduced temperature of 0.8. For a nematogen with a nematic-isotropic transition temperature of 400 K this would correspond to a nematic range of 80 K which is relatively long for a real nematogen. The dashed line in Figure 1.2b shows this hypothetical nematic range and it is seen that for the vast majority of the molecular biaxialities the uniaxial nematic phase is expected to freeze before the transition to the biaxial nematic can occur. Indeed the range of molecular biaxialities for which an enantiotropic biaxial nematic is predicted is extremely small, from approximately 0.39 to 0.42. Thus, for a material to form the biaxial nematic phase the biaxiality of the constituent molecules must be within a few percent of the maximum allowed biaxiality of $1/\sqrt{6}(\equiv 0.4082)$ [4]. It is not surprising, therefore, that the biaxial nemtic phase is proving to be elusive when the molecular biaxiality has to be to tightly defined. Offcourse, if the system can be prevented from freezing, as in lattice models where the orientational and translational order are decoupled, then it should certainly be possible for molecules interacting via a biaxial potential to form a biaxial nematic. This has been found to be the case for the biaxial analogue [21] of the seminal Lebwohl-Lasher model of uniaxial nematics [22].

We have, implicitly, been taking the biaxial molecules to be cuboidal but other molecular shapes also deviate from cylindrical symmetry. For example, V-shaped or banana molecules such as that in Figure 1.8 are also biaxial although many of these form new smectic phases with quite fascinating properties [**?**, 4]. Since the V-shaped molecule can be thought of as containing two cylindrically symmetric arms the extent of its biaxiality is determined simply by the angle between these two arms. The influence of

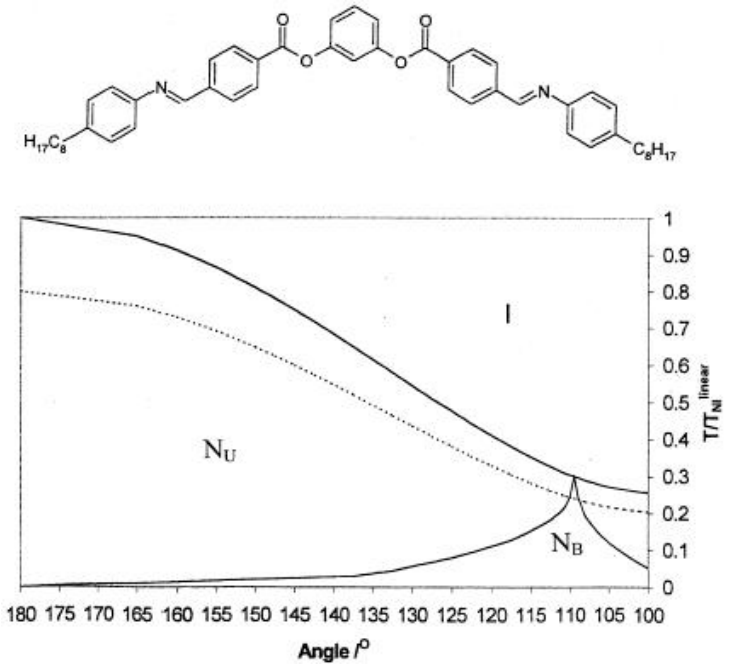

FIGURE 1.8. Phase behaviour predicted by molecular field theory for a V-shaped molecule, as a function of the angle θ between the two mesogenic arms. The dashed line indicates the freezing point which is taken to occur at a reduced temperature of 0.8.

this geometrical parameter on the phase behaviour is readily calculated using molecular field theory and the result is shown in Figure 1.7b [24]. When θ is 180^o the molecule is linear and so only a uniaxial nematic phase can be formed; similarly when the angle between the two arms is 90^o only a uniaxial nematic phase is possible when the molecule is essentially disc-like. In between these two limiting cases the uniaxial nematic-isotropic transition temperature falls as the molecule is bent. More importantly a biaxial nematic phase necessarily appears in the phase diagram and $T_{N_B N_U}$ increases, albeit rather slowly. Eventually the lines for $T_{N_B N_U}$ and $T_{N_U I}$ cross at the Landau point when there is a second-order transition directly from the isotropic to the biaxial nematic phase. The value of θ at the Landau point which is associated with the maximal molecular biaxiality is the tetrahedral angle of $\cos^{-1}(1/3)$, that is, 109.47^o. The appearance of this phase diagram has much in common with that obtained for hard V-shaped objects using a theoretical approach based on a second virial and bifurcation analysis [25]. The state variable for such a system is the density

which is related to the inverse temperature for thermotropic models. We see, therefore, that the conventional banana molecules where the angle between the mesogenic arms is close to 120^o are somewhat removed from the optimum tetrahedral value. To determine whether it is too far removed to yield an enantiotropic biaxial nematic it is necessary to include on the phase diagram the anticipated freezing point of the material. Again this is taken to occur at a reduced temperature of 0.8 and the line corresponding to this is shown as the dashed line in Figure 1.8. It is now apparent that the uniaxial nematic phase will freeze before the biaxial nematic phase is formed except for a very narrow range of angles θ, varying from 108.5^o to 110^o. It would appear that the conventional banana molecules will certainly not exhibit a biaxial nematic phase although one in which the two arms are linked by a methylene group should form this elusive phase. However, there is another problem with this strategy which is also apparent from the phase diagram in Figure 1.8. This is the dramatic reduction in the uniaxial nematic-isotropic transition temperature as the inter-arm angle decreases from 180^o; indeed by the time it has reached the tetrahedral angle T_{NI} has decreased to less than one-third of its original value. It seems, therefore, that the transition temperature of the linear mesogen, that is without the central carbon atom, should be above 900 K if T_{NI} for the V-shaped form is to be in excess of room temperature. This would require mesogenic arms with atleast three phenyl rings; however, such molecules do not exhibit a liquid crystal phase presumably because of their high melting points [24]. This high melting point can be reduced and the smectic forming tendency of the V-shaped molecules removed by placing a bulky substituent in the linking phenyl ring. The use of a hexyl chain is found to create a series of materials exhibiting monotropic nematic phases although the symmetry of these has yet to be determined [26].

If, as seems apparent from this discussion, the design of mesogenic molecules with sufficient biaxiality to form a biaxial nematic is such a delicate task then the use of

mixtures might prove to be more successful. This view is suggested by the observation that the stable arrangement for a rod-like and a disc-like molecule is one with their symmetry axes orthogonal to each other. This would result in the two directors associated with these two symmetry axes being orthogonal to each other in the nematic phase. Indeed this strategy for the formation of a biaxial nematic was apparently supported by a molecular field theory [27]. This showed that a binary mixture of rods and discs should form both uniaxial and biaxial nematic phases except for the equimolar mixture for which the isotropic phase should undergo a transition directly to the biaxial nematic. However, this theory ignored the possibility that the system might phase separate into two uniaxial nematic phases, one rich in rods and the other in discs. In fact this proves to be the stable state of the binary mixture of rods and discs, in preference to a biaxial nematic phase [28].

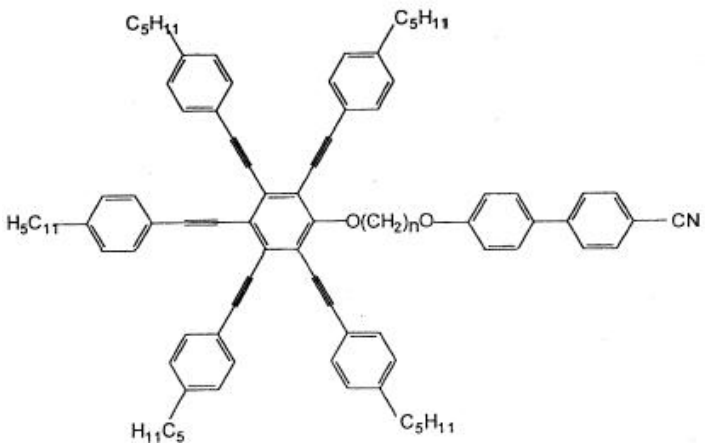

FIGURE 1.9. Molecular structure of a rod-disc dimer with high biaxiality.

The observation of this phase for such a mixture requires a method for inhibiting phase separation. This is readily achieved in computer simulation studies of lattice models where the rods and discs are randomly distributed and fixed on lattice sites. Such an idealized model with equal numbers of rods and discs is found to form a biaxial nematic phase although if exchange between lattice sites is allowed two uniaxial nematics are formed [29]. This strategy is clearly not possible for real mesogens and here it has been suggested that phase separation can be inhibited if the scalar

interaction between a rod and a disc is more favorable than the mean interaction between like particles [30]. Although attempts have been made to implement this theory led strategy at a practical level no biaxial nematics have yet been reported, possibly because the scalar rod-disc interactions are insufficiently strong. However, a limiting case which would certainly prevent phase separation would be to connect the rod-like and disc-like molecules covalently. It has been suggested by Fletcher and Luckhurst [49] that this can be achieved by using a flexible spacer to link the rod-like and disc-like moieties, an idea also explored by Praefcke and his colleagues [50]. However, it is necessary for the spacer with its different conformations to hold the effective symmetry axes of the two mesogenic moieties essentially perpendicular to each other so that their preferred alignment results in orthogonal directors. This approach has been attempted using a homologous series of $\alpha-$[(1,2,3,5,6- pentakis(4-pentylphenyl-ethynyl))-benzene-4-oxy]-ω-(4'-cyanobiphenyl)alkanes whose structure is shown in Figure 1.9. None of these materials gave a nematic phase although equimolar mixtures with 2,4,7-trinitro-9-fluorenone did yield monotropic nematics with small translational entropies [49] which is suggestive of a high molecular biaxiality. However, the monotropic nature of the nematic phase made it impossible to determine its symmetry using NMR spectroscopy. Nonetheless, this type of rod-disc dimer offers a wide range of opportunities both to stabilize the nematic phase and to enhance the molecular biaxiality, as we have discovered [51].

1.2.4. Ending Remarks. It is apparent that deuterium NMR spectroscopy provides a powerful technique with which to determine the symmetry of nematic phases especially as the system investigated is essentially free from surface perturbations. Application of this technique to several compounds for which thermotropic biaxial nematic phases have been claimed has shown them to be uniaxial nematics. This result is, at first sight, somewhat surprising because the constituent molecules certainly appear to have a high biaxiality and so might be expected to form a biaxial nematic. However, molecular field calculations predict that if a biaxial nematic is to

appear above the freezing point of a real uniaxial nematic then the molecular biaxiality must be within a few percent of its maximal value. It seems unlikely that such tightly constrained values can be easily achieved with real mesogenic molecules. An alternative route to molecule biaxiality is to bend a linear molecule thus giving a V- or banana-shaped molecule. Although this strategy seems attractive molecular field theory predicts that only a bond angle within a few degrees of the tetrahedral angle will allow the biaxial nematic to appear above the freezing point of a real uniaxial nematic. A quite different approach is based on the idea that mixtures of rods and discs should form a biaxial nematic were it not for the separation of the mixture into two uniaxial nematics. This phase separation can be prevented by linking the two mesogenic moieties to give a non-symmetric liquid crystal dimer. Such dimers provide a rich variety of molecular structures and prelimnary studies are supportive of this concept . At present, then, thermotropic biaxial nematics would appear to be fiction but there is every expectation that they will become fact in the near future.

1.3. Thesis organization

This chapter mentions some of the ongoing debates and unsolved problems in the area of Nematic Liquid Crystal Polymers. The introduction merely highlights a rich variety of problems, that seem to have little to do with each other. In this dissertation, we have specifically focused on one major problem in nematic lcps, namely the dynamics and rheology of flows of biaxial liquid crystal polymers, using the kinetic theory [85].

The thesis is organized as follows. Chapter 2 provides all the necessary tools and theorems needed to understand our work. The complete derivation of the rotational diffusion equation is then given in Chapter 3. Finally the results of the rheology and flows of biaxial lcps are presented in chapter 6. The three appendices towards the end, supplement our work.

Chapter 2

Mathematical Background

This Chapter provides the mathematical and the physical foundation which is necessary to understand this thesis on liquid crystals. Readers familiar with tensor notations are requested to skip the next section.

This chapter is organized as follows. Section 2.1 provides a detailed description of the tensor calculus needed to understand the various mathematical notations in subsequent chapters. While sections 2.2 and 2.3 gives all the quantum mechanical background needed to derive the rotational diffusion equation (described in the next chapter). Section 2.4 discusses how to construct the *"order parameters"* of interest for biaxial lcps. Finally, in section 2.5, we show an example of first order phase transition and explain the concept of tricritical point, which is necessary to understand our results (in chapter 6).

2.1. Tensors calculus

A scalar field describes a one-to-one correspondence between a single scalar number and a point. An n-dimensional vector field is described by a one-to-one correspondence between n-numbers and a point. Let us generalize these concepts by assigning n-squared numbers to a single point or n-cubed numbers to a single point. When these numbers obey certain transformation laws they become examples of tensor fields. In general, scalar fields are referred to as tensor fields of rank or order zero whereas vector fields are tensors of rank or order one. Closely associated with tensor calculus is the index notation.

2.1.1. Index Notation. A vector $\overrightarrow{A}$ can be expressed in the component form

$$\overrightarrow{A} = A_1\hat{\mathbf{e_1}} + A_2\hat{\mathbf{e_2}} + A_3\hat{\mathbf{e_3}}$$

(where $\hat{\mathbf{e_1}}$, $\hat{\mathbf{e_2}}$ and $\hat{\mathbf{e_3}}$ are orthogonal unit basis vectors), or as number triples: $\overrightarrow{A} = (A_1, A_2, A_3)$ or in the indicial notation, i.e.

$$A_i, \qquad i = 1, 2, 3$$

The indicial notion focuses attention only on the components of the vectors and employs a dummy subscript whose range over the integers is specified. The symbol A_i refers to all of the components of the vector $\overrightarrow{A}$ simultaneously. The dummy subscript i can have any of the integer values 1,2 or 3. For $i = 1$ we focus attention on the A_1 component of the vector $\overrightarrow{A}$. Setting $i = 2$ focuses attention on the second component A_2 component of the vector $\overrightarrow{A}$ and similarly when $i = 3$ we can focus attention on the third component of $\overrightarrow{A}$. The subscript i is a dummy subscript and may be replaced by another letter, say p, so long as one specifies the integer values that this dummy subscript can have .

Higher dimensional vectors may be defined as ordered n-tuples. For example, the vector

$$\overrightarrow{X} = (X_1, X_2, ..., X_N)$$

with components $X_i, i = 1, 2, ..., N$ is called a N-dimensional vector. Another notation used to represent this vector is

$$\overrightarrow{X} = X_1\hat{\mathbf{e_1}} + X_2\hat{\mathbf{e_2}} + ... + X_N\hat{\mathbf{e_N}}$$

where $(\hat{\mathbf{e_1}}, \hat{\mathbf{e_2}}, ..., \hat{\mathbf{e_N}})$ are linearly independent unit base vectors. Note that many of the operations that occur in the use of the index notation apply not only for three dimensional vectors, but also for N-dimensional vectors.

In future sections it is necessary to define quantities which can be represented by a letter with subscripts. Such quantities are referred to as systems. When these

quantities obey transformation laws they are referred to as tensor systems. Examples are;

$$A_{ijk} \quad e_{ijk} \quad \delta_{ij} \quad A_i \quad B_j$$

The number of subscripts determines the order of the system. A system with one index is a first order system. A system with N indices is called a Nth order system. A system with no indices is called a scalar or zeroth order system. The type of system depends upon the number of subscripts occurring in an expression. For example, A_{jk} and B_{st}, (all indices range 1 to N), are of the same type because they have the same number of subscripts.

There is a range convention associated with the indices. This convention states that whenever there is an expression where the indices occur unrepeated it is to be understood that each of the subscripts can take on any of the integer values 1,2,...N where N is a specified integer. For example the Kronecker delta symbol δ_{ij}, defined by $\delta_{ij} = 1$ if $i = j$ and $\delta_{ij} = 0$ if $i \neq j$, with i,j ranging over the values 1,2,3 represents the 9 quantities

$$\begin{aligned} \delta_{11} &= 1 \qquad \delta_{12} = 0 \qquad \delta_{13} = 0 \\ \delta_{21} &= 0 \qquad \delta_{22} = 1 \qquad \delta_{23} = 0 \\ \delta_{31} &= 0 \qquad \delta_{32} = 0 \qquad \delta_{33} = 1 \end{aligned}$$

The symbol δ_{ij} refers to all the components of the system simultaneously. As another example, consider the equation:

$$\hat{\mathbf{e}_\mathbf{m}} \cdot \hat{\mathbf{e}_\mathbf{n}} = \delta_{mn} \qquad\qquad m, n = 1, 2, 3 \tag{10}$$

the subscripts m,n occur unrepeated on the left side of the equation and hence must also occur on the right hand side of the equation. These indices are called "free" indices and can take on any of the values 1,2 or 3 as specified by the range. Since there are three choices for the value of m and three choices for a value of n we find that Eq.(10) represents nine equations simultaneously.

2.1.1.1. *Symmetric and Skew-Symmetric System.* A system defined by subscripts ranging over a set of values is said to be symmetric in two of its indices if the components are unchanged when the indices are interchanged. For example, the third order system T_{ijk} is symmetric in the indices i and k if

$$T_{ijk} = T_{kji} \qquad \text{for values of i,j,k}$$

A system defined by subscripts is said to be skew-symmetric in two of its indices if the components change sign when the indices are interchanged. For example, the fourth order system T_{ijkl} is skew-symmetric in indices i and l if

$$T_{ijkl} = -T_{ljki} \qquad \text{for values of i,j,k and l}$$

As another example, consider the third order system $a_{prs}, p, r, s = 1, 2, 3$ which is completely skew-symmetric in all of its indices. We would then have

$$a_{prs} = -a_{psr} = a_{spr} = -a_{srp} = a_{rsp} = -a_{rps}$$

This completely skew-symmetric system has 27 elements, 21 of which are zero. The 6 nonzero elements are all related to one another through the above equations when (p,r,s) = (1,2,3). This is expressed as saying that the above system has only one independent component.

2.1.2. Summation Convention. The summation convention states that whenever there arises an expression where there is an index which occurs twice on the same side of any equation, or term within an equation, it is understood to represent a summation on these repeated indices. The summation being over the integer values specified by the range. A repeated index is called a summation index, while an unrepeated index is called a free index. The summation convention requires that one must never allow a summation index to appear more than twice in any expression. Because of this rule it is sometimes necessary to replace one dummy summation symbol by some other dummy symbol in order to avoid having three or more indices occuring on the same side of the equation.

Example 1:

The two equations

$$y_1 = a_{11}x_1 + a_{12}x_2$$

$$y_2 = a_{21}x_1 + a_{22}x_2$$

can be represented as one equation by introducing a dummy index, say k, and expressing the above equations as

$$y_k = a_{k1}x_1 + a_{k2}x_2, \qquad \text{k=1,2}$$

The range convention states that k is free to have any one of the values 1 or 2, (k is a free index). This equation can now be written in the form

$$y_k = \sum_{i=1}^{2} a_{ki}x_i = a_{k1}x_1 + a_{k2}x_2$$

where i is the dummy summation index. When the summation sign is removed and the summation convention is adopted we have

$$y_k = a_{ki}x_i \;\; i,k = 1,2$$

Since the subscript i repeats itself, the summation convention requires that a summation be performed by letting the subscript take on the values specified by the range and then summing the results. The index k which appears only once on the left and only once on the right hand side of the equation is called free index. It should be noted that both k and i are dummy subscripts and can be replaced by other letters.

Example 2:

The two product of two vectors A_q, q = 1,2,3 and B_j, j = 1,2,3 can be represented with the index notation by the product $A_iB_i = AB\cos\theta \quad i = 1,2,3, \quad A = |\overrightarrow{A}|, \quad B = |\overrightarrow{B}|$. Since the subscript i is repeated it is understood to represent a summation index. Summing on i over the range specified, there results

$$A_1B_1 + A_2B_2 + A_3B_3 = AB\cos\theta$$

2.1.3. Addition, Multiplication and Contraction.

Addition:

The algebraic operation of addition or substraction applies to systems of the same type and order . That is we can add or subtract like components in systems. For example, the sum of A_{jk} and B_{jk} is again a system of the same type and is denoted by $C_{jk} = A_{jk} + B_{jk}$.

Outer Product:

The outer product of two systems is obtained by multiplying each component of the first system with each component of the second system. The order of the resulting product is the sum of the orders of the two systems involved in forming the product. For example, if A_{ij} is a second order system and B_{mnl} is a third order system, with all indices having the range 1 to N, then the product is fifth order and is denoted by $C_{ijmnl} = A_{ij}B_{mnl}$. The product system represents N^5 terms constructed from all possible products of the components from A_{ij} with the components from B_{mnl}. For any two tensors A and B, we denote the outer product as $C = A \otimes B$ or $C = AB$.

Contraction:

The operation of contraction occurs when two indices are set equal and the summation convention is invoked. For example, if we have a fifth order system C_{ijmnl} and we set $i = j$ and sum, then we form the system

$$C_{mnl} = C_{jjmnl} = C_{11mnl} + C_{22mnl} + ... + C_{NNmnl}$$

Here the symbol C_{mnl} is used to represent the third order system that results when the contraction is performed. The resulting system is always of order 2 less than the original system.

2.1.4. e-permutation and Kronecker delta. Two symbols that are used quite frequently with the indicial notation are the e-permutation symbol and the Kronecker

delta. The e-permutation symbol, sometimes referred to as the alternating tensor, deals with permutations of indices.

The e-permutation symbol is defined as:

$$e_{ijk\ldots l} = \begin{pmatrix} 1 & \text{if i,j,k...l is an even permutation of 123...n} \\ -1 & \text{if i,j,k...l is an odd permutation of 123...n} \end{pmatrix} \tag{11}$$

The Kronecker delta is defined:

$$\delta_{ij} = \begin{pmatrix} 1 & \text{if i} = \text{j} \\ 0 & \text{if i} \neq \text{j} \end{pmatrix} \tag{12}$$

Some of the useful properties of the two symbols are:

Property 1:

When an index of the Kronecker delta δ_{ij} is involved in the summation convention, the effect is that of replacing one index with a different index. For example, let a_{ij} denote the elements of an $N \times N$ matrix. Then the product

$$a_{ij}\delta_{ij} = a_{kj} \qquad \text{i,j} = 1,2,\ldots\text{N}$$

Property 2:

Using the summation convention, $\delta_{ii} = N$ i = 1,...,N

Property 3:

The determinant of a matrix A = (a_{ij}) can be represented in the indicial notation. Employing the e-permutation symbol the determinant of an $N \times N$ matrix is expressed as

$$|A| = e_{ij\ldots k}a_{1i}a_{2j}\ldots a_{Nk}$$

where $e_{ij\ldots k}$ is an Nth order system.

Property 4:

Given the vectors A_p, p = 1,2,3 and B_p, p=1,2,3 the cross product of these two vectors is a vector C_p, p = 1,2,3 with components

$$C_i = e_{ijk} A_j B_k, \qquad \text{i,j,k} = 1,2,3$$

The cross product of the unit vectors $(\hat{e}_1, \hat{e}_2, \hat{e}_3)$ can be represented in the index notation by

$$\hat{e}_i \times \hat{e}_j = \begin{pmatrix} \hat{e}_k & \text{if (i,j,k) is an even permutation of (1,2,3)} \\ -\hat{e}_k & \text{if (i,j,k) is an odd permutation of (1,2,3)} \\ 0 & \text{in all other cases} \end{pmatrix} \tag{13}$$

The result can be written in the form $\hat{e}_i \times \hat{e}_j = e_{ijk}\hat{e}_k$

Property 5: The $e - \delta$ identity

This identity, relating the e-permutation symbol and the Kronecker delta, can be expressed in different forms. The indicial form for this identity is

$$e_{ijk}e_{imn} = \delta_{jm}\delta_{kn} - \delta_{jn}\delta_{km}, \qquad \text{i,j,k,m,n} = 1,2,3$$

where i is the summation index and j,k,m,n are free indices.

In the next two sections there is a shift of focus towards the basic principles of quantum mechanics, necessary for understanding Liquid Crystal Theory.

2.2. Rotations in space

Rotations in 3 dimensional space are represented by unitary transformation. The unitary operator that rotates a state $|\psi>$ into $|\psi'>= U_R|\psi>$ has the form:

$$U_R = \exp\left(-\frac{\iota}{\hbar}\hat{n} \cdot \mathbf{L}\phi\right) \tag{14}$$

where **L**; the angular momentum operator and the generator of the 3-dimensional rotations; satisfy the commutation relations:

$$[L_i, L_j] = \iota\hbar\varepsilon_{ijk}L_k \tag{15}$$

In terms of it's components, the step-up and step-down operator for angular momentum $\mathbf{L} = (L_m, L_n, L_k)$ is:

$$L_\pm = L_n \pm iL_k \tag{16}$$

Some other properties of **L** are:

$$\begin{aligned} &L_k|jz>= z\hbar|jz>, \\ &L_\pm|jz>= \sqrt{j(j+1)-z(z\pm1)}\hbar|jz\pm1>, \\ &\mathbf{L}^2|jz>= j(j+1)\hbar|jz> \end{aligned} \tag{17}$$

where $\mathbf{L}^2 = L_m^2 + L_n^2 + L_k^2$. The system is rotationally invariant if $[\mathbf{L}, H] = 0$ where H is the hamiltonian of the system.

2.2.1. Three dimensional rotational group: Wigner matrices (D^l_{mn})

. Wigner rotation matrices or generalized spherical harmonics $D^J_{mn}(\alpha, \beta, \gamma)$ represent matrix elements of the operator performing a coordinate system rotation of Euler angles (α, β, γ) in an angular momentum basis. Following Rose's [86] convention:

$$D^l_{mn}(R) =< lm|U_R|ln >=< lm|\exp((-\frac{\iota}{\hbar}\hat{n}\cdot\mathbf{L}\phi))|ln > \tag{18}$$

where

$$U_R = exp(-\frac{\iota}{\hbar}\gamma\hat{z}\cdot\mathbf{L})exp(-\frac{\iota}{\hbar}\beta\hat{y}\cdot\mathbf{L})exp(-\frac{\iota}{\hbar}\alpha\hat{z}\cdot\mathbf{L}) \tag{19}$$

The explicit form of these matrices is:

$$
\begin{aligned}
D^l_{mn}(\alpha,\beta,\gamma) =& < lm|e^{-(\iota/\hbar)\alpha L_k}e^{-(\iota/\hbar)\beta L_n}e^{-(\iota/\hbar)\gamma L_k}|ln > \\
&= e^{-\iota\alpha m}e^{-\iota\gamma n} < lm|e^{-(\iota/\hbar)\beta L_n}|ln > \\
&= e^{-i(m\alpha+n\psi)}\sqrt{(l+m)!(l-m)!(l+n)!(l-n)!} \\
&\sum_s \frac{(-1)^s(\cos\beta/2)^{2l+n-m-2s}(-\sin\beta/2)^{m-n+2s}}{(l-m-s)!(l+n-s)!(s+m-n)!s!}
\end{aligned} \tag{20}
$$

where $0 \leq \alpha \leq 2\pi, 0 \leq \beta \leq \pi, 0 \leq \gamma \leq 2\pi$. The Wigner rotation matrices form an orthogonal basis set in the Euler angle space.

The **coupling rule** for these matrices can be written as

$$
\mathcal{D}^{j_1}_{\mu_1,m_1}\mathcal{D}^{j_2}_{\mu_2,m_2} = \sum_{j=|j_1-j_2|}^{j_1+j_2} C(j_1,j_2,j,\mu_1,\mu_2)C(j_1,j_2,j,m_1,m_2)\mathcal{D}^{j}_{\mu_1+\mu_2,m_1+m_2} \tag{21}
$$

We can decompose a Wigner rotation matrix as a linear combination of products of Wigner functions of lower rank,

$$
\begin{aligned}
\mathcal{D}^J_{mn} &= \sum C(J_1,J_2,J;m_1,m_2,m)C(J_1,J_2,J;n_1,n_2,n)\mathcal{D}^{J_1}_{m_1n_1}\mathcal{D}^{J_2}_{m_2n_2} \\
&\qquad\qquad \delta_{m_1+m_2,m}\delta_{n_1+n_2,n} \\
&= \sum C(J_1,J_2,J;m_1,m-m_1,m)C(J_1,J_2,J;n_1,n-n_1,n)\mathcal{D}^{J_1}_{m_1n_1}\mathcal{D}^{J_2}_{m-m_1n-n_1}
\end{aligned} \tag{22}
$$

where the sum is extended to all indices not appearing on the left hand side.
$C(a,b,c;d,e,f)$ are the Clebsch Gordon coefficients which are introduced next.

2.3. Clebsch-Gordon coefficients

Clebsch-Gordon (CG) coefficients play an essential role in a variety of problems involving addition of angular momenta and general tensor manipulation [86]. Apart

from more conventional applications in quantum mechanics Clebsch-Gordon coefficients are now employed in material science, statistical mechanics of condensed phases and in particular of anisotropic fluids such as liquid crystals [87].

2.3.1. Notations. There is an impressive number of different conventions for writing CG coefficients, even though many of them only differ in the symbols employed. We choose define the CG coefficients according to the phase convention of Rose [86], i.e. we write the coupling coefficient between the two states of angular momentum J_1 and J_2 to yield a state $|J_3 m_3>$ as

$$|J_3 m_3 >= \sum_{m_1 m_2} C(J_1, J_2, J_3; m_1, m_2, m_3)|J_1 m_1 > |J_2 m_2 > \tag{23}$$

where C(a,b,c;d,e,f) is a Clebsch-Gordon or vector coupling coefficient and J_1, J_2, J_3 can take non-negative integer or semi-integer values.

The angular momentum values J_1, J_2, J_3 are said to form a triangle $\triangle(J_1, J_2, J_3)$ in the sense that the following relations hold for the allowed values:

$$\triangle(J_1, J_2, J_3) = \begin{cases} J_1 + J_2 - J_3 \geq 0 \\ J_1 - J_2 + J_3 \geq 0 \\ -J_1 + J_2 + J_3 \geq 0 \end{cases} \tag{24}$$

where $(J_1 + J_2 + J_3)$ is an integer. The triangular relation is symmetric in the three angular momenta. CG coefficients formed with combinations of angular momenta not satisfying this rule are equal to zero. The angular momentum projection values m_1, m_2, m_3 can take the values

$$m_1 = -J_1, -J_1{+}1, .., J_1; \quad m_2 = -J_2, -J_2{+}1, .., J_2; \quad m_1 = -J_3, -J_3{+}1, .., J_3 \tag{25}$$

Explicit relations for the CG coefficients have been derived by Wigner [86]

$$C(j_1, j_2, j_3, m_1, m_2, m_3) = \delta_{m_3, m_1+m_2} \times \{(2J_3+1)$$

$$\frac{(J_3+J_1-J_2)!(J_3-J_1+J_2)!(J_1+J_2-J_3)!(J_3+m_3)!(J_3-m_3)!}{(J_1+m_1)!(J_1-m_1)!(J_2+m_2)!(J_2-m_2)!(J_1+J_2+J_3+1)!}\}^{1/2}\times \tag{26}$$

$$\sum_s \frac{(-1)^{s+J_2+m_2}(J_2+J_3+m_1-s)!(J_1-m_1+s)!}{s!(J_3-J_1+J_2-s)!(J_3+m_3-s)!(J_1-J_2-m_3+s)!}$$

and by Racah [89]

$$C(j_1, j_2, j_3, m_1, m_2, m_3) = \delta_{m_3, m_1+m_2}$$
$$\{(J_1+m_1)!(J_1-m_1)!(J_2+m_2)!(J_2-m_2)!(J_3+m_3)!(J_3-m_3)!\}^{1/2}\times$$
$$\{\frac{(2J_3+1)!(J_1+J_2-J_3)!(J_1+J_3-J_2)!(J_3+J_2-J_1)!}{(J_1+J_2+J_3+1)!}\}^{1/2}\times \tag{27}$$

$$\sum_s \frac{(-1)^s}{s!r_1!r_2!r_3!r_4!r_5!}$$

where $r_1 = (J_2+m_2-s); r_2 = (J_1-m_1-s); r_3 = (J_1+J_2-J_3-s); r_4 = (J_3-J_2+m_1+s); r_5 = (J_3-J_2-m_2+s)$ In Eq.(26) and eq.(27) the index s takes all the integral values leaving the argument of the various factorials non-negative. The CG coefficients are related to the often used and more symmetric $3j$ symbols introduced by Wigner [90]

$$C(j_1, j_2, j_3, m_1, m_2, m_3) = (-1)^{-J_1+J_2-m_3}(2J_3+1)^{\frac{1}{2}}\begin{pmatrix} J_1 & J_2 & J_3 \\ m_1 & m_2 & -m_3 \end{pmatrix} \tag{28}$$

2.3.2. Some useful relations.

2.3.2.1. *Symmetries.* There are various symmetry relations that can be derived e.g. from the general explicit expression for the CG coefficients given by Racah [89]. We have in particular:

$$\begin{aligned} C(J_1,J_2,J_3,m_1,m_2,m_3) &= (-1)^{J_1+J_2-J_3}C(J_1,J_2,J_3,-m_1,-m_2,-m_3) \\ &= (-1)^{J_1+J_2-J_3}C(J_2,J_1,J_3,m_2,m_1,m_3) \\ &= (-1)^{J_1-m_1}(\tfrac{2J_3+1}{2J_2+1})^{\frac{1}{2}}C(J_1,J_3,J_2,m_1,-m_3,-m_2) \end{aligned} \tag{29}$$

From these relations some other useful equations can in turn be derived

$$\begin{aligned} C(J_1,J_2,J_3,m_1,m_2,m_3) &= (-1)^{J_2+m_2}(\tfrac{2J_3+1}{2J_1+1})^{\frac{1}{2}}C(J_3,J_2,J_1,-m_3,m_2,-m_1) \\ &= (-1)^{J_1-m_1}(\tfrac{2J_3+1}{2J_2+1})^{\frac{1}{2}}C(J_3,J_1,J_2,m_3,-m_1,m_2) \\ &= (-1)^{J_2+m_2}(\tfrac{2J_3+1}{2J_1+1})^{\frac{1}{2}}C(J_2,J_3,J_1,-m_2,m_3,m_1) \end{aligned} \tag{30}$$

2.3.2.2. *Orthogonality.* The CG coefficients are elements of a unitary transformation and they satisfy orthogonality relations. These can be written as

$$\sum_{m_1,m_2} C(J_1,J_2,J,m_1,m_2,m)C(J_1,J_2,J',m_1,m_2,m') = \delta_{JJ'}\delta_{mm'} \tag{31}$$

or

$$\sum_{m_1} C(J_1,J_2,J,m_1,m-m_1,m)C(J_1,J_2,J',m_1,m-m_1,m) = \delta_{JJ'} \tag{32}$$

We also have

$$\sum_{J,m} C(J_1,J_2,J,m_1,m_2,m)C(J_1,J_2,J,m_1',m_2',m) = \delta_{m_1m_1'}\delta_{m_2m_2'} \tag{33}$$

or

$$\sum_{J} C(J_1,J_2,J,m_1,m-m_1,m)C(J_1,J_2,J,m_1',m'-m_1',m') = \delta_{m_1m_1'}\delta_{mm'} \tag{34}$$

2.3.2.3. *Sum rules.* Some of the useful formulas are [91]:

$$\sum_m C(J_1, J_2, J_1, -m, 0, -m) C(J_1', J_2, J_1', m-M, 0, m-M) = \frac{(-1)^{2M+J_2-2J_1-2J_1'}}{2J_2+1} \Big[\frac{(2J_1+1)(2J_1'+1)(2J_1-J_2)!(2J_1'+J_2+1)}{(2J_1'-J_2)!(2J_1+J_2+1)!} \Big]^{1/2}$$

$$\sum_{m_1,m_2,m} C(J_1, J_2, J, m_1, m_2, m)^2 = (2J+1)$$

$$\sum_m (-1)^m C(J, J, L, m, -m, 0) = (-1)^J (2J+1)^{1/2} \delta_{0L}$$

$$\sum_{J_1} \{C(J_1, J_2, J_3, 0, 0, 0)\}^2 =$$
$$(2J_3+1)\{(J_1+J_2-J_3-1)!!r!!\}/\{(J_1+J_2-J_3)!!(r+1)!!\}$$

$$\sum_{J_1=|J_3-J_2|, J_1 \neq k}^{J_2+J_3} (2J_1+1)\{C(J_1, J_2, J_3, 0, 0, 0)\}^2/\{J_1(J_1+1) - k(k+1)\} = 0 \tag{35}$$

where $r = J_1 + J_2 + J_3$. $J_3 - J_2 \leq k \leq J_3 + J_2$ and $k + J_3 + J_2$ odd, and the following two obtained by Morgon [92].

$$\sum_{J_2=0}^{J_1} \frac{\{(-1)^{J_1-J_2} C(J_1, J_2, J_1-J_2; 0, 0, 0)\}^2}{(2J_1 - 2J_2 + 1)} = \{(2J_1)!!/(2J_1+1)!!\}$$

$$\sum_{J_2=0}^{J_1} \{(-1)^{J_1-J_2} C(J_1, J_2, J_1-J_2; 0, 0, 0)\}^2/\{(2J_1-2J_2+1)(2J_2-1)^2\}$$
$$= 1 \qquad \text{if } J_1 = 0$$
$$= \{(2J_1)!!/(2J_1-2)!!\}/\{(2J_1+1)!!/(2J_1-1)!!\} \quad \text{if } J_1 \, \epsilon \, I^+ \tag{36}$$

2.3.2.4. *Recurrence relations.* We have two recurrence relations [86]. The first recurrence relation allows changing the angular momentum J

$$\{m_1 - m\frac{J_1(J_1+1) - J_2(J_2+1) + J(J+1)}{2J(J+1)}\}C(J_1, J_2, J; m_1, m-m_1, m) =$$
$$= \{\frac{(J^2-m^2)(J-J_1+J_2)(J+J_1-J_2)(J_1+J_2+J+1)(J_1+J_2-J+1)}{4J^2(2J-1)(2J+1)}\}^{1/2}$$
$$C(J_1, J_2, J-1; m_1, m-m_1, m)$$
$$+\{\frac{(r_1^2-m^2)(r_1-r_3)(r_1+r_3)(r_1+r_2+1)(r_2-J)}{4(J+1)^2(2J+1)(2J+3)}\}^{1/2}$$
$$C(J_1, J_2, J+1; m_1, m-m_1, m) \quad (37)$$

where $r_1 = J+1; r_2 = J_1+J_2; r_3 = J_1-J_2$. The second relation relates CG coefficients with the same angular momentum J_1, J_2, J but different components:

$$\{J(J+1) - J_1(J_1+1) - J_2(J_2+1) - 2m(M-m)\}C(J_1, J_2, J; m, M-m, M) =$$
$$= \{(J_1-m+1)(J_1+m)(J_2+M-m+1)(J_2-M+m)\}^{1/2}$$
$$C(J_1, J_2, J; m-1, M-m+1, M)$$
$$+\{(J_1+m+1)(J_1-m)(J_2-M+m+1)(J_2+M-m)\}^{1/2}$$
$$C(J_1, J_2, J; m+1, M-m-1, M) \quad (38)$$

2.3.2.5. *Some special formulas.* Formulas giving certain classes of vector coupling coefficients in algebraic form can be obtained specializing the general Eq.(26) and (27). Explicit formulas for coefficients with one of the angular momentum rank J=1,2 can be found in the celebrated book by Condon and Shortley [93]. For semi-integer ranks, formulas for J=1/2 are reported by Rose [86], while formulas for J=3/2, 5/2 are given by Saito and Morita [94]. Here we present a small collection of results which are particularly useful:

$$C(J,J',0,m,-m,0) = (-1)^{J-m}\delta_{J,J'}/(2J+1)^{1/2} \tag{39}$$

$$C(J_1,0,J_2,m_1,m_2,m_1+m_2) = \delta_{J_1,J_2}\delta_{m_2,0} \tag{40}$$

$$C(1,1,0;m,-m,0) = (-1)^{1-m}/3^{1/2} \tag{41}$$

$$C(1,1,1;m,-m,0) = m/2^{1/2} \tag{42}$$

$$C(1,1,2;m,-m,0) = (1/2)^{|m|}(2/3)^{1/2} \tag{43}$$

$$C(J,1,J;0,m,m) = -C(1,J,J;m,0,m) = -m/2^{1/2}; \quad J>0 \tag{44}$$

$$C(J,1,J+1;0,m,m) = C(1,J,J+1;m,0,m) = \sqrt{(J+2)/2(2J+1)}; \quad m\neq 0 \tag{45}$$

$$C(J,1,J-1;0,m,m) = C(1,J,J-1;m,0,m) = \sqrt{(J-1)/2(2J+1)}; \quad J>0, m\neq 0 \tag{46}$$

$$C(2,2,0;m,-m,0) = (-1)^m/\sqrt{5} \tag{47}$$

$$C(2,2,2;m,-m,0) = (-1)^m C(2,2,2;0,m,m) = (-1)^m(m^2-2)/\sqrt{14} \tag{48}$$

$$C(2,2,4;m,-m,0) = 24/\{\sqrt{70}(2+m)!(2-m)!\} \tag{49}$$

$$C(2,2,J;0,0,0) = (-12)^{J/2}\sqrt{(2J+1)(4-J)!/(5+J)!} \quad \text{if J = 0,2,4 and zero otherwise} \tag{50}$$

$$\begin{aligned} C(4,4,2;m,-m,0) &= (-1)^m\sqrt{5/9}C(4,2,4;m,0,m) \\ &= (-1)^m(3m^2-20)/(2\sqrt{693}) \end{aligned} \tag{51}$$

$$C(J_1,3,J;m,0,m)=$$
$$\{\frac{5(r_1+m+2)(r_1+m+1)(r_1-m+2)(r_1-m+1)(r_1-m)(r_1+m)}{(r_1+1)(r_1+2)(2r_1)(2r_1+1)(2r_1+3)(2r_1-1)}\}^{1/2}; \quad (52)$$
$$\text{if } J=J_1+3$$

$r_1=J_1+1$

$$C(J_1,3,J;m_1,3,m)=$$
$$\{\frac{(r_1+m_1+5)(r_1+m_1+4)(r_1+m_1+3)(r_1+m_1+2)(r_1+m_1+1)(r_1+m_1)}{(2r_1-1)(2r_1)(2r_1+1)(2r_1+2)(2r_1+3)(2r_1+4)}\}^{1/2};$$
$$\text{if } J=J_1+3 \quad (53)$$

$r_1=J_1+1$

$$C(J_1,J_2,(J_1+J_2);m_1,m_2,m_1+m_2)= \quad (54)$$
$$\{\frac{(2J_1)!(2J_2)!(J_1+J_2+m_1+m_2)!(J_1+J_2-m_1-m_2)!}{(2J_1+2J_2)!(J_1+m_1)!(J_1-m_1)!(J_2+m_2)!(J_2-m_2)!}\}^{1/2}$$

$$C(J_1,J_2,J_3;0,0,0)= \quad (55)$$
$$\begin{cases} 0 & \text{if } J_1+J_2+J_3 \text{ is odd} \\ (-1)^{(J_1+J_2+J_3)/2}\{\frac{2J_3+1}{J_1+J_2+J_3+1}\}^{1/2}\frac{\Gamma(J_1+J_2+J_3)}{\Gamma(J_1+J_2-J_3)\Gamma(J_1-J_2+J_3)\Gamma(-J_1+J_2+J_3)} \end{cases}$$

where $\Gamma(x)=(\frac{x}{2})!/(x!)^{1/2}$, if $J_1+J_2+J_3$ is an even integer.

2.3.2.6. *Asymptotic results.* A classical result due Brussaard and Toloehk:

$$C(J_1,J_2,J;m_1,m_2,m)\cong(-1)^{J_1+J_2-J}d^{J_1}_{m_1,J-J_2}(\vartheta) \quad (56)$$

where the small Wigner matrix d^J_{mn} is defined in [86] and $\cos\vartheta=m/J$; $J\gg 1$,

$J_1\ll J$

2.3.2.7. *Wigner-Eckart theorem.* The calculation of the matrix elements

$< J_1 m_1 | T^{J,m} | J_2 m_2 >$ of an irreducible tensor operator $T^{J,m}$ over an angular momentum basis set is simplified by the Wigner-Eckart theorem [86] according to which

$$< J_1 m_1 | T^{J,m} | J_2 m_2 >= K_{J_1,J_2} C(J_2, J, J_1; m_2, m, m_1) \tag{57}$$

where the quantity K_{J_1,J_2}, often written as $(J_1 \parallel T^J \parallel J_2)$, is called a reduced matrix element of the set of operator T^J and is independent on the angular momentum projection numbers.

2.3.2.8. *Gaunt formula.* This gives the integral of the three Wigner rotation matrices as

$$\int_0^{2\pi} d\alpha \int_0^{\pi} d\beta \int_0^{2\pi} d\gamma \mathcal{D}^{J_1}_{m_1 n_1}(\alpha\beta\gamma) \mathcal{D}^{J_2}_{m_2 n_2}(\alpha\beta\gamma) \mathcal{D}^{J_3}_{m_3 n_3}(\alpha\beta\gamma)^* = 8\pi^2 \delta_{m_1+m_2,m_3} \delta_{n_1+n_2,n_3} C(J_1, J_2, J_3; m_1, m_2, m_3) C(J_1, J_2, J_3; n_1, n_2, n_3)/(2J_3+1) \tag{58}$$

2.4. Measuring order and biaxiality

When one considers systems with orientational order, such as liquid crystals, there are various aspects of the ordering that one wishes to quantify. Two such properties are the overall director of the system and the extent to which it exhibits biaxiality. This section provides an introduction to some of the order parameters of interest in the study of liquid crystals.

In the following sections we will consider the problem of identifying an overall system director for a system of molecules, and quantifying the extent to which the system might be regarded as ordered. The simplest situation in which we can consider this is when the system comprises of molecules with one axis of rotational symmetry; if the molecules are not aligned with equal probability in every direction, the system is said

to exhibit nematic order, and we can use the axis of rotation, or the molecule director, to determine a preferred direction for the system, or the system director. It may also be that a system of such molecules picks out another preferred direction - if it does so, we say that the system is biaxial. We also consider this possibility. Next we consider the situation where each molecule can be associated with an orthonormal basis of unit vectors, i.e. the case where they do not have rotational symmetry about any axis; in this case the axes may be (for example) the eigenvectors of the molecule's inertia tensor. We can see once more how to identify a preferred direction for the system, and so a nematic order associated with one of its axes; and now we can investigate whether there is any other preferred direction associated with the remaining axes, i.e. whether the system is biaxial in this sense. Finally, we will briefly discuss the two notions of biaxiality that have been presented.

If a molecule has rotational symmetry, we associate with it a unit vector $\mathbf{m}$, which points along the axis of symmetry of the molecule. If it does not have rotational symmetry, then we associate with it an orthonormal set of vectors, $\mathbf{n}, \mathbf{k}, \mathbf{m}$, which may refer to the semi-axes of an ellipsoid which models the shape of the molecule, or its principle axis of inertia, but not in general. Whenever we consider the components of a vector, it will be with respect to some fixed laboratory set of axes, which we will denote E_x, E_y and E_z. Now, these vectors are attached to each molecule comprising the system under consideration; so if we label the molecules by i, where $i = 1...N$, then we have vectors $m^{(i)}$ or $n^{(i)}$, $k^{(i)}$, $m^{(i)}$ depending on the degree of symmetry of the molecules.

There are two ways of thinking about order parameters. One approach is to consider explicitly the orientational distribution function (PDF), and extract the order parameters from this PDF by using a spherical harmonic decomposition. This is analogous to expressing a function in terms of Fourier series and considering the Fourier coefficients as relative contributions of the various harmonics.

Another approach considers how to extract these same order parameters from tensors, or dyadics, constructed from the vectors $n^{(i)}$, $k^{(i)}$ and $m^{(i)}$. We define the dyadic Q^{zz} in two stages: first, we define P^{zz}, constructed from the vectors $m^{(i)}$:

$$P^{zz} = \frac{1}{N}(\sum_{i=1}^{N} m^{(i)}m^{(i)}) =< mm > \tag{59}$$

The angle brackets indicates the ensemble average. Finally, we define the Saupe order tensor [95] by

$$Q^{zz} = (3P^{zz} - I)/2 \tag{60}$$

The definitions of P^{xx}, P^{yy}, Q^{xx} and Q^{yy} are obtained by replacing $m^{(i)}$ by $n^{(i)}$ or $k^{(i)}$ appropriately.

Also, note the following two observations. First, the P and Q dyadics have the same eigenvectors, but that if v is an eigen vector of P with eigenvalue γ, then it is an eigenvector of Q with eigenvalue $(3\gamma - 2)/2$. Second, the Q dyadics are constructed to have trace zero, so that the sum of the eigenvalues of a Q dyadic is automatically 0. Because of this relationship between the P and Q dyadics, everything could be done entirely with reference to the Q dyadics, an approach used in [56]. The difference between that approach and the one followed here is that a different strategy is adopted for identifying the dominant eigenvalue.

2.4.1. Nematic order for Uniaxial Molecules. First we consider the case where the molecules have rotational symmetry about some axis, labeled as **m**. We also assume that the molecule has the symmetry of an ellipsoid of revolution, so that there is no way to distinguish **m** from $-\mathbf{m}$.

The question of how well the directors of a rotationally symmetric molecule, can be addressed in terms of a distribution function describing the proportion of molecules whose directors are in a neighborhood of a given angle away from some reference axis.

More precisely, fix a reference direction E_z and let $f(\theta)$ be such that $f(\theta)d\theta$ is the fraction of molecules in a sample whose directors make an angle between θ and $\theta + d\theta$ with the reference direction.

$f(\theta)$ can be expanded in various ways. One particularly useful expansion uses the Legendre polynomials [55];

$$f(\theta) = \sum_{l=0}^{\infty} p_l P_l(\cos(\theta)) \tag{61}$$

where the functions $P_l(\cos(\theta))$ satisfy the orthogonality relations

$$\int_0^{\pi} \sin(\theta) P_l(\cos(\theta)) P_m(\cos(\theta)) d\theta = \frac{2\delta_{lm}}{2l+1} \tag{62}$$

and also have the property that for even l, P_l is an even function while for odd l, P_l is odd. In our case, where there is no distinction between $\mathbf{m}$ and $-\mathbf{m}$, this implies that only the even Legendre polynomials contribute to P.

Using the orthogonality relationship, we have

$$p_l = \frac{2l+1}{2} < P_l > \tag{63}$$

where

$$< P_l >= \int_0^{\pi} \sin(\theta) P_l(\cos(\theta)) f(\theta) d\theta \tag{64}$$

and for a particular sample this can be computed by averaging the value of $P_l(\cos(\theta))$ over all the molecules in the sample. We thus obtain

$$f(\theta) = \frac{1}{2} + \frac{5}{2} < P_2 > P_2(\cos(\theta)) + ... \tag{65}$$

and $< P_2 >$ is the first order measure of how well the molecule directors are ordered in the direction E_z.

When E_z is the direction which maximizes this quantity, we regard E_z as the system director (describing the average axis along which the molecules may be regarded as aligned) and the order parameter is called S. This approach was first developed by Tsvetkov [54].

In particular, we note that if S is positive, then the directors of the molecules have E_z as the preferred direction; if S is negative, then the directors avoid E_z. An isotropic system, i.e. one with no preferred direction, has $S = 0$.

We can also obtain S in a more direct manner using one of the tensors defined above. For each molecule i specifies a unit vector, $m^{(i)}$, and we have the tensor Q^{zz} defined in the introduction. A natural way to associate special vectors with a matrix, is to consider its eigenvectors. Since Q^{zz} is symmetric, it has three orthogonal eigenvectors and all eigenvalues are real. One obvious candidate for a preferred direction for the system is the eigenvector associated with the dominant eigenvalue (i.e. the eigenvalue of the greatest absolute value).

Consider this by picking one particular direction for E_z, and some unit vector v. Then

$$v^T(3E_zE_z^T - I)/2v = (3\cos^2(\theta) - 1)/2 \tag{66}$$

where θ is the angle between E_z and v, and so

$$v^TQ^{zz}v =< (3\cos^2(\theta) - 1)/2 > \tag{67}$$

In this case we see immediately that if v is an eigenvector of Q^{zz} with associated eigenvalue λ, then $v^TQ^{zz}v = \lambda$. If M is any symmetric matrix, and v is a unit vector, then the largest value of $|v^TMv|$ is the modulus of the dominant eigenvalue of M, and this value is obtained when v is the associated eigenvector [53]. Thus the v which maximizes this quantity is exactly the director defined by Tsvetkov.

So we find that in this picture the eigenvector associated with the dominant eigenvalue of Q^{zz} is the system director, and the eigenvalue itself is the measure of how ordered the system is about that director.

We thus see from two different perspectives how an overall order parameter for the system may be defined, and that it may be easily computed once the Saupe order tensor is obtained.

Once we have our system director, we can ask how the molecule directors are distributed about it. The size and sign of S tell us how clustered the molecule directors are, and whether they are clustered in the direction of the director or orthogonal to it. We can also consider how the system behaves when it is rotated about the director. It may be that the system is symmetric under this operation, in which case it is uniaxial. On the other hand, if rotation about the director is not a symmetry, then there is a preferred direction orthogonal to the director, and the system is said to be biaxial.

To investigate this, we project the directors of the molecules to the plane orthogonal to the system director. If the director to a molecule is equally likely to point in any one of those directions, then the system has no biaxiality; on the other hand, if the director has a preferred direction, then the system does display biaxiality. To give some measure of this, we diagonalize the matrix Q^{zz}; in other words, we find its components in a basis built out of its eigenvectors. This gives a matrix of the form

$$\begin{bmatrix} q_x & 0 & 0 \\ 0 & q_y & 0 \\ 0 & 0 & q_z \end{bmatrix} \tag{68}$$

where $|q_z| \geq |q_y| \geq |q_x|$.

But we know that $q_z = S$, and that $q_x + q_y + q_z = 0$, so we can re-write this as

$$\begin{bmatrix} -S/2-\zeta & 0 & 0 \\ 0 & -S/2+\zeta & 0 \\ 0 & 0 & S \end{bmatrix} \tag{69}$$

So we can see that ζ, which is given by half the difference between the smaller eigenvalues of Q^{zz} measures the extent to which it is possible to distinguish a direction in the plane orthogonal to the director. If $\zeta = 0$, then the system is unchanged by a rotation about the director; if ζ is non-zero, there is a preferred direction orthogonal to the director, and we have a biaxial system.

This can be given a geometric interpretation as follows: we regard the density of molecule directors as determining an ellipsoid in space. Then the major axis of this ellipsoid lies along the system director, and its magnitude determines the order parameter. The difference between the minor axes is a measure of the extent to which the molecule directors are not equally scattered in all directions perpendicular to the system director, and gives the biaxiality parameter.

We can also see the connection between this measure of biaxiality and the distribution function for the molecule directors in the system by using a decomposition of the density function in terms of spherical harmonics. We fix a set of axes, E_x, E_y and E_z and consider the PDF $f(\theta, \phi)$ which describes the probability of a molecule director making an angle θ with E_z direction and its projection to the E_x, E_y plane making an angle of ϕ with the E_x direction.

The PDF $f(\theta, \phi)$ can now be expanded in terms of the usual spherical harmonics, $Y_{ln}(\theta, \phi)$; however, it is usual in this context to use instead the Wigner rotation matrices [86] which are multiples of the spherical harmonics. The rotation matrices which are relevant here are those of the form D^l_{0n}, where D^l_{0n} is a multiple of Y_{ln}, and the first few are given by

$$D^0_{00}(\theta,\phi) = 1$$

$$D^2_{00}(\theta,\phi) = P_2(\cos(\theta)) \tag{70}$$

$$D^2_{0\pm2} = \sqrt{\frac{3}{8}}\sin^2(\theta)exp(\mp 2\phi\iota)$$

In terms of these functions,

$$f(\theta,\phi) = \frac{1}{4\pi}\sum_{l=0}^{\infty}\sum_{n=-l}^{l}(2l+1) < D^{l*}_{0n} > D^l_{0n}(\theta,\phi) \tag{71}$$

where the averaged quantities are known as the orientational order parameters.

Now, the components of the unit vector determined by a molecule director with angular coordinates θ, ϕ in some coordinate system are given by $(\sin(\theta)\cos(\phi), \sin(\theta)\sin(\phi), \cos(\theta))$ and so the Saupe's matrix S^{zz} is obtained by averaging the matrix

$$\begin{bmatrix} \frac{3}{2}\sin^2(\theta)\cos^2(\phi) - \frac{1}{2} & \sin^2(\theta)\cos(\phi)\sin(\phi) & \sin(\theta)\cos(\theta)\cos(\phi) \\ \sin^2(\theta)\cos(\phi)\sin(\phi) & \frac{3}{2}\sin^2(\theta)\sin^2(\phi) - \frac{1}{2} & \sin(\theta)\cos(\theta)\sin(\phi) \\ \sin(\theta)\cos(\theta)\cos(\phi) & \sin(\theta)\cos(\theta)\sin(\phi) & \frac{3}{2}\cos^2(\theta) - \frac{1}{2} \end{bmatrix} \tag{72}$$

over the system.

Thus, if the axes E_x, E_y and E_z are chosen to be eigen directions of S^{zz} (with the z-direction associated with the dominant eigenvalue) then we have

$$S^{zz} = \begin{bmatrix} < \frac{3}{2}\sin^2(\theta)\cos^2(\phi) - \frac{1}{2} > & 0 & 0 \\ 0 & < \frac{3}{2}\sin^2(\theta)\sin^2(\phi) - \frac{1}{2} > & 0 \\ 0 & 0 & < \frac{3}{2}\cos^2(\theta) - \frac{1}{2} > \end{bmatrix} \tag{73}$$

which can be expressed in terms of the orientational order parameters listed above, giving

$$S^{zz} = \begin{bmatrix} \frac{\sqrt{6}}{2} Re < D^2_{02} > -\frac{1}{2} < D^2_{00} > & 0 & 0 \\ 0 & -\frac{\sqrt{6}}{2} Re < D^2_{02} > -\frac{1}{2} < D^2_{00} > & 0 \\ 0 & 0 & < D^2_{00} > \end{bmatrix} \tag{74}$$

From this we see that the biaxiality parameter identified above via the eigenanalysis of S^{zz} is given by $-\sqrt{6}Re < D^2_{02} > /2$, and so can be understood as arising from the spherical harmonic decomposition of the director's PDF in the appropriate coordinate system. This also enables an alternative computation of the order parameters, which can be used as a consistency check: once the appropriate axes have been found by diagonalization of Q^{zz}, the order parameters can be calculated by numerically finding the spherical harmonic decomposition of the distribution function for the molecule director in this coordinate system. Readers are requested to refer Zannoni's work [87] for more details.

2.4.2. Order for systems of Biaxial Molecules. In this section, we consider the case where the molecules have less symmetry, and so a set of three orthonormal axes can be attached to each molecule. Because of the loss of symmetry of the molecule, there is a new way in which biaxial behaviour can occur.

In the ideal case, we imagine a system of molecules where all the $m^{(i)}$ are perfectly aligned. Then the $n^{(i)}$ and $k^{(i)}$ all lie in a common plane, and it may be that these axes themselves determine preferred directions in this plane, which again we can regard as biaxial behaviour. Note that this form of biaxiality is distinct from the previous one, as ζ must be exactly 0 if all the directors are perfectly aligned.

We can now define three tensors, namely Q^{xx}, Q^{yy} and Q^{zz}. Again, we define an overall director for the system; but this time, we do not have a single molecular director to work with. The solution is straightforward. We find the dominant eigenvalue of

each of Q^{xx}, Q^{yy} and Q^{zz}, and the associated eigenvectors, and take as system director that eigenvector associated with the dominant eigenvalue of the greatest absolute value.

This provides us with an overall director for the system, and an order parameter that measures the extent to which the system is ordered in that direction. But now we can consider the possibility raised above, namely that the secondary molecular axes determine a preferred direction. So how do we measure the extent to which a system is biaxial in this sense?

One way is to consider axes perpendicular to the overall system director [52]; we will call the system director the E_z axis, and then E_x and E_y must be chosen to complete this to a right-handed orthonormal system, as usual. There are various possibilities for just which quantities we might consider constructing out of the Q^{xx} and Q^{yy} tensors, together with these new axes. If we have chosen E_x and E_y axes, with associate unit vectors X and Y respectively, then $X^T Q^{xx} X$ measures the extent to which the x-axes of the molecules are aligned with the E_x direction, and so on. We then see a measure of biaxiality is given by

$$B = \frac{1}{2}(X^T Q^{xx} X + Y^T Q^{yy} Y - X^T Q^{yy} X - Y^T Q^{xx} Y) \tag{75}$$

which is the difference between how well the molecules' x-axes and y-axes are aligned with the E_x and E_y direction respectively and how well they are aligned with the E_y and E_x directions respectively. If the molecules' x and y axes are perfectly aligned with the E_x and E_y directions respectively (or with the E_y and E_x directions respectively), this quantity is 1 (or -1), while if they are equally likely to point in any direction normal to E_y, it is 0. Thus a non-zero value for this indicates a degree of biaxiality in the system. As with the case of the uniaxial system, to give a measure of the biaxiality of the system, we want to find the X and Y axes which maximize this quantity; if the

maximum is zero, then the system does not distinguish any particular orientation in the plane orthogonal to Z, while if it is 1, then the x and y axes are perfectly ordered.

The question remains: how do we identify the X and Y axes that provide our biaxiality measure? We cannot just use the eigenvectors of Q^{xx} and Q^{yy}, because there is no guarantee that they will be orthogonal to Z, or to each other. (Though for highly ordered systems they are approximately so.) One approach, used by Allen [52] in the study of a system of ellipsoids, is to use the eigenvalues of Q^{xx} and Q^{yy}, and project the relevant one of these to the plane orthogonal to the system director.

Now, one might initially consider using the dominant eigenvalues of these, but this is not appropriate. For if the dominant eigenvalue of greatest magnitude is negative, then we are picking out a direction avoided by the molecular x or y axis, and in the case of a system with significant nematic order, this will be (approximately) orthogonal to the plane perpendicular to the system director - in other words it will be approximately parallel to the system director. In the extreme case where we have perfect nematic order, this eigenvector will in fact be parallel to the system director, and its projection to the plane orthogonal to the system director will vanish. Instead, we use the largest positive eigenvalue, and its associated eigenvector.

The projection orthogonal to Z of the eigenvector associated with the larger of these two is then taken to define the Y axis, and X is obtained by completing the set of axes to a right-handed orthogonal system. This procedure provides one with the required biaxiality parameter.

Again the parameter can be defined in terms the average value of a combination of the Wigner rotation matrices. To do this, we consider the Euler angles (θ, ϕ, ψ) associated with the rotation taking each molecule from some reference orientation to its orientation in the sample. For each state of the sample there is an associated PDF $f(\theta, \phi, \psi)$ given the probability that the orientation of any molecule in the system is

described by the Euler angles (θ, ϕ, ψ). The process is similar to that outlined in the case of uniaxial molecules, and more details can be found in [87].

2.4.3. The fourth order parameter. Since the order matrices Q^{xx}, Q^{yy} and Q^{zz} are constrained by the following relation

$$Q^{xx} + Q^{yy} + Q^{zz} = I \tag{76}$$

and the sum of eigenvalues of each of these matrices equals 1. We have just 4 independent eigenvalues for the triad (Q^{xx}, Q^{yy}, Q^{zz}). Hence they should naturally serve as the four order parameters. The fourth order parameter is constructed as follows:

$$S' = \frac{1}{2}(Z^T Q^{zz} Z + Y^T Q^{yy} Y - Z^T Q^{yy} Z - Y^T Q^{zz} Y) \tag{77}$$

This order parameter gives the phase biaxiality along with the order parameter ζ (described in section 2.4.1). However S' should only be used if $\zeta = 0$, because if $\zeta = 0$, then S' determines whether the system indeed shows phase biaxiality or not.

Hence we have seen that there are two ways in which biaxiality can arise in a system of molecules , and these two are essentially independent. One measures the residual ordering of the director of the molecules in the plane orthogonal to the system director, while the other measures the extent to which the molecules' other axes are ordered in the plane orthogonal to the system director.

In this section, we have explored just one way of describing orientational ordering in a biaxial system of molecules. However, this does not exhaust the possible ways in which biaxiality can arise in a system composed of molecules with at most uniaxial symmetry. If we interpret biaxial as any system with more than one direction picked out, then a system with significant S where the particles are confined to layers not orthogonal to Z is also biaxial; because the plane in which the molecules lie contains precisely one axis orthogonal to Z. This form of biaxiality (not considered in this

section) is related to the positional ordering of the system and is especially common in Smectic C phase of liquid crystals.

2.5. Phase transition and tricriticality

In this section, we give an example of first-order phase transition (Section 2.5.1) and then an example of a "tricritical" point (Section 2.5.2).

2.5.1. First-order nematic-to-isotropic transition. As discussed in Chapter 1, liquid crystals are composed of long, barlike molecules . In the isotropic fluid phase, the orientations and positions of the molecules are random. In the nematic phase, the positions of the molecules are still random, but their long axes are oriented on the average along a particular direction specified by a unit vector **n** called the director. Thus, the nematic phase is characterized by broken rotational but not translational symmetry. It is, therefore, tempting to associate the order parameter with the unit vector ν^α which points along the long axis of molecule α located at position $\mathbf{x}^\alpha$. However, since the nematic molecules either have a center of inversion or, if they do not, they have equal probability of pointing parallel or anti-parallel to any given direction, both ν^α and -ν^α contribute to the order. Thus any order parameter must be even in ν^α. Since a vector order parameter is insufficient, we can try a second rank tensor. We require the order parameter to be zero in the high-temperature isotropic phase. A symmetric traceless tensor will yield zero when averaged over directions, so we construct the order parameter from the symmetric traceless tensor formed from ν^α. Let

$$Q_{ij} = \frac{V}{N}\sum_\alpha (\nu_i^\alpha \nu_j^\alpha - \frac{1}{3}\delta_{ij})\delta(\mathbf{x} - \mathbf{x}^\alpha), \tag{78}$$

where ν_i^α is the ith component of ν^α. The factor of V/N is introduced in the definition of Q_{ij} to make it unitless as is conventionally done. Let $\underline{\mathrm{Q}}$ be the tensor with components Q_{ij}. Note that Tr $\underline{\mathrm{Q}} = 0$ since ν^α is a unit vector. In the ordered state

$\langle \underline{\mathrm{Q}} \rangle$ is not zero. In a coordinate system with one axis along the direction of molecular alignment, the matrix $\langle \underline{\mathrm{Q}} \rangle$ is diagonal:

$$\langle \underline{\mathrm{Q}} \rangle = \begin{pmatrix} \frac{2}{3}S & 0 & 0 \\ 0 & -\frac{1}{3}S + \eta & 0 \\ 0 & 0 & -\frac{1}{3}S - \eta \end{pmatrix} \tag{79}$$

If η is nonzero, $\underline{\mathrm{Q}}$ is *biaxial*, and there are two, rather than one, preferred directions. Except in exceptional cases, nematic liquid crystals are uniaxial so that $\eta = 0$. In this case,

$$\langle Q_{ij} \rangle = S(n_i n_j - \frac{1}{3}\delta_{ij}), \tag{80}$$

where the unit vector $\mathbf{n}$, called the Frank director, specifies the direction of the principal axis of $\langle Q_{ij} \rangle$. From Eq.(78)

$$S = \frac{1}{2}\langle 3(\nu^\alpha \cdot \mathbf{n})^2 - 1 \rangle = \frac{1}{2}\langle (3\cos^2\theta^{alpha} - 1) \rangle, \tag{81}$$

where θ^α is the angle between the molecular axis and the director $\mathbf{n}$.

We are now in a position to construct a Landau free energy for a nematic liquid crystal. The free energy density f must be invariant under all rotations. $\underline{\mathrm{Q}}$ transforms like a tensor under the rotation group. f must, therefore, only be a function of the scalar combinations Tr $\langle \underline{\mathrm{Q}} \rangle^p, p = 2, 3, \ldots$ that are invariant under rotations. The term with $p = 1$ is just the trace of $\langle \underline{\mathrm{Q}} \rangle$ and is by definition zero. Thus, there is no term linear in $\langle \underline{\mathrm{Q}} \rangle$ in the free energy. To fourth order in $\underline{\mathrm{Q}}$, we therefore have

$$\begin{aligned} f &= \tfrac{1}{2}r(\tfrac{3}{2}Tr\langle \underline{\mathrm{Q}} \rangle^2) - w(\tfrac{9}{2}Tr\langle \underline{\mathrm{Q}} \rangle^3) + u(\tfrac{3}{2}Tr\langle \underline{\mathrm{Q}} \rangle^2)^2, \\ &= \tfrac{1}{2}rS^2 - wS^3 + uS^4. \end{aligned} \tag{82}$$

In general, there should be two fourth-order terms proportional, respectively, to (Tr $\langle \underline{\mathrm{Q}} \rangle^2)^2$ and Tr $\langle \underline{\mathrm{Q}} \rangle^4$. However, for 3×3 symmetric traceless tensors, they are strictly

proportional, and we need only include the $(\mathrm{Tr}\ \langle \underline{Q} \rangle^2)^2$ term. As before, r is positive at high T and negative at low T. We choose

$$r = a(T - T^*) \tag{83}$$

u and w are independent of temperature.

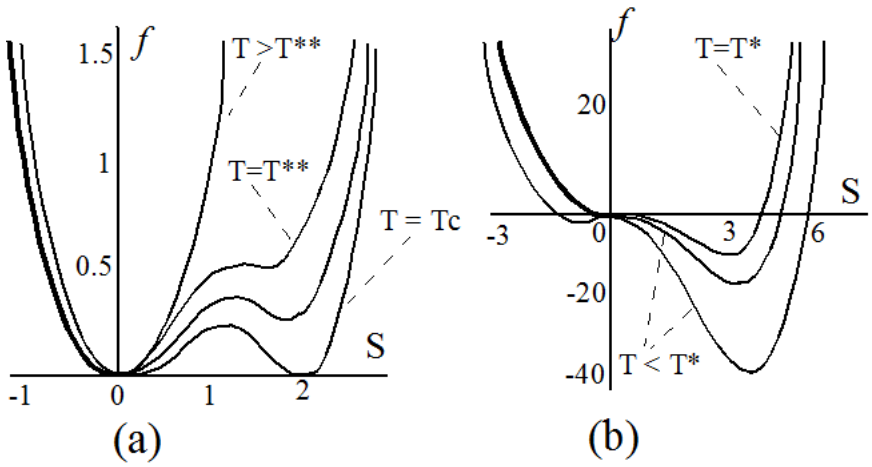

FIGURE 2.1. Free energy density f as a function of order parameter S for different T for the isotropic-nematic transition. The transition is first order. Note the limits of metastability for supercooling (T^*) and superheating(T^{**}).

The free energy of Eq.(82) differs from that of the Ising model by the presence of the third-order term $-wS^3$. If the order parameter for the nematic phase were a vector (as might be imagined if the constituent molecules lacked inversion symmetry) rather than a tensor, then odd order terms would be prohibited in the free energy by rotational symmetry. However, the rodlike molecules have a quadrupolar rather than a dipolar symmetry, and the order parameter is a tensor for which rotational invariance does not rule out the odd terms. Note that the quadrupole symmetry is also reflected in the form of the order parameter in Eqs.(80) and (81). f is sketched as a function of S for various values of T in Figure 2.1. Note that the cubic term leads to an asymmetry in f as a function of S and the emergence of a secondary minimum at finite S. The value of f at this minimum is greater than zero at high temperature but

becomes equal to zero at a critical temperature T_c that is greater than the temperature T^* at which the extremum at the origin develops negative curvature. Since f is less than zero at the secondary minimum for all $T < T_c$, there is a phase transition with a discontinuous change in S at T_c, i.e. there is a first-order transition at T_c. T^* is the *limit of metastability* of the isotropic phase since, for $T^* < T < T_c$, the origin is still a local minimum even though it is not a global minimum. The limit of metastability of the nematic phase occurs at the temperature T^{**} at which the secondary minimum disappears on heating.

The first-order transition temperature T_c and the value S_c of S at T_c are calculated by requiring that f be an extremum with respect to S in equilibrium and that the free energies of the disordered and the ordered phases be equal at the transition. The latter condition implies that the isotropic and the nematic phases can coexist at the transition temperature. If other variables, such as pressure or density, were included in our treatment, the two phases would coexist along a line rather than a single point. The equations determining T_c and S_c are, therefore,

$$\begin{aligned} \tfrac{\partial f}{\partial S} &= (r - 3wS + 4uS^2)S = 0 \\ f &= (\tfrac{1}{2}r - wS + uS^2)S^2 = 0 \end{aligned} \tag{84}$$

Thus,

$$S_c = \frac{w}{2u}, r_c = a(T_c - T^*) = \frac{w^2}{2u} \tag{85}$$

The entropy per unit volume of the disordered phase is zero in mean-field theory, whereas that of the nematic phase is negative. This result can be obtained from the free energy of the nematic phase, which to the lowest order in $r - r_c$ is

$$f = \frac{1}{2}(r - r_c)S_c^2 = \frac{1}{2}(r - r_c)(w/2u)^2 \tag{86}$$

The example of the isotropic-to-nematic transition is representative of phase transitions in which the order parameter possesses a third-order invariant. One expects in general that such transitions will be first order. Though the above Landau theory correctly predicts qualitative properties of first- order transitions, it certainly cannot make detailed quantitative predictions. This is because the order parameter is not zero at the transition. One is not justified, therefore, in truncating the power series expansion of f at fourth order. Even in mean-field theory, higher order terms in this expansion will lead to corrections both to T_c and S_c. If, however, the transition is nearly second order, as would be the case if the predicted value of $T_c - T^*$ is small, the truncated model is a reasonable approximation.

2.5.2. Tricritical points. In the preceding section, we found that third-order invariants lead to first-order transitions. First-order transitions can also occur if symmetry prohibits odd-order terms. Consider the follow Landau free energy:

$$f = \frac{1}{2} r\phi^2 + u_4\phi^4 + u_6\phi^6, \tag{87}$$

where $r = a(T - T*)$. If u_4 is positive, the sixth-order term can be neglected in the vicinity of the predicted second-order transition. If, on the other hand, u_4 is negative, the sixth- order term is required to maintain stability. In this case, secondary minima symmetrically placed about $\phi = 0$ develop as T is lowered, as shown in Fig. Figure 2.2. When the free energies of the secondary minima with $\phi \neq 0$ pass through zero, there is a first-order transition as in the isotropic-to-nematic example.

When $u_4 < 0$, the first-order transition temperature is determined by the conditions $f(r_c, \phi) = 0$ and $\partial f(r_c, \phi)/\partial\phi = 0$ just as for the nematic liquid crystal. This leads to

$$r_c = a(T_c - T^*) = \left\{ \begin{array}{ll} 0 & \text{if } u_4 > 0; \\ & \\ 1 & \text{if } u_4 < 0. \end{array} \right\} \tag{88}$$

The phase diagram described by this equation in the $r - u_4$ plane is shown in Figure 2.2. The line of second-order transitions for $u_4 > 0$ is called a *lambda line*. (first

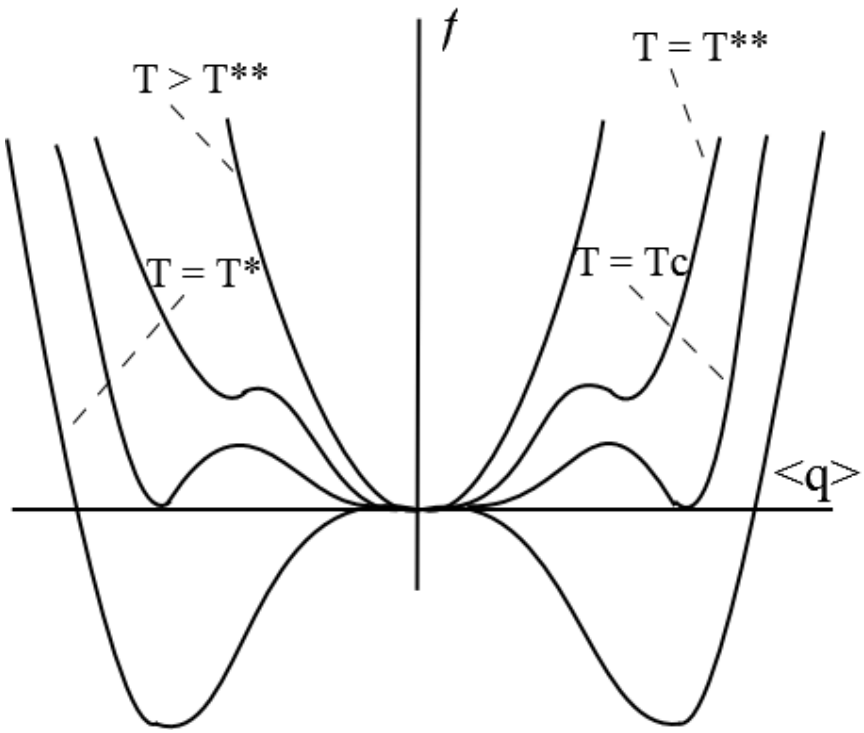

FIGURE 2.2. f for a ϕ^6 potential [Eq.(87)] with u_4 negative. There is a first-order transition at $T = T_c$, T^{**} and T^* are, respectively, the limits of metastability on heating and cooling.

observed at the normal-to-superfluid transition in liquid helium mixtures. The superfluid transition is often referred to as a λ transition.) It meets the line of first-order transitions for $u_4 < 0$ at a *tricritical point,* (r, u_4) = (0,0).

The value of the order parameter and the limit of metastability on heating can be calculated as in the previous section:

$$\begin{aligned} \phi_c &= \pm[|u_4|/(2u_6)]^{1/2}, \\ r^{**} &= a(T^{**} - T^*) = 2|u_4|^2/(3u_6). \end{aligned} \tag{89}$$

Notice that both ϕ_c and q go to zero at the tricritical point where there is no longer a first-order transition. Note also that along the first-order line there is coexistence of three phases: the disordered phase with $\phi = 0$ and two ordered phases with $\phi = \pm|\phi_c|$. When $u_4 = 0$, there is a second-order transition but with an order parameter critical exponent β of 1/4 rather than 1/2:

$$\phi = \pm[-r/6u_6]^{1/4}. \tag{90}$$

Similarly, when an external ordering field h is applied at the tricrical point,

$$\phi = [h/6u_6]^{1/5}, \tag{91}$$

implying that the exponent δ is 5 rather than 3. The other critical exponents, γ and ν, for the tricritical point are the same in mean-field theory for $u_4 = 0$ and $u_4 > 0$.

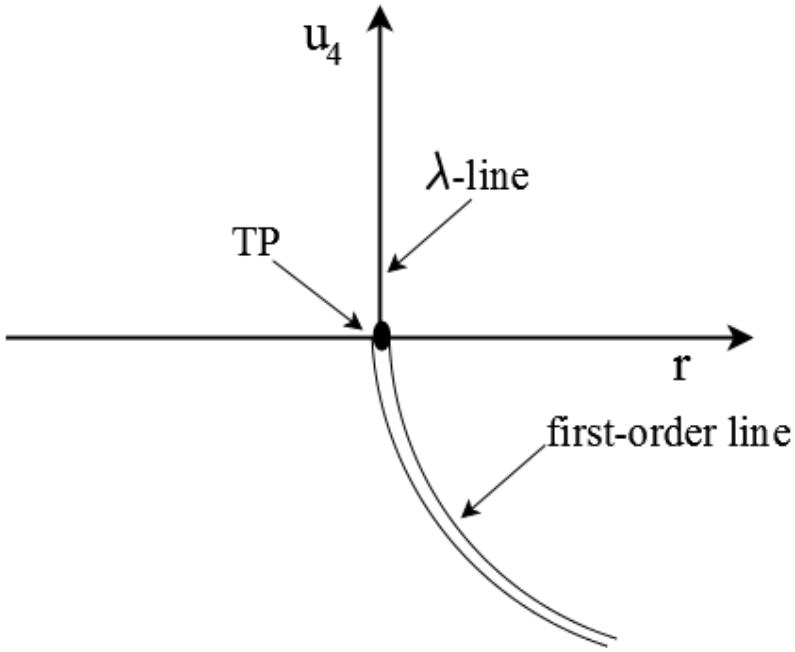

FIGURE 2.3. Phase diagram for the free energy of Eq.(87). The line $r = 0$, $u_4 > 0$ is a second-order lambda line, shown as a single line in the figure. The line $r = \frac{1}{2}|u_4|^2/u_6$ is a line of first-order transition, shown as a double line in the figure. The point TP, $r = 0$, $u_4 = 0$, is a tricritical point.

Figure 2.3 depicts the phase diagram in the vicinity of a tricritical point in the most natural variables for the model free energy of Eq.(87). In real systems, all of the potentials are functions of the experimentally controllable parameters such as temperature, pressure, chemical potential, concentration of species, or external magnetic field. Physical phase diagrams with tricritical points will thus be rotated and stretched version of Figure 2.3. We will now consider some physical systems exhibiting tricritical points, the microscopic models used to describe them, and how their mean-field energy can be cast into a form similar to Eq.(87).

Chapter 3

Rotational Diffusion Equation

In this Chapter we derive the rotational diffusion equation governing the orientational dynamics for rigid biaxial ellipsoids. In section 3.1, we provide the basic understanding of the kinetic theory developed in [85] and derive this equation in the molecular (or rotating) frame. Finally, in section 3.2, we describe the Wigner-Galerkin expansion of this equation.

3.1. Kinetic Equations: Doi Model

3.1.1. System with rigid constraints in macroscopic flow. Consider a system of particles (modeled a beads) in a macroscopic velocity gradient, subject to rigid constraints. This is necessary to deal with the problems of suspensions of a rigid body or polymers with rigid constraints (such as the rod like polymer, or the freely jointed model).

(i) In the freely jointed model, the beads (at position vector $\mathbf{R_n}$) are successively connected at constant distance b, so that

$$(\mathbf{R_n} - \mathbf{R_{n-1}})^2 - b^2 = 0, \qquad n = 1, 2, ..., N \tag{92}$$

(ii) In the rigid body model, the mutual distance between the beads is fixed.

When the constraints are introduced, the forces acting on the particles $\mathbf{F_m}$ is not a function of $\mathbf{R}$ and must be determined by the equation of motion, which is the hydrodynamic relation.

$$\mathbf{V_m} = \kappa \cdot \mathbf{R_m} + \Sigma_n \mathbf{H_{mn}} \cdot \mathbf{F_n} \tag{93}$$

where $\mathbf{V_m}$ is the velocity of particles and $\mathbf{H_{nm}}$ is the mobility matrix.

We use the method of generalized coordinates which are independent of each other, and specify the configuration of beads uniquely. The generalized coordinates stands for the three components of the position vector of the center of mass, and the three Euler angles specifying the orientation of the rigid body.

3.1.2. Method of generalized coordinates. Let $\{Q\} \equiv Q_1, Q_2, ..., Q_{N_f}$ be the set of generalized coordinates. The position vector $\mathbf{R_m}$ expressed as a function of $\{Q\}$ as

$$\mathbf{R_m} = \mathbf{R_m}(\{Q\}), \qquad m = 1, 2, ..., N \tag{94}$$

The velocity of the particle in terms of the velocity of the generalized coordinate V_a is

$$\mathbf{V_m} = \Sigma_{a=1}^{N_f} \frac{\partial \mathbf{R_m}}{\partial Q_a} V_a \tag{95}$$

Using the summation convention, we write Eq.(95) as

$$\mathbf{V_m} = \frac{\partial \mathbf{R_m}}{\partial Q_a} V_a \tag{96}$$

To obtain $\mathbf{F_m}$, we use the principle of virtual work. Consider the work necessary to change Q_a by δQ_a, which is

$$\delta(U + k_B T \ln \Psi) = [\frac{\partial}{\partial Q_a}(U + k_B T \ln \Psi)]\delta Q_a \tag{97}$$

Alternatively, work can also be calculated using the force $\mathbf{F_m}$ and the displacement $\delta \mathbf{R_m}$ caused by the change in Q_a, i.e.

$$\delta(U + k_B T \ln \Psi) = -\mathbf{F_m} \cdot \delta \mathbf{R_m} \tag{98}$$

where

$$\delta \mathbf{R_m} = \frac{\partial \mathbf{R_m}}{\partial Q_a} \delta Q_a \tag{99}$$

Hence, from Eqs. (97,98,99) we have

$$\mathbf{F_m} \cdot \frac{\partial \mathbf{R_m}}{\partial Q_a} = -\frac{\partial}{\partial Q_a}(U + k_B T \ln \Psi) \tag{100}$$

Eqs. (95,93,100) determine V_a and $\mathbf{F_m}$. To obtain $\mathbf{F_m}$ and V_a explicitly, we solve Eq.(93) for $\mathbf{F_n}$:

$$\begin{aligned} \mathbf{F_n} &= (\mathbf{H^{-1}})_{nm} \cdot (\mathbf{V_m} - \kappa \cdot \mathbf{R_m}) \\ &= (\mathbf{H^{-1}})_{nm} \cdot (\frac{\partial \mathbf{R_m}}{\partial Q_a} V_a - \kappa \cdot \mathbf{R_m}) \end{aligned} \tag{101}$$

From Eqs.(100,101), we have

$$\frac{\partial \mathbf{R_n}}{\partial Q_a} \cdot (\mathbf{H}^{-1})_{nm} \cdot [\frac{\partial \mathbf{R_m}}{\partial Q_b} V_b - \kappa \cdot \mathbf{R_m}] = -\frac{\partial}{\partial Q_a}(U + k_B T \ln \Psi) \tag{102}$$

Define

$$(h^{-1})_{ab} = \frac{\partial \mathbf{R_n}}{\partial Q_a} \cdot (\mathbf{H}^{-1})_{nm} \cdot \frac{\partial \mathbf{R_m}}{\partial Q_b} \tag{103}$$

and

$$F_a^E = -\frac{\partial}{\partial Q_a}(U + k_B T \ln \Psi) \tag{104}$$

and

$$V_a^{(V)} = h_{ab} \frac{\partial \mathbf{R_n}}{\partial Q_b} \cdot (\mathbf{H^{-1}})_{nm} \cdot \kappa \cdot \mathbf{R_m} \tag{105}$$

Hence

$$(h^{-1})_{ab}(V_b - V_b^{(V)}) = F_a^{(E)} \tag{106}$$

which can be solved using h_{ab}, the inverse of $(h^{-1})_{ab}$, giving

$$\begin{aligned} V_a &= V_a^{(V)} + h_{ab}F_b^{(E)} \\ &= -h_{ab}\frac{\partial}{\partial Q_b}(U + k_BT\ln\Psi) + V_a^{(V)} \end{aligned} \tag{107}$$

Hence

$$\mathbf{F_n} = (\mathbf{H}^{-1})_{nm} \cdot (\frac{\partial \mathbf{R_m}}{\partial Q_a} h_{ab}F_b^{(E)} + \frac{\partial \mathbf{R_m}}{\partial Q_a} V_a^{(V)} - \kappa \cdot \mathbf{R_m}) \tag{108}$$

In generalized coordinate space, the conservation equation is

$$\frac{\partial \Psi}{\partial t} = -\frac{1}{\sqrt{g}} \sum_{a=1}^{N_f} \frac{\partial}{\partial Q_a}[\sqrt{g}V_a\Psi] \tag{109}$$

where g is the determinant of the matrix g_{ab} defined by

$$g_{ab} = \frac{\partial \mathbf{R_m}}{Q_a} \cdot \frac{\partial \mathbf{R_m}}{Q_b} \tag{110}$$

Thus the diffusion equation is obtained as

$$\frac{\partial \Psi}{\partial t} = \frac{1}{\sqrt{g}} \frac{\partial}{\partial Q_a} \sqrt{g}[h_{ab}(k_BT\frac{\partial \Psi}{\partial Q_b} + \frac{\partial U}{\partial Q_b}\Psi) - V_a^{(V)}\Psi] \tag{111}$$

3.1.3. Rigid Ellipsoids. The molecular axis (**m**, **n**, **k**) in terms of the Euler angles (α, β, γ) are defined as

$$\begin{aligned} &\mathbf{m} = (\cos\alpha\sin\beta, \sin\alpha sin\beta, \cos\beta), \\ &\mathbf{n} = (\cos\alpha\cos\beta\cos\gamma - \sin\alpha\sin\gamma, \sin\alpha\cos\beta\cos\gamma + \cos\alpha\sin\gamma, -\sin\beta\cos\gamma), \\ &\mathbf{k} = (-\cos\alpha\cos\beta\sin\gamma - \sin\alpha\cos\gamma, -\sin\alpha\cos\beta\sin\gamma + \cos\alpha\cos\gamma, \sin\beta\sin\gamma) \end{aligned} \tag{112}$$

The position vector of a particle on the ellipsoid is $\mathbf{R} = (a\mathbf{m}, b\mathbf{n}, c\mathbf{k})$ where (a,b,c) are the lengths of the respective axis. Hence, using Eqs.(103,112), we have:

$$h = \begin{pmatrix} h_{11} & h_{12} & h_{13} \\ h_{21} & h_{22} & h_{23} \\ h_{31} & h_{32} & h_{33} \end{pmatrix} \tag{113}$$

where $h_{ij} = h_{ji}$ and

$$\begin{aligned} h_{11} &= \frac{a^2 + b^2\cos^2\gamma + c^2\sin^2\gamma}{(a^2+b^2)(a^2+c^2)\sin^2\beta}, \qquad h_{12} = -\frac{(b^2-c^2)\sin\gamma\cos\gamma}{(a^2+b^2)(a^2+c^2)\sin\beta}, \\ h_{13} &= -\cos\beta\frac{a^2 + b^2\cos^2(\gamma) + c^2\sin^2(\gamma)}{(a^2+b^2)(a^2+c^2)\sin^2\beta}, \quad h_{22} = \frac{a^2 + b^2\sin^2\gamma + c^2\cos^2\gamma}{(a^2+b^2)(a^2+c^2)}, \\ h_{23} &= \frac{(b^2-c^2)\sin\gamma\cos\gamma\cos\beta}{(a^2+b^2)(a^2+c^2)\sin\beta}, \end{aligned} \tag{114}$$

$$h_{23} = \frac{a^4\sin^2\beta + c^4\cos^2\beta\sin^2\gamma + b^4\cos^2\beta\cos^2\gamma + a^2c^2 + a^2b^2 + b^2c^2}{\sin^2\beta(a^2+b^2)(c^2+b^2)(c^2+a^2)}$$

The determinant (g) is

$$g = \sin^2\beta(a^2+b^2)(c^2+b^2)(a^2+c^2) \tag{115}$$

The derivatives in the fixed $(\mathbf{x}, \mathbf{y}, \mathbf{z})$ frame and the moving frame $(\mathbf{m}, \mathbf{n}, \mathbf{k})$ are related as

$$[\partial_\alpha, \partial_\beta, \partial_\gamma]^T = [L_m, L_n, L_k]^T A^T \tag{116}$$

where (L_m, L_n, L_k) are the derivatives in the molecular rotating frame (details in Appendix **??**) and the transformation matrix A is

$$A = \begin{pmatrix} \cos\beta & -\sin\beta\cos\gamma & \sin\beta\sin\gamma \\ 0 & \sin\gamma & \cos\gamma \\ 1 & 0 & 0 \end{pmatrix} \tag{117}$$

From Eq.(111) we have

$$\frac{\partial\Psi}{\partial t} = \frac{k_B T}{\sqrt{g}}(\frac{\partial}{\partial Q_a})^T \sqrt{g} h_{ab} \Psi (\frac{\partial}{\partial Q_b})\mu - \frac{1}{\sqrt{g}}(\frac{\partial}{\partial Q_a})^T \sqrt{g} h_{ab} \Psi \cdot \frac{\partial R_n}{\partial Q_b} \cdot K \cdot R_n \tag{118}$$

where $(Q_1, Q_2, Q_3) = (\alpha, \beta, \gamma)$ Define $\widetilde{\Psi} = \sqrt{g}\Psi$ and using Eq.(116), we get

$$\begin{aligned} \partial\widetilde{\Psi}/\partial t &= \mathbf{L}^* \cdot D \cdot \mathbf{L}\mu\widetilde{\Psi} - \mathbf{L}^* \cdot D \cdot \widetilde{\Psi}(\mathbf{L}R_n) \cdot K \cdot R_n \\ &= \mathbf{L}^* \cdot D \cdot \mathbf{L}\mu\widetilde{\Psi} - \mathbf{L}^* \cdot D \cdot \widetilde{\Psi}\overrightarrow{g} \end{aligned} \tag{119}$$

where D is the diffusion matrix given by

$$D = diag[\frac{\zeta}{b^2+c^2}, \frac{\zeta}{a^2+c^2}, \frac{\zeta}{a^2+b^2}] \tag{120}$$

and the vector $\overrightarrow{g}$ is

$$\begin{aligned} \overrightarrow{g} = \iota[&\tfrac{\mathbf{m}}{b^2+c^2}(\mathbf{K} : (b^2\mathbf{nk} - c^2\mathbf{kn})) + \tfrac{\mathbf{n}}{a^2+c^2}(\mathbf{K} : (c^2\mathbf{km} - a^2\mathbf{mk})) + \tfrac{\mathbf{k}}{a^2+b^2} \\ &(\mathbf{K} : (a^2\mathbf{mn} - b^2\mathbf{nm}))] \end{aligned} \tag{121}$$

In the fixed frame, the shear-flow tensor $\mathbf{K}'$ is

$$\mathbf{K}' = \begin{pmatrix} 0 & \nu & 0 \\ 0 & 0 & 0 \\ 0 & 0 & 0 \end{pmatrix} \tag{122}$$

In the molecular frame $(\mathbf{m}, \mathbf{n}, \mathbf{k})$ the tensor is

$$\mathbf{K} = \mathbf{R}^T \mathbf{K}' \mathbf{R} \tag{123}$$

3.2. Kinetic Equations: Galerkin Approximation

Having reviewed the neccessary Quantum Mechanical concepts in Chapter 2, we are now in a position to write the Wigner function expansion of the Smoluchowski Eq.(119) derived in Section 3.1.

3.2.1. Excluded Volume potential: $\mathcal{U}$. In almost every models of polymers, the interaction among the polymer segments is limited to within a few neighbours along the chain. In reality, however, segments distant along the chain do interact if they come close to each other in space. An obvious interaction is the steric effect: since the segment has finite volume, other segments cannot come into its own region. This interaction swells the polymer; the coil size of a chain with such an interaction is larger than that of the ideal chain which has no such interaction. Even when there are attractive forces, as long as the repulsive force dominates, the polymer will swell. This effect is called the *excluded volume effect*.

The excluded volume effect represents the effect of the interaction between segments which are far apart along the chain. (refer Figure 3.1a) Such an interaction is often called the *long range interaction* in contrast to the 'short range interaction' which represents the interaction among a few neighbouring segments. The terms 'long' and 'short' represent the distance along the chain, not the spatial seperation. The excluded volume effect was first discussed by Kuhn [65], and the modern development was initiated by Flory [66, 67]. Once the long range interaction is introduced, exact calculation becomes impossible. A great deal of work has been done on this problem and a detailed description is given in various literatures [70, 71, 68, 69].

We construct our intermolecular excluded volume potential based on the ideas given in [97, 98, 99, 100, 101, 102]. Biaxial molecules can be schematically described as bricks or platelets (refer Figure 3.1b)

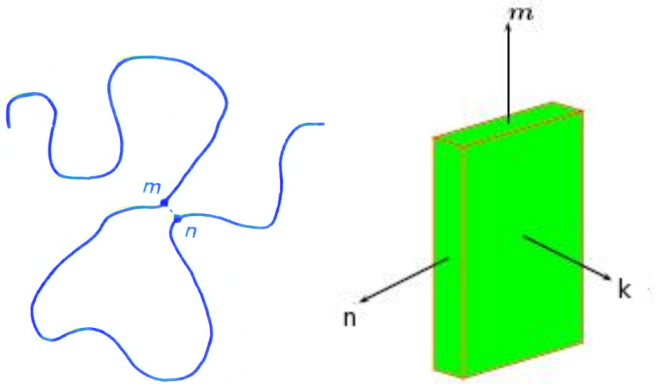

FIGURE 3.1. (a) Excluded volume interaction.(b) A simple biaxial molecule

In every platelet, we distinguish the major axis **m** from the two minor axes **n** and **k**.The anisotropic part of every molecular biaxial tensor can be described by two traceless, orthogonal components, defined as:

$$\begin{aligned} \mathbf{q} &= \mathbf{mm} - \tfrac{1}{3}\mathbf{I} \\ \mathbf{b} &= \mathbf{nn} - \mathbf{kk} \end{aligned} \tag{124}$$

If **m** is interpreted as the long molecular axis, then **q** is the uniaxial tensor representing the dominant geometric feature of the molecules, while **b** represents their secondary biaxiality. Let two molecules be described by the pairs of tensors (**q**,**b**) and (**q'**,**b'**). Straley [101] suggests that the most general orientational interaction energy or the excluded volume energy $\mathcal{U}$ between them, which is linear in each pair of tensors and invariant under their exchange, has the form:

$$\mathcal{U} = -\mathcal{U}_0\{\mathbf{q}\cdot\mathbf{q}' + \gamma_v(\mathbf{q}\cdot\mathbf{b}' + \mathbf{b}\cdot\mathbf{q}') + \lambda_v\mathbf{b}\cdot\mathbf{b}'\} \tag{125}$$

where $\mathcal{U}_0 > 0$ is a typical interaction energy and λ_v and γ_v are dimensionless material parameters. When $\lambda_v = \gamma_v = 0$, Eq.(125) represents the interaction energy put forward by Maier and Saupe [95], which depends only on the uniaxial molecular components.

The admissible range for the parameters λ_v and γ_v is given in reference [97] where it is assumed that the increment in excluded volume $\delta\mathcal{U}$ is positive definite under an arbitrary rotation of the second molecule with respect to the first one.

Using the Mean Field approach employed by Straley [101], the two independent tensors $\mathbf{Q}$ and $\mathbf{B}$ are defined as the ensemble averages $<\mathbf{q}>$ and $<\mathbf{b}>$ respectively. In the common, fixed eigen-frame of $\mathbf{Q}$ and $\mathbf{B}$, the molecular axes ($\mathbf{m}$,$\mathbf{n}$,$\mathbf{k}$), in terms of the Euler angles (α, β, γ), are given by Eq.(**??**) and the corresponding excluded volume potential of a molecule, in the mean field described by $\mathbf{Q}$ and $\mathbf{B}$, is given by

$$\mathcal{U} = -\mathcal{U}_v\{\mathbf{Q}\cdot\mathbf{q} + \gamma_v(\mathbf{Q}\cdot\mathbf{b} + \mathbf{B}\cdot\mathbf{q}) + \lambda_v\mathbf{B}\cdot\mathbf{b}\} \tag{126}$$

In our study, we consider a simplified version of the intermolecular potential (Eq. 126), which is given as follows:

$$\mathcal{U} = -\mathcal{U}_0\{\mathbf{M} : \mathbf{mm} + \gamma(\mathbf{M}\cdot\mathbf{nn} + \mathbf{N}\cdot\mathbf{mm}) + \lambda\mathbf{N}\cdot\mathbf{nn}\} \tag{127}$$

where $\mathbf{M}$ and $\mathbf{N}$ are the ensemble averages $<\mathbf{mm}>$ and $<\mathbf{nn}>$ respectively. The axes ($\mathbf{m}$,$\mathbf{n}$,$\mathbf{k}$) are related to the an orthonormal basis $\mathbf{n}_{1,2,3}$ through Eq. (112). The material parameters in the two models are related as

$$\gamma = \frac{2(\gamma_v + \lambda_v)}{1 + 2\gamma_v + \lambda_v}, \lambda = \frac{4\lambda_v}{1 + 2\gamma_v + \lambda_v}, \mathcal{U}_0 = \mathcal{U}_v(1 + 2\gamma_v + \lambda_v) \tag{128}$$

Rewriting Eq.(127) as

$$\begin{aligned}\mathcal{U} = -\mathcal{U}_0\{&< m_a m_b > m_a m_b + \gamma(< m_a m_b > n_a n_b + < n_a n_b > m_a m_b) \\ &+\lambda < n_a n_b > n_a n_b\}\end{aligned} \tag{129}$$

and using Eq.(112) in Section 3.1.3 for the euler angle expression for m and n, and finally rewriting them using Wigner functions (D^L_{mn}), we arrive at the series expansion for the excluded volume as follows

$$\mathcal{U} = A_1(t)D^2_{00} + A_2(t)(D^2_{20} + D^2_{-20}) + A_3(t)(D^2_{02} + D^2_{0-2}) + A_4(t)(D^2_{22} + D^2_{2-2} + D^2_{-22} + D^2_{-2-2}) + A_{12}(t)(D^2_{-20} - D^2_{20}) + A_{13}(t)(D^2_{-10} - D^2_{10}) + A_{23}(t)(D^2_{-10} + D^2_{10}) + B_{12}(t)(D^2_{-2-2} - D^2_{22} + D^2_{-22} - D^2_{2-2}) + B_{13}(t)(D^2_{-12} - D^2_{1-2} - D^2_{12} + D^2_{-1-2}) \tag{130}$$

where the time-dependent coefficients $A_i(t), A_{ij}(t)B_{ij}(t)$ are given in I. Note that the wigner functions are of the order $L = 2$. This is because the potential $\mathcal{U}$ is a second order polynomial of the trigonometric functions of the euler angles.

3.2.2. Rotational Diffusion Operator: $\mathbf{L}^* \cdot (D_r \mathbf{L}\mu f)$. Rotational diffusion equation ([105, 58, 104, 103, 59, 87]) has proved to be very useful for interpreting experimental spectroscopic data on molecules in isotropic [87] and uniaxial liquid crystalline phases [59, 60]. Techniques based on 2^{nd}-rank molecular properties such as ESR [59], NMR [60, 61] and fluorescence depolarization [62, 63] and first-rank properties such as IR [57] and dielectric relaxation [64] have been used. Molecular reorientation is characterized in the model by a 2^{nd}-rank diffusion matrix that is commonly assumed to be diagonal in the molecular frame.The 3 diffusion components D_{ii} in this frame quantify the ease of reorientation around the three axes.

Rod-like polymers do two kinds of Brownian motion, translation and rotation. The translational brownian motion is the random motion of the position vector $\mathbf{R}$ of the center of mass and the rotational Brownian motion is the random motion of the unit vector $\mathbf{u}$ which is parallel to the polymer.

To visualize the rotational Brownian motion we imagine the trajectory of $\mathbf{u}(t)$, which is on the surface of the sphere $|\mathbf{u}| = 1$ (Figure 3.2)

For short times, the random motion of $\mathbf{u}(t)$ can be regarded as Brownian motion on a $2-D$ flat surface, and the mean square displacement of $\mathbf{u}(t)$ in time t is written as

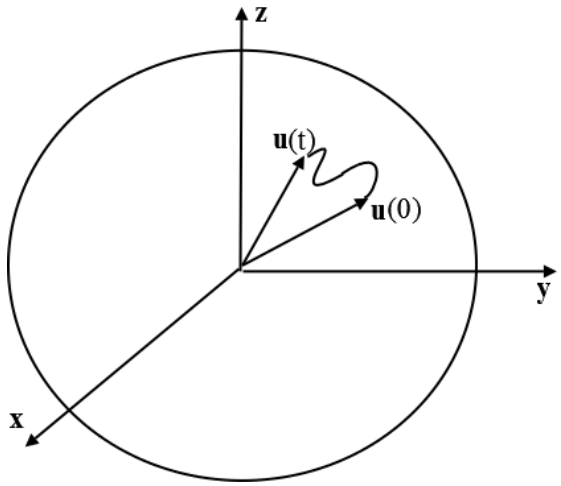

FIGURE 3.2. Rotational Diffusion

$$< (\mathbf{u}(t) - \mathbf{u}(0))^2 >= 4D_r t \qquad (\text{for} D_r t \ll 1) \tag{131}$$

D_r is the rotational diffusion constant. Note that the dimension of D_r is $(\text{time})^{(-1)}$, and is not the same as that of the translational diffusion constant, $((length)^2/time)$. Eq.(131) is correct only for $D_r \ll 1$. For the general case, readers are referred to Section 3.1.3.

We project the rotational diffusion operator (Eq.(119) derived in Section 3.1.3) onto the space spanned by the wigner rotation matrices and write the result in terms of a series expansion.

In the absence of external flow field, the probability density function (f) of a molecule undergoing rotational diffusion in an anisotropic potential $\mathcal{U}(\alpha, \beta, \gamma)$, evolves in time, according to the differential equation (refer Eq.(119))

$$\begin{aligned} \partial f/\partial t &= \mathbf{L}^* \cdot D_r \cdot \mathbf{L}\mu f \\ &= \hat{\Gamma} f \end{aligned} \tag{132}$$

where $\mathbf{L} = (L_n, L_k, L_m)$ is a dimensionless angular momentum operator, $\mathbf{D_r}$ is the diffusion tensor and $\hat{\Gamma}$ is the rotational diffusion operator. If we choose the molecule-fixed

frame of reference, then $\mathbf{D_r}$ is a diagonal matrix; $\mathbf{D} = diag(D_n, D_k, D_m)$. Writing $\mathbf{D}$ in a more convenient form as

$$\mathbf{D_r} = -\rho \begin{pmatrix} 1+\epsilon & 0 & 0 \\ 0 & 1-\epsilon & 0 \\ 0 & 0 & \eta \end{pmatrix} \tag{133}$$

where $\rho = \frac{1}{2}(D_n + D_k), \epsilon = \frac{D_n - D_k}{D_n + D_k}, \eta = \frac{2D_m}{D_n + D_k}$

The diffusion operator $\hat{\Gamma}$ is

$$\hat{\Gamma} = -\rho\{(1+\epsilon)(L_n^2 + L_n(L_n\mathcal{U})) + (1-\epsilon)(L_k^2 + L_k(L_k\mathcal{U})) + \eta(L_m^2 + L_m(L_m\mathcal{U}))\} \tag{134}$$

Using the following relations:

$$\begin{aligned} L_\pm &= L_n \pm \iota L_k \\ \nabla^2 &= L_n^2 + L_k^2 + \eta L_m^2 \end{aligned} \tag{135}$$

we arrive at

$$\hat{\Gamma} = -\rho[\nabla^2 + \nabla^2\mathcal{U}_0 + \tfrac{\epsilon}{2}(L_+^2 + L_-^2 + L_+^2\mathcal{U}_0 + L_-^2\mathcal{U}_0 + (L_+\mathcal{U}_0)L_+ + (L_-\mathcal{U}_0)L_-) +$$

$$\tfrac{1}{2}((L_+\mathcal{U}_0)L_- + (L_-\mathcal{U}_0)L_+) + \eta(L_m\mathcal{U}_0)L_m]f \tag{136}$$

The pdf is written in terms of the rotation wigner matrices, i.e.

$$f = \Sigma_{L',m',n'} C_{L',m',n'}(t) D_{L',m',n'}) \tag{137}$$

and using the Coupling-Rule (Eq.21) in Section 2.2.1 for the product of two wigner matrices, we get the following expansion. Note that the expansion of each terms of Eq. 136 in given in Appendix A.

$$\frac{-1}{\rho}\frac{\partial C_{L',m',n'}(t)}{\partial t} = \{\ [L'(L'+1)+(\eta-1)n'^2]C_{L',m',n'}(t)\ +\ \frac{\epsilon}{2}s_{n+1}s_{n+2}C_{L',m',n'+2}(t)$$
$$+\ \frac{\epsilon}{2}s_{n-1}s_{n_2}C_{L',m',n'-2}(t)+$$
$$\sum_{L=|L'-2|}^{L'+2}\sqrt{\tfrac{2L+1}{2L'+1}}\{\ C_{L,m',n'}(t)\{C(2,L,L',0,m)P_1(s_{n-1}C(2,L,L',1,n'-1)+s_{n+1}$$
$$C(2,L,L',-1,n'+1))+D_1C(2,L,L',0,m)C(2,L,L',0,n)\}\ +$$
$$C_{L,m'-2,n'}(t)\{C(2,L,L',2,m'-2)P_{4a}(s_{n-1}C(2,L,L',1,n'-1)+s_{n+1}$$
$$C(2,L,L',-1,n'+1))+D_{2a}C(2,L,L',2,m'-2)C(2,L,L',0,n')\}\ +$$
$$C_{L,m'+2,n'}(t)\{C(2,L,L',-2,m'+2)P_{4b}(s_{n-1}C(2,L,L',1,n'-1)+s_{n+1}$$
$$C(2,L,L',-1,n'+1))+D_{2b}C(2,L,L',-2,m'+2)C(2,L,L',0,n')\}\ +$$
$$C_{L,m'-2,n'-2}(t)C(2,L,L',2,m'-2)(P_{2a}s_{n-2}C(2,L,L',1,n'-1)+(D_{4a}+2(n'-2)$$
$$\eta(A_4-B_{12}))C(2,L,L',2,n'-2))\ +$$
$$C_{L,m'-2,n'+2}(t)C(2,L,L',2,m'-2)(P_{2a}s_{n+2}C(2,L,j,-1,n'+1)+(D_{4a}-2(n'+2)$$
$$\eta(A_4+B_{12}))C(2,L,L',-2,n'+2))\ +$$
$$C_{L,m'+2,n'-2}(t)C(2,L,L',-2,m'+2)(P_{2b}s_{n-2}C(2,L,L',1,n'-1)+(D_{4b}+2(n'-2)$$
$$\eta(A_4+B_{12}))C(2,L,L',2,n'-2))\ +$$
$$C_{L,m'+2,n'+2}(t)C(2,L,L',-2,m'+2)(P_{2b}s_{n+2}C(2,L,L',-1,n'+1)+(D_{4b}-$$
$$2(n'+2)\eta(A_4-B_{12}))C(2,L,j,-2,n'+2))\ +$$
$$C_{L,m',n'-2}(t)C(2,L,L',0,m')(P_3s_{n-2}C(2,L,L',1,n'-1)+(D_3+2(n'-2)\eta A_3)$$
$$C(2,L,L',2,n'-2))\ +$$
$$C_{L,m',n'+2}(t)C(2,L,L',0,m')(P_3s_{n+2}C(2,L,L',-1,n'+1)+(D_3-2(n'+2)\eta A_3)$$
$$C(2,L,L',-2,n'+2))\ +$$
$$C_{L,m'-1,n'}(t)C(2,L,L',1,m'-1)P_7(s_{n-1}C(2,L,L',1,n'-1)+s_{n+1}$$
$$C(2,L,L',-1,n'+1)+2\sqrt{6}C(2,L,L',0,n'))\ +$$
$$C_{L,m'+1,n'}(t)C(2,L,L',-1,m'+1)P_8(s_{n-1}C(2,L,L',1,n'-1)+s_{n+1}$$
$$C(2,L,L',-1,n'+1)+2\sqrt{6}C(2,L,L',0,n'))\ +$$
$$C_{L,m'-1,n'-2}(t)C(2,L,L',1,m'-1)(P_5s_{n-2}C(2,L,L',1,n'-1)+(D_5-2\eta B_{13}$$
$$(n'-2))C(2,L,L',2,n'-2))\ +$$

$$
\begin{aligned}
&C_{L,m'+1,n'+2}(t)C(2,L,L',-1,m'+1)(P_6 s_{n+2}C(2,L,L',-1,n'+1)+(D_6+\\
&\qquad 2\eta B_{13}(n'+2))C(2,L,L',-2,n'+2))+\\
&C_{L,m'-1,n'+2}(t)C(2,L,L',1,m'-1)(P_5 s_{n+2}C(2,L,L',-1,n'+1)+(D_5-\\
&\qquad 2\eta B_{13}(n'+2))C(2,L,L',-2,n'+2))+\\
&C_{L,m'+1,n'-2}(t)C(2,L,L',-1,m'+1)(P_6 s_{n-2}C(2,L,L',1,n'-1)+(D_6+\\
&\qquad 2\eta B_{13}(n'-2))C(2,L,L',2,n'-2))\}
\end{aligned}
\tag{138}
$$

where $s_{n-1}=\sqrt{L'(L'+1)-n'(n'-1)}$ $\qquad$ $s_{n+1}=\sqrt{L'(L'+1)-n'(n'+1)}$

$s_{n-2}=\sqrt{L'(L'+1)-(n'-1)(n'-2)}$ $\qquad$ $s_{n+2}=\sqrt{L'(L'+1)-(n'+1)(n'+2)}$

Time dependent coefficients involved in the above equation are given in Appendix A.

3.2.3. Flow Term: $\mathbf{L}^*\cdot(\mathbf{g}f)$. The flow operator is projected onto the space spanned by Wigner rotation matrices in a similar fashion as discussed in the previous section.

$$
\mathbf{L}^*\cdot(\mathbf{g}f)=-\{L_m(g_m f)+L_n(g_n f)+L_n(g_n f)\} \tag{139}
$$

Since the shear flow matrix has the form given in Eq.(122), the components of the flow vector ($\overrightarrow{g}$) are as follows:

$$
g_m = \frac{\nu}{b^2+c^2}(b^2k_1n_2-c^2n_1k_2) \tag{140}
$$

$$
g_n = \frac{\nu}{a^2+c^2}(c^2m_1k_2-a^2k_1m_2) \tag{141}
$$

$$
g_k = \frac{\nu}{a^2+b^2}(a^2n_1m_2-b^2m_1n_2) \tag{142}
$$

The euler angle expression for ($\mathbf{m}$,$\mathbf{n}$,$\mathbf{k}$) are given in Eq.(112). These expression are expanded in terms of the Wigner matrices, to arrive at the wigner function expansion of the ($\overrightarrow{g}$):

$$g_m = \nu[-\tfrac{1}{2}D^1_{00} - \tfrac{1}{4}\tfrac{b^2-c^2}{b^2+c^2}(D^2_{22} + D^2_{-2-2} - D^2_{2-2} - D^2_{-22})]$$

$$g_n = \nu[\tfrac{1}{2\sqrt{2}}(D^1_{01} - D^1_{0-1}) + \tfrac{1}{4}\tfrac{c^2-a^2}{c^2+a^2}D^2_{-2-1} + D^2_{2-1} - D^2_{21} - D^2_{-21})] \tag{143}$$

$$g_k = \nu[\tfrac{1}{2\sqrt{2}}(D^1_{01} - D^1_{0-1}) + \tfrac{1}{4}\tfrac{c^2-a^2}{c^2+a^2}(D^2_{-2-1} + D^2_{2-1} - D^2_{21} - D^2_{-21})]$$

Using the relations (135), we arrive at the final form of the flow operator:

$$\begin{aligned}\mathbf{L}^* \cdot (\mathbf{g}f) = L_m[(\tfrac{\nu}{r_c^2+r_b^2})(-\tfrac{r_c^2+r_b^2}{2}\mathrm{D}^1_{00} + \tfrac{r_c^2-r_b^2}{4}(\mathrm{D}^2_{2-2} + \mathrm{D}^2_{-22} - \mathrm{D}^2_{22} - \mathrm{D}^2_{-2-2})\ )]f\ + \\ \tfrac{\nu}{8}(L_+ + L_-)[\tfrac{r_c^2-1}{r_c^2+1}(\mathrm{D}^2_{-2-1} + \mathrm{D}^2_{2-1} - \mathrm{D}^2_{21} - \mathrm{D}^2_{-21})]f\ +\ \tfrac{\nu}{8}(L_+ - L_-) \\ [\tfrac{1-r_b^2}{1+r_b^2}(\mathrm{D}^2_{21} + \mathrm{D}^2_{-2-1} - \mathrm{D}^2_{2-1} - \mathrm{D}^2_{-21})]f\ -\ \tfrac{\nu}{2\sqrt{2}}[L_+\mathrm{D}^1_{0-1} - L_-\mathrm{D}^1_{01}]f\end{aligned} \tag{144}$$

$$\begin{aligned}= L_m[-\tfrac{\nu}{2}\mathrm{D}^1_{00} + \tfrac{\nu\alpha_{cb}}{4}(\mathrm{D}^2_{2-2} + \mathrm{D}^2_{-22} - \mathrm{D}^2_{22} - \mathrm{D}^2_{-2-2})\ ]f + \tfrac{\nu}{8}L_+[\eta_{c+b} \\ (\mathrm{D}^2_{21} - \mathrm{D}^2_{2-1}) + \eta_{c-b}(\mathrm{D}^2_{-21} - \mathrm{D}^2_{-2-1})]f + \tfrac{\nu}{8}L_-[\eta_{c-b}(\mathrm{D}^2_{21} - \mathrm{D}^2_{2-1}) + \eta_{c+b} \\ (\mathrm{D}^2_{-21} - \mathrm{D}^2_{-2-1})]f - \tfrac{\nu}{2\sqrt{2}}[L_+\mathrm{D}^1_{0-1} - L_-\mathrm{D}^1_{01}]f\end{aligned} \tag{145}$$

where $\alpha_{cb} = \frac{r_c^2-r_b^2}{r_c^2+r_b^2}$, $\eta_{c\pm b} = \frac{(1-r_c^2)}{(1+r_c^2)} \pm \frac{(1-r_b^2)}{(1+r_b^2)}$ $r_b = \frac{b}{a}, r_c = \frac{c}{a}$

Complete expansion of flow term is given as follows: (Details are given in Appendix A)

$$\frac{\partial C_{L',m',n'}(t)}{\partial t} = \frac{\nu}{2}\sum_{L=|L'-1|}^{L'+1}\sqrt{\frac{2L+1}{2L'+1}}C_{L,m',n'}(t)C(1,L,L',0,m')\{\sqrt{\frac{L'(L'+1)-n'(n'+1)}{2}}$$
$$C(1,L,L',1,n') + n'C(1,L,L',0,n') - \sqrt{\frac{L'(L'+1)-n'(n'-1)}{2}}C(1,L,L',-1,n')\}+$$
$$\sum_{L=|L'-2|}^{L'+2}\sqrt{\frac{2L+1}{2L'+1}}\ \{\ \frac{\nu\eta_{c+b}}{8}\sqrt{L'(L'+1)-n'(n'-1)}C(2,L,L',2,m'-2)\ \{$$
$$C(2,L,L',1,n'-2)C_{L,m'-2,n'-2}(t) - C(2,L,L',-1,n')C_{L,m'-2,n'}(t)\}+$$
$$\frac{\nu\eta_{c-b}}{8}\sqrt{L'(L'+1)-n'(n'-1)}C(2,L,L',-2,m'+2)\ \{\ C(2,L,L',1,n'-2)$$
$$C_{L,m'+2,n'-2}(t) - C(2,L,L',-1,n')C_{L,m'+2,n'}(t)\}+$$
$$\frac{\nu\eta_{c-b}}{8}\sqrt{L'(L'+1)-n'(n'+1)}C(2,L,L',2,m'-2)\ \{\ C(2,L,L',1,n')C_{L,m'-2,n'}(t)$$
$$-C(2,L,L',-1,n'+2)C_{L,m'-2,n'+2}(t)\}+$$
$$\frac{\nu\eta_{c+b}}{8}\sqrt{L'(L'+1)-n'(n'+1)}C(2,L,L',-2,m'+2)\ \{\ C(2,L,L',1,n')C_{L,m'+2,n'}(t)$$
$$-C(2,L,L',-1,n'+2)C_{L,m'+2,n'+2}(t)\}+$$
$$\frac{\alpha_{cb}}{4}n'C(2,L,L',2,m'-2)\{C(2,L,L',-2,n'+2)C_{L,m'-2,n'+2}(t) - C(2,L,L',2,n)$$
$$C_{L,m'-2,n'-2}(t)\} + \frac{\alpha_{cb}}{4}n'C(2,L,L',-2,m'+2)\{C(2,L,L',2,n'-2)C_{L,m'+2,n'-2}(t)$$
$$-C(2,L,L',-2,n'+2)C_{L,m'+2,n'+2}(t)\}\ \} \tag{146}$$

Chapter 4

Steady State Uniaxial Case

In this chapter, we show how to solve the Smoluchowski equation for solutions of rigid nematic polymers and suspensions under imposed elongational flow, magnetic or electric fields, respectively. Under the three imposed fields, we show that (1) the Smoluchowski equation can be cast into a generic form, (2) the external field must parallel to one of the eigenvectors of the second moment tensor in steady states, and (3) the steady state solution of the Smoluchowski equation (probability density function or simply pdf) is of the Boltzmann type parameterized by material parameters and two order parameters governed by two algebraic-integral equations. Then, we present a complete bifurcation diagram of the order parameters with respect to the material parameters by solving the algebraic-integral equations. The stability of the pdf solutions is inferred from the minimum of the free energy density. The solution method is extended to dilute solutions of dipolar, rigid nematic polymers under imposed electric field. The first moment of the steady state pdf is shown to parallel to the external field direction at sufficiently strong permanent dipole or relatively weak dipole-dipole interaction. In this case, the solution of the Smoluchowski equation is parameterized by one order parameter and material parameters in the Boltzmann form. Otherwise, the first moment is not necessarily parallel to the external field direction.

The chapter is organized as follows. In Section 4.1, we describe the well known kinetic theory and derive and solve the two implicit equations in order to find the steady state solutions of rigid nematic uniaxial lcps. Also, we state and proof an important result,

necessary for our solution procedure. In Section 4.2, we extend our study to a dilute solution of rigid nematic polymers.

4.1. Steady states under an imposed elongational flow, electric or magnetic field

We adopt the extended Doi-Hess model for solutions of rigid nematic polymers [85, 111, 112, 113, 114] with the well-known Maier-Saupe excluded volume potential

$$V_i(\mathbf{m}, \mathbf{x}, t) = -\frac{3NkT}{2}\langle \mathbf{mm} \rangle : \mathbf{mm} \tag{147}$$

where N is the dimensionless number density of the nematic polymer, $\mathbf{m}$ is a unit vector for the axis of symmetry of the molecule, which is modeled as a spheroid, $\langle \mathbf{mm} \rangle = \int_{\|\mathbf{m}\|=1} \mathbf{mm} f(\mathbf{m}, t) d\mathbf{m}$ is the second moment of $\mathbf{m}$ with respect to the probability density function $f(\mathbf{m}, t)$ [85, 113]. When the molecule (or nematic particle in the case of suspensions) is under an imposed electric or magnetic field, an induced dipole or magnetic moment in the molecule will occur even though it does not have an intrinsic dipole (non dipolar) or magnetic moment (non ferromagnetic). The potential due to the external field effect is given by the potential.

$$V_H = -\frac{\chi_\alpha}{2}(\mathbf{H} \cdot \mathbf{m})^2, V_E = -\frac{\alpha}{2}(\mathbf{E} \cdot \mathbf{m})^2 \tag{148}$$

respectively, where $\mathbf{H}$ is the magnetic field vector, and χ_α is the difference of the susceptibility parallel and perpendicular to the molecular direction; $\mathbf{E}$ is the electric field, and α is the difference between the polarizability parallel and perpendicular to the molecular direction. We note that, in this formulation, the mean-field dipole-dipole interaction due to the induced dipole is not accounted for.

The transport equation for the probability distribution function of the molecular orientation in monodomains is given by the Smoluchowski equation:

$$\frac{df}{dt} = \mathcal{R} \cdot [D_r f \mathcal{R} \mu_t] - \mathcal{R} \cdot [\mathbf{m} \times \dot{\mathbf{m}} f],$$
$$\dot{\mathbf{m}} = \mathbf{W} \cdot \mathbf{m} + a[\mathbf{D} \cdot \mathbf{m} - \mathbf{D} : \mathbf{mmm}] \tag{149}$$

where D_r is the rotary diffusivity (here it is assumed a constant), $\mathcal{R} = \mathbf{m} \times \frac{\partial}{\partial \mathbf{m}}$ is the rotational gradient operator, and $\frac{d}{dt}(\bullet)$ denotes the material derivative: $\frac{\partial}{\partial t}(\cdot) + \mathbf{v} \cdot \nabla(\cdot)$, $\mathbf{D}$ and $\mathbf{W}$ are the rate of strain tensor and vorticity tensor, respectively; a is a geometry or shape parameter defined by $a = \frac{r^2-1}{r^2+1}$ with the molecular aspect ratio r. $\mu = lnf + \frac{1}{kT} V_i$ is the normalized chemical potential and $\mu_t = \mu + \frac{1}{kT} V_H$ or $\mu_t = \mu + \frac{1}{kT} V_E$ is the extended chemical potential including the normalized external potential , respectively.

For an elongational flow field stretching ($\gamma > 0$, uniaxial elongation) or compressing ($\gamma < 0$, biaxial elongation) in the direction of $\mathbf{e}_3$, the velocity field is given by

$$\mathbf{v} = -\frac{\gamma}{2}(x\mathbf{e}_1 + y\mathbf{e}_2) + \gamma z \mathbf{e}_3 \tag{150}$$

It can be cast in the form of a potential effectively [116],

$$V_e = -\frac{3a\gamma}{4} kT \mathbf{e}_3 \mathbf{e}_3 : \mathbf{mm} \tag{151}$$

In fact,

$$-\mathbf{m} \times \dot{\mathbf{m}} = \frac{1}{kT} \mathcal{R} V_e \tag{152}$$

since $\mathbf{W} = 0$ in elongational flow fields. Therefore, the rotary convective term in the Smoluchowski equation can be absorbed into the extended chemical potential in Eq.(215).

Now that the external potentials for the elongational flow, magnetic and electric field are identical in form, we next illustrate the solution method for Smoluchowski

equation in the case of the elongational flow field only in the following. In this case, the Smoluchowski equation is rewritten in the form

$$\frac{df}{dt} = \mathcal{R} \cdot [D_r(a) f \mathcal{R} \mu_t] \tag{153}$$

where $\mu_t = lnf + \frac{1}{kT}(V_i + V_e)$. The steady state solution of the equation is given by

$$\mu_t = C \tag{154}$$

leading to

$$f = \frac{1}{Z} e^{-\frac{1}{kT}(V_i + V_e)}, \tag{155}$$

where Z is the normalizing constant to ensure $\langle 1 \rangle = 1$. We denote

$$\nu = \frac{a\gamma}{2} \tag{156}$$

and name it the effective Peclet number. Then, the total potential is given by

$$V = V_i + V_e = -\frac{3kT}{2}[N\langle \mathbf{mm} \rangle + \nu \mathbf{e}_3 \mathbf{e}_3] : \mathbf{mm} \tag{157}$$

We adopt a general representation of the second moment $\langle \mathbf{mm} \rangle$

$$\langle \mathbf{mm} \rangle = s(\mathbf{nn} - \mathbf{I}/3) + \beta(\mathbf{n}_\perp \mathbf{n}_\perp - \mathbf{I}/3) + \frac{\mathbf{I}}{3}, \tag{158}$$

where s and β are two order parameters and $\mathbf{n}$ and $\mathbf{n}_\perp$ are two eigenvectors of $\langle \mathbf{mm} \rangle$ [115]. It follows from Eq.(158) that

$$\begin{aligned} s &= 2\langle (\mathbf{n} \cdot \mathbf{m})^2 \rangle + \langle (\mathbf{n}_\perp \cdot \mathbf{m})^2 \rangle - 1, \\ \beta &= \langle (\mathbf{n} \cdot \mathbf{m})^2 \rangle + 2\langle (\mathbf{n}_\perp \cdot \mathbf{m})^2 \rangle - 1 \end{aligned} \tag{159}$$

If we parameterize the vector $\mathbf{m}$ relative to the orthonormal frame $(\mathbf{n}, \mathbf{n}_\perp, \mathbf{n}^*)$ as follows

$$\mathbf{m} = \cos\theta\mathbf{n} + \sin\theta\cos\phi\mathbf{n}_\perp + \sin\theta\sin\phi\mathbf{n}^* \tag{160}$$

where $\mathbf{n}^*$ is the third orthonormal eigenvector of $\mathbf{M}$ besides $\mathbf{n}$ and $\mathbf{n}_\perp$, and set $\mathbf{e}_3 = \mathbf{n}$, then

$$f = \frac{1}{Z} e^{\frac{3N}{2}[(s-\frac{\beta}{2})(\cos^2\theta - 1/3) + \frac{\beta}{2}\sin^2\theta\cos 2\phi] + \frac{3\nu}{2}\cos^2\theta} \tag{161}$$

with

$$Z = Z(s,\beta) = \int_{\|\mathbf{m}\|=1} e^{\frac{3N}{2}[(s-\frac{\beta}{2})(\cos^2\theta - \frac{1}{3}) + \frac{\beta}{2}\sin^2\theta\cos 2\phi] + \frac{3\nu}{2}\cos^2\theta} d\mathbf{m} \tag{162}$$

Substituting Eq.(161) into the formula of s and β, we arrive at the governing system of equations for the order parameters implicitly,

$$\begin{aligned} \beta &= \textstyle\int_{\|\mathbf{m}\|=1} \sin^2\theta\cos 2\phi f d\mathbf{m}, \\ s &= \textstyle\int_{\|\mathbf{m}\|=1} \frac{1}{2}(3\cos^2\theta - 1) f d\mathbf{m} + \frac{\beta}{2} \end{aligned} \tag{163}$$

Using a change of variable, we rewrite the order parameters as follows

$$\begin{aligned} \beta &= 4\textstyle\int_0^\pi \int_0^1 (1-z^2)\cos 2\phi f dz d\phi, \\ &= \textstyle\frac{1}{Z'}\int_0^1 (1-z^2) e^{3/2(N(s-\beta/2)+\nu)z^2} I_1(\zeta) dz, \\ s &= 4\textstyle\int_0^\pi \int_0^1 P_2(z) f dz + \beta/2, \\ &= \textstyle\frac{1}{Z'}\int_0^1 P_2(z) e^{3/2(N(s-\beta/2)+\nu)z^2} I_0(\zeta) dz + \beta/2, \\ f &= \textstyle\frac{1}{Z'} e^{\frac{3N}{2}[(s-\frac{\beta}{2})z^2 + \frac{\beta}{2}(1-z^2)\cos 2\phi] + \frac{3\nu}{2}z^2} \end{aligned} \tag{164}$$

where

$$Z'(s,\beta) = \int_0^1 e^{\frac{3}{2}(N(s-\beta/2)+\nu)z^2} I_0(\zeta) dz \tag{165}$$

$P_2(z) = \frac{1}{2}(3z^2-1)$ is the second order Legendre polynomial, and $\zeta = \frac{3N\beta}{4}(1-z^2)$. In the above, we used the definition for the modified Bessel function of the first kind:

$$\pi I_n(z) = \int_0^\pi e^{z\cos\phi} \cos n\phi d\phi, n = 0, \cdots, \infty \tag{166}$$

Noticing that $\beta = 0$ is a solution of Eq.(163), we deduce the implicit equation governing the uniaxial order parameter s:

$$\begin{aligned} s &= \int_{\|\mathbf{m}\|=1} \tfrac{1}{2}(3\cos^2\theta - 1)\tfrac{1}{Z(s,0)} e^{\frac{3N\,s}{2}(\cos^2\theta - 1/3) + \frac{3\nu}{2}\cos^2\theta} f d\mathbf{m} \\ &= \int_0^1 P_2(z) e^{\frac{3}{2}(N\,s+\nu)z^2} dz / (\int_0^1 e^{\frac{3}{2}(N\,s+\nu)z^2} dz) \end{aligned} \tag{167}$$

The free energy density of the nematic polymer system is given by

$$A[f] = \int_{\|\mathbf{m}\|=1} [kT\ln f + \frac{V_i}{2} + V_e] f d\mathbf{m} \tag{168}$$

From equation (155), we arrive at the free energy density at equilibrium:

$$\begin{aligned} A[f] &= \int_{\|\mathbf{m}\|=1} [-kTlnZ - \tfrac{V_i}{2}] f d\mathbf{m} \\ &= -kT[lnZ - \tfrac{N}{2}(s^2 - s\beta + \beta^2)] \end{aligned} \tag{169}$$

This formula will be used to infer the stability of the steady states. The stable steady state is the global minimum of the free energy density. The metastable equilibrium is a local minimum of the free energy, but not the global one.

4.1.1. Reduced symmetry. It is known that the Smoluchowski equation is invariant under the rotational transformation in $\mathcal{SO}_3$ when flows and external field effects are absent [117]. Namely,

$$\frac{d}{dt}f = \mathcal{R}_n \cdot D_r[f\mathcal{R}_n\mu] \tag{170}$$

where $\mathcal{R}_n = \mathbf{n} \times \frac{\partial}{\partial \mathbf{n}}$, $\mathbf{n} = \mathbf{U} \cdot \mathbf{m}$ for any $\mathbf{U} \in \mathcal{SO}_3$. With the imposed elongational flow of axis of symmetry $\mathbf{e}_3$, we denote the rotational group in the plane transverse to the axis by $\mathcal{SO}_2 = \{\mathbf{U} | \mathbf{U} \in \mathcal{SO}_3, \mathbf{U} \cdot \mathbf{e}_3 = \mathbf{e}_3\}$. Then, from the invariant property of the Smoluchowski equation, we deduce equation (215) is invariant under $\mathcal{SO}_2$ since

$$\mu_t = -\frac{3NkT}{2}\mathbf{mm} : \langle \mathbf{mm} \rangle - \frac{3\nu kT}{2}\mathbf{e}_3\mathbf{e}_3 : \mathbf{mm} = -\frac{3NkT}{2}\mathbf{nn} : \langle \mathbf{nn} \rangle - \frac{3\nu kT}{2}\mathbf{e}_3\mathbf{e}_3 : \mathbf{nn} \tag{171}$$

for $\mathbf{n} = \mathbf{U} \cdot \mathbf{m}$, where $\mathbf{U} \in \mathcal{SO}_2$. i.e., there exists a reduced symmetry in the Smoluchowski equation under the imposed field in the plane orthogonal to the field. Namely, if there exists a pdf solution of the Smoluchowski equation, there exists a family of pdf solutions parameterized by $\mathcal{SO}_2$.

In the extended Doi-Hess kinetic theory, the geometric parameter a can be exploited to model both rodlike ($a > 0$) and disklike ($a < 0$) molecules. Effectively, it is the effective Peclet number that matters in the steady state solution. When molecules are disklike, an uniaxial elongational flow ($\gamma > 0$) is effectively equivalent to a biaxial elongational flow of rodlike nematic polymers since they share the same effective Peclet number and vice versa. Given the asymmetric correspondence between the rodlike and disklike molecules in biaxial and uniaxial elongation, we will focus on the rodlike nematic polymer in the following ($a > 0$). The steady states of disklike nematic polymers can be obtained from the correspondence principle.

4.1.2. Uniaxial elongation. Stretching or uniaxial elongation for rodlike nematic polymers corresponds to $\nu > 0$. The steady state solutions consist of up to three uniaxial steady states with their uniaxial directors aligned in the direction of the flow and a family of biaxial solutions at sufficiently high polymer concentration

parameterized by $\mathcal{SO}_2$. The bifurcation diagram of the uniaxial steady states with respect to the dimensionless concentration has been documented in [115]: there are up to two stable prolate steady states at small Peclet number regime limited to a small window of nematic polymer concentration and there is only one in the regime of large Peclet numbers. The highly aligned nematic steady state is always stable. When two stable prolate steady states coexist in a window of small Peclet numbers and nematic polymer concentrations the lesser aligned one is metastable. Figure 4.1 depicts the uniaxial steady state solutions in the phase space (N, s) with ν = -0.1, -0.01, 0, 0.01, 0.1 respectively.

The biaxial steady states emerged at sufficiently high concentration represent the entire nematic equilibrium family (absent of flows) parameterized by $\mathcal{SO}_2$ with their major directors aligned in the plane perpendicular to the direction of elongation. However, these biaxial steady solutions are unstable. Figure 4.2 depicts all uniaxial steady states and a pair of biaxial steady state families with their major axes perpendicular to each other in the plane orthogonal to the direction of elongation.

4.1.3. Biaxial elongation. When nematic polymers are in biaxial elongation, $\nu < 0$, there exist up to three uniaxial steady states with their uniaxial directors aligned in the axis of the flow symmetry. At small concentration, the only uniaxial steady state is the oblate one; whereas there are two more prolate uniaxial steady states at sufficiently high concentration. At high enough concentration, a family of biaxial steady states parameterized by $\mathcal{SO}_2$ emerges. At low concentration, the only stable steady state is the oblate uniaxial one. At sufficiently high concentration, a family of biaxial steady state parameterized by $\mathcal{SO}_2$ is stable. The stable biaxial steady state is deformed from the prolate uniaxial equilibrium ($\nu = 0$) with their uniaxial director aligned in the plane orthogonal to the flow direction. Again, bistability may take place in the regime of small Peclet numbers for a limited range of

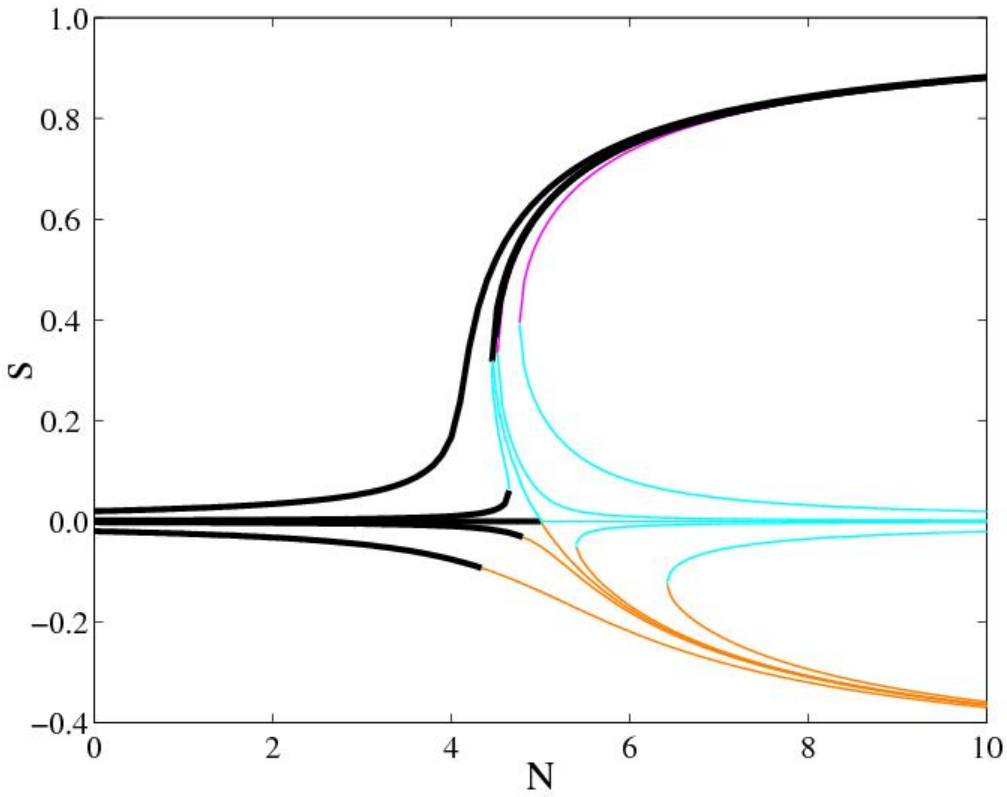

FIGURE 4.1. Phase bifurcation diagram for the steady state uniaxial order parameter at ν = -0.1,-0.01, 0,0.01,0.1 respectively. A bi-stability region exists for small magnitude Peclet numbers and in a small window of nematic polymer concentrations near the critical concentration N=5. If $\nu > 0$, the highly aligned prolate state ($s > 0$) is stable while the less aligned prolate steady state is metastable; whereas the oblate state ($s < 0$) is stable up to a certain critical concentration if $\nu < 0$. The thick curves represent the stable branches while the thin curves depict the unstable ones.

concentration. Figure 4.3 depicts a representative bifurcation diagram for all steady states as functions of the Peclet number and dimensionless concentration, respectively.

We have obtained solutions of the Smoluchowski equation semi-analytically by assuming the imposed field parallels to one of the eigenvector direction of the second moment tensor. Next, we show that this is a fact.

To prove it, we note that the imposed field direction can be parameterized in the frame of $\mathbf{n}, \mathbf{n}_\perp, \mathbf{n}^*$ as follows:

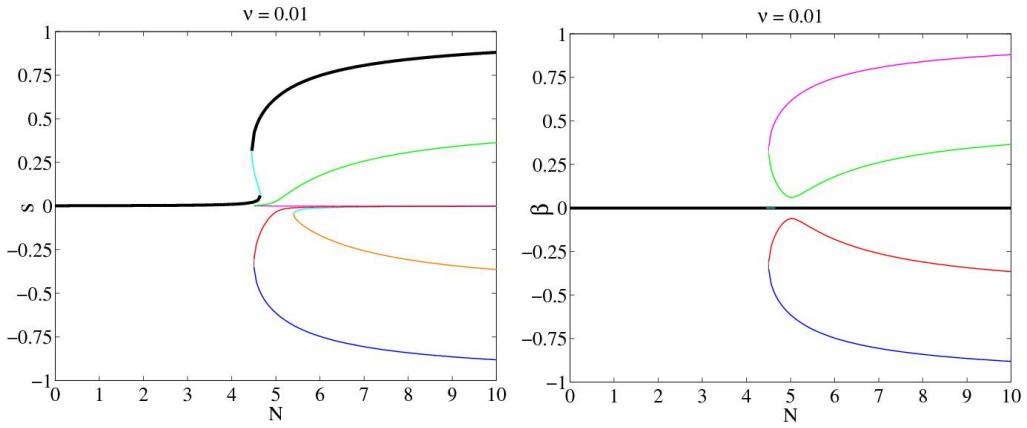

FIGURE 4.2. Phase bifurcation diagram for all the steady state order parameters in uniaxial elongation. The stable solutions are uniaxial prolate ones ($s > 0, \beta = 0$) of highly aligned and the less aligned. The biaxial states form a family of solutions parameterized by the rotational group $\mathcal{SO}_2$, which are unstable. The Peclet number here is $\nu = 0.01$. The thick curves depict the stable branches while the thin curves show the unstable ones.

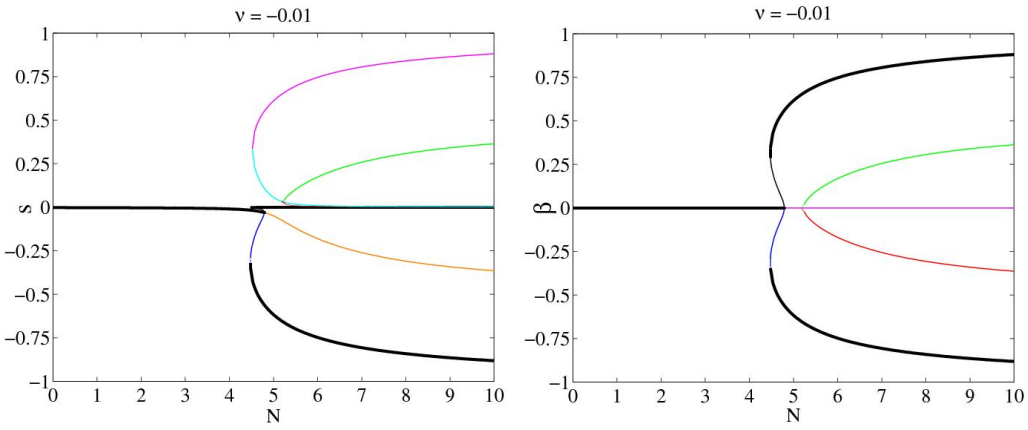

FIGURE 4.3. The phase bifurcation diagram for all the steady state order parameters in biaxial elongation. The stable solution is the oblate ($s < 0, \beta = 0$) one up to a critical concentration and then assumed by a family of biaxial solutions ($s \neq 0, \beta \neq 0$). The bistability region may exist in a small window of nematic polymer concentrations at small Peclet number regimes. The Peclet number here is $\nu = -0.01$. The thick curves depict the stable branches while the thin curves show the unstable ones.

$$\mathbf{e}_3 = \cos\theta'\mathbf{n} + \sin\theta'\cos\phi'\mathbf{n}_\perp + \sin\theta'\sin\phi'\mathbf{n}^* \tag{172}$$

where θ', ϕ' are constants. So,

$$\mathbf{e}_3 \cdot \mathbf{m} = \cos\theta\cos\theta' + \sin\theta\sin\theta'\cos(\phi - \phi') \tag{173}$$

The pdf solution of the Smoluchowski equation is given by

$$f = \frac{1}{Z} e^{\frac{3N}{2}[(s-\frac{\beta}{2})(\cos^2\theta - 1/3) + \frac{\beta}{2}\sin^2\theta\cos 2\phi] + \frac{3\nu}{2}(\cos\theta\cos\theta' + \sin\theta\sin\theta'\cos(\phi-\phi'))^2]} \tag{174}$$

where Z is the normalizing constant. From the definition of the second moment equation, we arrive at three additional identities

$$\mathbf{n}\cdot\mathbf{M}\cdot\mathbf{n}_\perp = 0, \mathbf{n}\cdot\mathbf{M}\cdot\mathbf{n}^* = 0, \mathbf{n}_\perp\cdot\mathbf{M}\cdot\mathbf{n}^* = 0 \tag{175}$$

where $\mathbf{M} = \langle\mathbf{mm}\rangle$. Next, we show that either $\theta' = 0$ or $\theta' = \pi/2$ together with $\phi' = 0$ or $\phi' = \pi/2$. This is equivalent to say that $\mathbf{e}_3$ is in one of the eigenvector directions of the second moment tensor $\mathbf{M}$.

It follows from Eq.(175)

$$\langle\cos\theta\sin\theta\cos(\phi - \phi')\rangle = 0 \tag{176}$$

for any values of ϕ'. We define

$$F(\lambda) = \int_{\|\mathbf{m}\|=1} \cos\theta\sin\theta\cos(\phi - \phi')e^h/Z d\mathbf{m} \tag{177}$$

where

$$\begin{aligned} h(\lambda) = {} & \tfrac{3N}{2}[(s - \tfrac{\beta}{2})(\cos^2\theta - 1/3) + \tfrac{\beta}{2}\sin^2\theta\cos 2\phi] + \tfrac{3\nu}{2}((\cos\theta\cos\theta')^2 + \\ & (\sin\theta\sin\theta'\cos(\phi - \phi'))^2 + 2\lambda\cos\theta\cos\theta'\sin\theta\sin\theta'\cos(\phi - \phi'))] \end{aligned} \tag{178}$$

We note that Eq.(176) implies

$$F(1) = 0 \tag{179}$$

Since the integrand in the integral of $F(0)$ is an analytical function of $\sin^2\theta$ multiplied by $\cos\theta$ which is an odd function about $\theta = \pi/2$, it can be easily shown to be zero. However,

$$F'(\lambda) = const \times \int_{\|\mathbf{m}\|=1} \sin 2\theta' \sin^2 2\theta \cos^2(\phi - \phi') e^h / Z d\mathbf{m} \neq 0 \tag{180}$$

provided

$$\sin 2\theta' \neq 0. \tag{181}$$

This contradicts the fact that $F(0) = F(1) = 0$ if (181) were true. Thus

$$\theta' = 0, \pi/2. \tag{182}$$

In the case of $\theta' = \pi/2$, we define

$$G(\lambda) = \int_{\|\mathbf{m}\|=1} \sin^2\theta \cos\phi \sin\phi e^g / Z d\mathbf{m} \tag{183}$$

where

$$\begin{aligned} g = \tfrac{3N}{2}[(s - \tfrac{\beta}{2})(\cos^2\theta - 1/3) + \tfrac{\beta}{2}\sin^2\theta\cos 2\phi] + \tfrac{3\nu}{2}\sin^2\theta(\cos^2\phi\cos^2\phi' + \\ \sin^2\phi\sin^2\phi' + 2\lambda\sin\phi\cos\phi\sin\phi'\cos\phi')] \end{aligned} \tag{184}$$

We recall that Eq.(175) implies $G(1) = 0$. At $\lambda = 0$, the integrand is given by an exponential function of $\cos 2\phi$ multiplied by $\sin 2\phi$. The integral in ϕ over $[0, 2\pi]$ is therefore equal to zero. i.e.,

$$G(0) = 0 \tag{185}$$

Then, using the same argument, we arrive at

$$G'(\lambda) = const \times \sin 2\phi' \int_{\|\mathbf{m}\|=1} \sin^4\theta \sin^2 2\phi e^g / Z d\mathbf{m} \neq 0 \tag{186}$$

provided $\sin 2\phi' \neq 0$. This contradicts to $G(0) = G(1) = 0$ if it were true. Hence, $\phi' = 0, \pi/2$. We then conclude that $\mathbf{e}_3$ must be in one of the principal axes or eigenvector directions of the second moment tensor $\mathbf{M}$.

Theorem 4.1.1. *When the Smoluchowski equation with the Maier-Saupe excluded volume potential is driven under an imposed magnetic, or electric field, or an elongational flow field, one of the principal axes of the second moment of the steady state probability density function solution must parallel to the imposed field direction.*

4.2. Effect of an imposed electric field on dilute solution of nematic polymers

We consider dilute solution of dipolar, rigid nematic polymers or suspensions, where the excluded volume effect is neglected. When the electric field is applied, the total potential consisting of the intermolecular (dipole-dipole) and external electric potential is given by

$$U = -\alpha \langle \mathbf{m} \rangle \cdot \mathbf{m} - \mu \mathbf{E} \cdot \mathbf{m} - \frac{\alpha_0}{2} \mathbf{E}\mathbf{E} : \mathbf{m}\mathbf{m} \tag{187}$$

where α_0 is the difference of the polarizability parallel and perpendicular to $\mathbf{m}$, μ is the strength of the permanent dipole and α is the strength of the intermolecular dipole-dipole interaction potential.

We set

$$\langle \mathbf{m} \rangle = s_1 \mathbf{q}_1, \|\mathbf{q}_1\| = 1 \tag{188}$$

where

$$s_1 = \langle(\mathbf{q}_1 \cdot \mathbf{m})\rangle \tag{189}$$

is an order parameter describing the averaged molecular orientation about the direction $\mathbf{q}_1$. We extend $\mathbf{q}_1$ into an orthonormal basis $\mathbf{q}_1$, $\mathbf{q}_2$ and $\mathbf{q}_3$ and parameterize $\mathbf{m}$ and $\mathbf{E}$ with respect to the basis:

$$\begin{aligned} \mathbf{m} &= \cos\theta\mathbf{q}_1 + \sin\theta\cos\phi\mathbf{q}_2 + \sin\theta\sin\phi\mathbf{q}_3, \\ \mathbf{E} &= \cos\theta'\mathbf{q}_1 + \sin\theta'\cos\phi'\mathbf{q}_2 + \sin\theta'\sin\phi'\mathbf{q}_3 \end{aligned} \tag{190}$$

Assuming $\mathbf{E}||\mathbf{q}_1$, we arrive at

$$\begin{aligned} f &= \tfrac{1}{Z} e^{\frac{1}{kT}[(\alpha s_1 + \mu E)\cos\theta + \frac{\alpha_0}{2}E^2\cos^2\theta]}, \\ s_1 &= \langle\cos\theta\rangle = \textstyle\int_{-1}^{1} z e^{\frac{1}{kT}[(\alpha s_1 + \mu E)z + \frac{\alpha_0}{2}E^2 z^2]} dz/Z, \\ Z &= \textstyle\int_{-1}^{1} e^{\frac{1}{kT}[(\alpha s_1 + \mu E)z + \frac{\alpha_0}{2}E^2 z^2]} dz. \end{aligned} \tag{191}$$

Figure 4.4 depicts the bifurcation diagram in the phase space (s_1, α, E) at selected values of μ, α_0. The stable branch is identified by examining the free energy density

$$A = \int_{\|\mathbf{m}\|=1} kT(flnf) - [\frac{\alpha}{2}\langle\mathbf{m}\rangle\cdot\mathbf{m} + \mu\mathbf{m}\cdot\mathbf{E} + \frac{\alpha_0}{2}\mathbf{EE}:\mathbf{mm}]fd\mathbf{m} = [\frac{\alpha}{2}s_1^2 - kTlnZ] \tag{192}$$

At zero electric field strength, the order parameter goes through a second order phase transition as α increases. The critical concentration is $\alpha^* = 3$. When the electric field is applied, the symmetric phase diagram is broken so that a single branch of positive (negative) s_1 forms for all values of α and positive (negative) values of E and two branches of the order parameter s_1 of negative (positive) values emerge through a saddle node bifurcation. The single branch order parameter is stable, indicating that the averaged molecular orientation favors the direction of the external field.

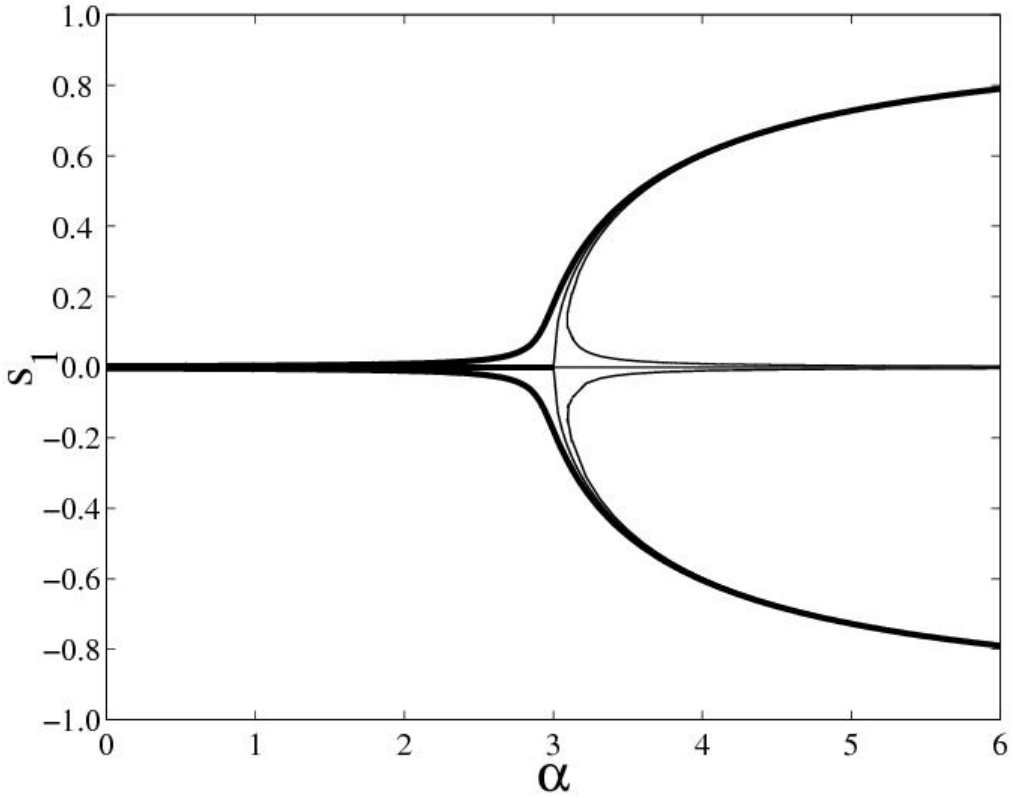

FIGURE 4.4. Phase bifurcation diagram for the steady state uniaxial order parameter s_1 as functions of α. The parameter values are kT=1, α_0=0.2, μ=0.1, E=-0.1,0,0.1. The steady state bifurcation diagram is symmetric about $s_1 = 0$ and occurs at $\alpha_c = 3$. When $E > 0$, the symmetry is broken in such a way that a stable and positive order parameter exists for all $\alpha > 0$ while a pair of negative order parameters emerge at sufficiently large values of α. Whereas $E < 0$, a stable negative order parameter persists for all $\alpha > 0$ while a pair of positive order parameters emerge at sufficiently large values of α. This indicates that nematic polymers incline to orient in the direction of the externally imposed electric field. The thick curves depict the stable branches while the thin curves show the unstable ones.

We next show that $\mathbf{q}_1$ must parallel to $\mathbf{E}$ under certain conditions, i.e. the orientational axis of the first moment is dictated by the external field. From the parametrization of the electric field, we have

$$f = \frac{1}{Z} e^{\frac{1}{kT}[(\alpha s_1)\cos\theta + \mu E(\cos\theta\cos\theta' + \sin\theta\sin\theta'\cos(\phi-\phi')) + \frac{\alpha_0}{2}E^2(\cos\theta\cos\theta' + \sin\theta\sin\theta'\cos(\phi-\phi'))^2]} \tag{193}$$

where Z is the normalizing constant. The other conditions that we can use are

$$\mathbf{q}_2 \cdot \langle \mathbf{m} \rangle = \mathbf{q}_3 \cdot \langle \mathbf{m} \rangle = 0 \tag{194}$$

This translates to

$$\langle \sin\theta \sin\phi \rangle = \langle \sin\theta \cos\phi \rangle = 0. \tag{195}$$

It follows from (195) that

$$\langle \sin\theta \cos(\phi - \tilde{\phi}) \rangle = 0. \tag{196}$$

for any values of $\tilde{\phi}$.

Theorem 4.2.1. *When the solution of dipolar, rigid nematic polymers is driven by an imposed electric field, the first moment of the steady state probability density function must be parallel to the external field direction provided* $|\mu| \geq |\alpha_0 E|$.

Proof. We first assume $s_1 \neq 0$ since the first moment is zero vector otherwise. We set $\tilde{\phi} = \phi'$ in (196) and define

$$H = \int_{\|\mathbf{m}\|=1} \sin\theta \cos(\phi - \phi') e^{\psi} d\mathbf{m} \tag{197}$$

where

$$\begin{aligned} \psi = \tfrac{1}{kT}[(\alpha s_1)\cos\theta + \mu E(\cos\theta\cos\theta' + \sin\theta\sin\theta'\cos(\phi-\phi'))+ \\ \tfrac{\alpha_0}{2}E^2(\cos\theta\cos\theta' + \sin\theta\sin\theta'\cos(\phi-\phi'))^2]. \end{aligned} \tag{198}$$

We denote

$$\begin{aligned} \psi = \tfrac{1}{kT}[\alpha s_1 \cos\theta + \mu E\cos\theta\cos\theta' + \tfrac{\alpha_0}{2}E\cos^2\theta\cos^2\theta' + \\ a(\theta)\cos(\phi-\phi') + b(\theta)\cos^2(\phi-\phi')] \end{aligned} \tag{199}$$

where

$$a(\theta) = (\mu E + \alpha_0 E^2 \cos\theta \cos\theta') \sin\theta \sin\theta',$$
$$b(\theta) = \tfrac{\alpha_0}{2} E^2 \sin^2\theta \sin^2\theta'. \tag{200}$$

Taking into account the periodicity of the trigonometric functions, we observe that H does not depend on ϕ'. Without loss of generality, we set $\phi' = 0$. Through a series of variable changes, we arrive at

$$H = \int_0^{\pi/2}\int_0^{\pi/2} \sin^2\theta \cos\phi e^{\frac{1}{kT}[\frac{\alpha_0}{2}E^2\cos^2\theta\cos^2\theta' + b(\theta)\cos^2\phi]}[\sinh(a(\theta)\cos\phi/kT)$$
$$e^{\frac{1}{kT}[\alpha s_1\cos\theta + \mu E\cos\theta\cos\theta']} + \sinh(a(\pi-\theta)\cos\phi/kT) e^{\frac{-1}{kT}[\alpha s_1\cos\theta + \mu E\cos\theta\cos\theta']}] d\theta d\phi \tag{201}$$

If $|\mu| \geq |\alpha_0 E|$, $a(\theta)a(\pi-\theta) \geq 0$. Thus, if $\sin\theta' \neq 0$, $H > 0$, which contradicts to $H = 0$. This implies, $\sin\theta' = 0$. i.e., the magnetic field is parallel to the direction of the first moment $\mathbf{q}_1$.

The condition on the size of the parameters in Theorem 4.2.1 is necessary for some values of α. In fact, if $|\mu| < |\alpha_0 E|$ and α is large enough, then the direction of $< \mathbf{m} >$ may be different from that of $\mathbf{E}$ (which will be shown below by numerical calculations). This result can be illustrated by an intuitive physical argument. Each polymer rod is subject to two potentials: 1) the external potential caused by the electric field and 2) the (mutual) intermolecular potential caused by other polymer rods in the ensemble. It is known that in the absence of the external potential, there is an I-N phase transition caused by the dipole-dipole interaction between polymer rods when $\alpha > 3kT$ [108, 109, 110]. In other words, for $\alpha > 3kT$, polymer rods tend to form a cluster with a distinguished direction (director). In the absence of the external potential, the director of the cluster is arbitrary. In the presence of the external potential, however, the director of the cluster is no longer arbitrary. If the director of the cluster is not a stationary point of the external potential, then the

cluster cannot be a steady state solution. The external potential has at least two stationary points for any values of $\mu, \alpha_0, \mathbf{E}$. To continue the discussion, we need to switch to a spherical system different from the one used above. We select the z-axis as the direction of $\mathbf{E}$ and the y-axis perpendicular to the plane spanned by $< \mathbf{m} >$ and $\mathbf{E}$ (assuming $< \mathbf{m} >$ and $\mathbf{E}$ are not parallel to each other of course) . In this coordinate system,

$$\mathbf{E} = E(0, 0, 1), \quad < \mathbf{m} >= (r_1, 0, r_3) \tag{202}$$

In spherical coordinates, the external potential is given by

$$U_{Ext}(\theta, \phi) = -\mu E \cos\theta - \frac{\alpha_0}{2} E^2 \cos^2\theta = -\alpha_0 E^2 (\frac{\mu}{\alpha_0 E} \cos\theta + \frac{1}{2} \cos^2\theta) \tag{203}$$

When $|\mu| < |\alpha_0 E|$, the external potential has a third stationary point, θ_0, determined by

$$\cos(\theta_0) = -\frac{\mu}{\alpha_0 E} \tag{204}$$

The stationary point θ_0 is between 0 and π. Therefore, the intuitive analysis indicates that when $|\mu| < |\alpha_0 E|$ and $\alpha \neq 0$, there can be a steady state cluster whose director is different from the direction of $\mathbf{E}$. □

We next prove that when $0 < |\mu| < |\alpha_0 E|$, there is a critical value α^* such that for $\alpha \leq \alpha^*$, all steady state solutions satisfy that $< \mathbf{m} >$ is parallel to $\mathbf{E}$ (i.e. $r_1 = 0$). For $\alpha > \alpha^*$, we show numerically that there exists a steady state solution where $< \mathbf{m} >$ is not parallel to $\mathbf{E}$ (i.e. $r_1 \neq 0$).

In the Cartesian coordinate system with the direction of $\mathbf{E}$ as the z-axis:

$$\mathbf{m} = (m_1, m_2, m_3), \quad \mathbf{E} = E(0,0,1), \quad <\mathbf{m}>= (r_1, 0, r_3),$$

$$U(\mathbf{m}) = -\alpha\, r_1\, m_1 - (\mu\, E + \alpha\, r_3)\, m_3 - \tfrac{\alpha_0}{2}\, E^2\, m_3^2, \tag{205}$$

$$\rho(\mathbf{m}) = \frac{\exp\left(\frac{1}{kT}[\alpha\, r_1\, m_1 + (\mu\, E + \alpha\, r_3)\, m_3 + \frac{\alpha_0}{2}\, E^2\, m_3^2]\right)}{\int_S \exp\left(\frac{1}{kT}[\alpha\, r_1\, m_1 + (\mu\, E + \alpha\, r_3)\, m_3 + \frac{\alpha_0}{2}\, E^2\, m_3^2]\right)\, d\mathbf{m}}.$$

In the spherical coordinate system:

$$\mathbf{m} = (\sin\theta\, \cos\phi, \sin\theta\, \sin\phi, \cos\theta),$$

$$U(\theta,\phi) = -\alpha\, r_1\, \sin\theta\, \cos\phi - (\mu\, E + \alpha\, r_3)\, \cos\theta - \tfrac{\alpha_0}{2}\, E^2\, \cos^2\theta,$$

$$\rho(\theta,\phi) = \frac{\exp\left(\frac{1}{kT}[\alpha\, r_1\, \sin\theta\, \cos\phi + (\mu\, E + \alpha\, r_3)\, \cos\theta + \frac{\alpha_0}{2}\, E^2\, \cos^2\theta]\right)}{\int_{\|\mathbf{m}\|=1} \exp\left(\frac{1}{kT}[\alpha\, r_1\, \sin\theta\, \cos\phi + (\mu\, E + \alpha\, r_3)\, \cos\theta + \frac{\alpha_0}{2}\, E^2\, \cos^2\theta]\right) d\mathbf{m}} \tag{206}$$

where $\int_{\|\mathbf{m}\|=1} d\mathbf{m} = \int_0^\pi \int_0^{2\pi} \sin\theta d\theta d\phi$ The nonlinear integral equations governing r_1 and r_3 are

$$\begin{aligned} r_1 &= \int_0^\pi \int_0^{2\pi} \sin\theta\, \cos\phi\, \rho(\theta,\phi)\, d\phi\, \sin\theta\, d\theta, \\ r_3 &= \int_0^\pi \int_0^{2\pi} \cos\theta\, \rho(\theta,\phi)\, d\phi\, \sin\theta\, d\theta. \end{aligned} \tag{207}$$

Theorem 4.2.2. *When $|\mu| < |\alpha_0 E|$, there exists a critical α^* such that all solutions of Eq. (207) satisfy $r_1 = 0$ if $\alpha < \alpha^*$.*

Proof. We first prove that all solutions of Eq. (207) satisfy $r_1 = 0$ if $\alpha < kT$. We prove it by contradiction. Suppose there is a solution of (207) satisfying $r_1 \neq 0$. In the probability density $\rho(\theta,\phi)$ above, we replace r_1 by r and treat it as a variable. We consider the function

$$f(r) = r - < \sin\theta \, \cos\phi > \tag{208}$$

which satisfies

$$f(0) = f(r_1) = 0. \tag{209}$$

The derivative of $\rho(\theta, \phi)$ with respect to r is

$$\frac{d\rho(\theta,\phi)}{dr} = \frac{\alpha}{kT}(\sin\theta \, \cos\phi - < \sin\theta \, \cos\phi >) \, \rho(\theta,\phi) \tag{210}$$

The derivative of $f(r)$ is

$$\begin{aligned} \frac{df(r)}{dr} &= 1 - \frac{\alpha}{kT} < \sin\theta \, \cos\phi(\sin\theta \, \cos\phi - < \sin\theta \, \cos\phi >) > \\ &= 1 - \tfrac{\alpha}{kT} \operatorname{Var}(\sin\theta \, \cos\phi) > \left\{ \begin{array}{ll} 1, & \alpha \leq 0, \\ 1 - \langle \sin^2\theta \, \cos^2\phi \rangle, & 0 < \alpha < kT, \end{array} \right\} > 0, \end{aligned} \tag{211}$$

where Var denotes the variance. Clearly, $\frac{df}{dr} > 0$ when $\alpha < kT$, which contradicts to (209). Thus, the only solution for r_1 is zero when $\alpha < kT$. Let

$$\alpha^* = \inf\{\alpha | \text{Eq.(207) has a solution with } r_1 \neq 0\} \tag{212}$$

Clearly, α^* exists and $\alpha^* \geq kT$. Then, $r_1 = 0$ is the only solution if $\alpha < \alpha^*$. □

Figure 4.5 depicts the steady state solution whose director is not parallel to **E**. In Figure 4.5, $< m_1 >$ (i.e. r_1) and $- < m_3 >$ (i.e. $-r_3$) are shown as functions of α. The parameters used here are $\mu = 0.6kT$, $\alpha_0 = kT$, and $E = 1$. For this set of parameters $\alpha^* \approx 5.7226567kT$.

4.2.1. Reduced symmetry. The direction of the first moment is arbitrary in equilibrium. However, it is no longer arbitrary when the electric field is imposed. When the first moment is parallel to the external field direction, for instance $\alpha > \alpha^*$ when $|\mu| < |\alpha_0 E|$ or when $|\mu| > |\alpha_0 E|$, the solution is invariant with respect to the rotational group $\mathcal{SO}_2$ defined in the previous section . Otherwise, the direction of the

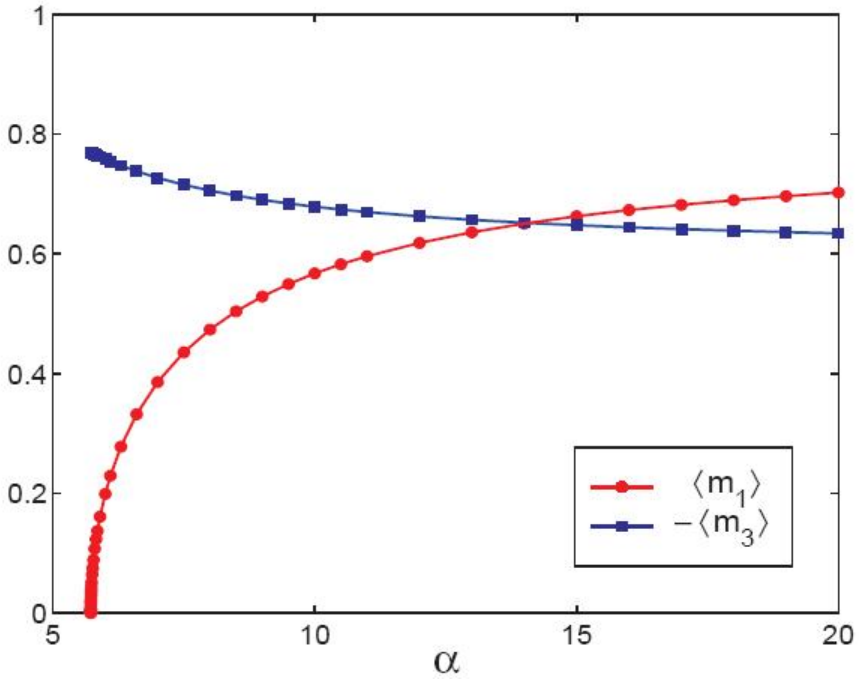

FIGURE 4.5. The plot of $\langle m_1 \rangle$ *(i.e.* r_1*)* and $\langle m_3 \rangle$ *(i.e.* $-r_3$*)* as functions of α with kT=1. It shows the existence of the first moment that is not parallel to any eigenvectors of the second moment.

first moment is well-defined and the pdf solution of the Smoluchowski equation may no longer be invariant under $\mathcal{SO}_2$.

4.3. CONCLUSION

We have demonstrated the projection method for solving the Smoluchowski equation with Maier- Saupe potential and the dipole-dipole interaction potential coupled with external fields. The method is general and can be used to solve the Smoluchsowki equation with any potential that is a function of the finite sum of spherical harmonic functions plus the external potential. The solution is always of the Boltzmann type and parameterized by a finite set of order parameters. The stability of the pdf solution can be inferred from the free energy density function within the order parameter space.

Chapter 5

Mono domain dynamics for rigid rod and platelet suspensions

In Chapter 4 we provided a detailed description of the steady state solution of the Smoluchowski equation for the molecules with uniaxial symmetry. In this chapter, we will discuss the case of time dependent solutions of the Smoluchowski equation.

We organize our discussion as follows. In sections 5.1 and 5.2, we state and prove the reciprocity principle of the Doi-Hess kinetic theory which provides a reduction of the Smoluchowski equation from a 5 parameter family of coplanar linear flows and magnetic fields to a 2 parameter target model. The target model distinguishes planar flows with a rotational component, which map to simple shear and a transverse magnetic field; and irrotational flows, which reduce to pure extension and a transverse magnetic field which is equivalent to a three-dimensional biaxial extension flow.

In section 5.3, we discuss the case of rotational flows with coplanar magnetic field where we predict transition phenomena associated with each robust class of sheared monodomain attractors (tumbling, kayaking, and chaotic) as a magnetic field is turned on and amplified. This numerical study of the target model requires a simple extension of a shear kinetic code [75, 76] to a coupled transverse magnetic field.

The case for the for irrotational flows coupled with a magnetic field is described in section 5.4. We explicitly show equilibria of the Smoluchowski equation are given by a Boltzmann distribution parameterized by a pair of order parameters, providing a natural extension of results on extensional flow-induced equilibria [72]. All stable

and unstable equilibria are then explored numerically, with the result that PDFs are generically biaxial, with principal axis either at a preferred angle in the flow-magnetic field plane, or orthogonal to it.

Finally, in section 5.5, we provide a summary of results.

5.1. Mathematical formulation

We briefly review the mathematical formulation of the Doi-Hess kinetic theory for homogeneous flows of rigid spheroids (rods or platelets) immersed in a viscous solvent subject to an imposed magnetic field [120, 111, 112, 113]. We allow a general excluded volume potential

$$V_i(\mathbf{m}, \mathbf{x}, t) = \nu kT \int_{\|\mathbf{m}'\|=1} B(\mathbf{m}, \mathbf{m}') f(\mathbf{m}', \mathbf{x}, t) d\mathbf{m}', \tag{213}$$

where ν is the number density of spheroids, $\mathbf{m}$ and $\mathbf{m}'$ are unit vectors for the axes of symmetry of a given spheroid, $B(\mathbf{m}, \mathbf{m}')$ is the excluded volume and f is the orientational probability density function (PDF) of the ensemble of spheroids. In the presence of an imposed magnetic field, an induced magnetic moment develops; we assume intrinsic magnetic moments and their magnetic dipole-dipole interaction are negligible (nonferromagnetic spheroids). For such systems, the potential due to the external field is given by [85, 84, 118].

$$V_H = -\frac{\chi_\alpha}{2}(\mathbf{H} \cdot \mathbf{m})^2 \tag{214}$$

where $\mathbf{H}$ is the magnetic field vector, and χ_α (normally positive for paramagnetic materials and negative for diamagnetic materials) is the difference between the susceptibility parallel and perpendicular to the spheroid principal axis, also known as the magnetic anisotropy.

The rotational transport equation for the orientational PDF is given by the Smoluchowski equation of Doi and Hess [85, 111, 118]:

$$\begin{aligned} \tfrac{df}{dt} &= \mathcal{R}\cdot[D_r(a) f \mathcal{R}(\mu + \tfrac{1}{kT}V_H)] - \mathcal{R}\cdot[\mathbf{m}\times\dot{\mathbf{m}}f], \\ \dot{\mathbf{m}} &= \mathbf{W}\cdot\mathbf{m} + a[\mathbf{D}\cdot\mathbf{m} - \mathbf{D}:\mathbf{mmm}], \end{aligned} \tag{215}$$

where $D_r(a)$ is the rotational diffusivity (assumed to be constant in this study), $\mathcal{R} = \mathbf{m}\times\frac{\partial}{\partial\mathbf{m}}$ is the rotational gradient operator, and $\frac{d}{dt}(\bullet)$ denotes the material derivative: $\frac{\partial}{\partial t}(\cdot) + \mathbf{v}\cdot\nabla(\cdot)$, $\mathbf{D}$ and $\mathbf{W}$ are the rate-of-strain and vorticity tensor, respectively; a is a geometry or shape parameter defined by $a = \frac{r^2-1}{r^2+1}$ in terms of the spheroidal aspect ratio r; $\mu = \ln f + \frac{1}{kT}V_i$ is the normalized chemical potential.

In [73], we show the Smoluchowski equation can be rewritten into a form with a modified Jeffery orbit equation for $\mathbf{m}$ containing a transport term due to magnetic forcing:

$$\begin{aligned} \mathbf{m}\times(\dot{\mathbf{m}} + \chi\mathbf{HH}\cdot\mathbf{m}) = \mathbf{m}\times\{\mathbf{W}\cdot\mathbf{m} + [a\mathbf{D} + \chi(\mathbf{HH} \\ -\tfrac{H^2}{k}\mathbf{I})]\cdot\mathbf{m} - [a\mathbf{D} + \chi(\mathbf{HH} - \tfrac{H^2}{l}\mathbf{I})]:\mathbf{mmm}\}, \end{aligned} \tag{216}$$

where$\chi = \frac{D_r\chi_\alpha}{kT}$ is a normalized magnetic anisotropy, k, l can be any non zero numbers and $H = \|\mathbf{H}\|$.

Recall the Smoluchowski equation absent of external fields is invariant under orthogonal transformations, which reflects orientational degeneracy of ordered equilibria f_{eq} due to excluded volume interactions. That is, nematic equilibria have a specified Boltzmann distribution function and unique uniaxial order parameter, but the principal axis of orientation is arbitrary. If $\mathbf{n} = \mathbf{U}\cdot\mathbf{m}$, where $\mathbf{U}$ is an orthogonal matrix, then Eq.(215) leads to

$$\frac{d\tilde{f}}{dt} = \mathcal{R}_n \cdot [D_r(a)\tilde{f}\mathcal{R}_n\tilde{\mu}] - \mathcal{R}_n \cdot [\mathbf{n} \times (\dot{\mathbf{n}} + \chi\tilde{\mathbf{H}}\tilde{\mathbf{H}} \cdot \mathbf{n})\tilde{f}], \tag{217}$$

where the pdf $\tilde{f} = \tilde{f}(\mathbf{n}, \mathbf{x}, t) = f(\mathbf{U}^t \cdot \mathbf{n}, \mathbf{x}, t)$, $\mathcal{R}_n = \mathbf{n} \times \frac{\partial}{\partial \mathbf{n}}$, $\tilde{\mathbf{H}} = \mathbf{U} \cdot \mathbf{H}$ is the rotated external field, and $\tilde{\mu} = \ln \tilde{f} + \frac{1}{kT} V_i(\mathbf{n}, \mathbf{x}, t)$. If we denote $SU(2, \mathbf{H}) = \{\mathbf{U} | \mathbf{U} \cdot \mathbf{H} = \mathbf{H}\}$, the Smoluchowski equation is invariant under $SU(2, \mathbf{H})$.

5.2. Reduced target models based on reciprocity relations

We briefly recall the reduction from the Smoluchowski equation for coplanar flow and magnetic fields to the target models [73].

Consider a linear planar flow field

$$\mathbf{v} = (v_{11}x + v_{12}y, v_{21}x - v_{11}y, 0), \tag{218}$$

where v_{ij} are constants, with gradient

$$\nabla\mathbf{v} = \begin{pmatrix} v_{11} & v_{12} & 0 \\ v_{21} & -v_{11} & 0 \\ 0 & 0 & 0 \end{pmatrix}, \tag{219}$$

and a coplanar magnetic field $\mathbf{H} = (H_1, H_2, 0)^T$. Let

$$p = \frac{1}{2}(v_{12} + v_{21}), \qquad q = \frac{1}{2}(v_{12} - v_{21}). \tag{220}$$

$q \neq 0$ corresponds to a rotational flow field with non-vanishing vorticity tensor. By choosing $k = l = 2$ in Eq.(216), the upper left 2×2 sub-matrix qualifies as an effective rate- of-strain tensor. Then, $\mathbf{W} = q\mathbf{W}_0$ and

$$a\mathbf{D} + \mathbf{H}\mathbf{H} - \frac{H^2}{2}(\mathbf{e}_1\mathbf{e}_1 + \mathbf{e}_2\mathbf{e}_2) = \lambda\mathbf{U}^T \cdot \mathbf{D}_0 \cdot \mathbf{U} \tag{221}$$

where $\mathbf{W}_0$ and $\mathbf{D}_0$ are normalized vorticity and rate-of-strain tensors for the pure shear velocity field $\mathbf{v} = (2y, 0, 0)$,

$$\mathbf{W}_0 = \begin{pmatrix} 0 & 1 & 0 \\ -1 & 0 & 0 \\ 0 & 0 & 0 \end{pmatrix}, \mathbf{D}_0 = \begin{pmatrix} 0 & 1 & 0 \\ 1 & 0 & 0 \\ 0 & 0 & 0 \end{pmatrix}, \mathbf{U} = \begin{pmatrix} \cos\theta & \sin\theta & 0 \\ -\sin\theta & \cos\theta & 0 \\ 0 & 0 & 1 \end{pmatrix},$$

$$\cos 2\theta = \frac{b}{\sqrt{b^2+c^2}}, \quad \sin 2\theta = -\frac{c}{\sqrt{b^2+c^2}}, \tag{222}$$

$$b = ap + \chi H_1 H_2, \quad c = av_{11} + \chi \tfrac{H_1^2 - H_2^2}{2}, \quad \lambda = \sqrt{b^2+c^2}.$$

In the new configurational coordinates $\mathbf{n} = \mathbf{U} \cdot \mathbf{m}$, the Smoluchowski equation takes the form

$$\begin{aligned} \tfrac{d\tilde{f}}{dt} &= \mathcal{R}_n \cdot [D_r(a)\tilde{f}\mathcal{R}_n\tilde{\mu}] - \mathcal{R}_n \cdot [\mathbf{n} \times (\dot{\mathbf{n}} - \tfrac{\chi H^2}{2}\mathbf{e}_3\mathbf{e}_3 \cdot \mathbf{n})\tilde{f}], \\ \dot{\mathbf{n}} &= \tilde{\mathbf{W}} \cdot \mathbf{n} + \tilde{a}\,[\tilde{\mathbf{D}} \cdot \mathbf{n} - \tilde{\mathbf{D}} : \mathbf{nnn}], \end{aligned} \tag{223}$$

where $\tilde{\mathbf{W}} = q\,\mathbf{W}_0$, $\tilde{\mathbf{D}} = q\,\mathbf{D}_0$, and $\tilde{a} = \lambda/q$

This transformed system Eq.(223), by comparison with Eq.(215), corresponds to a simple shear flow with effective shear rate 2q, a modified shape parameter $\tilde{a}$, together with an imposed magnetic field in the direction $\mathbf{e}_3$ normal to the shearing plane, and most importantly, the anisotropy $-\frac{\chi}{2}$ is opposite to the original one for the same material. *The response to any coupled coplanar rotational flow and magnetic field is now given in terms of the solution of the target kinetic model (223), which we provide by a shear flow code extended to incorporate a transverse magnetic field component.*

When $q = 0$, the flow is irrotational, i.e., the vorticity tensor is zero. Here, we can choose

$$\cos 2\theta = \frac{c}{\sqrt{b^2 + c^2}}, \quad \sin 2\theta = \frac{b}{\sqrt{b^2 + c^2}} \tag{224}$$

so that the rate of strain tensor is transformed into a diagonal form $\lambda \mathbf{D}_1$, where

$$\mathbf{D}_1 = \begin{pmatrix} 1 & 0 & 0 \\ 0 & -1 & 0 \\ 0 & 0 & 0 \end{pmatrix} \tag{225}$$

Now, the corresponding flow is a planar extension or elongation

$$\mathbf{v} = \lambda(x, -y, 0) \tag{226}$$

which is a potential flow with the corresponding normalized potential given by

$$V_e = -\frac{a\lambda}{2D_r}\mathbf{D}_1 : \mathbf{mm} \tag{227}$$

The problem can be written in terms of a scalar potential with the total normalized potential given by

$$V = -\frac{3N}{2}\mathbf{M} : \mathbf{mm} - \frac{a\lambda}{2D_r}\mathbf{D}_1 : \mathbf{mm} + \frac{\chi}{4D_r}H^2\mathbf{e}_3\mathbf{e}_3 : \mathbf{mm} \tag{228}$$

The Smoluchowski equation is simplified to

$$\frac{d}{dt}f = \mathcal{R} \cdot D_r(\mathcal{R}f + \mathcal{R}Vf) \tag{229}$$

Thus, steady states are given by a Boltzmann distribution [72],

$$f(\mathbf{m}) = \frac{1}{Z}e^{-V} \tag{230}$$

The proof of the above result can be found in Appendix. In addition, in steady states, the ensemble averaged torque vanishes

$$\langle \mathcal{R}V \rangle = 0 \tag{231}$$

which is equivalent to

$$\epsilon_{ijk}(\frac{a\lambda}{2D_r}\mathbf{D}_1 - \frac{\chi H^2}{4D_r}\mathbf{e}_3\mathbf{e}_3)_{il} \cdot \mathbf{M}_{lj} = 0 \tag{232}$$

This in turn implies

$$M_{12} = M_{13} = M_{23} = 0 \tag{233}$$

if $a\lambda \neq -\frac{\chi H^2}{2}$. If $a\lambda = -\frac{\chi H^2}{2}$, $M_{12} = M_{23} = 0$; if $a\lambda = \frac{\chi}{2}$, $M_{12} = M_{13} = 0$. In these latter cases, it can be shown $\mathbf{M}$ is diagonal [**?**]. Thus, the principal axes of the rate of strain tensor coincide with those of the second moment tensor and both share the external field direction $\mathbf{e}_3$ as a principal axis.

The total potential can be recast into

$$V = -\frac{3N}{2}\mathbf{M} : \mathbf{mm} - \frac{1}{2}\mathbf{D}_{ex} : \mathbf{mm} + const \tag{234}$$

where

$$\mathbf{D}_{ex} = \frac{1}{D_r} diag(a\lambda + \frac{\chi H^2}{6}, -a\lambda + \frac{\chi H^2}{6}, -\frac{\chi H^2}{3}) \tag{235}$$

is an effective rate of strain tensor corresponding to an asymmetric elongational flow with all three stretching rates unequal in general.

In the coordinate system with basis given by the three orthonormal eigenvectors of the second moment tensor, the second moment is diagonal with diagonal components given by

$$\langle m_i^2 \rangle = \int_{\|\mathbf{m}\|=1} m_i^2 f(\mathbf{m}) d\mathbf{m}, i = 1, 2, 3. \tag{236}$$

We non dimensionalize the Smoluchowski equation by the time scale set by rotary diffusivity $t_0 = \frac{1}{D_r}$. Then

$$\hat{q} = qt_0, \hat{\lambda} = \lambda t_0, \hat{\chi} = \chi H_0^2 t_0 \tag{237}$$

where H_0 is a characteristic field strength. We identify $Pe = 2\hat{q}$ as the Peclet number in simple shear or $Pe = \tilde{a}\lambda$ as the effective Peclet number in planar extension.

5.3. Simple shear flows coupled with a transverse magnetic field and a negative anisotropy

We now study parametric behavior of the reduced or target model for simple shear coupled to a transverse magnetic field of variable strength. From the formula for the stretching rate

$$\tilde{a} = \frac{1}{q}\sqrt{(\frac{\chi}{2}(H_1^2 - H_2^2))^2 + (a\,p + \chi H_1 H_2)^2} \tag{238}$$

we note that the magnetic field strength alters $\tilde{a}$. We discretize the Smoluchowski equation using a spherical harmonic expansion

$$f(\mathbf{m}, t) = \sum_{l=0}^{L} \sum_{m=-l}^{l} a_{lm}(t) Y_l^m(\mathbf{m}) \tag{239}$$

where Y_l^m are complex spherical harmonic functions, and L is the order of truncation in the Galerkin approximation. After this discretization, the Smoluchowski equation is transformed to a system of ordinary differential equations for the coefficients a_{lm}. For the simulation results described below, we choose $L = 10$ and we get 65 differential equations. This choice gives robust results for small to moderate concentration N and magnetic field strength χH^2.

Note that in-plane attractors are characterized by the property that $a_{lm} = 0$ for all odd integers m; otherwise, the attractor is out-of-plane. We utilize the continuation software AUTO [119] to produce the bifurcation diagrams presented below.

As noted in [73] based on second-moment closure predictions, the impact of the transverse magnetic field for materials with a negative anisotropy is to assert an

attraction toward the flow plane, or equivalently, a repulsion of the principal axis away from the vorticity axis. One anticipates any steady or transient attractor to have reduced out of plane components compared to zero magnetic field strength. We will address the impact of the transverse magnetic field with respect to several representative regimes of the effective Peclet number. In the following discussion, we decouple $\tilde{a}$ from $\tilde{\mathbf{H}}$ to investigate how the variation in anisotropy and field strength $\tilde{\mathbf{H}}$ affect the dynamics of the system at fixed values of $(q, \tilde{a})$.

We first fix $\tilde{a} = 1, N = 5.5$, and vary the Peclet number $Pe = 2q$. We have found in [76] that, absent of the magnetic field, there are 7 distinct intervals of Pe with different attractors or multiplicity of attractors, and with transitions between them at the boundaries of each interval. Now we study the consequences of turning on a magnetic field and raising its amplitude for one representative attractor in each of these 7 intervals.

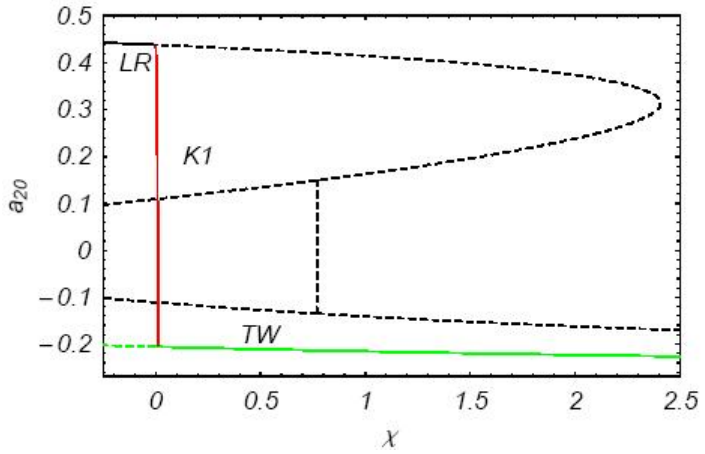

FIGURE 5.1. Bifurcation diagram of a_2^0, the coefficient of spherical harmonic mode Y_2^0 (time averaged for periodic states), as a function of entropy χ at parameter values $Pe = 1$, $\tilde{a} = 1$ and N = 5.5. As χ increases, the logrolling (LR) steady states undergo a sharp unsteady transition to kayaking states (K_1) and then collapse onto in-plane tumbling-wagging $(T-W)$ orbits. The solid green and black curves indicate stability and other curves are unstable.

As shown in Figure 5.1, when the magnetic field is absent, the stable attractor at parameter values $Pe = 1.5, \tilde{a} = 1, N = 5.5$ is a so-called logrolling state (LR). This means the principal axis of the PDF is aligned with the vorticity axis, and the solution is steady. When we turn on the field and increase its strength with negative anisotropy, the steady LR states persists up to a critical strength, then stiffly transitions to an in-plane tumbling limit cycle, which then transitions at some higher strength to a wagging limit cycle (finite amplitude oscillation of the peak of the PDF). This stiff transition is mediated by a steady-unsteady transition from vorticity-aligned steady states to kayaking limit cycles, where the peak of the PDF rotates around the vorticity axis. Presumably, the closed path of the peak of the PDF migrates from near the vorticity axis all the way to the shear plane over this short parameter range.

Thus, we find the magnetic field forces vorticity-aligned sheared steady states to in-plane periodic orbits. This is not a transition scenario that one might have predicted *a priori* on intuitive grounds. This phenomenon is furthermore *not* captured by closure models, which except for one special closure of Hinch and Leal, do not yield logrolling stable states.

Next, we shift to $Pe = 3$, holding $\tilde{a} = 1$ and $N = 5.5$, with solutions versus magnetic field strength shown in Figure 5.2. The shear response is a K_1 limit cycle at zero anisotropy $\chi = 0$. As χ increases, the K_1 attractor "collapses" to a tumbling/wagging orbit (TW) in a hysteresis bifurcation. The bistable K_1 and tumbling/wagging solutions coexist in a very narrow band of χ. This is once again a rather non-intuitive response diagram.

When the Peclet number is further increased to $Pe = 4$ with fixed $\tilde{a} = 1$, $N = 5.5$, there are bistable K_1 and tumbling/wagging orbits for pure shear, $\chi = 0$. The stable tumbling/wagging solution persists for all $\chi > 0$ shown here, whereas the K_1

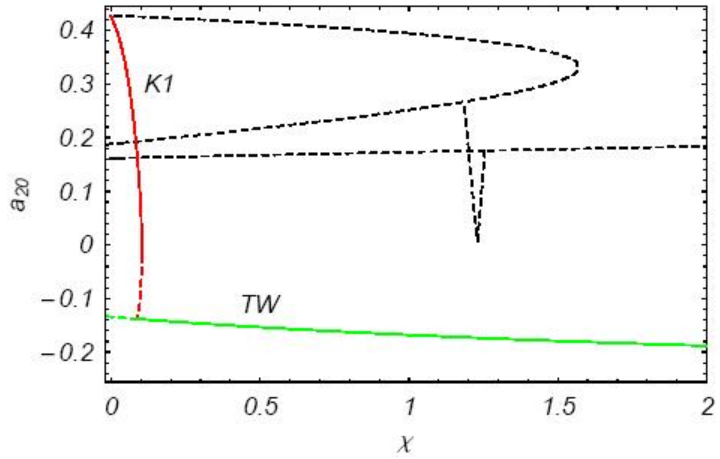

FIGURE 5.2. Bifurcation diagram of a_2^0, the coefficient of spherical harmonic mode Y_2^0 (time averaged for periodic states), as a function of entropy χ at parameter values $Pe = 3$, $\tilde{a} = 1$ and N = 5.5. The response is K_1 for zero anisotropy $\chi = 0$. As $|\chi|$ increases, the K_1 attractor collapses to a tumbling/wagging orbit (TW). In a very narrow band of χ, the K_1 and TW attractors coexist.

solution survives up to a certain value of $\chi > 0$ and then vanishes by a turning point bifurcation. The solution as a function of the anisotropy χ is shown in Figure 5.3.

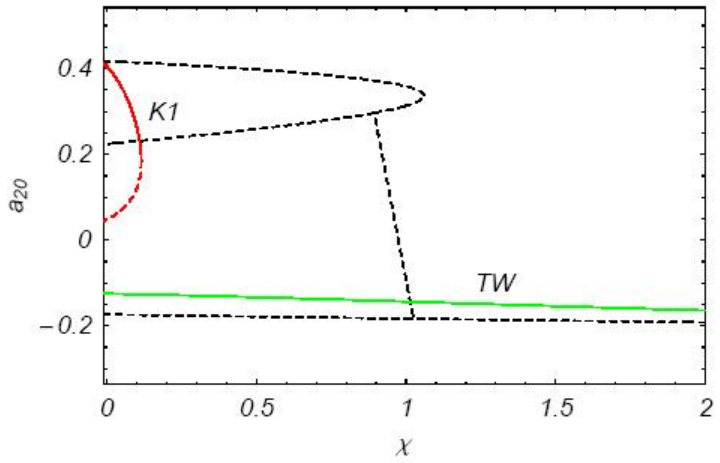

FIGURE 5.3. Bifurcation diagram of a_2^0, the coefficient of spherical harmonic mode Y_2^0 (time averaged for periodic states), as a function of entropy χ at parameter values $Pe = 4$, $\tilde{a} = 1$ and N = 5.5. In this parameter regime, the bi-stable attractors are K_1 orbits in pure shear ($\chi = 0$) and the tumbling/wagging orbit (TW). As $|\chi|$ increases, the out-of-plane K_1 orbits disappear, leaving only the in-plane, tumbling/ wagging orbit.

At $Pe = 5, \tilde{a} = 1$ and $N = 5.5$, the K_1 solution branch behaves qualitatively the same as in the case of $Pe = 4$. However, at small anisotropy, a pair of stable K_2 solutions exist. They merge into the tumbling/wagging solution as the anisotropy enhances. So, at small anisotropy, the two distinct kayaking solutions are bi-stable. Figure 5.4 depicts the bifurcation diagram.

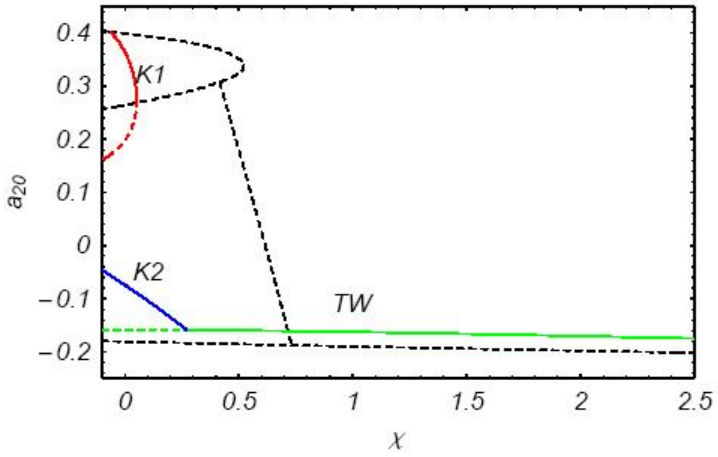

FIGURE 5.4. Bifurcation diagram of a_2^0, the coefficient of the spherical harmonic mode Y_2^0 (time averaged for periodic states), as a function of anisotropy χ at parameter values $Pe = 5, \tilde{a} = 1$ and $N = 5.5$. In this parameter regime, two stable attractors (K_1 and K_2) co-exist at small χ. K_1 disappears after a turning point, leaving K_2 as a single attractor for a short interval of χ. Then the out-of-plane tilted kayaking orbit K_2 transitions into an in-plane tumbling/wagging orbit TW as χH^2 increases.

At $Pe = 6, \tilde{a} = 1$ and $N = 5.5$, the zero anisotropy limit is dominated by the stable K_1 solution. As the anisotropy increases, the stable PDF goes through a pair of out-of-plane steady states and then aligns in the flow direction. Ironically, the anisotropy later destabilizes the flow-aligning steady state to generate a tumbling/wagging solution at high anisotropy. This is a phenomenon that requires further investigation. Figure 5.5 depicts the bifurcation diagram.

For $\tilde{a} = 1$ and $N = 5.5$, at $Pe = 6.5$ or $Pe = 7$, the bifurcation diagram is essentially the same as for $Pe = 6$ shown in Figure 5.6.

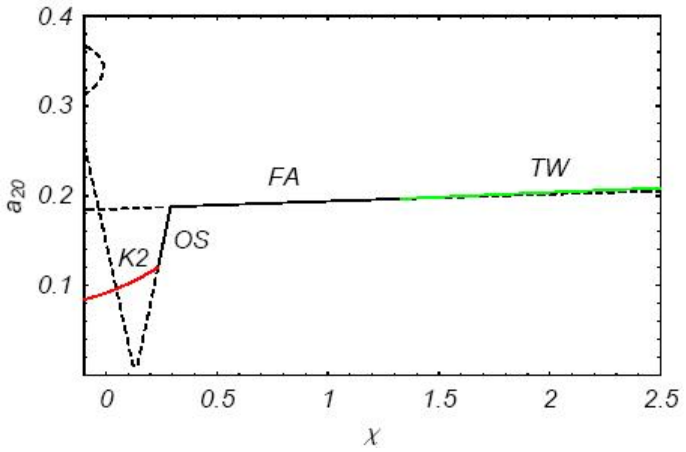

FIGURE 5.5. Bifurcation diagram of a_2^0, the coefficient of the spherical harmonic mode Y_2^0 (time averaged for periodic states), as a function of anisotropy χ at parameter values $Pe = 6, \tilde{a} = 1$ and $N = 5.5$. In this parameter regime, the stable attractor at small χ is K_2. It connects to a stable out-of-plane (OS) orbit as χ increases; the OS orbit comes down to a flow-aligning state as χ increases further. A tumbling/wagging orbit emerges at large values of χ!

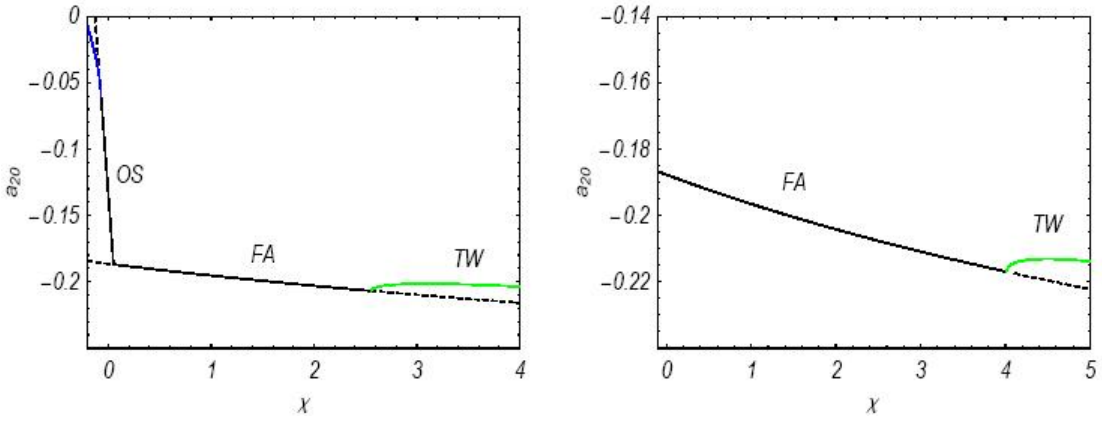

FIGURE 5.6. Bifurcation diagram of a_2^0, the coefficient of the spherical harmonic mode Y_2^0 (time averaged for periodic states), as a function of anisotropy χ at parameter values $\tilde{a} = 1$, $N = 5.5$ and $Pe = 6.5$ (left), $Pe = 7$ (right). For $Pe = 6.5$, the stable sheared attractor absent of a magnetic field is a pair of out-of-plane stable states OS. They collapse onto a flow-aligning state as χ increases. For $Pe = 7$, the stable attractor absent of magnetic field is a steady flow-aligned state FA. For both cases, a tumbling/wagging orbit emerges from the FA branch at large values of χ!

This sequence of numerical experiments shows that the impact of the magnetic field imposed perpendicular to the flow plane coupled with a negative anisotropy is to drive the out-of-plane peak axis of the PDF to a PDF with peak axis in-plane. However, at high Peclet numbers, the effect of anisotropy is two-fold: time-periodic motion is arrested at intermediate magnetic field strengths, but then limit cycle behavior is predicted to obtain at large anisotropy. This nonlinear effect of the anisotropy is a manifestation of the nonlinear material response to the external field, and experimental verification would be helpful to validate the theory.

Now we move on to four other sheared responses absent of the magnetic field. The first two are pictured in Figure 5.7 for $N = 5.1$, $\tilde{a} = 1$ and two values of Pe. For $Pe = 3$ (left), the stable attractors absent of the magnetic field are $K1$ and a chaotic orbit, CH. As χ increases, the $K1$ attractor disappears, leaving only the chaotic state. Then through period halving, the chaotic attractor disappears and a pair of $K2$ attractors emerge. Then, the $K2$ attractors sharply transition to steady OS and then onto in-plane steady states FA. Finally, at higher field strength, TW states emerge. For $Pe = 3.6$ (right), the bifurcation is similar. One of the main differences is that, absent of the magnetic field, only the chaotic response is an attractor.

The other two scenarios are pictured in Figure 5.8 for $N = 6$, $\tilde{a} = 1$, and two values of Pe. For $Pe = 7$ (left), the stable attractors absent of a magnetic field are LR and TW. As χ increases, the LR attractor becomes the periodic $K1$ attractor. Then at a turning point, $K1$ disappears. The TW state persists for all χ. For $Pe = 8.2$ (right), the stable attractor absent of a magnetic field is TW. This state persists as the magnetic filed is coupled.

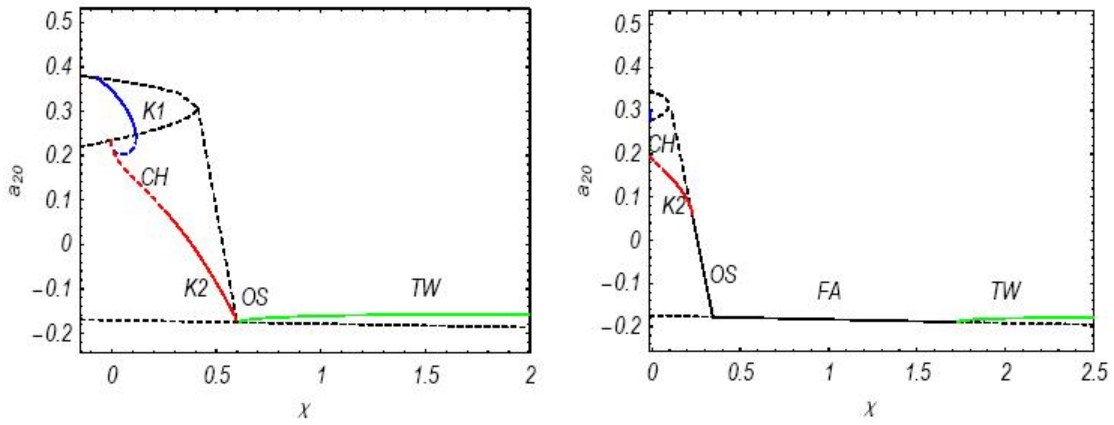

FIGURE 5.7. Bifurcation diagram of a_2^0, the coefficient of the spherical harmonic mode Y_2^0 (time averaged for periodic states), as a function of anisotropy χ at parameter values $\tilde{a} = 1$, $N = 5.1$ and $Pe = 3$ (left), $Pe = 3.6$ (right) . For $Pe = 3$ (left), the stable attractors absent of a magnetic field are $K1$ and CH. As χ increases , the $K1$ attractor disappears, leaving only the chaotic state. Then through period halving, the chaotic attractor transitions to a pair of $K2$, then OS steady out-of-plane states, then in-plane steady states FA, and finally TW limit cycles at sufficiently high amplitude. For $Pe = 3.6$ (right), the bifurcation sequence is similar.

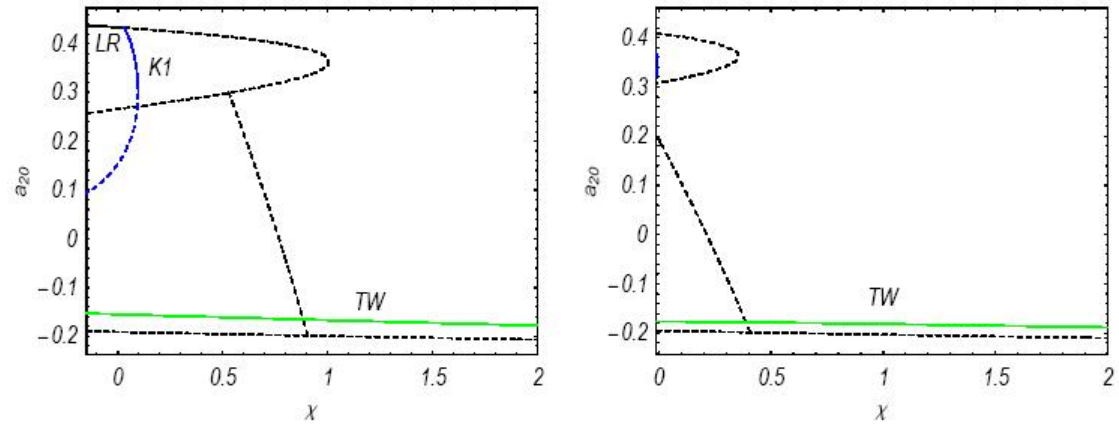

FIGURE 5.8. Bifurcation diagram of a_2^0, the coefficient of the spherical harmonic mode Y_2^0 (time averaged for periodic states), as a function of anisotropy χ at parameter values $\tilde{a} = 1$, $N = 5.1$ and $Pe = 7$ (left), $Pe = 8.2$ (right). For $Pe = 7$ (left), the stable attractors absent of a magnetic field are LR and TW. As χ increases, the LR transitions to $K1$ limit cycles, which disappear at a turning point, leaving only the TW limit cycle branch. For $Pe = 8.2$ (right), the stable attractor absent of a magnetic field is the TW limit cycle, which persists as the magnetic field turns on and amplifies.

5.4. Planar extensional flows coupled with a coplanar magnetic field

In dimensionless variables, the steady state solutions of the Smoluchowski equation are governed by the Boltzmann distribution with the potential Eq.(234), where

$$V = -\frac{3N}{2}\mathbf{M} : \mathbf{mm} - \frac{1}{2}D_e : \mathbf{mm}, \tag{240}$$

$$D_e = diag(Pe + \tfrac{\chi}{6}, -Pe + \tfrac{\chi}{6}, -\tfrac{\chi}{3}).$$

We choose coordinates to align with the three principal axes of the second moment tensor $\mathbf{M}$, $\mathbf{n}_{1,2,3}$, where $\mathbf{n}_3$ is the transverse external field direction. We parametrize the unit vector $\mathbf{m}$ by

$$\mathbf{m} = \cos\theta\mathbf{n}_1 + \sin\theta\cos\phi\mathbf{n}_2 + \sin\theta\sin\phi\mathbf{n}_3. \tag{241}$$

The second moment tensor also admits a biaxial representation

$$\mathbf{M} = s(\mathbf{n}_1\mathbf{n}_1 - \frac{\mathbf{I}}{3}) + \beta(\mathbf{n}_2\mathbf{n}_2 - \frac{\mathbf{I}}{3}) \tag{242}$$

where s and β are the two order parameters which describe degrees of anisotropy of the PDF . If either vanishes or equal, the PDF is uniaxial; if neither vanish nor equal, the PDF is fully biaxial. In the above parametrization, s and β satisfy the following equations

$$s - \frac{\beta}{2} = \langle\tfrac{3}{2}\cos^2\theta - \tfrac{1}{2}\rangle, \tag{243}$$

$$\beta = \langle\sin^2\theta\cos 2\phi\rangle,$$

where

$$\langle(\bullet)\rangle = \int_{\|\mathbf{m}\|=1}(\bullet) f d\mathbf{m},$$

$$f = \tfrac{1}{Z} e^{h},$$

$$h = \tfrac{3N}{2}[(s-\beta/2)\cos^2\theta + \tfrac{\beta}{2}\sin^2\theta\cos 2\phi] + \tag{244}$$

$$\tfrac{1}{2}[\tfrac{3}{2}(Pe+\tfrac{\chi}{6})\cos^2\theta + (\tfrac{-1}{2}Pe+\tfrac{\chi}{4})\sin^2\theta\cos 2\phi].$$

We first note that $\beta \neq 0$ unless $(-\frac{1}{2}Pe + \frac{\chi}{4}) = 0$. In fact, we can show steady states are all biaxial if

$$-\frac{1}{2}Pe + \frac{\chi}{4} \neq 0, Pe \neq 0 \tag{245}$$

Therefore, the steady states are primarily biaxial except in very special cases. We also note that for planar extension flows, we only need to discuss the case where $Pe \geq 0$ since $Pe < 0$ can be obtained through a 90^o planar rotation within the extension plane.

We denote the three non-negative eigenvalues of the second moment tensor by $d_{1,2,3}$, which characterize the degree of orientation with respect to each director $\mathbf{n}_{1,2,3}$, respectively. Then,

$$s = d_1 - d_3, \beta = d_2 - d_3 \tag{246}$$

Figure 5.9 depicts the steady state solutions at three selected values of the Peclet number $Pe = 0.01, 0.1, 1$, respectively, with $\chi = 1$. When $Pe = 0.01$, the effective rate of strain tensor is

$$D_e = diag(0.01 + 1/6, -0.01 + 1/6, -1/3) \tag{247}$$

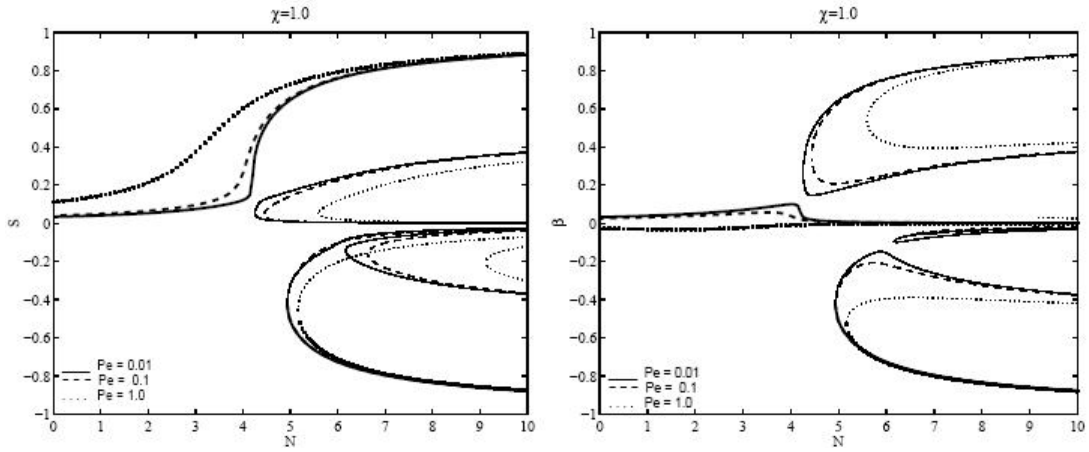

FIGURE 5.9. Order parameter s and β as functions of N at selected Peclet number $Pe = 0.01, 0.1, 1$. The anisotropy parameter is set at $\chi = 1$. The flow-aligning and the logrolling state (the major director is perpendicular to the flow) are the two stable states, in which the logrolling state is metastable. The solid black curves represent the stable branches.

All three directors align with the coordinate directions. The director in the flow direction $\mathbf{e}_1$ corresponds to a stable steady state where the order parameters satisfy $s > 0, \beta > 0, s > \beta$, implying

$$d_3 < d_2 < d_1 \tag{248}$$

We infer stability by examining the second variation of the generalized free energy density. Since the extension rate in $\mathbf{e}_1$ is the largest, the degree of orientation is the largest in that direction as well. In addition, the degrees of orientation correlate with the extension rate, i.e., the order of the degrees of orientation follows that of the extension rates. The scenario persists in the case of $Pe = 0.1$. However, when $Pe = 1$, the extension rate along $\mathbf{e}_3$ exceeds that along $\mathbf{e}_2$, the order of the degrees of orientation switches to

$$d_2 < d_3 < d_1 \tag{249}$$

This is captured from $\beta < 0$. Besides the stable steady state, there is another metastable state (a linearized stable state, but not a global minimum of the generalized free energy) given by a solution with the major director pointing in the direction perpendicular to the flow plane, for which $s < 0, \beta < 0$. This is shown by the second family of solutions in Figure 5.9, labeled dark solid. This is the so-called logrolling solution. We remark that this branch is unstable in the closure model due to the closure approximation [73].

At fixed value of Pe, the role of χ is to increase the extension rate in the plane while reducing it in the perpendicular direction. We expect the degree of orientation to increase in the flow direction in the flow-aligning stable steady state while decrease in the logrolling stable steady state. At concentrations less than $N = 5$, the logrolling steady state only survives up to a finite value of χ. However, when $N > 5$, it exists for all χ in the range we studied. Figure 5.10 and Figure 5.11 depict the steady states at selected Peclet number for $N = 4.7$ and $N = 6$, respectively.

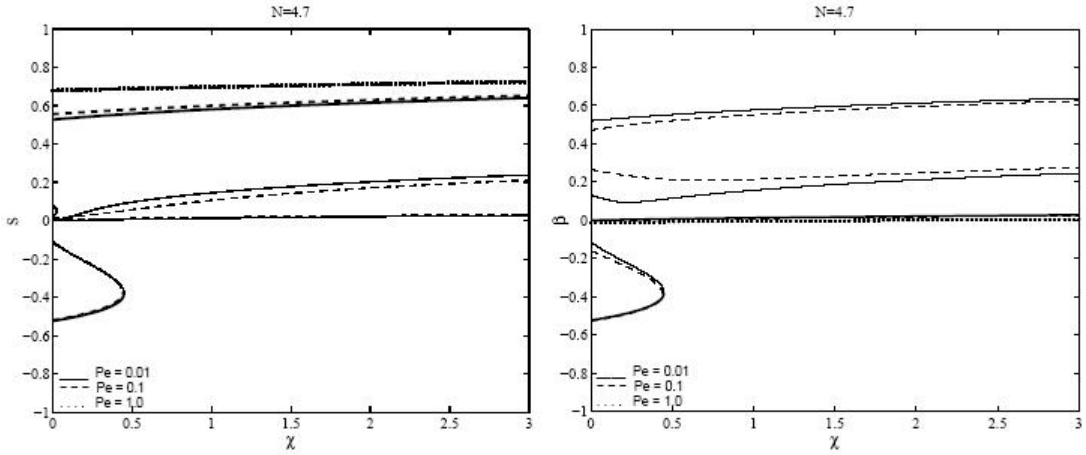

FIGURE 5.10. Order parameters s and β as functions of χ at selected Peclet numbers $Pe = 0.01, 0.1, 1$ and concentration $N = 4.7$. The flow-aligning and the logrolling state (the major director is perpendicular to the flow) are the two stable states, in which the logrolling state is metastable surviving only at small anisotropy. The solid black curves represent the stable branches.

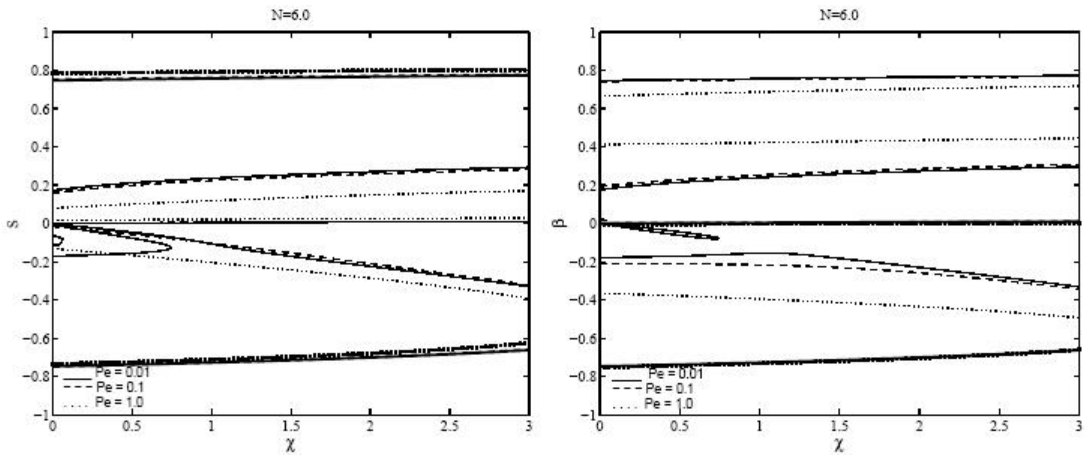

FIGURE 5.11. Order parameters s and β as functions of χ at selected Peclet numbers $Pe = 0.01, 0.1, 1$ and concentration $N = 6.0$. The flow-aligning and the logrolling state (the major director is perpendicular to the flow) are the two stable states, in which the logrolling state is metastable. The solid black curves represent the stable branches.

5.5. CONCLUSION

We have explored various phenomena associated with the strong coupling of coplanar linear flow and magnetic fields in rigid rod suspensions. The approach is based on a reciprocity relation of the Doi-Hess kinetic theory model, derived on [73], which reduces the problem to either of two simpler kinetic models, depending on whether the linear planar flow is rotational or irrotational. In the rotational case, we solve the kinetic equation with a new spherical harmonic Galerkin method, coupled with the continuation software AUTO. Various predictions are made, indicating a regularizing influence of a coplanar magnetic field on each type of sheared monodomain attractor. For irrotational flow, analytical results are given first based on a Boltzmann distribution for the PDF, followed by numerical solution of the resulting steady state equilibrium equations.

Chapter 6

Orientational dynamics of sheared BLCPs

In this Chapter, we present the nematodynamics of a mesoscopic system consisting of sheared biaxial liquid crystalline polymers (BLCPs) using a hydrodynamical kinetic theory developed in Chapter 3 in which the BLCP is modeled as rigid, biaxial, ellipsoidal molecules immersed in viscous solvent. The governing Smoluchowski equation in the model is solved in selected regions of the material parameter space and a range of accessible shear rates using the Wigner-Galerkin spectral method. In addition to the truly biaxial flow-aligning steady states, logrolling states and out-of-plane steady states, we report the presence of two new time-periodic motions, chaotic motion and associated phase transitions in the range of shear rates and selected material parameters. Rheological signatures of the sheared mesoscopic system are identified with predominant shear thinning in all phases and alternating signs between the normal stress differences in steady vs time-dependent motions. Finally, we detail the rheological responses in the range of accessible shear rates and selected material parameters.

6.1. Introduction

It was predicted in the 1970's that biaxial nematogens in liquid crystals may exhibit mesoscopic biaxiality at equilibrium under certain conditions besides the uniaxial symmetry reported earlier [42, 101, 102]. The theoretical prediction of the biaxial phase of biaxial nematogens by Freiser [102] was confirmed by computer simulations of biaxial liquid crystals in the 1990's and early 21st century [52, 36, 37, 33, 45]. It was not until 2004, when several groups of experimentalists, independently discovered

the biaxial phase using different biaxial nematogens [43, 31, 44, 47, 39]. In the past, studies on biaxial liquid crystals and their interactions with external fields were concentrated either on uniaxial phases of biaxial molecules [48] or on flow or external field induced biaxial phases of purely uniaxial molecules [74, 72, 75, 76]. Very few studies in this direction have touched upon the biaxial phases due to biaxial molecules. Leslie and his coworkers [107, 35] extended the well-known Ericksen-Leslie continuum theory to biaxial liquid crystals, where they derived the theory based on a single second order tensor. Recently, Virga *et al.* [97, ?, 34, 100] developed a self-consistent mean field theory for thermotropic biaxial liquid crystals employing two second order, trace-less biaxial tensors that account for both the intrinsic biaxiality and the induced mesoscopic phase biaxiality at equilibrium. This model was built upon the fundamental belief that D_{2h} symmetry remains in the biaxial system when coarse-grained to mesoscopic level. In addition to the thermotropic biaxial liquid crystals discovered recently [43, 31, 44, 47, 39], there had been lyotropic biaxial liquid crystal systems exhibiting biaxial phases being identified in the past [17, 32, 40]. However, in the presence of an asymmetric external field (like shear flow), the D_{2h} symmetry of the BLCP disappears and the two second order tensors ceases to have a common eigen-frame. The skewness between these two tensors highlights a drastically different mesoscale orientational structure in contrast to the equilibrium state. Hence, in this chapter we pursue the extension of the previously proposed thermodynamic mean-field theories [101, 97] to allow the hydrodynamic coupling between the biaxial nematogens and small molecule solvent in solutions of the BLCPs to study shear induced phases, motions, and phase transitions as well as associated rheological responses [78].

The chapter is organized as follows. In Sec.6.2, we briefly describe the kinetic theory for flows of BLCPs (derived in chapter 3), present the Smoluchowski equation

for a homogenous flow of BLCPs, modeled as ellipsoidal suspensions in viscous solvent and provide the Wigner- Galerkin spectral scheme required to solve the system (Sec.6.2.3). In Sec.6.3, we report and discuss the various aspects of the numerical results in sheared BLCPs: the presence of the newly discovered time-periodic and chaotic motions in addition to the steady-states; the associated *nematic order* and the mixed moments or correlation matrices with respect to the *orientational distribution function* which are used to describe the mesoscale material structures in fast motion ESR [64] and NMR [38] experiments (Sec.6.3.1). The rheological response of this sheared liquid crystal system is elucidated in Sec.6.3.2 . The chaotic regime is elaborated in Sec.6.3.3. The details on the derivation of the associated stress constitutive equation are supplemented in the Appendix A.

6.2. Kinetic theory and numerical method

We first present the kinetic theory for monodomain solution of BLCPs, in which the BLCP molecule is modeled as a rigid, ellipsoidal (or brick) shaped object immersed in viscous solvent. A Galerkin spectral method based on the Wigner function is developed to solve the Smoluchowski equation in the kinetic theory in the monodomain regime.

6.2.1. Kinetic theory. Let $f(\Omega, t)$ be the orientational *probability density function* (PDF) of the ellipsoidal (or brick-shaped), rigid biaxial nematogens, where $\Omega = (\alpha, \beta, \gamma)$ denotes the Euler angle triplet describing the instantaneous orientation of the mutually orthogonal molecular axes $(\mathbf{m}, \mathbf{n}, \mathbf{k})$ with respect to the fixed Cartesian frame (x, y, z). $\mathbf{m}$ is indentified as the longest semiaxis of length a, $\mathbf{n}$ the second longest of length b, and $\mathbf{k}$ the shortest of length c of the ellipsoidal molecule. i.e., $a > b > c > 0$. The transport of the PDF is governed by the kinetic or Smoluchowski equation in mesoscale accounting for the configurational space flux due to the Brownian motion of the molecules, the excluded volume or steric effect among the biaxial nematogens, and the flow-induced flux. The Smoluchowski equation in the molecular

(or rotating) frame is derived using the phase-space diffusion theory with constraints [85] and given by

$$\frac{\partial}{\partial t}f + \nabla(\mathbf{v}f) = \mathbf{L}^* D_r \cdot (\mathbf{L}f + \frac{1}{k_B T} f \mathbf{L}\mathcal{U}) - \mathbf{L}^* \cdot (\mathbf{g}f) \tag{250}$$

where

$$D_r = D_{r0}\zeta \; Diag(\frac{1}{1+r_b^2}, \frac{1}{r_b^2+r_c^2}, \frac{1}{1+r_c^2})$$

is the rotational diffusivity (assumed a constant matrix), D_{r0} is the rotational diffusivity of perfectly rigid spheres in an isotropic state, ζ is a scaling constant ($\zeta = 2$ when the ellipsoid degenerates into a sphere), $r_b = \frac{b}{a}, r_c = \frac{c}{a}$ are the two aspect ratios of the biaxial molecule; $\mathbf{L} = i\mathbf{x} \times \frac{\partial}{\partial \mathbf{x}}$ is the angular momentum operator; k_B is the Boltzmann constant, T is the absolute temperature; $\mathbf{g}$ is the torque due to the flow given by

$$\begin{aligned}\mathbf{g} = i[&\tfrac{\mathbf{m}}{r_b^2+r_c^2}(\nabla\mathbf{v} : (r_b^2\mathbf{nk} - r_c^2\mathbf{kn})) + \tfrac{\mathbf{n}}{1+r_c^2}(\nabla\mathbf{v} : (r_c^2\mathbf{km} - \mathbf{mk})) + \tfrac{\mathbf{k}}{1+r_b^2} \\ &(\nabla\mathbf{v} : (\mathbf{mn} - r_b^2\mathbf{nm}))],\end{aligned} \tag{251}$$

$\nabla\mathbf{v}$ is the velocity gradient of the velocity field $\mathbf{v}$; $\mathcal{U}$ is the excluded volume potential given by

$$\mathcal{U} = -\frac{3}{2} N k_B T[\xi_0 \mathbf{M} : \mathbf{mm} + \gamma_0(\mathbf{N} : \mathbf{mm} + \mathbf{M} : \mathbf{nn}) + \lambda_0 \mathbf{N} : \mathbf{nn}], \tag{252}$$

where $\mathbf{M} = \langle \mathbf{mm} \rangle$ and $\mathbf{N} = \langle \mathbf{nn} \rangle$ are the second moment tensors of $\mathbf{m}$ and $\mathbf{n}$ with respect to the pdf, respectively,

$$\langle (\bullet) \rangle = \int (\bullet) f(\Omega) d\Omega$$

denotes the ensemble average with respect to the pdf (f). N is dimensionless parameter measuring the strength of the potential, known as the strength of the intermolecular potential or dimensionless concentration [85], $(\xi_0, \lambda_0, \gamma_0)$ are two dimensionless material parameters characterizing the full range of the excluded volume potential and are linearly related to the parameters (γ, λ) of the Straley's pair-potential [101] as follows:

$$\xi_0 = 1 + 2\gamma + \lambda,\ \gamma_0 = 2(\gamma + \lambda),\ \lambda_0 = 4\lambda. \tag{253}$$

The free energy for the ensemble of the ellipsoidal suspension, consisting of the rotational Brown motion and the excluded volume interaction is given by

$$\mathcal{A}[f] = \nu \int_G [k_B T(lnf - f) + \frac{\mathcal{U}}{2}] f d\Omega, \tag{254}$$

where ν is the number density of the ellipsoidal molecules and G is the domain occupied by the ensemble system. The chemical potential is given by the variation of the free energy with respect to the number density:

$$\frac{\delta \mathcal{A}}{\nu \delta f} = k_B T[lnf + \frac{\mathcal{U}}{k_B T}]. \tag{255}$$

We introduce a normalized chemical potential denoted by

$$\mu = lnf + \frac{\mathcal{U}}{k_B T}. \tag{256}$$

6.2.2. Nondimensionalization. We consider an imposed plane shear flow field in this study

$$\mathbf{v} = (\dot{\gamma} y, 0, 0,) \tag{257}$$

where $\dot{\gamma}$ is the shear rate. We define the Peclet number as the dimensionless shear rate

$$Pe = \dot{\gamma} t_0 \tag{258}$$

We choose the characteristic time scale as

$$t_0 = \frac{1}{D_{r0}\zeta} \tag{259}$$

The dimensionless flow field for the plane shear in the Cartesian coordinate is then given by

$$\mathbf{v} = Pe(y, 0, 0). \tag{260}$$

After non-dimensionalization with the time-scale ($t_0 = \frac{1}{\zeta D_{r0}}$), Eq.(250) becomes:

$$\frac{\partial}{\partial \tilde{t}} f = \mathbf{L}^* \tilde{D}_r \cdot (\mathbf{L} f + \frac{1}{k_B T} f \mathbf{L}\mathcal{U}) - \mathbf{L}^* \cdot (\tilde{\mathbf{g}} f), \tag{261}$$

where $\tilde{D}_r = Diag(\frac{1}{1+r_b^2}, \frac{1}{r_b^2+r_c^2}, \frac{1}{r_c^2+1})$ and $\tilde{\mathbf{g}} = \tilde{\mathbf{g}}(Pe)$ which is the flow flux with the rate of strain tensor replaced by its dimensionless form. In our studies to follow, we will drop the tilde ˜ on the dimensionless quantities.

6.2.3. Numerical method. We employ a Wigner function based Galerkin spectral method to solve the Smoluchowski equation numerically. Using the Wigner function $\mathcal{D}^L_{mn}(\Omega)$ as the basis, we discretize the orientational PDF f as follows [75, 76]

$$f(t, \Omega) = \sum_{L=0, |m|, |n| \leq L}^{L_0} C_{Lmn}(t) \mathcal{D}^L_{mn}(\Omega), \tag{262}$$

where $C_{Lmn}(t)$ are the time-dependent generalized Fourier coefficients [62]. The discretized equations are obtained by enforcing the residual of the equation system to be orthogonal to the set spanned by the basis function

$$\{\mathcal{D}^L_{mn}(\Omega), |m|, |n| \leq L, 0 \leq L \leq L_0\}. \tag{263}$$

We solve for the coefficients $C_{Lmn}(t)$ with the initial conditions $C_{Lmn}(0)$ obtained at $f(0,\Omega) = f_0(\Omega)$, where $f_0(\Omega)$ is the equilibrium PDF [97, 100, 72, 74]. In the calculations, we use $L_0 = 10$ and the four-step Runge-Kutta scheme with the step size $\Delta t = 10^{-3}$ to advance the system in time.

Extensive numerical convergent tests have been done to ensure the code is indeed convergent as we increase the number of modes in the discretized system. The number of modes chosen in the computation is primarily based on the consideration of efficiency. For $L = 10$, the error of approximation is about 1%. It reduces to 0.1% should a much large L (say $L = 20$) is adopted. For practical purposes, the resolution at $L = 10$ suffices.

6.3. Numerical results in shear flows

The governing system of equations includes one flow parameter Pe, two molecular geometrical parameters r_b and r_c, and three material parameters associated with the steric interaction among molecules. Given the six-dimensional parameter space, an exhaustive search of the parameters is clearly beyond our reach. We therefore settle with numerical investigations carried out with selected sets of parameters in the parameter space. We first fix the molecular geometry parameters at $r_b = 0.51, r_c = 0.36$. Our analysis then focuses on the various orientational phases/structures and their transitions in a selected set of material parameter regimes and accessible shear rates along with the analysis of the order parameters, the mixed moment tensors and the rheological responses.

The $\mathcal{SO}_2$ rotational symmetry with respect to the molecular axis $\mathbf{m}$ and the D_{2h} symmetry in uniaxial liquid crystals ensures that the second moment $\langle \mathbf{mm} \rangle$ is sufficient to render the mesoscopic orientational information about the LCP ensemble. When the contiguous rotational symmetry is broken in the biaxial molecule, six second moments must be taken into account. From the autocorrelation matrices, we have already extracted four invariants named order parameters discussed in the previous

section. What orientational information do the major directors of the autocorrelation matrices and other three mixed moments $\langle \mathbf{mn} \rangle, \langle \mathbf{mk} \rangle, \langle \mathbf{nk} \rangle$ convey is an issue we will discuss next.

First, the three molecular axes $\mathbf{m}, \mathbf{n}, \mathbf{k}$ of the biaxial molecule are mutually orthogonal

$$\mathbf{m} \cdot \mathbf{n} = \mathbf{n} \cdot \mathbf{k} = \mathbf{m} \cdot \mathbf{k} = 0. \tag{264}$$

These scale up to the mesoscale to yield the following three trace conditions on the mixed moments

$$tr(\langle \mathbf{mn} \rangle) = tr(\langle \mathbf{mk} \rangle) = tr(\langle \mathbf{nk} \rangle) = 0. \tag{265}$$

Secondly, the mixed moments are the correlation matrices among the pairs of the molecular axes. Therefore, they provide additional mesoscopic information of molecular orientation, correlation and phase. We study these mixed moments by defining, what we term as, the effective *Orientational Correlation Functions* (OCF), for any pair of unit vectors $\mathbf{r}_i$ and $\mathbf{r}_j$,

$$\begin{aligned} \phi^{\mathbf{mn}}(\mathbf{r}_i, \mathbf{r}_j) &= \mathbf{r}_i^T \cdot \langle \mathbf{mn} \rangle \cdot \mathbf{r}_j \\ &= \langle (\mathbf{r}_i \cdot \mathbf{m})(\mathbf{r}_j \cdot \mathbf{n}) \rangle \\ &= \langle (\cos \angle \mathbf{r}_i \mathbf{m})(\cos \angle \mathbf{r}_j \mathbf{n}) \rangle \end{aligned} \tag{266}$$

which is the mean value of the product of the direction cosines of the angle between the pair of vectors $(\mathbf{r}_i,\ \mathbf{m})$ and the pair of vectors $(\mathbf{r}_j, \mathbf{n})$. Hence, $\phi^{\mathbf{mn}}$ gives the correlation between the projection of $\mathbf{m}$ onto the direction $\mathbf{r}_i$ and $\mathbf{n}$ onto the direction $\mathbf{r}_j$. Similarly, its *Auto Correlation Function* (ACF) ($\psi(\mathbf{r}_i) = \mathbf{r}_i \cdot \langle \mathbf{mn} \rangle \cdot \mathbf{r}_i$) is defined as the correlation between the degree of orientation of $\mathbf{m}$ and that of $\mathbf{n}$ in direction $\mathbf{r}_i$. The choice of $\mathbf{r}_i$ is fairly flexible depending on the problem investigated. We restrict our qualitative analysis in this paper to vectors $\{\mathbf{r}_i, \mathbf{r}_j\} \in \{\mathbf{m}_1, \mathbf{n}_1, \mathbf{k}_1\}$, where

$(\mathbf{m}_1, \mathbf{n}_1, \mathbf{k}_1)$ are the major directors of the second moments (**M**,**N**,**K**) respectively. Hence, by definition, the OCFs give measures of the correlational alignment of the molecular axes $(\mathbf{m}, \mathbf{n}, \mathbf{k})$ with respect to the mesoscale major directors $(\mathbf{m}_1, \mathbf{n}_1, \mathbf{k}_1)$.

Given the recent studies of Bisi et al. [34] on the equilibrium phase diagram of the biaxial liquid crystal using an extended Straley's potential, we focus on a few selected points in the material parameter space that are representatives of various biaxial phases and study how shear will alter the various biaxial states. Our numerical studies are carried out in the range of the shear strength $0.0 \leq Pe \leq 14.0$ and for LCP concentrations $N = 4.9, 5.5, 6.28, 7.84$, respectively. Based on the equilibrium phase behavior, we divide the admissible material parameters in the (γ, λ)-space into four regions (Figure 6.1). Region(A): $\lambda \geq 1.0$, where the excluded volume attractive interaction is highly biaxial (large value of λ; the coefficient of the purely biaxial term $\mathbf{N} : \mathbf{nn}$ in the potential); Region B: the region inside the space $\gamma^2 \leq \lambda < 1.0$ and bounded below by the tricritical curve C_1C_3 (refer to [34]), where a first order, temperature induced, phase transition from *isotropic* $\rightarrow$ *biaxial* phase in equilibrium was reported in [97]; Region C: the region inside the space $\lambda \geq \gamma^2$ and bounded above by C_1C_3, where the nature of the transition in region B changes to a second order transition from *isotropic*$\rightarrow$*uniaxial*$\rightarrow$*biaxial* phase, across the tricritical curve C_1C_3; Region D: $0 \leq \lambda < \gamma^2; |2\gamma| \leq 1 + \lambda$. The excluded volume potential in region (D) is not convex (partially repulsive). A detailed exercise in this region showed that the equilibrium free energy may not have a global minimum and hence the steady-state solution is obtained via a minimax principle [100, 34].

6.3.1. Orientational dynamics, phases and correlation functions. The nematic phases in equilibrium are torque-free in the presence of the excluded volume interaction. When shear is imposed, the external shear exerts a shear torque to the biaxial molecules to break down the D_{2h} rotational symmetry and to rotate the molecules. In response, the excluded volume potential exerts the elastic torque to

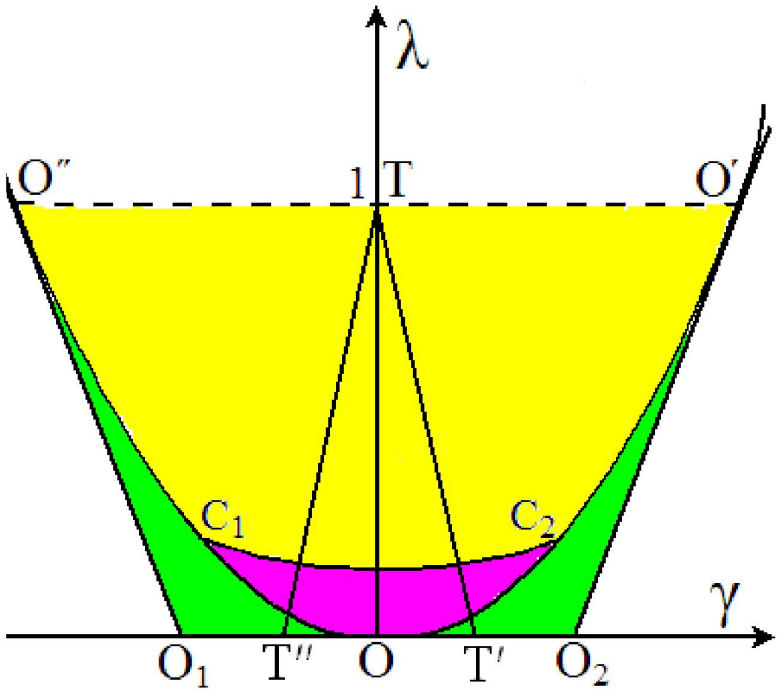

FIGURE 6.1. Range of admissible values of the material parameters (γ, λ) of the excluded volume potential, described in Eq.(252). The regions have the following color scheme: Region (A):white; Region (B):yellow; Region (C):magenta and Region (D):green. The curves TT', TT" and TO are explained in Section **??**. The coordinates of the labeled points are as follows: $O_1 : (-0.5, 0), T$" $: (-0.1634, 0), O : (0, 0), T' : (0.1634, 0), O_2 : (0.5, 0), O' : (1, 1), T : (0, 1), O$" $: (-1, 1), C_1 : (-0.469, 0.22), C_2 : (0.469, 0.22)$

counter the shear induced one. Various new states and motions arise out of the balance/inbalance between the two competing torques under shear. We note that in all our investigations major director of **M**, $\mathbf{m}_1$, is always the distinguished direction in the mesoscale ensemble and thereby maintains the major director of the system. The various orientational phases and structures found by our numerical investigations are (a) Log -Rolling **LR**, (b) Flow-Alignment **FA**, and (c) Out-of-Plane **OS** steady states; and periodic responses (d) Mixed-Kayaking **MK**, (e) Fluttering-Kayaking **FK**, and (f) Chaotic **CH** motion. The representative of each is shown in Figure 6.2, respectively. It is widely believed that the sets of eigenvectors of the two second moments **M** and **N** coincide in quiescent state. When the flow is present, however, they no long do so that **M** and **N** becomes skewed in their in-plane eigenvectors. In this

section, we describe the orientational dynamics, phases/states, and state transitions that occur at the four different regions of the material parameter space as we vary the Peclet number and the corresponding behavior of the order parameters and the correlation matrices. We discuss the results for each of the four regions, respectively.

6.3.1.1. *Region A.* In region(A), the sequence of orientational response is: **LR→OS →FA** via an out-of-plane steady state (OS). This is reminiscent of the flow-driven uniaxial liquid crystals in some concentration regime predicted using the Doi-Hess kinetic theory [76, 85]. The logrolling state, where the major director of the second moment tensor **M** aligns in the vorticity direction, is the one subject to the minimum elastic torque counter-balancing the flow-induced torque and is therefore the preferred stable steady state for the LCP at small Pe. As the shear strength increases, the strength of the flow-induced torque enhances. When the flow-induced torque exceeds a critical value, the counterbalancing elastic torque is sufficiently large to sustain the flow-aligning state so that the system suddenly switches to the flow-aligned (**FA**) steady state beyond the critical Pe^*, where the major director of the system $\mathbf{m}_1$ aligns approximately in the flow direction and remains so for all larger Pe. The value of this critical shear strength increases with the LCP concentration (N) because the excluded volume interaction becomes stronger with higher values of N.

Next, we detail the behavior of the order parameters $(s_1, \beta_1, s_2, \beta_2)$ at the point $(\gamma = 0.0, \lambda = 1.0)$ for steady states in region (A) (Figure 6.3). The critical value of shear at which the system goes through a phase transition is $Pe^* = 9.51$ (for N=4.9), $Pe^* = 9.72$ (for N=5.5), $Pe^* = 10.1$ (for N=6.28) and $Pe^* = 10.75$ (for N=7.84) respectively. In the LR state, the *intrinsic* uniaxial order parameter (s_1) decreases steadily and reaches its minimum at the end of the **LR** phase, when the major director ($\mathbf{m}_1$) is about to change its alignment from the vorticity to the flow velocity-gradient direction; in the FA state, the order parameter becomes monotonically increasing with respect to Pe. This can be interpreted statistically as follows: some of the biaxial

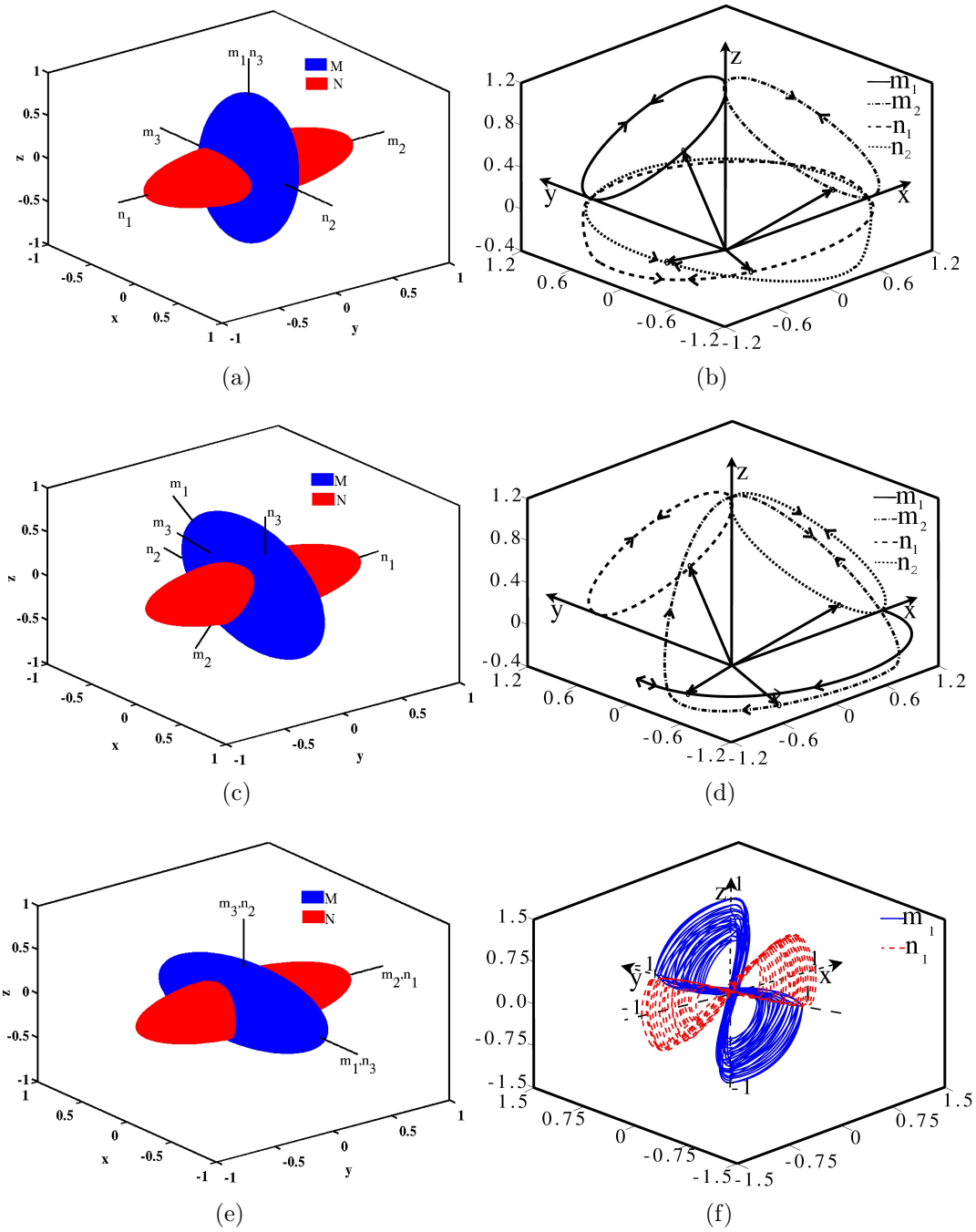

FIGURE 6.2. Orientational phases and motions: (a) Log-Rolling state ($Pe = 1.0, N = 7.84, \gamma = 0.08167, \lambda = 0.5$) (b) Periodic Mixed-Kayaking ($Pe = 7.6, N = 7.84, \gamma = 0.08167, \lambda = 0.5$ and Period T = 4.98) (c) Out-of-Plane steady state ($Pe = 9.0, N = 7.84, \gamma = 0.1389, \lambda = 0.15$) (d) Periodic Fluttering-Kayaking ($Pe = 9.7, N = 7.84, \gamma = 0.08167, \lambda = 0.5$ and Period T = 4.92) (e) Flow-Aligning state ($Pe = 12.0, N = 7.84, \gamma = 0.08167, \lambda = 0.5$) (f) Chaotic motion ($Pe = 1.32, N = 4.9, \gamma = 0.45, \lambda = 0.0093654$)

molecules simply rotate their long axis toward the flow direction as the shear strength increases leading to the reduced mesoscopic order in the vorticity direction; whereas when $\mathbf{m}_1$ is in the flow-aligned direction, more biaxial molecules turn their long axis to the direction enhancing the uniaxial order parameter.

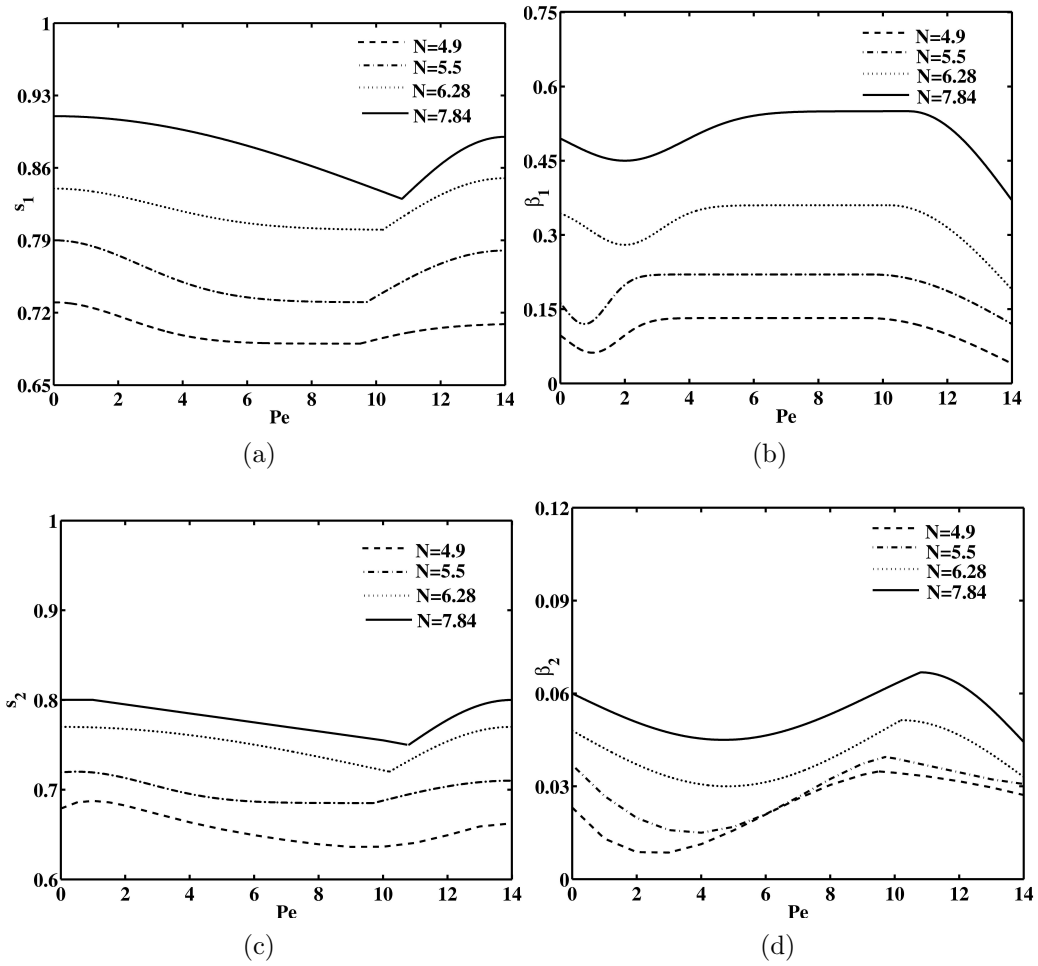

FIGURE 6.3. Order Parameters 'vs' non-dimensional shear strength (Pe) at ($\gamma = 0.0, \lambda = 1.0$) for different nematic concentrations (N).

Phase biaxial order parameter β_1 experiences an initial decline and then increase until the FA transition point, indicating an internal microstructure shakeup for the ensemble of biaxial molecules during the variation of Pe. The *intrinsic* or the *molecular* biaxiality parameter (β_2) first decreases and then shows a steady increase at intermediate shear correlating with the variation of β_1. This is not an coincidence since both measure the orientational discrepancy of biaxial molecular axes projected onto

the flow-velocity gradient plane. They bottom up at different location of Pe though, β_1 at a smaller Pe than β_2. Analogously, the overall biaxial order parameter s_2 varies in sync with the uniaxial order parameter s_1. At the critical value of shear strength (Pe^*), a continuous curve with a kink (jump in its derivative) in order parameters is observed in the three cases of $N = 5.5, 6.28, 7.84$ visibly but less so in the case of $N = 4.9$. In the **FA** phase, (s_1) shows a sudden and progressive increase (showing the tendency of $\mathbf{m}_1$ to progressively improve alignment along the flow direction) while (β_1 and β_2) decrease rapidly (relative to their mean value). The other order parameter (s_2), following a similar pattern as the order parameter (s_1), increases with Pe. The angle that the major director $\mathbf{m}_1$ makes with the flow axis (x-axis) is called the primary Leslie angle in the FA state; whereas the angle $\mathbf{n}_2$ makes with the velocity gradient direction is called the secondary Leslie angle. Figure 6.4 shows the behavior of the Leslie angles at ($\gamma = 0.0, \lambda = 1.0, N = 7.84$) for one representative solution. At the **LR** state, the secondary Leslie angle is negative while the primary Leslie angle is not defined. At the **FA** state, the primary angle is positive while the secondary Leslie angle is negative. Both the Leslie angles gradually decay to zero as Pe increases. Notice that the secondary Leslie angle varies continuously from the **LR** state into the **FA** state despite that the underlying state undergoes **LR**-→**FA** transition.

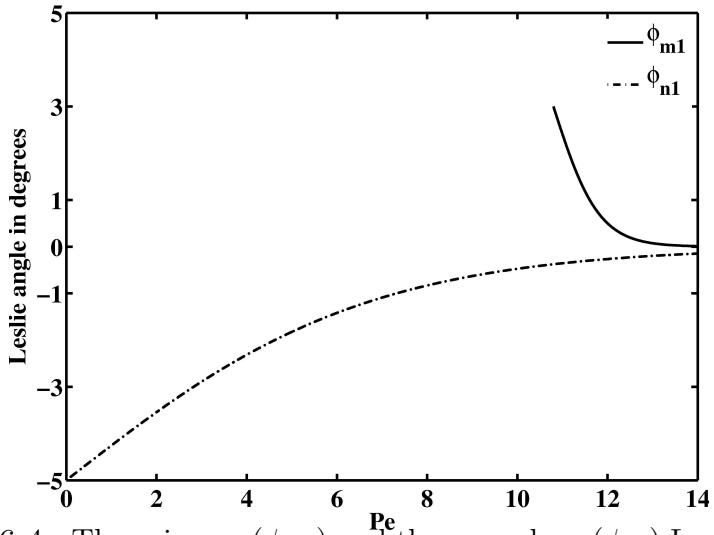

FIGURE 6.4. The primary ($\phi_{\mathbf{m}_1}$) and the secondary ($\phi_{\mathbf{n}_1}$) Leslie angles at ($\gamma = 0.0, \lambda = 1.0, N = 7.84$), a point in Region(A)

Correlation functions ($\langle\mathbf{mn}\rangle, \langle\mathbf{nk}\rangle, \langle\mathbf{km}\rangle$) at ($\gamma = 0.0, \lambda = 1.0, N = 7.84$) are shown in Figure 6.5. At equilibrium (Pe=0.0), the OCFs and ACFs are zero or nearly zero (within the limits of numerical error), suggesting a complete lack of correlation among the molecular axes in equilibrium. This also suggests that the eigen-frames of the second moments (**M,N,K**) are identical at equilibrium. However, as the shear strength increases, this alignment is rapidly distorted. As a result, they diverge monotonically from their equilibrium values. The absolute values of the OCFs converge to two localized band centered at 0.25 and 0.5, respectively. The ACFs ($\psi(\mathbf{mn}), \psi(\mathbf{nk}), \psi(\mathbf{km})$) remain close to zero in the weak shear regime and converge progressively towards a non-zero value as the shear strength increases. They converge to a band of values near 0.5 in absolute values at high shear strength (i.e. Pe $\geq$ 10); suggesting that an overall enhanced correlation among the molecular axes exists in the high shear region. These correlation functions seem not to be sensitive to the phase/state transition from LR to FA.

6.3.1.2. *Region B.* In region (B), at high concentration (N=5.5,6.28,7.84), the major director $\mathbf{m}_1$ of the second moment **M**, changes its alignment from the **LR** state at low Peclet numbers to the **FA** state at high Peclet numbers via a couple of exotic out-of-plane time periodic motions termed as the mixed- kayaking (**MK**) and the fluttering-kayaking (**FK**) motion, depicted in Figure 6.2. The **MK** motion is a tilted kayaking of $\mathbf{m}_1$ combined with the full kayaking of the major director $\mathbf{n}_1$ of the second moment **N** [41, 106, 77, 75, 76]. In the **MK** phase, $\mathbf{m}_1$ and $\mathbf{m}_2$ (the second eigenvector of **M**) collectively go through a coordinated tilted motion about their respective tilted axis; whereas, $\mathbf{n}_1$ and $\mathbf{n}_2$ (the second eigenvector of **N**) rotate about the vorticity axis in a weakly non-planar fashion, imitating a full-blown kayaking move against the flow velocity-gradient plane. In the **FK** motion, $\mathbf{m}_1$ wags in the flow velocity-gradient plane while $\mathbf{m}_2$ goes through a truly nonplanar circular motion. The coordinated motion of $\mathbf{m}_1$ and $\mathbf{m}_2$ is reminiscent of the fluttering fall of a leaf or a feather in the air. In the meantime, $\mathbf{n}_1$ and $\mathbf{n}_2$ rotate around two tilted

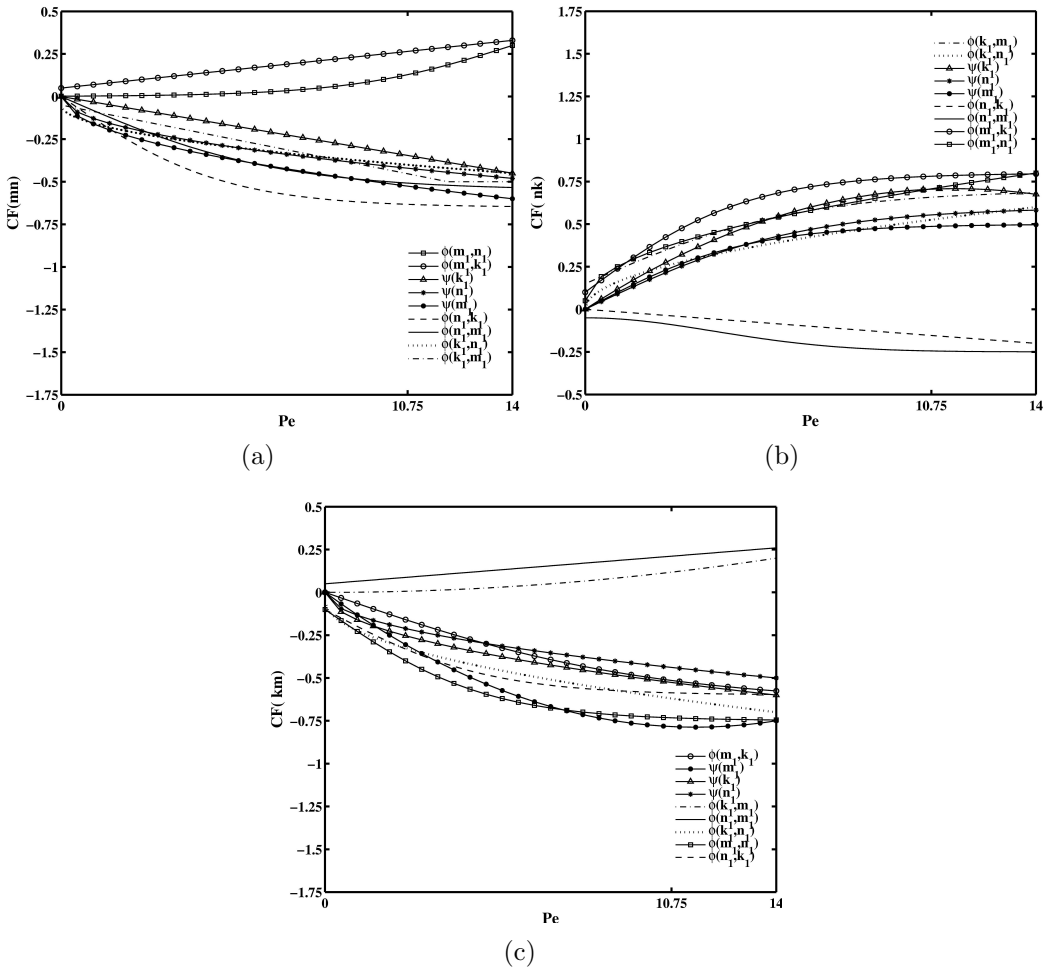

FIGURE 6.5. *Orientational Correlation Functions* of (a) $\langle \mathbf{mn} \rangle$ (b)$\langle \mathbf{nk} \rangle$ (c)$\langle \mathbf{km} \rangle$ at $(\gamma = 0.0, \lambda = 1.0, N = 7.84)$. The meso-structure makes a transition **LR**→**FA** at $\nu^* = 10.75$. However, the correlation functions seem not to be affected.

axes coordinately, analogous to the major director motion of the tilted kayaking. In both the **MK** and the **FK** motion, the orbits of the pair of directors going through the tilted kayaking osculate each other near the vorticity axis. The motion of the two second moment tensors **M** and **N** is skewed most of the time in these time-periodic motion and the angle between $\mathbf{m}_1$ and $\mathbf{n}_1$ oscillates between 40^o and 140^o within a period (Figure 6.6).

In the **LR** state, the secondary Leslie angle is negative with a decaying magnitude as Pe increases. It vanishes at the Pe value where the **MK** motion ensues. The primary

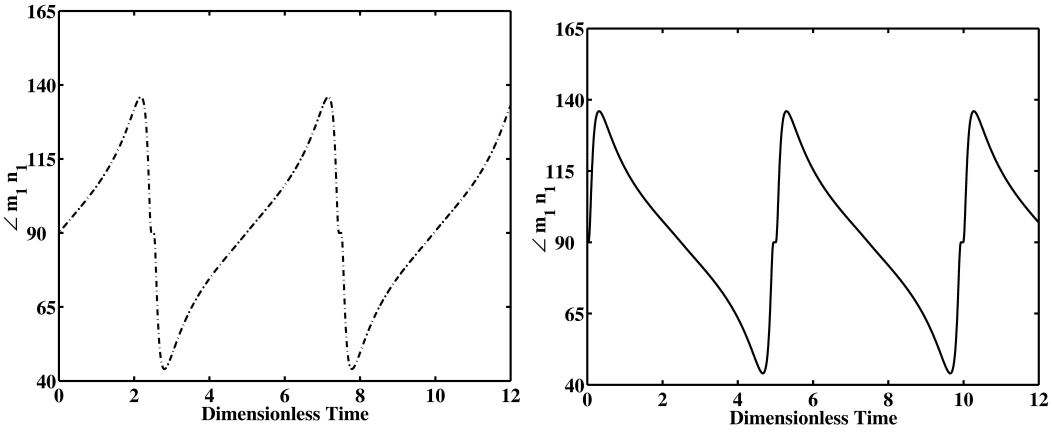

FIGURE 6.6. Angle between $\mathbf{m_1}$ and $\mathbf{n_1}$ in (a) **MK** phase (b) **FK** phase

Leslie angle emerges positive while the secondary one negative at the beginning of the FA state. As Pe increases, they both converge to zero. Figure 6.7 depicts the two Leslie angles as functions of Pe.

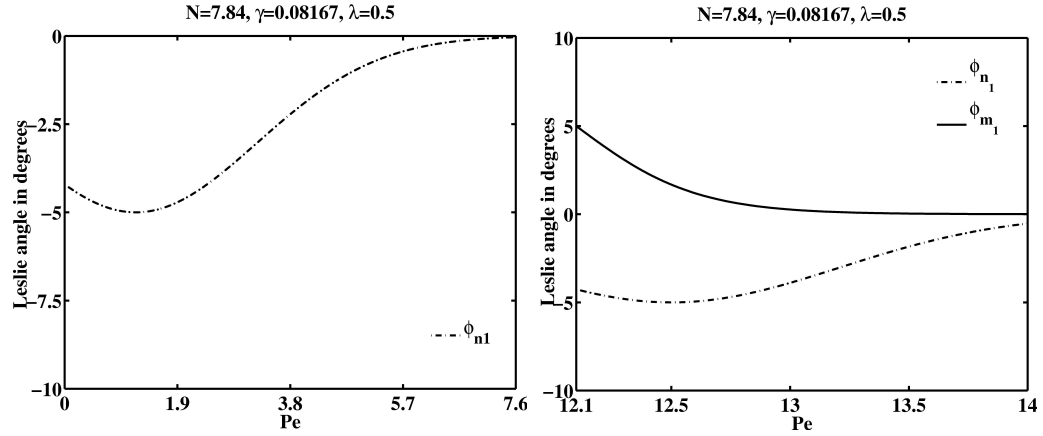

FIGURE 6.7. The primary ($\phi_{\mathbf{m}_1}$) and the secondary ($\phi_{\mathbf{n}_1}$) Leslie angles in the steady (a)Log-rolling phase (b)Flow-aligning phase at a point in Region(C)

The eigenvalues of $\mathbf{M}$ corresponding to $\mathbf{m}_1$ and $\mathbf{m}_2$, which measure the degree of orientation about the eigenvectors, fluctuates within 2% of their mean value (refer Figure 6.8a ,Figure 6.8b). The wagging motion of the primary major director $\mathbf{m}_1$ yield a time-periodic change of the degree of orientation about the major axis by the long molecular axis abruptly at the moment when the director swings back. In

the absence of any out-of-plane steady state (**OS**) in this region, there is an abrupt transition of the out-of-plane state of the directors from the **MK** state to the in-plane (x-y plane) wagging in the **FK** state which resembles a first order "phase transition". The time-averaged free energy density captures this abrupt change from the **MK** state to the **FK** state , shown in (Figure 6.8c). Hence, the sequence of phase changes in this region is: **LR**→**MK**→**FK**→**FA** for $N = 5.5, 6.28$. At $N = 7.84$, the jump in the time-averaged free energy density disappears so that the transition improves to a second order phase transition. At any phase/state transition, the free energy density shows either a kink or a jump discontinuity in Figure 6.8. This reveals that the transition between other adjacent states resembles the second order transition! At lower concentration (N=4.9), this sequence reduces to: **LR**→**OS**→**FA**. The transition resembles a second order phase transition.

The order parameters $(s_1, \beta_1, s_2, \beta_2)$ at the point $(\gamma = 0.0817, \lambda = 0.5)$ in region (B) are shown in Figure 6.9. The critical values of shear at which the system experiences a phase transition is $Pe^* = 5.8$ (for N=4.9); $Pe^* = 5.1, 6.3$ and 8.2 (for N=5.5); $Pe^* = 6.4, 8.3$ and 10.5 (for N=6.28) and $Pe^* = 7.6, 9.7$ and 12.1 (for N=7.84) respectively. As usual, irrespective of the nematic concentration (N), s_1 decreases steadily in the **LR** phase and reaches a minimum value at the end of this phase. At N=5.5,6.28,7.84; when the system undergoes the periodic **MK**-phase; the order parameter s_1 shows a non-monotonic behavior, i.e. s_1 increases, reaches a peak at an optimal value of Pe and then decreases thereby reaching a minimum value at the end of this phase. This trend repeats in the following periodic **FK**-phase. This indicates that the long axis of the BLCP molecule can be more aligned in the direction of the major director of the system at some Pe during the periodic motions; near the transition Pe, the nematic order tends to get frustrated and thereby reduces. A persistent improvement in the nematic order for $\mathbf{m}_1$ is only seen in the FA state as Pe increases. These *bumps* in s_1 are not visible at N=4.9 since the periodic phases are absent for this value of BLCP concentration. The order parameter variation with

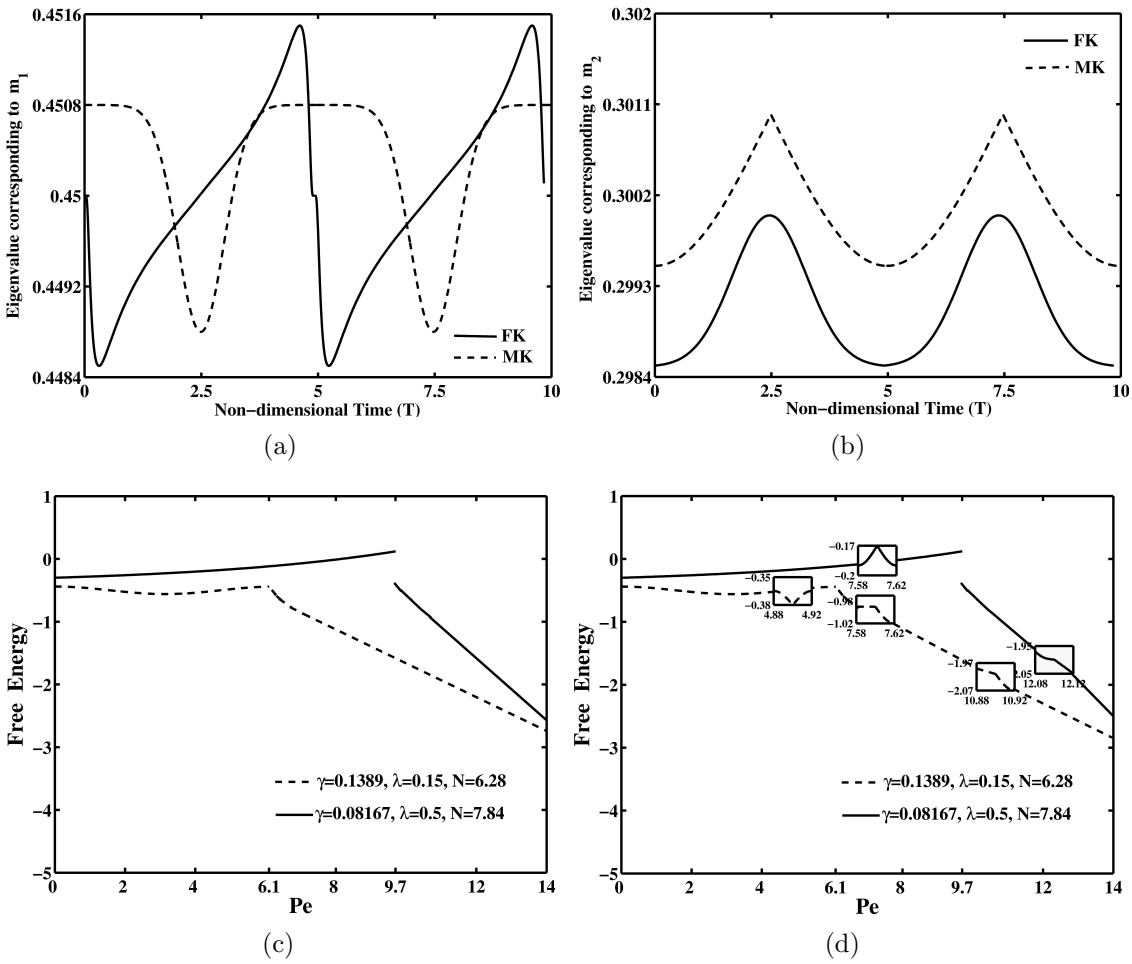

FIGURE 6.8. Eigen-values in the periodic **MK** and **FK** motion corresponding to the eigen-vector (a)$\mathbf{m}_1$ (b)$\mathbf{m}_2$ (c) The time-averaged free energy density versus Pe. A first order transition at Pe=9.7 in region (B) (dashed line) and a 2^{nd} order transition at Pe=6.1 in region (C) (solid line) is shown. (d) The same free energy data, highlighting the *small* second order transitions at critical Pe-values

respect to Pe in s_1, s_2 and β_2 are an analogous to the scenario alluded to in Region A. The biaxial order β_1, however, shows monotonic decreasing in LR state and increasing in FA state.

The *phase* biaxial parameter β_1, decreases in the **LR** and in the subsequent **MK**- and largely in the **FK**-phase. In the **FA**-phase it remains more or less a concave-down shape. The *molecular* biaxiality (β_2) first decreases and then shows a slight increase in the **LR** phase. Its variation in the subsequent phases is nonmonotone and perhaps

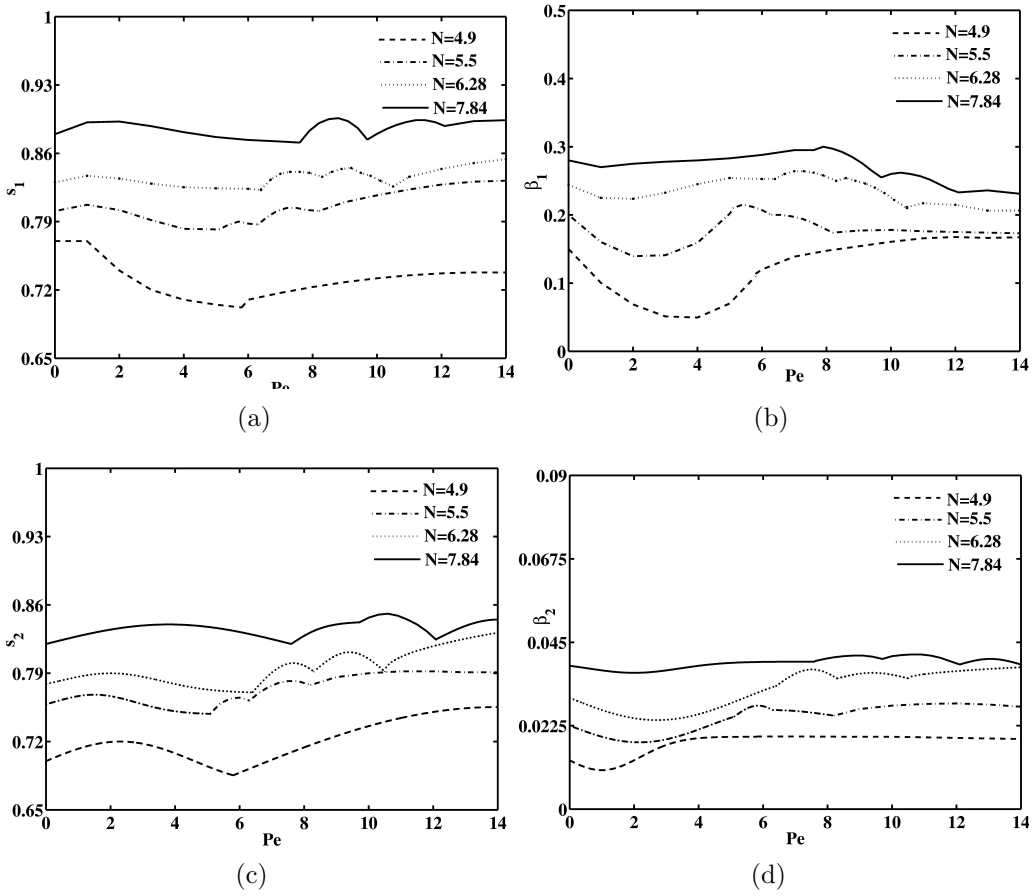

FIGURE 6.9. Order Parameters 'vs' non-dimensional shear strength (Pe) at ($\gamma = 0.0817, \lambda = 0.5$) for different nematic concentrations (N).

negligible. The *overall* biaxiality parameter s_2 varies in a pattern which is similar to s_1. Each of these order parameters show a visible second order discontinuity at the critical Pe-values at which the system undergoes a phase transition. The correlation functions (OCF) and the auto correlations (ACF) (refer Figure 6.10) diverge away progressively from their values at equilibrium with an increase in the shear strength. We observe like in Region A, there exist exactly two OCFs in each subplot converge to a narrow and around 0.25 while the rest go to a band centered at 0.5. Between the two OCFs, one converges to 0.25 while the other -0.25. The correlation functions are insensitive to the state/phase transitions shown in the figure.

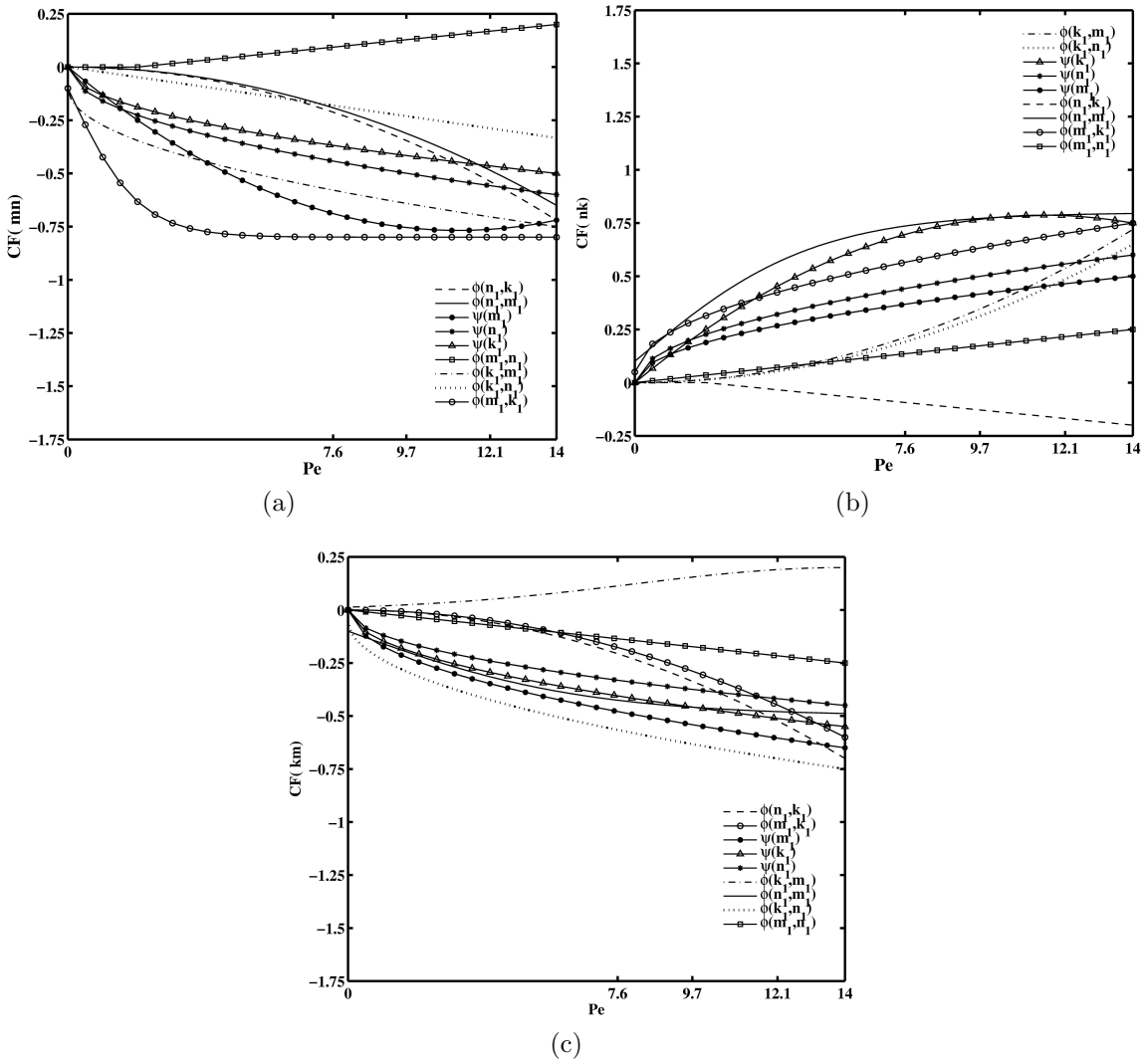

FIGURE 6.10. *Orientational Correlation Functions* of (a) $\langle \mathbf{mn} \rangle$ (b)$\langle \mathbf{nk} \rangle$ (c)$\langle \mathbf{km} \rangle$ at $(\gamma = 0.0817, \lambda = 0.5, N = 7.84)$. The meso-structure makes the transition **LR**→**MK**→**FK**→**FA** at $(\nu^* = 7.6, 9.7, 12.1)$ respectively.

6.3.1.3. *Region C.* In region (C), the state at concentrations $N = 5.5, 6.28, 7.84$ changes gradually in the sequence **LR**→**MK**→**OS**→**FK**→**FA**; as the shear rate increases. At a lower concentration (N=4.9), the sequence is **LR** → **OS** → **FA**, with the transitions occurring at (Pe^*=4.7, 5.9), respectively. At N=4.9 , a weaker excluded volume potential induces a smaller elastic torque to balance the imposed shear torque. The system prefers to remain in one of the steady states and the periodic

transitions vanish. The existence of the out-of-plane steady state **OS** (where the major director $\mathbf{m}_1$ points away from the flow velocity-gradient plane), implies that the transition of $\mathbf{m}_1$ from the out-of-plane unsteady **MK** phase to the in-plane unsteady **FK** phase is a continuous (or *second order*) phase/motion transition. This fact is corroborated by the free-energy diagram in Figure 6.8. The second moment tensors **M** and **N** are primarily skewed and non-planar during these unsteady motions. Even in the **LR** and the **FA** state, **M** and **N** share the vorticity axis as the common eigenvector direction, but the two tensors are skewed on the flow velocity-gradient plane signifying a shear-induced broken symmetry. In the transitional out-of-plane steady state (**OS**), all eigenvectors are skewed leading to additional broken symmetries. The difference between the steady states at $N = 4.9$ and the steady states in region A is that the OS state in this sequence exists on a computational resolvable interval of Pe while it virtually jumps to **FA** state from **LR** in region A.

The order parameters at $(\gamma = 0.1389, \lambda = 0.15)$, a point in region (C) are shown in Figure 6.11. The critical shear strengths at which the phase transitions occur are at Pe^*=4.7,5.9 (for N=4.9); Pe^*=4.2, 5.1, 6.3 and 9.3 (for N=5.5); Pe^*=4.9, 6.1, 7.6 and 10.9 (for N=6.28); and Pe^*=5.8, 7.3, 9.1 and 13.0 (for N=7.84) respectively. The *intrinsic* uniaxiality parameter, (s_1) , varies slowly on a concave-down curve in the **LR**-phase and then increases monotonically at the beginning of the next phase in various rates in different phases. The *intrinsic* biaxiality (β_2) , first shows a dip and then rises steadily in the **LR** phase. At higher nematic concentration, the maximum value of (β_2) is obtained at the end of the **MK** phase and at the beginning of the out- of-plane steady state phase (**OS**). The other two order parameters (s_2 and β_1) follow the pattern which is similar to order parameter (s_1 and β_2) respectively. Unlike in Region (B), the choice of the material parameters (γ, λ) forces s_1 (and s_2) monotonically increase starting from the periodic **MK**-phase. In the Out-of-Plane steady state (**OS**), all the order parameters evolve linearly: $s_{1,2}$ increase while $\beta_{1,2}$

decrease demonstrating a refocusing effect for the long axis of the BLCP molecule to the major director direction of the system. s_1 increases linearly with a slope: 0.0096 (at N=4.9), 0.0097 (at N=5.5), 0.0105 (at N=6.28) and 0.0111 (at N=7.84). β_1 decays with a slope: -0.0082 (at N=4.9), -0.0121 (at N=5.5), -0.0200 (at N=6.28) and -0.0361 (at N=7.84). The slope of s_2 is: 0.0167 (at N=4.9), 0.0250 (at N=5.5), 0.0340 (at N=6.28) and 0.0310 (at N=7.84), respectively, while the slope of β_2 is: -0.0021 (at N=4.9), -0.0020 (at N=5.5), -0.0013 (at N=6.28) and -0.0011 (at N=7.84), respectively.

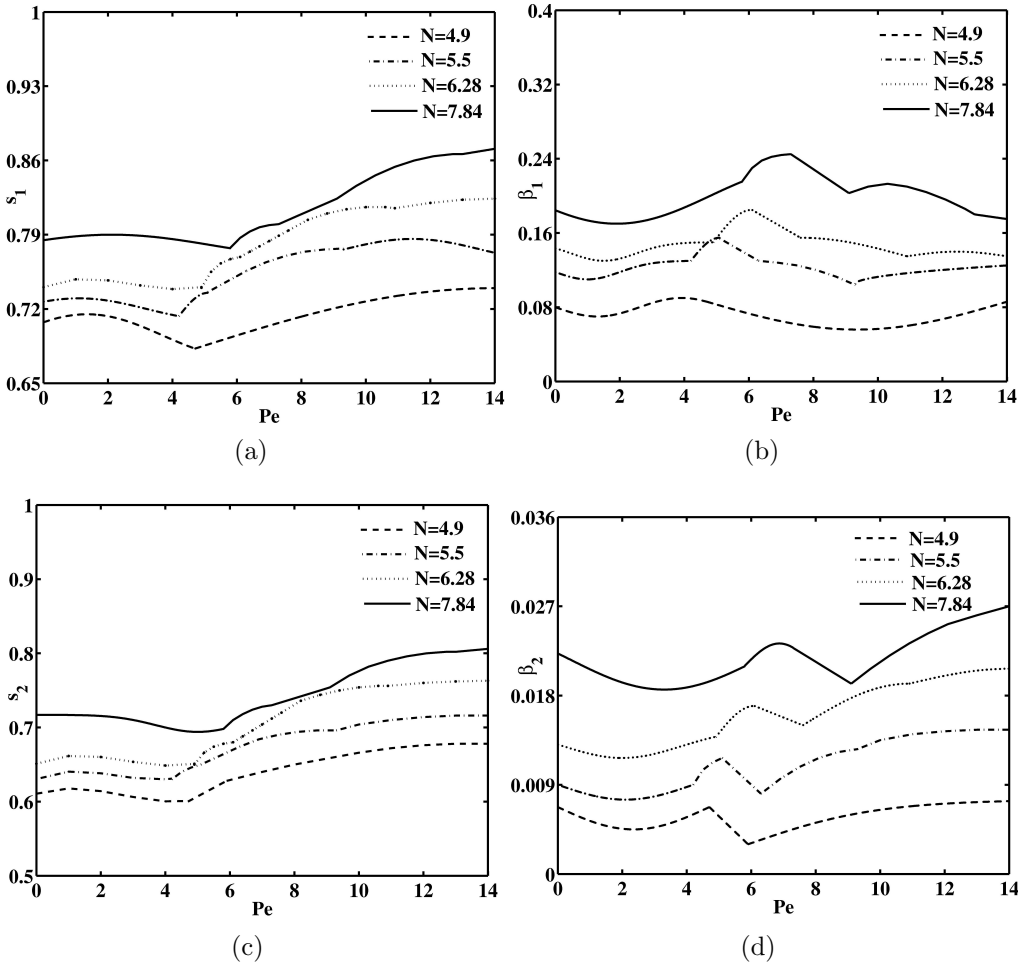

FIGURE 6.11. Order Parameters 'vs' non-dimensional shear strength (Pe) at (γ=0.1389, λ=0.15) for different nematic concentrations (N).

The correlation functions at ($\gamma = 0.1389, \lambda = 0.15, N = 7.84$) remain close to zero in the weak shear regime and we again see a rapid divergence of the OCFs and the

ACFs towards a non-zero value with an increase in shear strength. Noticeably, one OCF shows distinctive sign than the rest of the correlation functions analogous to the scenario seen in Region B.

6.3.1.4. *Region D.* Finally in region (D), we observe two different sequences of states as Pe varies. At γ= 0.16198, λ=0.0093654 and N=5.5,6.28,7.84, we have the sequence **MK**→**OS**→**FK**→**FA**. At lower LCP concentration (N=4.9), this sequence reduces to **OS**→**FK**→**FA**. The other sequence is **MK**→**CH**→**FK**→**FA** at γ=0.45, λ=0.0093654 and N=4.9, where **CH** stands for the chaotic state. The logrolling phase is absent in this region because the repulsive excluded volume interaction is weakly biaxial (smaller value of λ) and the torque due to shear dominates.

The chaotic solution (**CH**) arises at N=4.9 from the periodic **MK** state, inside the Peclet window $1.15 \leq Pe \leq 2.5$. The solution shows period-doubling bifurcations, which leads to a harmonic cascade (see Table Table 6.1), starting from a periodic rotation of $\mathbf{m}_1$ about a tilted axis. Figure 6.12a shows the evolution of $\mathbf{m}_1$ and $\mathbf{n}_1$ in this chaotic regime, where two attractors for the major director $\mathbf{m}_1$ in the vicinity of the two tilted axes in the **CH** motion can be easily identified. An estimate of the maximal Lyapunov exponent was performed with the method used in [121]. Figure 6.12b depicts the stretching factor versus the non- dimensional iteration time after an initial transient. The slope of the function (indicated by the dashed line) at intermediate time, gives an estimate of the maximal Lyapunov exponent. This quantity is positive ($\lambda_1 \sim 0.228$) and thus confirms the chaotic motion.

During the chaotic motion, the degrees of order measured by the eigenvalues of the second moments oscillate irregularly. The range of oscillation for the largest eigenvalue of the second moment tensor **M** is about 6% while the largest eigenvalue of **N** fluctuates about 8% (Figure 6.13).

The order parameters at ($\gamma = 0.16198, \lambda = 0.0093654$) are shown in Figure 6.14. The critical shear strengths at which the phase transitions occur are at ν^*=3.7, 5.1

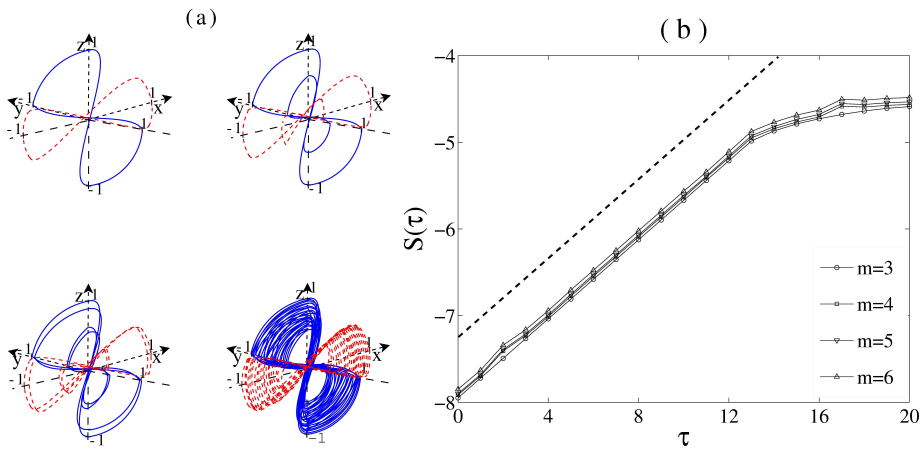

FIGURE 6.12. (a) The trajectory of the eigenvectors $\mathbf{m_1}$ (marked solid blue) and $\mathbf{n_1}$ (marked dashed red) after an initial transient. The parameter values are N=4.9 , γ=0.45, λ=0.0093654 and (i) Pe=1.15; (ii) Pe=1.22; (iii) Pe=1.26; (iv) Pe=1.32. (b) Stretching factor (details in [**?**]) versus the iteration time at different embedding dimensions 'm' and $Pe = 2.00$. The starting distance between any two trajectories is $\epsilon = 0.002$. The dashed line indicates the slope at intermediate time.

Label	Pe	F = $\frac{Pe_i - Pe_{i-1}}{Pe_{i+1} - Pe_i}$
PDL_1	1.161	...
PDL_2	1.225	1.575
PDL_3	1.266	1.819
PDL_4	1.289	1.951
PDL_5	1.300	...
PDR_1	2.472	...
PDR_2	2.381	2.299
PDR_3	2.341	1.988
PDR_4	2.321	...

TABLE 6.1. Column: (a) Shear strength corresponding to period doubling bifurcations. (b)Feigenbaum number (F) which approaches the limit $F \to 1.958$, a typical feature of harmonic cascading.

(for N=4.9); ν^*= 3.4, 4.6 and 5.8 (for N=5.5); ν^*=4.0, 5.5 and 7.3 (for N=6.28) and ν^*=5.2, 7.0 and 9.1 (for N= 7.84) respectively. The *intrinsic* uniaxiality parameter (s_1) shows an increase of about 11% while the *molecular* biaxiality (β_2) increases by about 40%, as the shear strength increases from 0 to 14. The increase in the *overall* biaxiality (s_2) is about 16%. The *phase* uniaxiality (β_1) decreases by about 50% of it's initial value at Pe=0.0. In this region and for all N investigated, the uniaxial

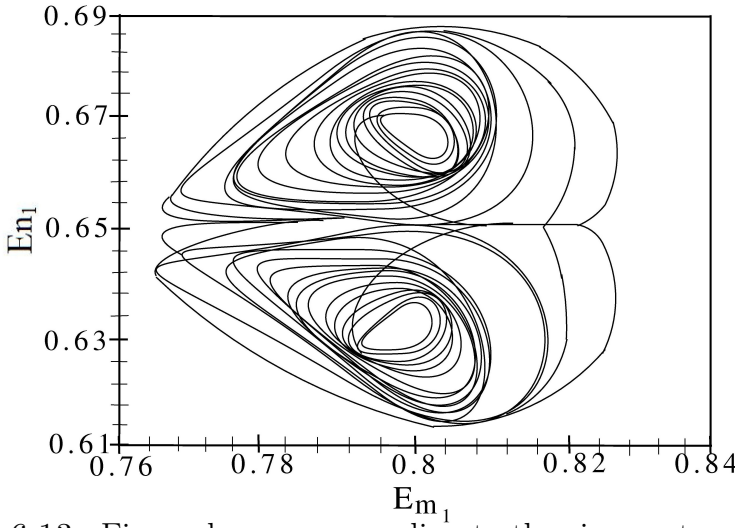

FIGURE 6.13. Eigenvalues corresponding to the eigenvectors $\mathbf{m_1}$ and $\mathbf{n_1}$ after an initial transient. The parameter values are N=4.9, γ=0.45, λ=0.0093654 and Pe=1.32.

order parameter s_1 increase monotonically with the shear strength. In the Out -of-Plane steady state (**OS**), the order parameters either increase or decreases linearly. s_1 increases linearly with a slope: 0.0041 (at N=4.9), 0.0167 (at N=5.5), 0.0200 (at N=6.28) and 0.0333 (at N=7.84). β_1 decays with a slope: -0.0041 (at N=4.9), -0.025 (at N=5.5), -0.0083 (at N=6.28) and -0.0056 (at N=7.84). The slope of s_2 is: 0.0054 (at N=4.9), 0.0667 (at N=5.5), 0.0668 (at N=6.28) and 0.0668 (at N=7.84) while the slope of β_2 is: -0.0011 (at N=4.9), -0.00083 (at N=5.5), -0.0008 (at N= 6.28) and -0.00079 (at N=7.84). The biaxial order parameter β_2 exhibits small numerical values consistently in the region.

The correlation and the auto correlation functions at ($\gamma = 0.16198, \lambda = 0.0093654, N = 7.84$) in region D show similar behavior as in region B indicating enhanced correlation in the mesoscopic system at higher shear strength.

6.3.2. Rheology. In this section, we discuss the rheological responses (normal stress differences N_1, N_2, shear stress τ_{12} and the apparent viscosity τ_{app}) of flows of BLCPs in the four regions of the material parameter space. The friction coefficients (η, ζ_0) in the viscous stress are chosen as (0.01,0.035) respectively. The choice of

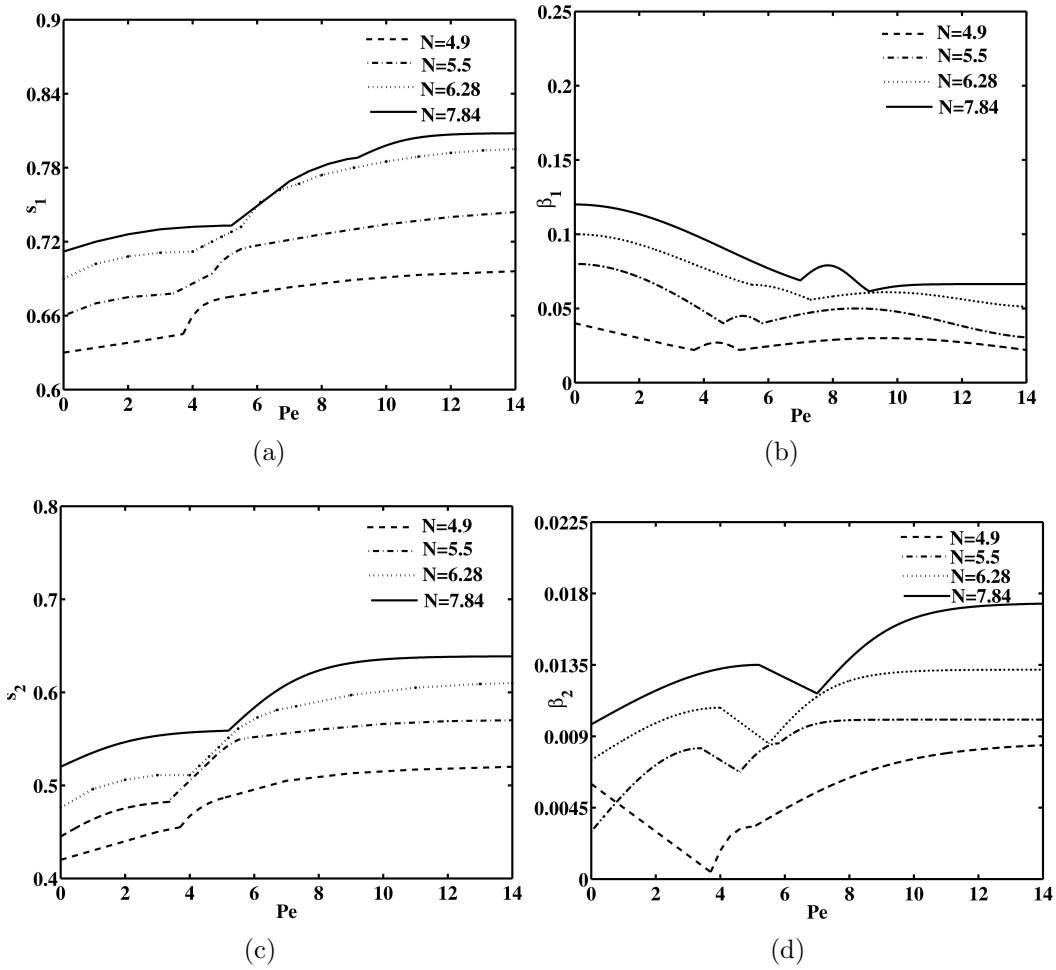

FIGURE 6.14. Order Parameters 'vs' non-dimensional shear strength (Pe) at (γ=0.16198, λ=0.0093654) for different nematic concentrations (N).

these constants apparently highlights the elastic stress in the total composition of the stress.

In all cases, the second normal stress difference, N_2, is one order of magnitude smaller than the first normal stress difference, N_1. The shear viscosity decreases with an increasing concentration (N), irrespective of the shear strength applied, highlighting the role of the nematic order to the reduction of the shear viscosity in the flow. Uniformly, we predict a shear thinning behavior for the entire range of the shear strength under study (i.e. the apparent viscosity (τ_{app}) decreases with increasing

shear strength). At the time-dependent states, a time-averaged value is adopted. Next, we detail the behavior in each of the four regions.

6.3.2.1. *Region A.* Figure 6.15 presents the rheological responses at $\gamma = 0.0, \lambda = 1.0$ (a point representing region-A). The first normal stress difference (N_1) is positive while the second stress difference (N_2) is negative for all the values of LCP concentrations (N=4.9,5.5,6.28,7.84) and the range of Pe investigated. In both states, **LR** and **FA**, the first normal stress difference increases while the second normal stress difference decreases monotonically with Pe. The rate of increase (decrease) of N_1 (N_2) in **LR** (**FA**) phase is more quickly than that in **FA** (**LR**) phase. The phase transition behavior is shown in the normal stress differences by a kinks at the transitional Pe. The shear viscosity demonstrate shear thinning behavior in all cases. It enhances in the **FA** phase. The shear stress is mostly constant in the **LR** state except that it enhances near the transitional shear strength and then decays in the **FA** state.

6.3.2.2. *Region B and C.* In Figure 6.16, we present rheological responses at $\gamma = 0.0817, \lambda = 0.5$ (a point representing region-B) and at N=4.9,5.5,6.28,7.84. The first normal stress difference N_1 steadily attains a positive value (with a large positive slope) in the **LR** phase (vice-versa for N_2 with a negative slope). N_1 changes it's sign from positive to negative in the periodic **MK** phase and back from negative to positive in the **FK** phase (N_2 changes its sign in exactly the opposite manner in both of these states). In the **FA** phase, N_1 is positive with a positive slope and N_2 is negative with a negative slope again. The transition from **FK** to **FA** is barely shown in these rheological functions. The shear stress (τ_{12}) increases and then reaches a maximum in the **LR** state and then gradually decays towards a constant non-zero value. The overall change in the shear stress is less than 10% of it's value at Pe=0.0. The shear viscosity (τ_{app}) shows shear thinning behavior at a decaying rate which changes continuously with respect to different orientational states.

To analyze the respective contribution of the viscous and elastic stress to the rheological functions, we plot in Figure 6.17 the elastic and the viscous normal stress

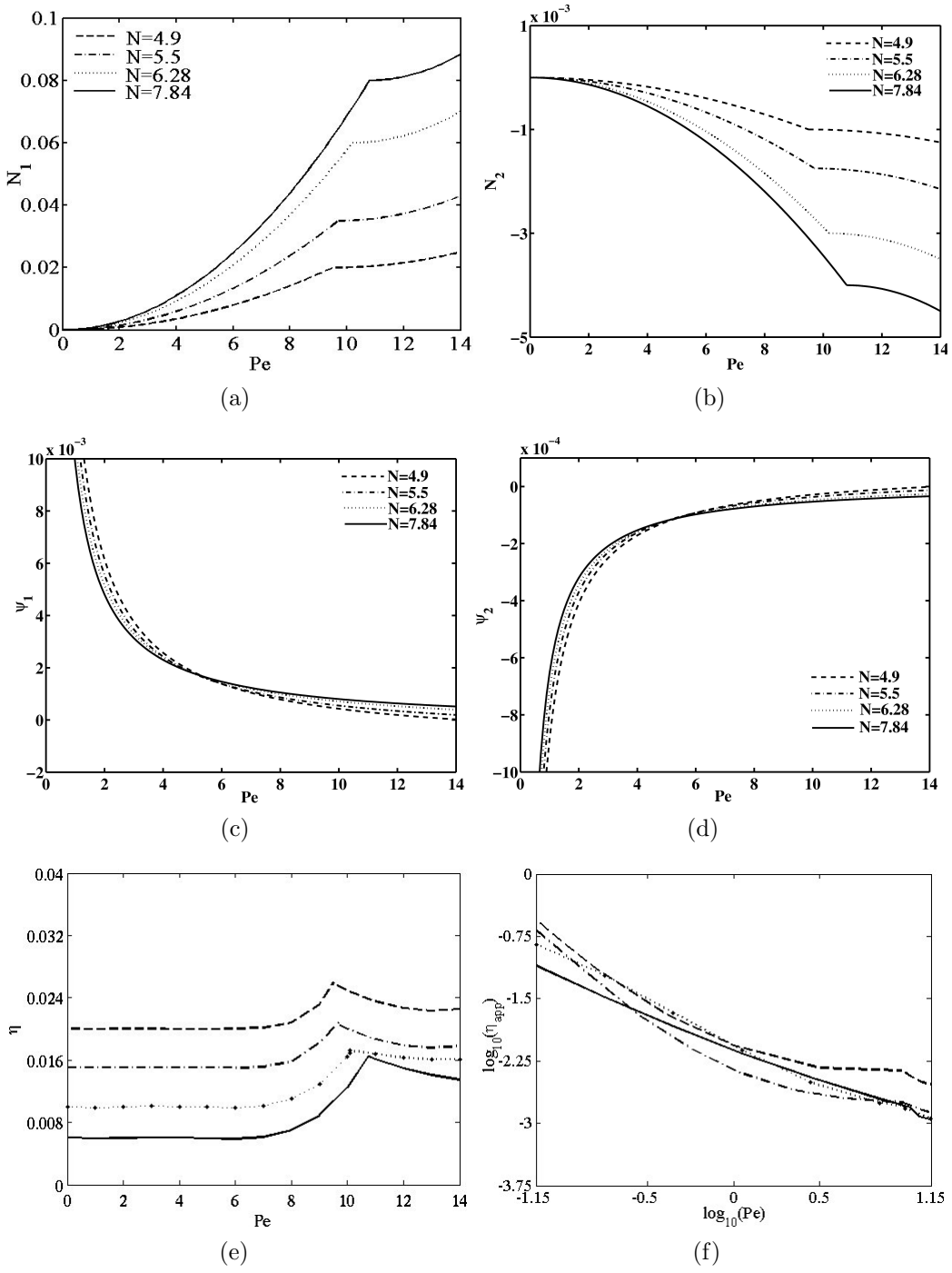

FIGURE 6.15. (a) 1^{st} normal stress difference ($N_1 = \tau_{xx} - \tau_{yy}$) (b) 2^{nd} normal stress difference ($N_2 = \tau_{yy} - \tau_{zz}$) (c) 1^{st} normal stress coefficient ($\psi_1 = N_1/Pe^2$) (d) 2^{nd} normal stress coefficient ($\psi_2 = N_2/Pe^2$) (e) shear stress (τ_{12}) (f) apparent viscosity: ($\tau_{app} = \tau_{12}$/Pe) at (γ=0.0, λ= 1.0) for different nematic concentrations (N).

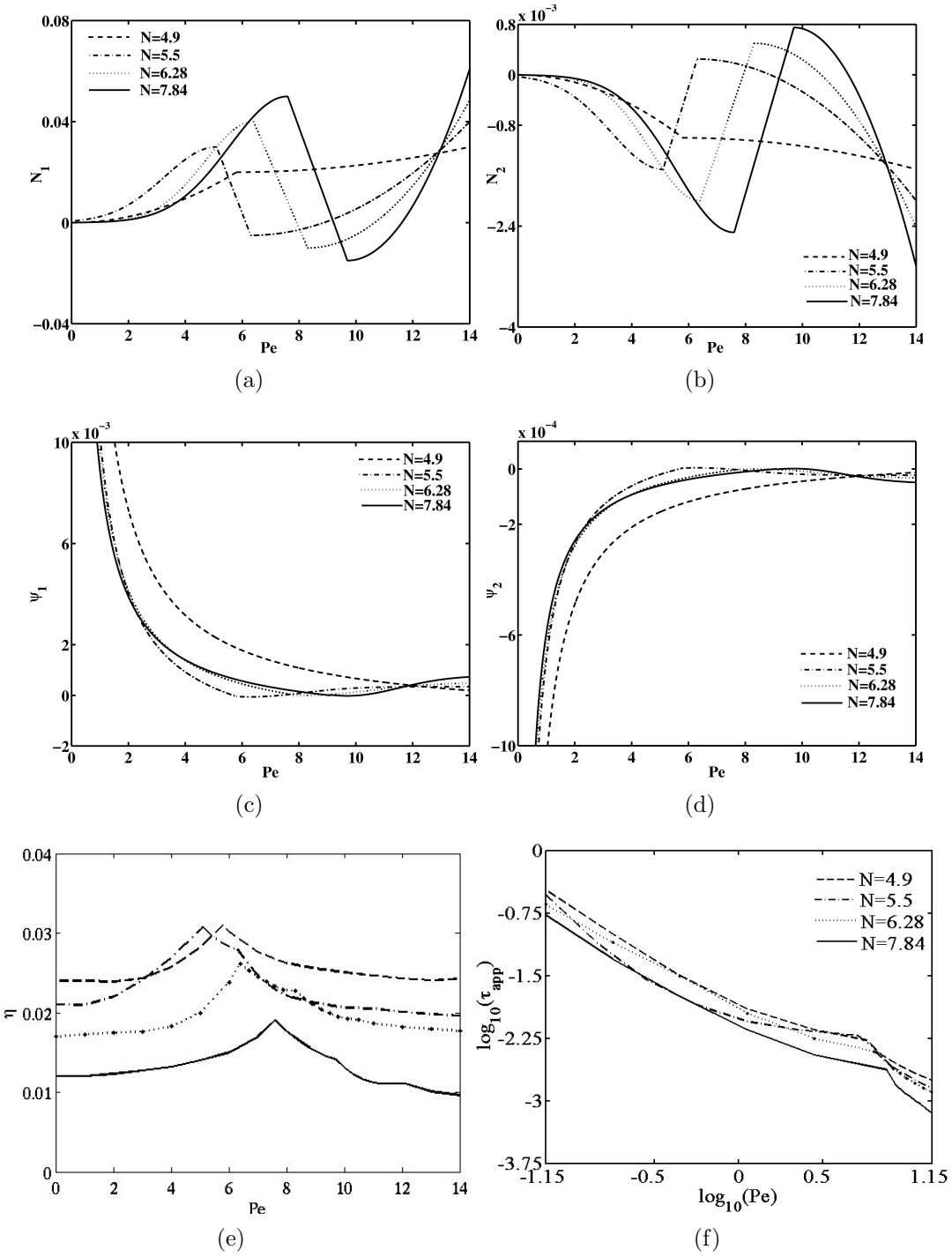

FIGURE 6.16. (a) 1^{st} normal stress difference ($N_1 = \tau_{xx} - \tau_{yy}$) (b) 2^{nd} normal stress difference ($N_2 = \tau_{yy} - \tau_{zz}$) (c) 1^{st} normal stress coefficient ($\psi_1 = N_1/Pe^2$) (d) 2^{nd} normal stress coefficient ($\psi_2 = N_2/Pe^2$) (e) shear stress (τ_{12}) (f) apparent viscosity: ($\tau_{app} = \tau_{12}$/Pe) at (γ=0.0817, λ=0.5) for different nematic concentrations (N). In the steady **OS**-phase, N_1 decays linearly with a slope: -0.0292 (at N=5.5), -0.0293 (at N=6.28), -0.0310 (at N=7.84); N_2 rises at the rate:0.0015 (at N=5.5, 6.28), 0.0016 (at N=7.84) and τ_{app} decays linearly at a rate: -0.3650 (at N= 4.9), -0.3600 (at N=5.5), -0.3750 (at N=6.28, 7.84).

differences, separately. We present these separate components in region (B) only to highlight the general effect of these components on the global behavior of the normal stress differences. The behavior of the elastic stresses is similar to the experimental results given in [106, 41]. Clearly, due to the choice of our viscosity coefficients ($\eta = 0.01, \zeta_0 = 0.035$), the elastic normal stress difference dominates in the entire range of high shear strength region. It clearly show that the viscous contribution to normal stress differences is exactly opposite to that of the elastic one.

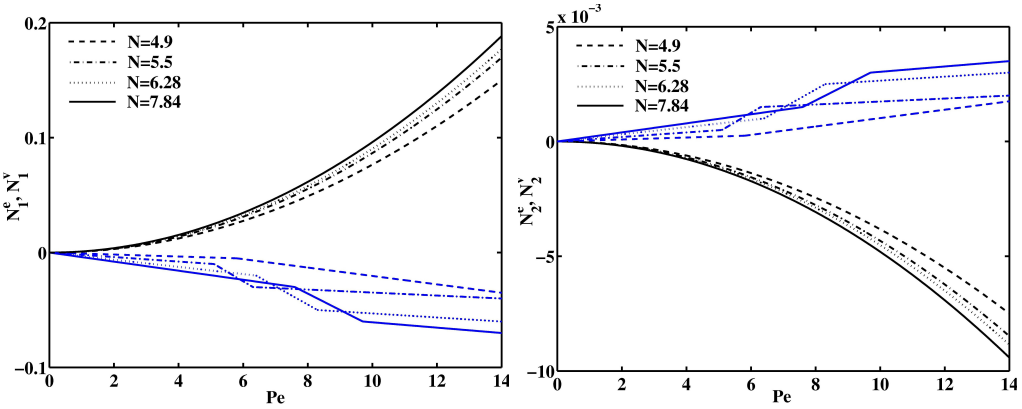

(a) (b)

FIGURE 6.17. (a) 1^{st} normal elastic and viscous stress differences ($N_1^e = \tau_{xx}^e - \tau_{yy}^e, N_1^v = \tau_{xx}^v - \tau_{yy}^v$) (b) 2^{nd} normal elastic and viscous stress differences ($N_2^e = \tau_{yy}^e - \tau_{zz}^e, N_1^v = \tau_{yy}^v - \tau_{zz}^v$) at (γ=0.0, λ=1.0) for different nematic concentrations (N). The elastic stresses are marked black and the viscous stresses marked blue.

The rheological responses in region C are qualitatively the same as in region B. The difference between the states in this region and region B is that there exists an OS state between MK and FK states. The numerical results show that N_1 at the OS state is negative while N_2 is positive.

6.3.2.3. *Region D.* Figure 6.18 presents rheological responses at material parameters ($\gamma = 0.16198, \lambda = 0.0093654$), a point in region-D, and at nematic concentrations $N = 4.9, 5.5, 6.28, 7.84$ respectively. The absence of the steady **LR** phase and the presence of the periodic **MK** phase in the sequence of phase transitions for $N = 5.5, 6.28, 7.84$ in this region, implies that the normal stress differences (N_1, N_2)

acquires negative values immediately at very low value of shear ($Pe \leq 2.0$). The signs of both N_1 and N_2 are retained in the next phase, namely, the steady **OS**-phase. There is again a change in the sign of N_1 from negative to positive (vice-versa for N_2) in the periodic **FK** phase . Finally, in the **FA**-phase, N_1 regains its positive value while N_2 obtains negative one. The scenario for the rheological functions at $N = 4.9$ resembles the case discussed in region A.

The graphs of the normal stress coefficients show a rapid decay (ψ_1 and ψ_2) with varying rate for different nematic concentrations (N=5.5, 6.28, 7.84) at small Pe. For a fixed BLCP concentration in this group and at the end of the Pe range, the shear stress (τ_{12}) undergoes non- monotonic variation and decreases at $Pe = 14$ by about 50% of it's value at Pe=0.0. The maximum value of τ_{12} is achieved at the end of the **OS** phase. The apparent shear viscosity thins by about 400% of it's initial value, with varying rates of decay.

6.3.3. Choatic Regime. A chaotic motion is observed at ($\gamma = 0.45$, $\lambda = 0.0093654$, $N = 4.9$), a point in Region (D) of the material parameter space. The sequence of phase transitions here is: **MK**→**CH**→**FK**→**FA**. The critical shear strength at which these transitions occur are at ($Pe^* = 1.15, 2.5, 4.6$). Figure 6.19 presents the order parameters and the rheological response functions at these states as Pe varies from 0 to 14. The values plotted are period-averaged quantities along periodic states and a finite-time averaged quantities at the chaotic state, where the time interval for the averaging is [5, 15].

The order parameters (s_1, s_2) increase slightly, while β_1, β_2 decay marginally in the periodic and the steady states. The stress difference N_1 and the stress coefficient ψ_1 change signs from positive to negative in the periodic **MK** phase and back to positive in the **FK** phase (vice-versa for the N_2, ψ_2). In the **CH**-phase, however, the signs of both the stress differences and the stress coefficients fluctuate. The plots of shear stress (τ_{12}) and apparent viscosity (τ_{app}) highlight a shear thinning behavior (except in the chaotic regime), of the order of 300 % and 500 %, respectively.

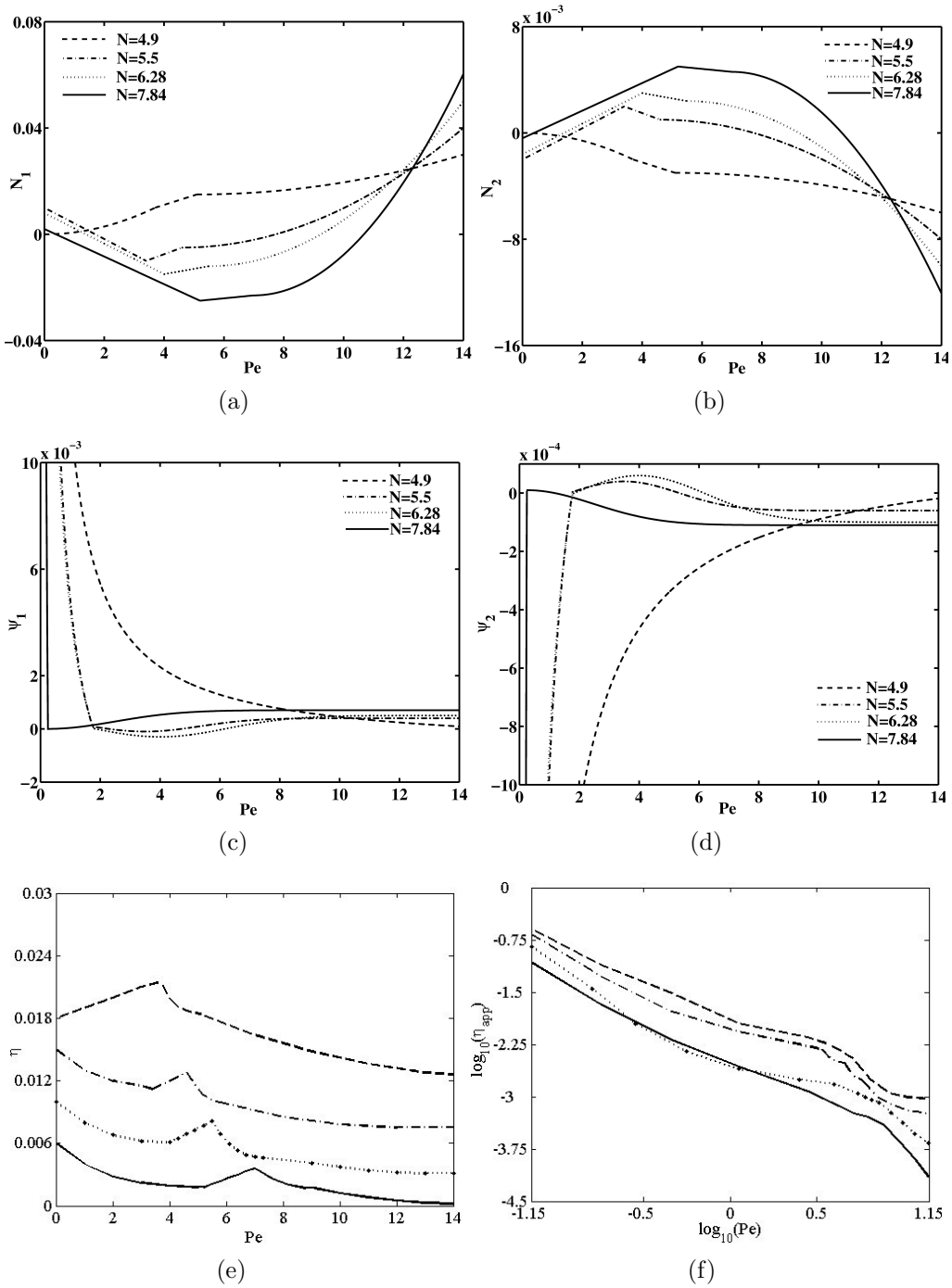

FIGURE 6.18. (a) 1^{st} normal stress difference ($N_1 = \tau_{xx} - \tau_{yy}$) (b) 2^{nd} normal stress difference ($N_2 = \tau_{yy} - \tau_{zz}$) (c) 1^{st} normal stress coefficient ($\psi_1 = N_1/Pe^2$) (d) 2^{nd} normal stress coefficient ($\psi_2 = N_2/Pe^2$) (e) shear stress (τ_{12}) (f) apparent viscosity: ($\tau_{app} = \tau_{12}$/Pe) at (γ=0.16198, λ=0.0093654) for different nematic concentrations (N). In the steady the **OS**-phase N_1 increases linearly with a slope: 0.0011 (at N=4.9, 7.84), 0.0042 (at N=5.5), 0.002 (at N=6.28); N_2 rises at the rate:0.0002 (at N=4.9, 7.84), 0.0008 (at N=5.5), 0.0004 (at N=6.28) and τ_{app} decays linearly at a rate: -0.3550 (at N=4.9, 5.5, 6.28), -0.3700 (at N=7.84).

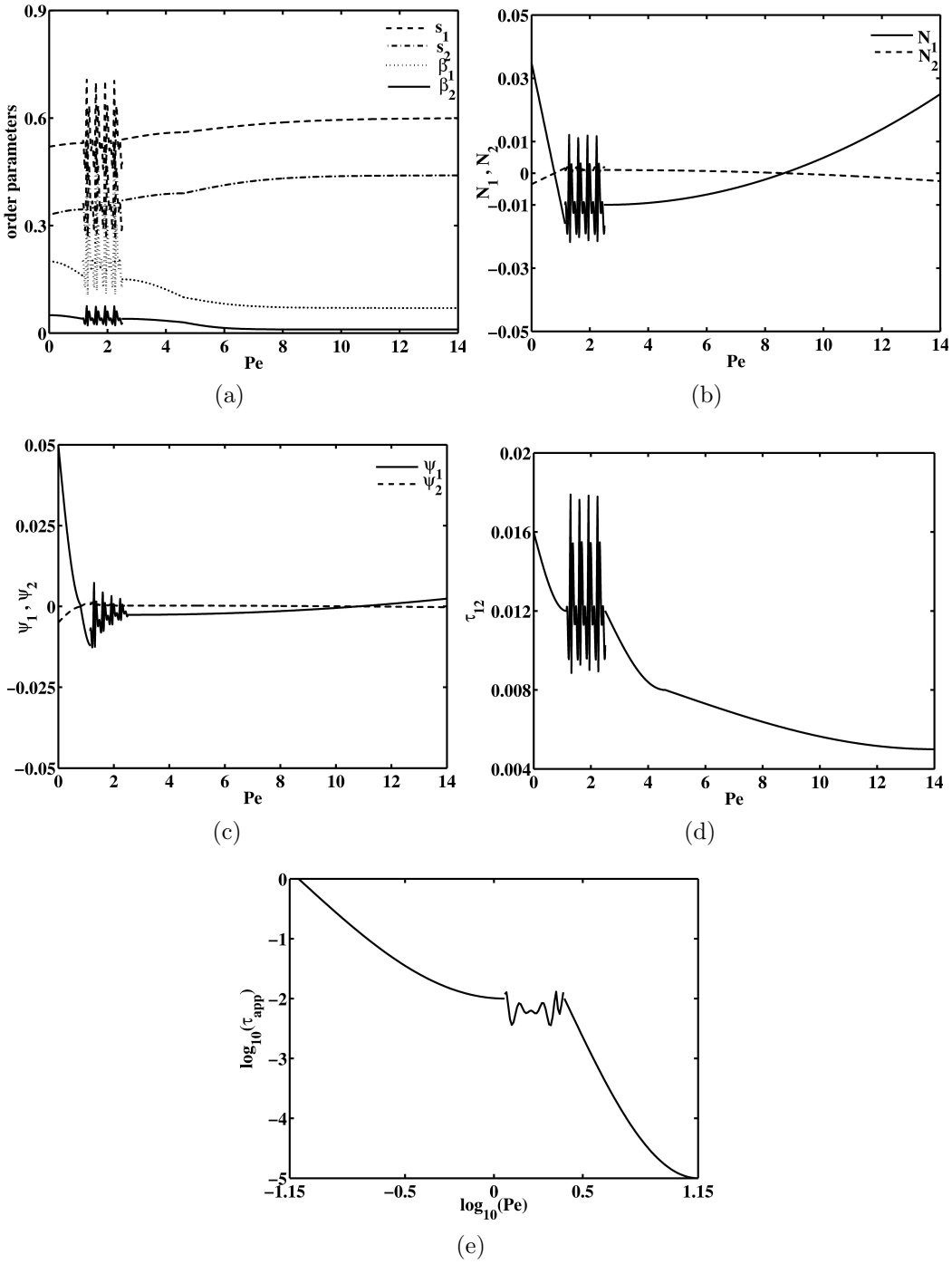

FIGURE 6.19. (a) The order parameters $(s_1, \beta_1, s_2, \beta_2)$ (b) 1^{st} and the 2^{nd} normal stress difference (N_1, N_2) (c) 1^{st} and the 2^{nd} normal stress coefficients (ψ_1, ψ_2) (d) shear stress (τ_{12}) (f) apparent viscosity: $(\tau_{app} = \tau_{12}/\text{Pe})$ at $(\gamma = 0.45, \lambda = 0.0093654, N = 4.9$. The shear window $1.15 \leq Pe \leq 2.5$ represents the chaotic regime. The normal stress differences are linear in the **MK**-phase with slopes: (-0.044,0.004) for N_1, N_2 respectively.

6.4. Conclusion

We have shown that the shear flow breaks the rotational symmetry in BLCPs producing two exotic out-of-plane time periodic motions along with the biaxial logrolling, flow-aligning, out-of-plane steady state and the robust chaotic structure. Various flow induced cascades are observed in the selected material parameter regions as the shear strength enhances. The shear induced skewness between the second moments **M** and **N** in all the dynamical states suggests a enhanced *orientational correlation* among the molecular axes in the mesoscopic ensemble. The biaxial liquid crystal polymer system demonstrates strong shear thinning behavior in all states and motions except for the uncertain chaotic states. The rheological signature in the first normal stress difference shows a robust positive value in the **LR** and **FA** state and possibly negative value in the time-dependent states on average. We believe that these dynamical and steady states serve as the genesis of the complex morphology in inhomogeneous flows of BLCPs. The current study sets the launching point for the challenging study ahead for the structure formation, evolution and dynamics of defects in the inhomogeneous BLCPs

Bibliography

[1] R. Shashidhar (Ed.), Liquid Crystal Materials, Devices and Displays (Proc. SPIE) (1995). 1.2

[2] R.J. Twieg, V. Chu, N. Nguyen, C.M. Dannels, C. Viney, Liq. Cryst. 20 (1996) 287. 1.2

[3] N.Boccarra, R.Mejdani, L. De Seze, J. Phys. **38** (1977) 149. 1.2.1, 1.2.1

[4] A.Ferrarini, G.R.Luckhurst, P.L.Nordio, S.J.Roskilly, J.Chem.Phys. **100** 1460 (1994). 1.2.1, 1.2.2, 1.2.3, 1.2.3

[5] (a) J.Malthete, H.T.Nguyen, A.M.Levelut, J.Chem. Soc. Chem. Commun. 1548 (1986); (b) J.Malthete, H.T.Nguyen, A.M.Levelut, J.Chem. Soc. Chem. Commun. 40 (1987); (c) J.Malthete, H.T.Nguyen, A.M.Levelut, Y.Galerne, Compt. Rend. Acad. Sci. Paris 303 (1986) 1073. 1.2.1, 1.2.2

[6] (a) S.Chandrasekhar, B.K.Sadashiva, B.R.Ratna, N.V.Raja, Pramana **30** (1988) L491.; (b) S.Chandrashekar, B.K.Sadashiva, B.R.Ratna, N.V.Raja, Mol. Cryst. Liq. Cryst. 165 (1988) 123. 1.2.1, 1.2.2

[7] K.Praefcke, B.Kohne, D.Singer, D.Demus, G.Pelzl, S.Diele, Liq. Cryst. **7** (1990) 589. 1.2.1

[8] Y.Galerne, Mol. Cryst. Liq. Cryst. **323** (1998) 211. 1.2.2, 1.2.2

[9] K.Praefcke, B.Kohne, B.Gundogan, D.Demus, G.Pelzl, S.Diele, Mol. Cryst. Liq. Cryst. Lett.**7** (1990) 27. 1.2.2, 1.2.2

[10] R.Y.Dong, Nuclear Magnetic Resonance of Liquid Crystals, Springer-Verlag, New York, 1994. 1.2.2

[11] S.G.Carr, G.R.Luckhurst, R.Poupko, H.J.Smith, Chem.Phys. **7** (1975) 278. 1.2.2

[12] S.M.Fan, I.D.Fletcher, B.Gundogan, N.J.Heaton, G.Kothe, G.Luckhurst, K.Praefcke, Chem.Phys. Lett. **204** (1993) 517. 1.2.2, 1.2.2, 1.2.2, 1.2.2

[13] J.R.Hughes, G.Kothe, G.R.Luckhurst, J.Malthete, M.E.Neubert, I.Shenouda, B.A.Timimi, M. Tittlebach, J.Chem.Phys. **107** (1997) 9252. 1.2.2, 1.2.2, 1.2.2

[14] (a) S.Chandrasekhar, G.G.Nair, D.S.Shankar Rao, S.Krishna Prasad, K.Praefcke, D.Singer, Mol. Cryst. Liq. Cryst. **288** (1996) 7; (b) S.Chandrashekar, G.G.Nair, D.S.Shankar Rao, S.Krishna Prasad, K.Praefcke, D.Blunk, Liq. Cryst. **24** (1998) 67. 1.2.2

[15] S.Chandrashekar, G.G.Nair, D.S.Shankar Rao, S.Krishna Prasad, K.Praefcke, D.Blunk, Cur. Sci. **75** (1998) 1042. 1.2.2

[16] R. Alapati, A.J.Cook, C.T.Imrie, G.R.Luckhurst, D. de Silva and B.A. Timimi, in preparation. 1.2.2, 1.2.2

[17] L.J. Yu, A.Saupe, Phys. Rev. Lett. **45** (1980) 1000. 1.2.2, 6.1

[18] V.Berejnov, V.Cabnil, R.Perzynski, Yu Raikher, J.Phys.Chem.B **102** (1998) 7132. 1.2.2

[19] E.A.Oliveira, L.Liebert, A.M.Figueiredo Neto, Liq. Cryst. **5** (1989) 1669. 1.2.2

[20] F.P.Nicoletta, G.Chidichimo, A.Golemme, N.Picci, Liq.Cryst. **10** (1991) 665. 1.2.2, 1.2.2

[21] G.R.Luckhurst, S.Romano, Mol. Phys. **40** (1980) 129; 1.2.3

[22] P.A. Lebwohl, G.Lasher, Phys.Rev.A **6** (1972) 426. 1.2.3

[23] J. Feng, G. Sgalari, L. G. Leal, J. Rheol. **44** 1085-1101 (2000). C.2

[24] M.Lehmann, G.R.Luckhurst, S.J.Perkins and J.L.Serrano, in preparation. 1.2.3

[25] P.I.C. Teixeira, A.J.Masters, B.M.Mulder, Mol. Cryst. Liq. Cryst. **323** (1998) 167 1.2.3

[26] J.Matraszek, J.Mieczkowski, J.Szydlowska, E.Gorecka, Liq.Cryst. **27** (2000) 429. 1.2.3

[27] R.Alben, J. Chem. Phys. **59** (1973) 4299. 1.2.3

[28] P.Palffy-Muhoray, J.R. de Bruyn, D.A. Dunmur, J. Chem. Phys. **82** (1985) 5294. 1.2.3

[29] R. Hashim, G.R. Luckhurst, S. Romano, Liq. Cryst. **15** (1993) 283. 1.2.3

[30] (a) S.R.Sharma, P.Palffy-Muhoray, B.Bergersen, D.A. Dunmur, Phys.Rev.A **32** (1985); (b) A.G.Vanakaras, S.C.McGrother, G.Jackson, D.Photinos, Mol. Cryst. Liq. Cryst. **323** (1998) 199. 1.2.3

[31] B.R. Acharya, A. Primak & S. Kumar, Phys. Rev. Lett. **92**, 145506 (2004). 6.1

[32] V. Berjnov, V. Cabuil, R., Perzynski and Y. Raikher, J. Phys. Chem. B, **102**, 7132 (1998). 6.1

[33] R. Bernardi and C. Zannoni, J. Chem. Phys., **113**, 5971 (2000). 6.1

[34] F. Bisi, E.G. Virga, E.C. Gartland, G. De Matteis, A. M. Sonnet and G.E. Durand, Phys. Rev. E, **73**, 051709 (2006). 6.1, 6.3

[35] T. Carlsson and F. Leslie, Liq. Cryst., **10**, 325 (1991). 6.1

[36] F. Biscarini, C. Chiccoli, P. Pasini, F. Semeria and C. Zannoni, Phys. Rev. Lett., **75**, 1803 (1995). 6.1

[37] C. Chiccoli, P. Pasini, F. Semeria, and C. Zannoni, Lecture Notes in Computer Science, **2110**, 555-560 (2001). 6.1

[38] J.W. Emsley *Nuclear Magnetic Resonance of Liquid Crystals*, (1985). 6.1

[39] J. L. Figyeirinhas, C. Cruz, D. Filip, G. Feio, A. C. Ribeiro, Y. Frere, T. Meyer and G. H. Mehl, Phys. Rev. Lett., **94**, 107802 (2005). 6.1

[40] A. A. De Melo Filho, A. Laverde and F. Y. Fujiwara, Langmuir, **19**, 1127 (2003). 6.1

[41] R.G. Larson, Macromolecules, **23**, 3983-3992 (1990). 6.3.1.2, 6.3.2.2

[42] G.R. Luckhurst, Nature (London) **430**, 413 (2004). 6.1

[43] L.A. Madsen, T.J. Dingemans, M. Nakata and E.T. Samulski, Phys. Rev. Lett. **92**, 145505 (2004). 6.1

[44] K. Merkel, A. Kocot, J. K. Vij, R. Korlacki, G. H. Mehl, and T. Meyer, Phys. Rev. Lett., **93** 237801 (2004). 6.1

[45] J. Pelaez and M. Wilson, Phys. Rev. Lett., **97**, 267801 (2006). 6.1

[46] R. Roscoe, J. Fluid Mech. **28**, 273-293 (1976). C.1

[47] K. Severing and K. Saalwachter, Phys. Rev. Lett., **92**, 125501 (2004). 6.1

[48] B. Tjipto-Margo, J. Chem. Phys. **94** 4546-4556 (1991). 6.1

[49] I.D.Fletcher, G.R.Luckhurst, Liq.Cryst. **18** (1995) 175. 1.2.3

[50] K.Praefcke, private communication. 1.2.3

[51] J.L.Hunt, R.W.Date, B.A.Timimi, G.R.Luckhurst, D.W.Bruce, submitted to J. Am. Chem. Soc. 1.2.3

[52] M.P. Allen, *Liquid Crystals*, **8**, p499 (1990). 2.4.2, 2.4.2, 6.1

[53] P.R. Halmos, *Finite Dimensional Vector Spaces*, van Nostrand Reinhold (1958) 2.4.1

[54] V. Tsvetkov, Acta Physicoch USSR **10**, p557 (1939) 2.4.1

[55] M. Abramowitz & I.A. Stegun, *Handbook of Mathematical Functions*, Dover. 2.4.1

[56] R Memmer, Liquid Crystals, **15** p 345 (1993). 2.4

[57] B. Rosi, M.P.Fontana, I. Dozov and N. Kiroz, Phys. Rev. A, **36**, 2879 (1987). 3.2.2

[58] W. Huntress Jr., Adv. magn. Reson.,**4**, 1 (1970). 3.2.2

[59] C.F. Polnaszek, G.V. Bruno and U. Segre, J.Chem.Phys., **58**, 3185. 3.2.2

[60] J.Bulthuis and L.Plomp, J.Phys.Paris, **51**, 2581 (1990). 3.2.2

[61] A.M. Figuereido, Y.Galerne and L.Liebert, Liq. Crys., **10**, 751, (1991). 3.2.2

[62] C. Zannoni, Molec. Phys., **38**, 1813, (1979). 3.2.2, 6.2.3

[63] A. Archioni, R. Tarroni and C. Zannoni, Polarized Spectroscopy of Ordered Systems, edited by B. Samori and E. Thulstrup, p.421 (1988). 3.2.2

[64] P.L. Nordio, G. Rigatti and U. Segre, Molec.Phys., **25**, 129 (1973). 3.2.2, 6.1

[65] W. Kuhn, Kolloid Z. **68**, 2 (1934). 3.2.1

[66] P.J. Flory, J.Chem. Phys. **17**, 303 (1949). 3.2.1

[67] P.J. Flory, Principles of Poly. Chem., *Cornell Univ. Press*, (1953). 3.2.1

[68] P.G. DeGennes, Scaling Concepts in Poly. Phys., *Cornell Univ. Press*, (1979). 3.2.1

[69] Y. Oono, Adv.Chem. Phys.,**61**, 301 (1985). 3.2.1

[70] S.F. Edwards, (eds. R. Balian and G. Weill). Gordon and Breach, London (1976). 3.2.1

[71] K.F. Freed, Adv.Chem.Phys. **22**, 1 (1972). 3.2.1

[72] Q. Wang, S. Sircar and H. Zhou, Comm. Math. Sci., Vol 3, **4**, 605-620 (2005). 5, 5.2, 6.1, 6.2.3

[73] M.G. Forest, Q. Wang and R. Zhou, J. Rheol., Vol 51, **1**, 1-21 (2007). 5.1, 5.2, 5.3, 5.4, 5.5, B

[74] M.G. Forest, S. Sircar, Q. Wang and R. Zhou, Phys. Fluids, **18**, 103102 (2006). 6.1, 6.2.3, B

[75] M.G. Forest, Q. Wang and R.Zhou, Rheol. Acta, Vol 43, 17-37 (2003). 5, 6.1, 6.2.3, 6.3.1.2, B

[76] M.G. Forest, Q. Wang and R.Zhou, Rheol. Acta, Vol 44, 80-93 (2004). 5, 5.3, 6.1, 6.2.3, 6.3.1.1, 6.3.1.2, B

[77] M.G. Forest, Q. Wang, Rheol. Acta **42** (2003) 20-46. 6.3.1.2

[78] M. C. Calderer, M. G. Forest and Q. Wang, J. Non-Newtonian Fluid Mech., **120**, 69-78 (2004). 6.1

[79] P.Palffy-Muhoray, B.Bergersen, H.Liu, R.B.Meyer and Z. Racz, S. Kai ed.,(1991) 505-518. 1

[80] Weinan E and P. Palffy-Muhoray, J. Nonlinear Sci.,**9**(1999) 417-437. 1

[81] J. Eriksen, Arch. Rat. Mech. Anal.,**113**(1991) 97-120. 1.1

[82] M.G.Forest, Q.Wang and H.Zhou, Phys. Fluids, **12** (2000) 490-498. 1.1

[83] F. Alouges and A. Soyeur, Nonlinear Analysis, Theory Methods and Applications, Vol. **18**, No. 11 (1992) 1071-1084. 1

[84] P.G. de Gennes and J. Prost, "The Physics of Liquid Crystals, second edition, Oxford University Press, 1993. 1, 1.1, 1.1, 5.1

[85] M. Doi and S.F. Edwards, The Theory of Polymer Dynamics, Oxford University Press, 1986 1.3, 3, 4.1, 4.1, 5.1, 5.1, 6.2.1, 6.2.1, 6.3.1.1, C, C.2

[86] M.E. Rose, Elementary Theory of Angular Momentum (Wiley, 1957). 2.2.1, 2.3, 2.3.1, 2.3.1, 2.3.2.4, 2.3.2.5, 2.3.2.6, 2.3.2.7, 2.4.1

[87] G.R. Luckhurst and G.W. Gray, The Molecular Physics of Liquid Crystals (Academic Press, 1979). 2.3, 2.4.1, 2.4.2, 3.2.2

[88] G.R. Luckhurst, C. Zannoni, P.L. Nordio and U. Segre, Mol. Phys., Vol 30, **5**, 1345-1358 (1975). 1.2.1, 1.2.1

[89] G. Racah, Phys. Rev. Lett.**62**, 438 (1942). 2.3.1, 2.3.2.1

[90] E.P. Wigner, Group Theory (Academic Press, 1959) 2.3.1

[91] B.I. Dunlap and B.R. Judd, J. Math. Phys. **16**, 318 (1975). 2.3.2.3

[92] J.D. Morgon, J. Phys. A: Math. Gen. **10**, 1059 (1977). 2.3.2.3

[93] E.U. Condon and G.H. Shortley, Cambridge Univ. Press (1935). 2.3.2.5

[94] R. Saito and M. Morita, Prog. Theor. Phys. **13**, 540 (1955). 2.3.2.5

[95] W. Maier and A. Saupe, Z.Naturforsch. **14a**, 882 (1959). 2.4, 3.2.1

[96] G.K. Batchelor, J.Fluid Mech., Vol 41 **3**, 545-570 (1970). C.1, C.1

[97] A.M. Sonnet, E.G. Virga and G. E. Durand, Phys. Rev. E, **67**, 061701 (2003). 3.2.1, 3.2.1, 6.1, 6.2.3, 6.3

[98] G. De Matteis and E. G. Virga, Phys. Rev. E, **71**, 061703 (2005). 3.2.1

[99] G. De Matteis, S.Romano and E.G. Virga, Phys. Rev. E, **72**, 041706 (2005). 3.2.1

[100] L. Longa, P. Grzybowski, S. Romano and E.G. Virga, Phys. Rev. E, **71**, 051714 (2005). 3.2.1, 6.1, 6.2.3, 6.3

[101] J.P. Straley, Phys. Rev. A, Vol 10, **5**, 1881 (1974). 1.2.1, 1.2.1, 3.2.1, 3.2.1, 3.2.1, 6.1, 6.2.1

[102] M.J. Freiser, Phys. Rev. Lett., Vol 24, **19**, 1041 (1970). 1.2, 1.2.1, 1.2.1, 3.2.1, 6.1

[103] P.L. Nordio, G. Rigatti & U. Segre, J.Chem. Phys., **56**, **5**, 2117 (1972). 3.2.2

[104] P.L. Nordio and P. Busolin, J.Chem. Phys., Vol 55, **12**, 5485 (1971). 3.2.2

[105] J.H. Freed, J.Chem. Phys., Vol 41, **7**, 2077 (1964). 3.2.2

[106] R. G. Larson and H. C. Ottinger, Macromolecules 24 (1991), 6270-6282. 6.3.1.2, 6.3.2.2

[107] F. M. Leslie, Advances in Liq. Crystals 4 (1979), 1-81. 6.1

[108] I. Fatkullin and V. Slastikov, preprint, submitted to nonlinearity (2005). 4.2

[109] H. Liu, H. Zhang, and P. Zhang, Comm. Math. Sci. 3 (2005), 201-218. 4.2

[110] H. Zhou, H. Wang, M. G. Forest, and Q. Wang, Nonlinearity **18** (2005), 2815-2825. 4.2

[111] S. Hess, Z Naturforschung 31a (1976), 1034-1037. 4.1, 5.1, 5.1

[112] N. Kuzuu, and M. Doi, J. Phys. Soc. of Japan, 52 (1983), 3486-3494. 4.1, 5.1

[113] Q. Wang, J. Chem. Phys. **116** (2002), 9120-9136. 4.1, 4.1, 5.1, C.2

[114] Q. Wang, M. G. Forest, and R. Zhou, J. Fluid Eng., **126** (2004), 180-188. 4.1

[115] Q. Wang, J. of Non-Newtonian Fluid Mech. 72 (1997), 141-162. 4.1, 4.1.2

[116] H. See, M. Doi, and R. G. Larson, J. Chem. Phy. 92(1) (1990), 792-800. 4.1

[117] M. G. Forest, Q. Wang, R. Zhou, and E. Coate, J. of Non-Newtonian Fluid Mechanics, 118(1) (2004), 17-31. 4.1.1

[118] A. S. Bhandar & J. M. Wiest, J. Col. & Interf. Sci., **257** 371-382 (2003). 5.1, 5.1

[119] E.J. Doedel, A.R.Champneys, T.F. Fairgrive, Y.A. Kuznetsov, B. Sandstede, X. Wang, **AUTO97**, Concordia University, 1997. 5.3

[120] A. Isihara, J. Chem. Phys. **19** (1951) 1142-1147. 5.1

[121] M. Grosso, R. Keunings, S. Crescitelli, P.L. Maffettone, Phys. Rev. Lett. **86** (2001) 3184-3187. 6.3.1.4

[122] G.R. Luckhurst, Thin Solid Films, **393**, pp 40-52 (2001). 1.2

Appendix A

Parameters and Coefficients

In this chapter we list all the time-dependent parameters and coefficients involved in the rotational diffusion equation derived in Chapter 3. This chapter is organised as follows. Section A.1 provides a list of time-dependent parameters used in the excluded volume potential $\mathcal{U}$. Section A.2 gives a series expansion of the each of the terms involved in the rotational diffusion part. Finally, section A.3 list the series expansion of the various terms involved in the flow part.

A.1. Time dependent parameters of $\mathcal{U}$

The time-dependent coefficients $A_i(t), A_{ij}(t), B_{ij}(t)$ of the excluded volume potential $\mathcal{U}$ in Eq.(130) are given as

$$
\begin{aligned}
&A_1(t) = 2\alpha(bC_{200}(t) + \gamma a(C_{202}(t) + C_{20-2}(t)))\\
&A_2(t) = \alpha(b(C_{220}(t) + C_{2-20}(t)) + \gamma a(C_{222}(t) + C_{22-2}(t) + C_{2-22}(t) + C_{2-2-2}(t)))\\
&A_3(t) = 2\alpha(\gamma a C_{200}(t) + \lambda c(C_{202}(t) + C_{20-2}(t)))\\
&A_4(t) = \alpha(\gamma a(C_{220}(t) + C_{2-20}(t)) + \lambda c(C_{222}(t) + C_{22-2}(t) + C_{2-22}(t) + C_{2-2-2}(t)))\\
&A_{12}(t) = -\alpha(b(C_{2-20}(t) - C_{220}(t)) + \gamma a(C_{2-2-2}(t) - C_{222}(t) + C_{2-22}(t) - C_{22-2}(t)))\\
&A_{13}(t) = \alpha(b(C_{2-10}(t) - C_{210}(t)) + \gamma a(C_{2-12}(t) - C_{21-2}(t) - C_{212}(t) + C_{2-1-2}(t)))\\
&A_{23}(t) = 2\alpha(\sqrt{\tfrac{2}{3}}\gamma a - \tfrac{b}{2} - \tfrac{\lambda c}{3})(C_{2-10}(t) + C_{210}(t))\\
&B_{12}(t) = -\alpha(\gamma a(C_{2-20}(t) - C_{220}(t)) + \lambda c(C_{2-2-2}(t) - C_{222}(t) + C_{2-22}(t) - C_{22-2}(t)\\
&B_{13}(t) = \alpha(\gamma a(C_{2-10}(t) - C_{210}(t)) + \lambda c(C_{2-12}(t) - C_{21-2}(t) - C_{212}(t) + C_{2-1-2}(t)))\\
&(a = \frac{2\pi}{\sqrt{15}}, \qquad b = \frac{2\pi}{3}\sqrt{\frac{2}{5}}, \qquad c = \pi\sqrt{\frac{2}{5}})
\end{aligned}
\tag{267}
$$

A.2. Expansion Coefficients for the Diffusion Operator: $\hat{\Gamma}$

In this section, we present the full derivation of each of the terms in the rotational diffusion operator in the order as they appear in Eq.(136)

$$(\nabla^2 f) = [L^{'}(L^{'}+1) + n^{'^2}(\eta - 1)]C_{L^{'},m^{'},n^{'}}(t) \tag{268}$$

$$\frac{\epsilon}{2}(L_{+}^{2} f) = \frac{\epsilon}{2}(\sqrt{[L'(L'+1) - n'(n'-1)]}\sqrt{[L'(L'+1) - (n'-1)(n'-2)]}) \; C_{L',m',n'-2}(t) \tag{269}$$

$$\frac{\epsilon}{2}(L_{-}^{2} f) = \frac{\epsilon}{2}(\sqrt{[L'(L'+1) - n'(n'+1)]}\sqrt{[L'(L'+1) - (n'+1)(n'+2)]}) \; C_{L',m',n'+2}(t) \tag{270}$$

$$\begin{aligned}
(\nabla^2 \mathcal{U}) f = \sum_{L=|L'-2|}^{L^{'}+2} \sqrt{\tfrac{2L+1}{2L'+1}} \; \{ \; & 6A_1 C(2,L,L^{'},0,m^{'})C(2,L,L^{'},0,n^{'})C_{L,m^{'},n^{'}}(t) \\
& +6(A_2 - A_{12})C(2,L,L^{'},2,m^{'}-2)C(2,L,L^{'},0,n^{'})C_{L,m^{'}-2,n^{'}}(t) \\
& +6(A_2 + A_{12})C(2,L,L^{'},-2,m^{'}+2)C(2,L,L^{'},0,n^{'})C_{L,m^{'}+2,n^{'}}(t) \\
& +6(A_{23} - A_{13})C(2,L,L^{'},1,m^{'}-1)C(2,L,L^{'},0,n^{'})C_{L,m^{'}-1,n^{'}}(t) \\
& +6(A_{23} + A_{13})C(2,L,L^{'},-1,m^{'}+1)C(2,L,L^{'},0,n^{'})C_{L,m^{'}+1,n^{'}}(t) \\
& +2A_3(1+2\eta)C(2,L,L^{'},0,m^{'})C(2,L,L^{'},2,n^{'}-2)C_{L,m^{'},n^{'}-2}(t) \\
& +2A_3(1+2\eta)C(2,L,L^{'},0,m^{'})C(2,L,L^{'},-2,n^{'}+2)C_{L,m^{'},n^{'}+2}(t) \\
& +2(A_4 - B_{12})(1+2\eta)C(2,L,L^{'},2,m^{'}-2)C(2,L,L^{'},2,n^{'}-2) \\
& \qquad C_{L,m^{'}-2,n^{'}-2}(t) \\
& +2(A_4 + B_{12})(1+2\eta)C(2,L,L^{'},-2,m^{'}+2)C(2,L,L^{'},-2,n^{'}+2) \\
& \qquad C_{L,m^{'}+2,n^{'}+2}(t) \\
& +2(A_4 - B_{12})(1+2\eta)C(2,L,L^{'},2,m^{'}-2)C(2,L,L^{'},-2,n^{'}+2) \\
& \qquad C_{L,m^{'}-2,n^{'}+2}(t) \\
& +2(A_4 + B_{12})(1+2\eta)C(2,L,L^{'},-2,m^{'}+2)C(2,L,L^{'},2,n^{'}-2) \\
& \qquad C_{L,m^{'}+2,n^{'}-2}(t)
\end{aligned}$$

$$
\begin{aligned}
&-2B_{13}(1+2\eta)C(2,L,L^{'},1,m^{'}-1)C(2,L,L^{'},2,n^{'}-2)C_{L,m^{'}-1,n^{'}-2}(t)\\
&+2B_{13}(1+2\eta)C(2,L,L^{'},-1,m^{'}+1)C(2,L,L^{'},-2,n^{'}+2)C_{L,m^{'}+1,n^{'}+2}(t)\\
&-2B_{13}(1+2\eta)C(2,L,L^{'},1,m^{'}-1)C(2,L,L^{'},-2,n^{'}+2)C_{L,m^{'}-1,n^{'}+2}(t)\\
&+2B_{13}(1+2\eta)C(2,L,L^{'},-1,m^{'}+1)C(2,L,L^{'},2,n^{'}-2)C_{L,m^{'}+1,n^{'}-2}(t)\}
\end{aligned}
\tag{271}
$$

$$
\begin{aligned}
\eta(L_m\mathcal{U})(L_mf) = 2\eta\sum_{L=|L^{'}-2|}^{L^{'}+2}\sqrt{\tfrac{2L+1}{2L^{'}+1}}\ \{&\\
&A_3(n'-2)C(2,L,L^{'},0,m^{'})C(2,L,L^{'},2,n^{'}-2)C_{L,m^{'},n^{'}-2}(t)\\
&-A_3(n'+2)C(2,L,L^{'},0,m^{'})C(2,L,L^{'},-2,n^{'}+2)C_{L,m^{'},n^{'}+2}(t)\\
&+(A_4-B_{12})(n'-2)C(2,L,L^{'},2,m^{'}-2)C(2,L,L^{'},2,n^{'}-2)\\
&\qquad\qquad C_{L,m^{'}-2,n^{'}-2}(t)\\
&-(A_4-B_{12})(n'+2)C(2,L,L^{'},-2,m^{'}+2)C(2,L,L^{'},-2,n^{'}+2)\\
&\qquad\qquad C_{L,m^{'}+2,n^{'}+2}(t)\\
&-(A_4+B_{12})(n'+2)C(2,L,L^{'},2,m^{'}-2)C(2,L,L^{'},-2,n^{'}+2)\\
&\qquad\qquad C_{L,m^{'}-2,n^{'}+2}(t)\\
&+(A_4+B_{12})(n'-2)C(2,L,L^{'},-2,m^{'}+2)C(2,L,L^{'},2,n^{'}-2)\\
&\qquad\qquad C_{L,m^{'}+2,n^{'}-2}(t)\\
&-B_{13}(n'-2)C(2,L,L^{'},1,m^{'}-1)C(2,L,L^{'},2,n^{'}-2)C_{L,m^{'}-1,n^{'}-2}(t)\\
&+B_{13}(n'+2)C(2,L,L^{'},-1,m^{'}+1)C(2,L,L^{'},-2,n^{'}+2)C_{L,m^{'}+1,n^{'}+2}(t)\\
&-B_{13}(n'+2)C(2,L,L^{'},1,m^{'}-1)C(2,L,L^{'},-2,n^{'}+2)C_{L,m^{'}-1,n^{'}+2}(t)\\
&+B_{13}(n'-2)C(2,L,L^{'},-1,m^{'}+1)C(2,L,L^{'},2,n^{'}-2)C_{L,m^{'}+1,n^{'}-2}(t)\}
\end{aligned}
\tag{272}
$$

$$
\begin{aligned}
\tfrac{\epsilon}{2}(L_+\mathcal{U})(L_+f) = \tfrac{\epsilon}{2}\sum_{L=|L^{'}-2|}^{L^{'}+2}\sqrt{\tfrac{2L+1}{2L^{'}+1}}\sqrt{L(L+1)-(n'-2)(n'-1)}\ \{&\\
\sqrt{6}A_1C(2,L,L^{'},0,m^{'})C(2,L,L^{'},1,n^{'}-1)C_{L,m^{'},n^{'}-2}(t)&
\end{aligned}
$$

$$
\begin{aligned}
&+\sqrt{6}(A_2 - A_{12})C(2, L, L^{'}, 2, m^{'} - 2)C(2, L, L^{'}, 1, n^{'} - 1) \\
&\qquad\qquad C_{L,m^{'}-2,n^{'}-2}(t) \\
&+\sqrt{6}(A_2 + A_{12})C(2, L, L^{'}, -2, m^{'} + 2)C(2, L, L^{'}, 1, n^{'} - 1) \\
&\qquad\qquad C_{L,m^{'}+2,n^{'}-2}(t) \\
&+\sqrt{6}(A_{23} - A_{13})C(2, L, L^{'}, 1, m^{'} - 1)C(2, L, L^{'}, 1, n^{'} - 1) \\
&\qquad\qquad C_{L,m^{'}-1,n^{'}-2}(t) \\
&+\sqrt{6}(A_{23} + A_{13})C(2, L, L^{'}, -1, m^{'} + 1)C(2, L, L^{'}, 1, n^{'} - 1) \\
&\qquad\qquad C_{L,m^{'}+1,n^{'}-2}(t)\} \\
&+\sqrt{L(L+1) - n'(n'+1)}\ \{\ 2A_3 C(2, L, L^{'}, 0, m^{'}) \\
&\qquad\qquad C(2, L, L^{'}, -1, n^{'} + 1)C_{L,m^{'},n^{'}}(t) \\
&+2(A_4 - B_{12})C(2, L, L^{'}, 2, m^{'} - 2)C(2, L, L^{'}, -1, n^{'} + 1)C_{L,m^{'}-2,n^{'}}(t) \\
&+2(A_4 + B_{12})C(2, L, L^{'}, -2, m^{'} + 2)C(2, L, L^{'}, -1, n^{'} + 1)C_{L,m^{'}+2,n^{'}}(t) \\
&-2B_{13}C(2, L, L^{'}, 1, m^{'} - 1)C(2, L, L^{'}, -1, n^{'} + 1)C_{L,m^{'}-1,n^{'}}(t) \\
&+2B_{13}C(2, L, L^{'}, -1, m^{'} + 1)C(2, L, L^{'}, -1, n^{'} + 1)C_{L,m^{'}+1,n^{'}}(t)\}
\end{aligned}
\tag{273}
$$

$$
\begin{aligned}
\tfrac{1}{2}(L_+\mathcal{U})(L_-f) = \tfrac{1}{2}\textstyle\sum_{L=|L^{'}-2|}^{L^{'}+2}\sqrt{\frac{2L+1}{2L^{'}+1}}\sqrt{L(L+1) - n'(n'-1)}\ \{ \\
&\sqrt{6}A_1 C(2, L, L^{'}, 0, m^{'})C(2, L, L^{'}, 1, n^{'} - 1)C_{L,m^{'},n^{'}}(t) \\
&+\sqrt{6}(A_2 - A_{12})C(2, L, L^{'}, 2, m^{'} - 2)C(2, L, L^{'}, 1, n^{'} - 1)C_{L,m^{'}-2,n^{'}}(t) \\
&+\sqrt{6}(A_2 + A_{12})C(2, L, L^{'}, -2, m^{'} + 2)C(2, L, L^{'}, 1, n^{'} - 1)C_{L,m^{'}+2,n^{'}}(t) \\
&+\sqrt{6}(A_{23} - A_{13})C(2, L, L^{'}, 1, m^{'} - 1)C(2, L, L^{'}, 1, n^{'} - 1)C_{L,m^{'}-1,n^{'}}(t) \\
&+\sqrt{6}(A_{23} + A_{13})C(2, L, L^{'}, -1, m^{'} + 1)C(2, L, L^{'}, 1, n^{'} - 1)C_{L,m^{'}+1,n^{'}}(t)\} \\
&+\sqrt{L(L+1) - (n'+2)(n'+1)}\ \{\ 2A_3 C(2, L, L^{'}, 0, m^{'}) \\
&\qquad\qquad C(2, L, L^{'}, -1, n^{'} + 1)C_{L,m^{'},n^{'}+2}(t)
\end{aligned}
$$

$$
\begin{aligned}
&+2(A_4 - B_{12})C(2,L,L^{'},2,m^{'}-2)C(2,L,L^{'},-1,n^{'}+1)C_{L,m^{'}-2,n^{'}+2}(t)\\
&+2(A_4 + B_{12})C(2,L,L^{'},-2,m^{'}+2)C(2,L,L^{'},-1,n^{'}+1)C_{L,m^{'}+2,n^{'}+2}(t)\\
&-2B_{13}C(2,L,L^{'},1,m^{'}-1)C(2,L,L^{'},-1,n^{'}+1)C_{L,m^{'}-1,n^{'}+2}(t)\\
&+2B_{13}C(2,L,L^{'},-1,m^{'}+1)C(2,L,L^{'},-1,n^{'}+1)C_{L,m^{'}+1,n^{'}+2}(t)\}
\end{aligned}
\tag{274}
$$

$$
\begin{aligned}
\tfrac{\epsilon}{2}(L_{-}\mathcal{U})(L_{-}f) = \tfrac{\epsilon}{2}\textstyle\sum_{L=|L^{'}-2|}^{L^{'}+2}\sqrt{\frac{2L+1}{2L^{'}+1}}\sqrt{L(L+1)-(n^{\prime}+2)(n^{\prime}+1)}\ \{\\
&\sqrt{6}A_1C(2,L,L^{'},0,m^{'})C(2,L,L^{'},-1,n^{'}+1)C_{L,m^{'},n^{'}+2}(t)\\
&+\sqrt{6}(A_2 - A_{12})C(2,L,L^{'},2,m^{'}-2)C(2,L,L^{'},-1,n^{'}+1)\\
&\qquad C_{L,m^{'}-2,n^{'}+2}(t)\\
&+\sqrt{6}(A_2 + A_{12})C(2,L,L^{'},-2,m^{'}+2)C(2,L,L^{'},-1,n^{'}+1)\\
&\qquad C_{L,m^{'}+2,n^{'}+2}(t)\\
&+\sqrt{6}(A_{23} - A_{13})C(2,L,L^{'},1,m^{'}-1)C(2,L,L^{'},-1,n^{'}+1)\\
&\qquad C_{L,m^{'}-1,n^{'}+2}(t)\\
&+\sqrt{6}(A_{23} + A_{13})C(2,L,L^{'},-1,m^{'}+1)C(2,L,L^{'},-1,n^{'}+1)\\
&\qquad C_{L,m^{'}+1,n^{'}+2}(t)\}\\
&+\sqrt{L(L+1)-n^{\prime}(n^{\prime}-1)}\ \{\ 2A_3C(2,L,L^{'},0,m^{'})\\
&\qquad C(2,L,L^{'},1,n^{'}-1)C_{L,m^{'},n^{'}}(t)\\
&\quad +2(A_4 - B_{12})C(2,L,L^{'},2,m^{'}-2)C(2,L,L^{'},1,n^{'}-1)\\
&\qquad C_{L,m^{'}-2,n^{'}}(t)\\
&\quad +2(A_4 + B_{12})C(2,L,L^{'},-2,m^{'}+2)C(2,L,L^{'},1,n^{'}-1)\\
&\qquad C_{L,m^{'}+2,n^{'}}(t)\\
&\quad -2B_{13}C(2,L,L^{'},1,m^{'}-1)C(2,L,L^{'},1,n^{'}-1)C_{L,m^{'}-1,n^{'}}(t)\\
&\quad +2B_{13}C(2,L,L^{'},-1,m^{'}+1)C(2,L,L^{'},1,n^{'}-1)C_{L,m^{'}+1,n^{'}}(t)\}
\end{aligned}
\tag{275}
$$

$$\begin{aligned}
\tfrac{1}{2}(L_{-}\mathcal{U})(L_{+}f) = \tfrac{1}{2}\textstyle\sum_{L=|L^{'}-2|}^{L^{'}+2}\sqrt{\tfrac{2L+1}{2L^{'}+1}}\sqrt{L(L+1)-n'(n'+1)}\ \{ \\
&\sqrt{6}A_1 C(2,L,L^{'},0,m^{'})C(2,L,L^{'},-1,n^{'}+1)C_{L,m^{'},n^{'}}(t) \\
&+\sqrt{6}(A_2-A_{12})C(2,L,L^{'},2,m^{'}-2)C(2,L,L^{'},-1,n^{'}+1) \\
&\qquad\qquad C_{L,m^{'}-2,n^{'}}(t) \\
&+\sqrt{6}(A_2+A_{12})C(2,L,L^{'},-2,m^{'}+2)C(2,L,L^{'},-1,n^{'}+1) \\
&\qquad\qquad C_{L,m^{'}+2,n^{'}}(t) \\
&+\sqrt{6}(A_{23}-A_{13})C(2,L,L^{'},1,m^{'}-1)C(2,L,L^{'},-1,n^{'}+1) \\
&\qquad\qquad C_{L,m^{'}-1,n^{'}}(t) \\
&+\sqrt{6}(A_{23}+A_{13})C(2,L,L^{'},-1,m^{'}+1)C(2,L,L^{'},-1,n^{'}+1) \\
&\qquad\qquad C_{L,m^{'}+1,n^{'}}(t)\} \\
&+\sqrt{L(L+1)-(n'-2)(n'-1)}\ \{\ 2A_3 C(2,L,L^{'},0,m^{'}) \\
&\qquad\qquad C(2,L,L^{'},1,n^{'}-1)C_{L,m^{'},n^{'}-2}(t) \\
&\quad +2(A_4-B_{12})C(2,L,L^{'},2,m^{'}-2)C(2,L,L^{'},1,n^{'}-1) \\
&\qquad\qquad C_{L,m^{'}-2,n^{'}-2}(t) \\
&\quad +2(A_4+B_{12})C(2,L,L^{'},-2,m^{'}+2)C(2,L,L^{'},1,n^{'}-1) \\
&\qquad\qquad C_{L,m^{'}+2,n^{'}-2}(t) \\
&-2B_{13}C(2,L,L^{'},1,m^{'}-1)C(2,L,L^{'},1,n^{'}-1)C_{L,m^{'}-1,n^{'}-2}(t) \\
&+2B_{13}C(2,L,L^{'},-1,m^{'}+1)C(2,L,L^{'},1,n^{'}-1)C_{L,m^{'}+1,n^{'}-2}(t)\}
\end{aligned} \tag{276}$$

where the time-dependent parameters used in the series expansion above are as follows

$$\begin{aligned}
&P_1 = \sqrt{\tfrac{3}{2}}A_1 + \epsilon A_3, \qquad P_{2a} = \sqrt{\tfrac{3}{2}}\epsilon(A_2 - A_{12}) + (A_4 - B_{12}), \\
&P_{2b} = \sqrt{\tfrac{3}{2}}\epsilon(A_2 + A_{12}) + (A_4 + B_{12}), \qquad P_3 = \sqrt{\tfrac{3}{2}}\epsilon A_1 + A_3, \\
&P_{4a} = \sqrt{\tfrac{3}{2}}(A_2 - A_{12}) + \epsilon(A_4 - B_{12}), \qquad P_{4b} = \sqrt{\tfrac{3}{2}}(A_2 + A_{12}) + \epsilon(A_4 + B_{12}), \\
&P_5 = \sqrt{\tfrac{3}{2}}\epsilon(A_{23} - A_{13}) - B_{13}, \qquad P_6 = \sqrt{\tfrac{3}{2}}\epsilon(A_{23} + A_{13}) + B_{13},
\end{aligned}$$

$$
\begin{aligned}
&P_7 = \sqrt{\tfrac{3}{2}}(A_{23} - A_{13}) - \epsilon B_{13}, \qquad P_8 = \sqrt{\tfrac{3}{2}}(A_{23} + A_{13}) + \epsilon B_{13}, \\
&D_1 = 2\sqrt{6}P_1, \qquad D_{2a} = 2\sqrt{6}P_{4a}, \qquad D_{2b} = 2\sqrt{6}P_{4b}, \qquad D_3 = 2P_3 + 4\eta A_3, \\
&D_{4a} = 2P_{2a} + 4\eta(A_4 - B_{12}), \qquad D_{4b} = 2P_{2b} + 4\eta(A_4 + B_{12}) \\
&D_5 = 2P_5 - 4\eta B_{13}, \qquad D_6 = 2P_6 + 4\eta B_{13}
\end{aligned}
\tag{277}
$$

A.3. Expansion Coefficients of the flow operator

In this section, we present the full derivation of each of the terms in the flow operator in the order as they appear in Eq.(145):

$$
\begin{aligned}
&L_m(\mathrm{D}^1_{00}f) = \textstyle\sum_{L=|L'-1|}^{L'+1} n'\sqrt{\frac{2L+1}{2L'+1}}C(1,L,L',0,m')C(1,L,L',0,n')C_{L,m',n'}(t) \\
&L_+(\mathrm{D}^1_{0-1}f) = \textstyle\sum_{L=|L'-1|}^{L'+1} \sqrt{L'(L'+1)-n'(n'-1)}\sqrt{\frac{2L+1}{2L'+1}}C(1,L,L',0,m') \\
&\qquad\qquad C(1,L,L',-1,n')C_{L,m',n'}(t) \\
&L_-(\mathrm{D}^1_{01}f) = \textstyle\sum_{L=|L'-1|}^{L'+1} \sqrt{L'(L'+1)-n'(n'+1)}\sqrt{\frac{2L+1}{2L'+1}}C(1,L,L',0,m') \\
&\qquad\qquad C(1,L,L',1,n')C_{L,m',n'}(t) \\
&L_+[\eta_{c+b}(D^2_{21} - D^2_{2-1})f] = \eta_{c+b}\textstyle\sum_{L=|L'-2|}^{L'+2}\sqrt{\frac{2L+1}{2L'+1}}C(2,L,L',2,m'-2) \\
&\sqrt{L'(L'+1)-n'(n'-1)}\{C(2,L,L',1,n'-2)C_{L,m'-2,n'-2}(t) - \\
&\qquad\qquad C(2,L,L',-1,n')C_{L,m'-2,n'}(t)\} \\
&L_+[\eta_{c-b}(D^2_{-21} - D^2_{-2-1})f] = \eta_{c-b}\textstyle\sum_{L=|L'-2|}^{L'+2}\sqrt{\frac{2L+1}{2L'+1}}C(2,L,L',-2,m'+2) \\
&\sqrt{L'(L'+1)-n'(n'-1)}\{C(2,L,L',1,n'-2)C_{L,m'+2,n'-2}(t) - \\
&\qquad\qquad C(2,L,L',-1,n')C_{L,m'+2,n'}(t)\} \\
&L_-[\eta_{c-b}(D^2_{21} - D^2_{2-1})f] = \eta_{c-b}\textstyle\sum_{L=|L'-2|}^{L'+2}\sqrt{\frac{2L+1}{2L'+1}}C(2,L,L',2,m'-2) \\
&\sqrt{L'(L'+1)-n'(n'+1)}\{C(2,L,L',1,n')C_{L,m'-2,n'}(t) - \\
&\qquad\qquad C(2,L,L',-1,n'+2)C_{L,m'-2,n'+2}(t)\} \\
&L_-[\eta_{c+b}(D^2_{-21} - D^2_{-2-1})f] = \eta_{c+b}\textstyle\sum_{L=|L'-2|}^{L'+2}\sqrt{\frac{2L+1}{2L'+1}}C(2,L,L',-2,m'+2)
\end{aligned}
$$

$$\sqrt{L'(L'+1)-n'(n'+1)}\{C(2,L,L',1,n')C_{L,m'+2,n'}(t)-$$
$$C(2,L,L',-1,n'+2)C_{L,m'+2,n'+2}(t)\}$$
$$L_m(\mathrm{D}^2_{2-2}f)=\sum_{L=|L'-2|}^{L'+2}n'\sqrt{\tfrac{2L+1}{2L'+1}}C(2,L,L',2,m'-2)C(2,L,L',-2,n'+2)$$
$$C_{L,m'-2,n'+2}(t)$$
$$L_m(\mathrm{D}^2_{-2-2}f)=\sum_{L=|L'-2|}^{L'+2}n'\sqrt{\tfrac{2L+1}{2L'+1}}C(2,L,L',-2,m'+2)$$
$$C(2,L,L',-2,n'+2)C_{L,m'+2,n'+2}(t)$$
$$L_m(\mathrm{D}^2_{-22}f)=\sum_{L=|L'-2|}^{L'+2}n'\sqrt{\tfrac{2L+1}{2L'+1}}C(2,L,L',-2,m'+2)$$
$$C(2,L,L',2,n'-2)C_{L,m'+2,n'-2}(t)$$
$$L_m(\mathrm{D}^2_{22}f)=\sum_{L=|L'-2|}^{L'+2}n'\sqrt{\tfrac{2L+1}{2L'+1}}C(2,L,L',2,m'-2)C(2,L,L',2,n'-2)$$
$$C_{L,m'-2,n'-2}(t) \tag{278}$$

Appendix B

Moment Equations

Moment equations provides an alternative approach to investigate the flow-phase behavior of the a mesoscopic system liquid crystals. Although compared with the kinetic equation, this approach considerably reduces the number of coupled partial differential equations; we are left with a choice of coming up with a suitable moment closure equations to reduce the higher moments [75, 76, 74, 73]. The numerical solution is very sensitive to the choice of these closure equations. Nevertheless, we provide an overview of this approach, should the need arise to use them in future.

In section B.1, we describe all the tools and lemmas necessary to understand the derivation. Finally, in section B.2, we derive and list these set of equations.

B.1. Calculus Lemmas in SO_3

Let (**m**,**n**,**k**) be the unit vectors for an arbitrary rotation in 3-D space with respect to a fixed frame(**x**,**y**,**z**). Eq.(112) provides a relation between these two frames in terms of the euler angles (α, β, γ). The angular momentum operator (w.r.t. this fixed frame) is:

$$\mathbf{L} = \mathbf{m}L_m + \mathbf{n}L_n + \mathbf{k}L_k \tag{279}$$

where

$$\begin{aligned} L_m &= i\tfrac{\partial}{\partial\gamma}, \\ L_n &= i(\cos\gamma\cot\beta\tfrac{\partial}{\partial\gamma} + \sin\gamma\tfrac{\partial}{\partial\beta} - \tfrac{\cos\gamma}{\sin\beta}\tfrac{\partial}{\partial\alpha}), \\ L_k &= i(-\sin\gamma\cot\beta\tfrac{\partial}{\partial\gamma} + \cos\gamma\tfrac{\partial}{\partial\beta} + \tfrac{\sin\gamma}{\sin\beta}\tfrac{\partial}{\partial\alpha}) \end{aligned} \tag{280}$$

The differentiation properties of angular momentum operator **L** is given by:

$$L_p(q) = i[p \times q] \qquad where(p,q,r) = (\mathbf{m},\mathbf{n},\mathbf{k}) \tag{281}$$

Lemma 1: For two scalar functions f and g

$$\int (L_i f(\Omega)) g(\Omega) d\mathbf{\Omega} = -\int f(\Omega) L_i g(\Omega) d\mathbf{\Omega} \qquad i = (m,n,k) \tag{282}$$

where $\int \mathbf{d\Omega} = \int_0^\pi \sin\beta d\beta \int_0^{2\pi} d\alpha \int_0^{2\pi} d\gamma$

Lemma 2: For a scalar and a vector function g and $\mathbf{F}$

$$\int g\mathbf{L}\cdot\mathbf{F} d\mathbf{\Omega} = -\int \mathbf{F}\cdot\mathbf{L} g d\mathbf{\Omega} \tag{283}$$

Lemma 3: For an $m^{'}$-th order tensor A and an $n^{'}$-th order tensor B

$$\int A_{i_1\ldots i_{m^{'}}} \mathbf{L}_k B_{j_1\ldots k\ldots j_{n^{'}}} d\mathbf{\Omega} = -\int \mathbf{L}_k A_{i_1\ldots i_{m^{'}}} B_{j_1\ldots k\ldots j_{n^{'}}} d\mathbf{\Omega} \tag{284}$$

B.2. Moment equations

Using the calculus lemmas and Eq.(119) we arrive at the moment equations as follows. From Eq.(127), the excluded volume potential of a biaxial molecule is given by:

$$\mathcal{U} = -\tfrac{3N}{2}\{M:\mathbf{mm} + \gamma(M:\mathbf{nn} + N:\mathbf{mm}) + \lambda N:\mathbf{nn}\}$$

$$= -\frac{3N}{2}\{< m_a m_b > m_a m_b + \gamma(< m_a m_b > n_a n_b + < n_a n_b > m_a m_b) + \lambda < n_a n_b > n_a n_b\}$$

where (γ,λ) are the material parameters.

The application of the angular momentum operator $\mathbf{L}$ on the excluded volume potential gives:

$$
\begin{aligned}
L_n(\mathcal{U}_0) &= -\tfrac{3N\iota}{2}\{< m_a m_b > (-k_a m_b - m_a k_b) + \gamma < n_a n_b > (-k_a m_b - m_a k_b) \\
&= \tfrac{3N\iota}{2}\{(< m_a m_b > + \gamma < m_a k_b >)(k_a m_b + m_a k_b)\} \\
&= \tfrac{3Ni}{2}\{(\mathbf{M} + \gamma\mathbf{N}) : (\mathbf{km} + \mathbf{mk})\}
\end{aligned}
\tag{285}
$$

Similarly:

$$
L_k(\mathcal{U}_0) = -\frac{3Ni}{2}\{((1-\gamma)\mathbf{M} + (\gamma - \lambda)\mathbf{N}) : (\mathbf{mn} + \mathbf{nm})\} \tag{286}
$$

$$
L_m(\mathcal{U}_0) = -\frac{3N\iota}{2}\{(\gamma\mathbf{M} + \lambda\mathbf{N}) : (\mathbf{kn} + \mathbf{nk})\} \tag{287}
$$

Using Eq.(119) and the relations above, the moment equations are derived as follows:

$$
\dot{\mathbf{M}} = \int\int\int_\Omega \mathbf{mm}L^* \cdot (D_r L\mu f) - \int\int\int_\Omega \mathbf{mm}L^* \cdot (\mathbf{gf}) \qquad D_r = diag(D_1, D_2, D_3)
$$

$$
= \quad \mathbf{I} \quad + \quad \mathbf{II}
$$

$$
\mathbf{I} = \int\int\int -\mathbf{L}^*(\mathbf{mm}) \cdot (\mathbf{D_r L}\mu\mathbf{f})
$$

$$
= \int\int\int -\{L_i^*(m_\alpha)m_\beta + m_\alpha L_i^*(m_\beta)\} D_i \{L_i f + L_i(\mathcal{U})f\}
$$

$$
= -\iota[\int\int\int \{k_\alpha m_\beta + m_\alpha k_\beta\} D_2 \{L_n f + L_n(\mathcal{U})f\} - \int\int\int \{n_\alpha m_\beta + m_\alpha n_\beta\} D_3 \{L_k f + L_k(\mathcal{U})f\}]
$$

$$
= -\iota[-\int\int\int D_2 \{L_n(k_\alpha m_\beta + m_\alpha k_\beta)\} f \;+\; \int\int\int D_3 \{L_k(n_\alpha m_\beta + m_\alpha n_\beta)\} f
$$

$$
+ \int\int\int D_2 \{k_\alpha m_\beta + m_\alpha k_\beta\} L_n(\mathcal{U}) f \;-\; \int\int\int D_3 \{n_\alpha m_\beta + m_\alpha n_\beta\} L_k(\mathcal{U}) f]
$$

$$
= \int\int\int 2D_2(k_\alpha k_\beta - m_\alpha m_\beta) f \;+\; \int\int\int 2D_3(n_\alpha n_\beta - m_\alpha m_\beta) f +
$$

$$
-\iota[\int\int\int_\Omega D_2 \{k_\alpha m_\beta + m_\alpha k_\beta\} L_n(\mathcal{U}) f \;-\; \int\int\int_\Omega D_3 \{n_\alpha m_\beta + m_\alpha n_\beta\} L_k(\mathcal{U}) f]
$$

$$
= 2D_2\mathbf{K} + 2D_3\mathbf{N} - 2(D_2 + D_3)\mathbf{M} + \tfrac{3N}{2} D_2(\mathbf{M} + \gamma\mathbf{N}) : (< \mathbf{kmkm} > + < \mathbf{mkkm} > +
$$

$$
< \mathbf{kmmk} > + < \mathbf{mkmk} >) + \tfrac{3N}{2} D_3((1-\gamma)\mathbf{M} + (\gamma - \lambda)\mathbf{N}) : (< \mathbf{nmnm} > +
$$

$$< \mathbf{mnnm} > + < \mathbf{nmmn} > + < \mathbf{mnmn} >)$$

$$\mathbf{II} = \int\int\int_{\mathbf{\Omega}} \mathbf{L}^*(\mathbf{mm}) \cdot (\mathbf{gf})$$

$$= \int\int\int \{L_i^*(m_\alpha)m_\beta + m_\alpha L_i^*(m_\beta)\} g_i f$$

$$= -\int\int\int \{k_\alpha m_\beta + m_\alpha k_\beta\} g_n f + \int\int\int_\Omega \{n_\alpha m_\beta + m_\alpha n_\beta\} g_k f$$

$$= -\tfrac{\mathbf{K}}{a^2+c^2} : (c^2 < \mathbf{mkkm} > -a^2 < \mathbf{kmkm} > +c^2 < \mathbf{mkmk} > -a^2 < \mathbf{kmmk} >)$$

$$+\tfrac{\mathbf{K}}{a^2+b^2} : (a^2 < \mathbf{nmmn} > -b^2 < \mathbf{mnmn} > +a^2 < \mathbf{nmnm} > -b^2 < \mathbf{mnnm} >)$$

The complete system of equations is given by:

$$\begin{aligned}
&\dot{\mathbf{M}} = 2D_2\mathbf{K} + 2D_3\mathbf{N} - 2(D_2 + D_3)\mathbf{M} \\
&+\tfrac{3N}{2} D_2(\mathbf{M} + \gamma\mathbf{N}) : (< \mathbf{kmkm} > + < \mathbf{mkkm} > + < \mathbf{kmmk} > + < \mathbf{mkmk} >) \\
&+\tfrac{3N}{2} D_3((1-\gamma)\mathbf{M} + (\gamma - \lambda)\mathbf{N}) : (< \mathbf{nmnm} > + < \mathbf{mnnm} > + < \mathbf{nmmn} > + \\
&\qquad\qquad < \mathbf{mnmn} >) \\
&-\tfrac{\mathbf{K}}{a^2+c^2} : (c^2 < \mathbf{mkkm} > -a^2 < \mathbf{kmkm} > +c^2 < \mathbf{mkmk} > -a^2 < \mathbf{kmmk} >) \\
&+\tfrac{\mathbf{K}}{a^2+b^2} : (a^2 < \mathbf{nmmn} > -b^2 < \mathbf{mnmn} > +a^2 < \mathbf{nmnm} > -b^2 < \mathbf{mnnm} >)
\end{aligned} \tag{288}$$

$$\begin{aligned}
&\dot{\mathbf{N}} = 2D_1\mathbf{K} + 2D_3\mathbf{M} - 2(D_1 + D_3)\mathbf{N} \\
&+\tfrac{3N}{2} D_1(\gamma\mathbf{M} + \lambda\mathbf{N}) : (< \mathbf{knnk} > + < \mathbf{knkn} > + < \mathbf{nkkn} > + < \mathbf{nknk} >) \\
&-\tfrac{3N}{2} D_3((1-\gamma)\mathbf{M} + (\gamma - \lambda)\mathbf{N}) : (< \mathbf{nmnm} > + < \mathbf{mnnm} > + < \mathbf{nmmn} > + \\
&\qquad\qquad < \mathbf{mnmn} >) \\
&+\tfrac{\mathbf{K}}{b^2+c^2} : (b^2 < \mathbf{nkkn} > -c^2 < \mathbf{knkn} > +b^2 < \mathbf{nknk} > -c^2 < \mathbf{knnk} >) \\
&-\tfrac{\mathbf{K}}{a^2+b^2} : (a^2 < \mathbf{nmmn} > -b^2 < \mathbf{mnmn} > +a^2 < \mathbf{nmnm} > -b^2 < \mathbf{mnnm} >)
\end{aligned} \tag{289}$$

$$\dot{\mathbf{K}} = 2D_1\mathbf{N} + 2D_2\mathbf{M} - 2(D_1+D_2)\mathbf{K}$$
$$-\tfrac{3N}{2}D_1(\gamma\mathbf{M}+\lambda\mathbf{N}) : (<\mathbf{knnk}> + <\mathbf{knkn}> + <\mathbf{nkkn}> + <\mathbf{nknk}>)$$
$$-\tfrac{3N}{2}D_2(\mathbf{M}+\gamma\mathbf{N}) : (<\mathbf{kmkm}> + <\mathbf{mkkm}> + <\mathbf{kmmk}> + <\mathbf{mkmk}>)$$
$$-\tfrac{\mathbf{K}}{b^2+c^2} : (b^2 <\mathbf{nkkn}> - c^2 <\mathbf{knkn}> + b^2 <\mathbf{nknk}> - c^2 <\mathbf{knnk}>)$$
$$+\tfrac{\mathbf{K}}{a^2+c^2} : (c^2 <\mathbf{mkkm}> - a^2 <\mathbf{kmkm}> + c^2 <\mathbf{mkmk}> - a^2 <\mathbf{kmmk}>) \tag{290}$$

$$<\dot{\mathbf{km}}> = -(D_1+2D_2+D_3) <\mathbf{km}> - 2D_2 <\mathbf{mk}>$$
$$-\tfrac{3N}{2}D_1(\gamma\mathbf{M}+\lambda\mathbf{N}) : (<\mathbf{knnm}> + <\mathbf{nknm}>)$$
$$+\tfrac{3N}{2}D_2(\mathbf{M}+\gamma\mathbf{N}) : (<\mathbf{kmkk}> + <\mathbf{mkkk}> - <\mathbf{kmmm}> - <\mathbf{mkmm}>)$$
$$+\tfrac{3N}{2}D_3((1-\gamma)\mathbf{M}+(\gamma-\lambda)\mathbf{N}) : (<\mathbf{mnkn}> + <\mathbf{nmkn}>)$$
$$-\tfrac{\mathbf{K}}{b^2+c^2} : (b^2 <\mathbf{nknm}> - c^2 <\mathbf{knnm}>) - \tfrac{\mathbf{K}}{a^2+b^2} : (a^2 <\mathbf{nmkn}> - b^2 <\mathbf{mnkn}>)$$
$$+\tfrac{\mathbf{K}}{a^2+c^2} : (c^2 <\mathbf{mkmm}> - a^2 <\mathbf{kmmm}> - c^2 <\mathbf{mkkk}> + a^2 <\mathbf{kmkk}>) \tag{291}$$

$$<\dot{\mathbf{mn}}> = -(D_1+D_2+2D_3) <\mathbf{mn}> - 2D_3 <\mathbf{nm}>$$
$$+\tfrac{3N}{2}D_1(\gamma\mathbf{M}+\lambda\mathbf{N}) : (<\mathbf{knmk}> + <\mathbf{nkmk}>) + \tfrac{3N}{2}D_2(\mathbf{M}+\gamma\mathbf{N}) :$$
$$(<\mathbf{kmkn}> + <\mathbf{mkkn}>)$$
$$+\tfrac{3N}{2}D_3((1-\gamma)\mathbf{M}+(\gamma-\lambda)\mathbf{N}) : (<\mathbf{mnnn}> + <\mathbf{nmnn}> - <\mathbf{mnmm}> -$$
$$<\mathbf{nmmm}>)$$
$$+\tfrac{\mathbf{K}}{b^2+c^2} : (b^2 <\mathbf{nkmk}> - c^2 <\mathbf{knmk}>) - \tfrac{\mathbf{K}}{a^2+c^2} : (c^2 <\mathbf{mkkn}> - a^2 <\mathbf{kmkn}>)$$
$$+\tfrac{\mathbf{K}}{a^2+b^2} : (a^2 <\mathbf{nmnn}> - b^2 <\mathbf{mnnn}> - a^2 <\mathbf{nmmm}> + b^2 <\mathbf{mnmm}>) \tag{292}$$

$$< \mathbf{n\dot{k}} > = -(2D_1 + D_2 + D_3) < \mathbf{nk} > -2D_1 < \mathbf{kn} > -\tfrac{3N}{2} D_2(\mathbf{M} + \gamma\mathbf{N}) : (< \mathbf{kmnm} > + < \mathbf{mknm} >)$$
$$+\tfrac{3N}{2} D_1(\gamma\mathbf{M} + \lambda\mathbf{N}) : (< \mathbf{knkk} > + < \mathbf{nkkk} > - < \mathbf{knnn} > - < \mathbf{nknn} >)$$
$$-\tfrac{3N}{2} D_3((1-\gamma)\mathbf{M} + (\gamma - \lambda)\mathbf{N}) : (< \mathbf{mnmk} > + < \mathbf{nmmk} >)$$
$$+\tfrac{\mathbf{K}}{b^2+c^2} : (b^2 < \mathbf{nkkk} > -c^2 < \mathbf{knkk} > -b^2 < \mathbf{nknn} > +c^2 < \mathbf{knnn} >) + \tfrac{\mathbf{K}}{a^2+c^2} : (c^2 < \mathbf{mknm} > -a^2 < \mathbf{kmnm} >) - \tfrac{\mathbf{K}}{a^2+b^2} : (a^2 < \mathbf{nmmk} > -b^2 < \mathbf{mnmk} >) \tag{293}$$

$$< \mathbf{m\dot{k}} > = -(D_1 + 2D_2 + D_3) < \mathbf{mk} > -2D_2 < \mathbf{km} > -\tfrac{3N}{2} D_1(\gamma\mathbf{M} + \lambda\mathbf{N}) : (< \mathbf{knmn} > + < \mathbf{nkmn} >)$$
$$+\tfrac{3N}{2} D_2(\mathbf{M} + \gamma\mathbf{N}) : (< \mathbf{kmkk} > + < \mathbf{mkkk} > - < \mathbf{kmmm} > - < \mathbf{mkmm} >)$$
$$+\tfrac{3N}{2} D_3((1-\gamma)\mathbf{M} + (\gamma - \lambda)\mathbf{N}) : (< \mathbf{mnnk} > + < \mathbf{nmnk} >)$$
$$-\tfrac{\mathbf{K}}{b^2+c^2} : (b^2 < \mathbf{nkmn} > -c^2 < \mathbf{knmn} >) - \tfrac{\mathbf{K}}{a^2+b^2} : (a^2 < \mathbf{nmnk} > -b^2 < \mathbf{mnnk} >)$$
$$+\tfrac{\mathbf{K}}{a^2+c^2} : (c^2 < \mathbf{mkmm} > -a^2 < \mathbf{kmmm} > -c^2 < \mathbf{mkkk} > +a^2 < \mathbf{kmkk} >) \tag{294}$$

$$< \mathbf{n\dot{m}} > = -(D_1 + D_2 + 2D_3) < \mathbf{nm} > -2D_3 < \mathbf{mn} >$$
$$+\tfrac{3N}{2} D_1(\gamma\mathbf{M} + \lambda\mathbf{N}) : (< \mathbf{knkm} > + < \mathbf{nkkm} >) + \tfrac{3N}{2} D_2(\mathbf{M} + \gamma\mathbf{N}) : (< \mathbf{kmnk} > + < \mathbf{mknk} >)$$
$$+\tfrac{3N}{2} D_3((1-\gamma)\mathbf{M} + (\gamma - \lambda)\mathbf{N}) : (< \mathbf{mnnn} > + < \mathbf{nmnn} > - < \mathbf{mnmm} > - < \mathbf{nmmm} >)$$
$$+\tfrac{\mathbf{K}}{b^2+c^2} : (b^2 < \mathbf{nkkm} > -c^2 < \mathbf{knkm} >) - \tfrac{\mathbf{K}}{a^2+c^2} : (c^2 < \mathbf{mknk} > -a^2 < \mathbf{kmnk} >)$$
$$+\tfrac{\mathbf{K}}{a^2+b^2} : (a^2 < \mathbf{nmnn} > -b^2 < \mathbf{mnnn} > -a^2 < \mathbf{nmmm} > +b^2 < \mathbf{mnmm} >) \tag{295}$$

$$
\begin{aligned}
&< \dot{\mathbf{kn}} > = -(2D_1 + D_2 + D_3) < \mathbf{kn} > -2D_1 < \mathbf{nk} > \\
&+\tfrac{3N}{2} D_1(\gamma \mathbf{M} + \lambda \mathbf{N}) : (< \mathbf{knkk} > + < \mathbf{nkkk} > - < \mathbf{knnn} > - < \mathbf{nknn} >) \\
&-\tfrac{3N}{2} D_2(\mathbf{M} + \gamma \mathbf{N}) : (< \mathbf{kmmn} > + < \mathbf{mkmn} >) \\
&-\tfrac{3N}{2} D_3((1-\gamma)\mathbf{M} + (\gamma - \lambda)\mathbf{N}) : (< \mathbf{mnkm} > + < \mathbf{nmkm} >) \\
&+\tfrac{\mathbf{K}}{b^2+c^2} : (b^2 < \mathbf{nkkk} > -c^2 < \mathbf{knkk} > -b^2 < \mathbf{nknn} > +c^2 < \mathbf{knnn} >) + \tfrac{\mathbf{K}}{a^2+c^2} : (c^2 \\
&< \mathbf{mkmn} > -a^2 < \mathbf{kmmn} >) - \tfrac{\mathbf{K}}{a^2+b^2} : (a^2 < \mathbf{nmkm} > -b^2 < \mathbf{mnkm} >)
\end{aligned}
\tag{296}
$$

Appendix C

Viscous and Elastic Stresses

The macroscopic stress tensor consists of three parts: the isotropic pressure, the extra elastic stress and the extra viscous stress. The elastic stress is due to the BLCP molecular interaction while the viscous stress is the result of the interaction between BLCP molecules and solvent molecules as well as among the solvent molecules. They are derived separately. In this chapter, we derive in detail the viscous and the elastic stresses involved in the shear induced polymeric flows. Section C.1 gives the detailed series expansion of the viscous stress components. Next, in section C.2 we derive the elastic stresses using the virtual work principle given in [85]. Finally, in section C.3, we provide the series expansion of the elastic stress components.

C.1. Viscous Stress

The viscous stress for biaxial LCPs follows from the work of Batchelor [96] and Roscoe [46] on ellipsoidal suspensions in viscous solvent

$$\tau^v = 2\eta\mathbf{D} + 3\nu kT\zeta_0\mathcal{B} : \mathbf{D} \tag{297}$$

where η is the viscosity of the solvent, $\mathcal{B}$ is the fourth order strain rate concentration tensor, $\mathbf{D}$ is the second order strain rate tensor, given by $\mathbf{D} = \frac{1}{2}(\nabla\mathbf{v} + \nabla\mathbf{v}^T)$ and ζ_0 is a shape dependent friction coefficient proportional to the volume of the ellipsoidal suspension. Replacing the volume average by the ensemble average in [96], it follows

that

$$\tau^v = 2\eta\mathbf{D} + \nu kT\zeta_0[\tfrac{4}{3(J_1J_2+J_2J_3+J_1J_3)}((J_1\langle\mathbf{mmmm}\rangle + J_2\langle\mathbf{nnnn}\rangle + J_3\langle\mathbf{kkkk}\rangle) : \mathbf{D} -$$

$$\tfrac{\mathbf{I}}{3}(J_1\langle\mathbf{mm}\rangle + J_2\langle\mathbf{nn}\rangle + J_3\langle\mathbf{kk}\rangle) : \mathbf{D}) + \tfrac{2}{3}(\tfrac{1}{I_1}(\langle\mathbf{nk}+\mathbf{kn}\rangle)(\langle\mathbf{nk}+\mathbf{kn}\rangle) : \mathbf{D} +$$

$$\tfrac{1}{I_2}(\langle\mathbf{mn}+\mathbf{nm}\rangle)(\langle\mathbf{mn}+\mathbf{nm}\rangle) : \mathbf{D} + \tfrac{1}{I_3}(\langle\mathbf{mk}+\mathbf{km}\rangle)(\langle\mathbf{mk}+\mathbf{km}\rangle) : \mathbf{D})]. \tag{298}$$

Here, the shape constants $(J_i, I_i), i = 1, 2, 3$ in Eq. 298 are:

$$I_1 = \int_0^\infty \tfrac{abc(a^2+c^2)d\lambda}{\Delta(c^2+\lambda)(a^2+\lambda)}, I_2 = \int_0^\infty \tfrac{abc(b^2+a^2)d\lambda}{\Delta(b^2+\lambda)(a^2+\lambda)}, I_3 = \int_0^\infty \tfrac{abc(b^2+c^2)d\lambda}{\Delta(b^2+\lambda)(c^2+\lambda)},$$

$$J_1 = \int_0^\infty \tfrac{abc\lambda d\lambda}{\Delta(a^2+\lambda)(c^2+\lambda)}, J_2 = \int_0^\infty \tfrac{abc\lambda d\lambda}{\Delta(a^2+\lambda)(b^2+\lambda)}, J_3 = \int_0^\infty \tfrac{abc\lambda d\lambda}{\Delta(b^2+\lambda)(c^2+\lambda)} \tag{299}$$

and $\Delta^2 = (a^2+\lambda)(b^2+\lambda)(c^2+\lambda)$. The series expansion of each of the normal components (τ^v_{ii}) and the viscous shear component (τ^v_{12}) is as follows:

$$\tau_{11}^{v} = \tfrac{4}{3}k_B T\zeta_0\nu[\tfrac{J_1}{\triangle J}\{$$
$$-\tfrac{4\pi^2}{3\iota}[\tfrac{2}{35}\sqrt{\tfrac{2}{3}}(C_{2-20}(t)-C_{220}(t))+\tfrac{1}{27}\sqrt{\tfrac{2}{3}}(C_{420}(t)-C_{4-20}(t))-\tfrac{2}{35}(C_{22-2}(t)+$$
$$C_{222}(t)-C_{2-2-2}(t)-C_{2-22}(t))-\tfrac{1}{14}(C_{32-2}(t)+C_{3-2-2}(t)-C_{322}(t)-C_{3-22}(t))$$
$$-\tfrac{1}{42}(C_{42-2}(t)+C_{422}(t)-C_{4-2-2}(t)-C_{4-22}(t))]\}\quad+\quad\tfrac{J_2}{\triangle J}\{\tfrac{\pi^2}{27\iota}[3\sqrt{\tfrac{2}{35}}(C_{440}(t)-$$
$$C_{4-40}(t))+\tfrac{36}{35}(C_{22-2}(t)-C_{2-2-2}(t)+C_{222}(t)-C_{2-22}(t))+\tfrac{3}{7}(C_{422}(t)$$
$$-C_{4-2-2}(t)+C_{42-2}(t)-C_{4-22}(t))+\tfrac{3}{2}(C_{444}(t)+C_{4-44}(t)-C_{44-4}(t)-C_{4-4-4}(t)$$
$$)+\tfrac{3}{\sqrt{70}}(C_{404}(t)-C_{40-4}(t))+\tfrac{36}{35}\sqrt{\tfrac{3}{2}}(C_{20-2}(t)-C_{202}(t))+\tfrac{3}{7\sqrt{10}}(C_{40-2}(t)-C_{402}(t)$$
$$)+\tfrac{3}{\sqrt{7}}(C_{4-4-2}(t)-C_{442}(t)+C_{4-42}(t)-C_{44-2}(t))+\tfrac{9}{7}\sqrt{\tfrac{3}{10}}(C_{302}(t)-C_{30-2}(t))+$$
$$\tfrac{3}{2\sqrt{7}}(C_{4-2-4}(t)+C_{42-4}(t)-C_{424}(t)-C_{4-24}(t))-\tfrac{36}{35}\sqrt{\tfrac{2}{3}}(2C_{2-20}(t)+C_{220}(t))+$$
$$0.136C_{4-20}(t)-0.407C_{420}(t)\}]\quad+\quad\tfrac{J_3}{\triangle J}\{\tfrac{\pi^2}{27\iota}[3\sqrt{\tfrac{2}{35}}(C_{4-40}(t)-C_{440}(t))+\tfrac{36}{35}$$
$$(C_{22-2}(t)-C_{2-2-2}(t)+C_{222}(t)-C_{2-22}(t))+\tfrac{3}{7}(C_{42-2}(t)-C_{4-22}(t))+\tfrac{3}{2}(C_{444}(t)$$
$$+C_{4-44}(t)-C_{44-4}(t)-C_{4-4-4}(t))+\tfrac{3}{\sqrt{70}}(C_{404}(t)-C_{40-4}(t))+\tfrac{36}{35}\sqrt{\tfrac{3}{2}}(C_{20-2}(t)-$$
$$C_{202}(t))+\tfrac{3}{7\sqrt{10}}(C_{402}(t)-C_{40-2}(t))+\tfrac{3}{\sqrt{7}}(C_{4-42}(t)-C_{44-2}(t))+\tfrac{9}{7}\sqrt{\tfrac{3}{10}}(C_{302}(t)$$
$$-C_{30-2}(t))+\tfrac{3}{2\sqrt{7}}(C_{4-2-4}(t)+C_{42-4}(t)-C_{424}(t)-C_{4-24}(t))+\tfrac{36}{35}\sqrt{\tfrac{2}{3}}(2C_{220}(t)+$$
$$C_{2-20}(t))+0.407C_{4-20}(t)-0.136C_{420}(t)\}]\quad+\quad\tfrac{8}{I_{1\iota}}(\tfrac{\pi^2}{5})^2[C_{2-2-2}(t)-C_{222}(t)$$
$$+C_{22-2}(t)-C_{2-22}(t)+\sqrt{\tfrac{2}{3}}(C_{202}(t)-C_{20-2}(t))][C_{2-2-2}(t)+C_{222}(t)-C_{22-2}(t)$$
$$-C_{2-22}(t)]\quad+\quad\tfrac{8}{I_{2\iota}}(\tfrac{\pi^2}{5})^2[C_{221}(t)-C_{2-2-1}(t)-C_{2-21}(t)+C_{22-1}(t)-\sqrt{\tfrac{2}{3}}(C_{201}(t)$$
$$-C_{20-1}(t))][C_{221}(t)+C_{2-2-1}(t)+C_{22-1}(t)+C_{2-21}(t)]\quad+\quad\tfrac{8}{I_{3\iota}}(\tfrac{\pi^2}{5})^2[C_{22-1}(t)+$$
$$C_{2-21}(t)-C_{2-2-1}(t)-C_{221}(t)+\sqrt{\tfrac{2}{3}}(C_{20-1}(t)+C_{201}(t))][C_{221}(t)-C_{2-2-1}(t)+$$
$$C_{2-21}(t)-C_{22-1}(t)]$$

(300)

$$\tau_{22}^{v} = \tfrac{4}{3}k_BT\zeta_0\nu[\tfrac{J_1}{\triangle J}\{$$
$$-\tfrac{4\pi^2}{3\iota}[\tfrac{2}{35}\sqrt{\tfrac{2}{3}}(C_{2-20}(t)-C_{220}(t))+\tfrac{1}{27}\sqrt{\tfrac{2}{3}}(C_{420}(t)-C_{4-20}(t))+\tfrac{2}{35}(C_{22-2}(t)+$$
$$C_{222}(t)-C_{2-2-2}(t)-C_{2-22}(t))+\tfrac{1}{14}(C_{32-2}(t)+C_{3-2-2}(t)-C_{322}(t)-C_{3-22}(t))$$
$$+\tfrac{1}{42}(C_{42-2}(t)+C_{422}(t)-C_{4-2-2}(t)-C_{4-22}(t))]\}\quad+\quad\tfrac{J_2}{\triangle J}\{\tfrac{\pi^2}{27\iota}[3\sqrt{\tfrac{2}{35}}(C_{4-40}(t)$$
$$-C_{440}(t))+\tfrac{36}{35}(C_{222}(t)-C_{2-2-2}(t)+C_{22-2}(t)-C_{2-22}(t))+\tfrac{3}{7}(C_{422}(t)-C_{4-2-2}(t)$$
$$+C_{42-2}(t)-C_{4-22}(t))-\tfrac{3}{2}(C_{444}(t)-C_{4-44}(t)+C_{44-4}(t)-C_{4-4-4}(t))-\tfrac{3}{\sqrt{70}}($$
$$C_{40-4}(t)-C_{404}(t))+\tfrac{36}{35}\sqrt{\tfrac{3}{2}}(C_{20-2}(t)+C_{202}(t))+\tfrac{3}{7\sqrt{10}}(C_{40-2}(t)+C_{402}(t))-\tfrac{3}{\sqrt{7}}($$
$$C_{4-4-2}(t)-C_{442}(t)+C_{4-42}(t)-C_{44-2}(t))+\tfrac{9}{7}\sqrt{\tfrac{3}{10}}(C_{30-2}(t)-C_{302}(t))+\tfrac{3}{2\sqrt{7}}($$
$$C_{42-4}(t)+C_{424}(t)-C_{4-24}(t)-C_{4-2-4}(t))-\tfrac{36}{35}\sqrt{\tfrac{2}{3}}(C_{2-20}(t)-C_{220}(t))+0.136$$
$$C_{420}(t)+0.407C_{4-20}(t)\}]\quad+\quad\tfrac{J_3}{\triangle J}\{\tfrac{\pi^2}{27\iota}[3\sqrt{\tfrac{2}{35}}(C_{440}(t)-C_{4-40}(t))-\tfrac{72}{35}(C_{222}(t)-$$
$$C_{2-2-2}(t)+C_{22-2}(t)-C_{2-22}(t))-\tfrac{6}{7}(C_{42-2}(t)-C_{4-22}(t)+C_{422}(t)-C_{4-2-2}(t))$$
$$-\tfrac{3}{2}(C_{444}(t)-C_{4-44}(t)+C_{44-4}(t)-C_{4-4-4}(t))+\tfrac{3}{\sqrt{70}}(C_{404}(t)-C_{40-4}(t))$$
$$+\tfrac{36}{35}\sqrt{\tfrac{3}{2}}(C_{20-2}(t)+C_{202}(t))+\tfrac{3}{7\sqrt{10}}(C_{402}(t)+C_{40-2}(t))+\tfrac{3}{\sqrt{7}}(C_{4-42}(t)-C_{44-2}(t)$$
$$+C_{4-4-2}(t)-C_{442}(t))+\tfrac{9}{7}\sqrt{\tfrac{3}{10}}(C_{302}(t)-C_{30-2}(t))+\tfrac{3}{2\sqrt{7}}(C_{4-2-4}(t)+C_{4-24}(t)$$
$$-C_{42-4}(t)-C_{424}(t))+\tfrac{144}{35}\sqrt{\tfrac{2}{3}}(C_{2-20}(t)-C_{220}(t))+0.677(C_{4-20}(t)-C_{420}(t))\}]$$
$$+\quad\tfrac{8}{I_{1\iota}}(\tfrac{\pi^2}{5})^2[C_{2-22}(t)-C_{22-2}(t)+C_{222}(t)-C_{2-2-2}(t)+\sqrt{\tfrac{2}{3}}(C_{202}(t)-C_{20-2}(t))]$$
$$[C_{2-2-2}(t)+C_{222}(t)-C_{22-2}(t)-C_{2-22}(t)]\quad+\quad\tfrac{8}{I_{2\iota}}(\tfrac{\pi^2}{5})^2[C_{2-2-1}(t)+C_{2-21}(t)-$$
$$C_{221}(t)-C_{22-1}(t)+\sqrt{\tfrac{2}{3}}(C_{20-1}(t)-C_{201}(t))][C_{221}(t)+C_{2-2-1}(t)+C_{22-1}(t)+$$
$$C_{2-21}(t)]\quad+\quad\tfrac{8}{I_{3\iota}}(\tfrac{\pi^2}{5})^2[C_{22-1}(t)+C_{2-21}(t)+C_{2-2-1}(t)+C_{221}(t)+\sqrt{\tfrac{2}{3}}(C_{20-1}(t)+$$
$$C_{201}(t))][C_{221}(t)-C_{2-2-1}(t)+C_{2-21}(t)-C_{22-1}(t)] \tag{301}$$

$$\tau_{33}^{v} = \tfrac{4}{3}k_BT\zeta_0\nu[\tfrac{J_1}{\triangle J}\{$$
$$\tfrac{8\pi^2}{3\iota}[\tfrac{2}{35}\sqrt{\tfrac{2}{3}}(C_{2-20}(t)-C_{220}(t))+\tfrac{1}{27}(C_{420}(t)-C_{4-20}(t))]\}\quad+\quad\tfrac{J_2}{\triangle J}\{\tfrac{2\pi^2}{27\iota}[-\tfrac{36}{35}(C_{222}(t)$$
$$-C_{2-2-2}(t)+C_{22-2}(t)-C_{2-22}(t))-\tfrac{3}{7}(C_{422}(t)-C_{4-2-2}(t)+C_{42-2}(t)-C_{4-22}(t))$$
$$+\tfrac{36}{35}\sqrt{\tfrac{2}{3}}(C_{220}(t)-C_{2-20}(t))+0.407(C_{420}(t)-C_{4-20}(t))+\tfrac{3}{2\sqrt{7}}(C_{42-4}(t)+C_{424}(t)-$$
$$C_{4-2-4}(t)-C_{4-24}(t))]\}\quad+\quad\tfrac{J_3}{\triangle J}\{\tfrac{2\pi^2}{27\iota}[\tfrac{36}{35}(C_{222}(t)-C_{2-2-2}(t)+C_{22-2}(t)-C_{2-22}(t))$$

$$+\tfrac{3}{7}(C_{422}(t)-C_{4-2-2}(t)+C_{42-2}(t)-C_{4-22}(t))+\tfrac{36}{35}\sqrt{\tfrac{2}{3}}(C_{220}(t)-C_{2-20}(t))$$
$$+0.407(C_{420}(t)-C_{4-20}(t))+\tfrac{3}{2\sqrt{7}}(C_{42-4}(t)+C_{424}(t)-C_{4-2-4}(t)-C_{4-24}(t))]\}$$
$$-\tfrac{16}{I_{1\iota}}\sqrt{\tfrac{2}{3}}(\tfrac{\pi^2}{5})^2\{C_{202}(t)-C_{20-2}(t)\}\{C_{2-2-2}(t)+C_{222}(t)-C_{22-2}(t)-C_{2-22}(t)\}-$$
$$\tfrac{16}{I_{2\iota}}\sqrt{\tfrac{2}{3}}(\tfrac{\pi^2}{5})^2\{C_{20-1}(t)-C_{201}(t)\}\{C_{2-2-1}(t)+C_{221}(t)+C_{22-1}(t)+C_{2-21}(t)\}-$$
$$\tfrac{16}{I_{3\iota}}\sqrt{\tfrac{2}{3}}(\tfrac{\pi^2}{5})^2\{C_{20-1}(t)+C_{201}(t)\}\{C_{221}(t)-C_{2-2-1}(t)+C_{2-21}(t)-C_{22-1}(t)\}] \tag{302}$$

The shear component of the viscous stress is given by:

$$\tau_{12}^v=\eta\nu+\tfrac{2}{3}k_BT\zeta_0\nu[\tfrac{2J_1}{\triangle J}\{\tfrac{8\pi^2}{9}[-\tfrac{1}{\sqrt{70}}($$
$$C_{440}(t)+C_{4-40}(t))+\tfrac{1}{35}C_{400}(t)-\tfrac{6}{35}C_{200}(t)+\tfrac{6}{5}C_{000}(t)]\}\ +\ \tfrac{2J_2}{\triangle J}\{-\tfrac{\pi^2}{9}[\tfrac{3}{\sqrt{70}}(C_{440}(t)$$
$$+C_{4-40}(t))-6C_{000}(t)-\tfrac{3}{35}C_{400}(t)-\tfrac{24}{35}C_{200}(t)+\tfrac{1}{2}(C_{444}(t)+C_{4-4-4}(t)+C_{44-4}(t)$$
$$+C_{4-44}(t))-\tfrac{2}{\sqrt{70}}(C_{404}(t)+C_{40-4}(t))-\tfrac{1}{\sqrt{7}}(C_{442}(t)+C_{44-2}(t)+C_{4-4-2}(t)$$
$$+C_{4-42}(t))+\tfrac{36}{35}\sqrt{\tfrac{2}{3}}(C_{20-2}(t)+C_{202}(t))+\tfrac{1}{7}\sqrt{\tfrac{2}{5}}(C_{40-2}(t)+C_{402}(t))]\ +\ \tfrac{2J_3}{\triangle J}\{-\tfrac{\pi^2}{9}[$$
$$\tfrac{3}{\sqrt{70}}(C_{440}(t)+C_{4-40}(t))-6C_{000}(t)-\tfrac{3}{35}C_{400}(t)-\tfrac{24}{35}C_{200}(t)+\tfrac{1}{2}(C_{444}(t)+C_{4-4-4}(t)$$
$$+C_{44-4}(t)+C_{4-44}(t))-\tfrac{2}{\sqrt{70}}(C_{404}(t)+C_{40-4}(t))+\tfrac{1}{\sqrt{7}}(C_{442}(t)+C_{44-2}(t)+$$
$$C_{4-4-2}(t)+C_{4-42}(t))-\tfrac{36}{35}\sqrt{\tfrac{2}{3}}(C_{20-2}(t)+C_{202}(t))-\tfrac{1}{7}\sqrt{\tfrac{2}{5}}(C_{40-2}(t)+C_{402}(t))]+$$
$$\tfrac{16}{I_1}(\tfrac{\pi^2}{5})^2[C_{2-2-2}(t)+C_{222}(t)-C_{22-2}(t)-C_{2-22}(t)]^2\ -\ \tfrac{16}{I_2}(\tfrac{\pi^2}{5})^2[C_{221}(t)+C_{2-2-1}(t)$$
$$+C_{2-21}(t)+C_{22-1}(t)]^2\ +\ \tfrac{16}{I_3}(\tfrac{\pi^2}{5})^2[C_{221}(t)-C_{2-2-1}(t)+C_{2-21}(t)-C_{22-1}(t)]^2\ ] \tag{303}$$

C.2. Elastic Stress

The extra elastic stress tensor is calculated by an extended virtual work principle [85] . Let $\delta u=\nabla\mathbf{v}\delta t$ be the virtual deformation of the macroscopic system of biaxial lcps [23, 113]. Then the virtual work principle states that the variation of the free energy density equals the work done on the material volume:

$$\int\delta\mathcal{A}d\mathbf{x}=\int[\tau_e:\nabla\mathbf{v}-\mathbf{v}\cdot\mathbf{F_e}]\delta td\mathbf{x} \tag{304}$$

where τ_e is the elastic stress and $\mathbf{F_e}$ is the elastic body force. The variation of the free energy is expressed as the rate of change of the *PDF* $f(\Omega, t)$

$$\delta\mathcal{A} = \int \frac{\delta\mathcal{A}}{\delta f}\delta f d\Omega = \int \frac{\delta\mathcal{A}}{\delta f}\frac{\partial f}{\partial t}\delta t d\Omega \tag{305}$$

For biaxial molecules, undergoing an impulsive elastic deformation,

$$\frac{\partial f}{\partial t} = -\nabla\cdot(\mathbf{v}f) - L^*\cdot(\mathbf{g}f) \tag{306}$$

From eqs.(304,305,306),

$$\begin{aligned}\int \delta\mathcal{A} d\mathbf{x} &= -\int\int \frac{\delta\mathcal{A}}{\delta f}[\nabla\cdot(\mathbf{v}f) + L^*\cdot(\mathbf{g}f)]\delta t d\mathbf{x} d\Omega \\ &= -\int\int \mathbf{v}\cdot(-\nabla\frac{\delta\mathcal{A}}{\delta f})f\delta t d\mathbf{x} d\Omega + \int\int L\tfrac{\delta\mathcal{A}}{\delta f}\cdot\mathbf{g}^* f\delta t d\mathbf{x} d\Omega.\end{aligned} \tag{307}$$

Comparing the terms containing $\nabla\mathbf{v}$ in eqs.(304,307):

$$\tau_e : \nabla\mathbf{v} = \int \mathbf{L}\frac{\delta\mathcal{A}}{\delta f}\cdot\mathbf{g}^* f d\Omega. \tag{308}$$

Using the notation for the chemical potential, we arrive at

$$\begin{aligned}\int \mathbf{L}\frac{\delta\mathcal{A}}{\delta f}\cdot\mathbf{g}^* f d\Omega &= \nu\int_\Omega(\mathbf{L}\tilde{\mu}_t f)\cdot\mathbf{g}^* d\Omega \\ &= \nu k_B T\langle\mathbf{L}\mu\cdot\mathbf{g}^*\rangle\end{aligned} \tag{309}$$

where $\tilde{\mu}_t = k_B T\mu$. Using the equation for the flow vector $\overrightarrow{g} = K : \alpha_m\mathbf{m} + K : \alpha_n\mathbf{n} + K : \alpha_k\mathbf{k}$ (Eq. 251), we arrive at the expression for the elastic stress tensor

$$\begin{aligned}\tau_e^{\alpha\beta} &= \nu k_B T\langle\alpha_m^{*\alpha\beta}L_m\mu + \alpha_n^{*\alpha\beta}L_n\mu + \alpha_k^{*\alpha\beta}L_k\mu\rangle \\ &= -\nu k_B T\langle\mathbf{L}^*\cdot\vec{\alpha}^{\alpha\beta}\rangle + \langle\alpha_m^{*\alpha\beta}L_m\mathcal{U} + \alpha_n^{*\alpha\beta}L_n\mathcal{U} + \alpha_k^{*\alpha\beta}L_k\mathcal{U}\rangle,\end{aligned} \tag{310}$$

where $\vec{\alpha}^{\alpha\beta} = (\alpha_m^{\alpha\beta}, \alpha_n^{\alpha\beta}, \alpha_k^{\alpha\beta})$ is a third order tensor and $\mathbf{L}^* \cdot \vec{\alpha}^{\alpha\beta} = \sum_{i=1}^{3} L_i \alpha_i^{\alpha\beta}$. The elastic force is identified as $\mathbf{F}_e = -\langle \nabla \tilde{\mu}_t \rangle$. For an incompressible, homogeneous fluid system, this term can be absorbed into the pressure and is therefore ignored from now on.

C.3. Elastic Stress: Series Expansion

First we note the following useful identities necessary for the series expansion of the elastic stress:

$$
\begin{aligned}
m_1 n_1 &= \tfrac{1}{4}[D^2_{-2-1} - D^2_{21} - D^2_{2-1} + D^2_{-21} + \sqrt{\tfrac{2}{3}}(D^2_{01} - D^2_{0-1})] \\
m_2 n_2 &= \tfrac{1}{4}[D^2_{21} - D^2_{-2-1} - D^2_{-21} + D^2_{2-1} + \sqrt{\tfrac{2}{3}}(D^2_{01} - D^2_{0-1})] \\
m_3 n_3 &= -\tfrac{1}{2}\sqrt{\tfrac{2}{3}}(D^2_{01} - D^2_{0-1}) \\
n_1 k_1 &= \tfrac{1}{4\iota}[D^2_{22} - D^2_{-2-2} + D^2_{-22} - D^2_{2-2} + \sqrt{\tfrac{2}{3}}(D^2_{0-2} - D^2_{02})] \\
n_2 k_2 &= \tfrac{1}{4\iota}[D^2_{2-2} - D^2_{-22} + D^2_{-2-2} - D^2_{22} + \sqrt{\tfrac{2}{3}}(D^2_{0-2} - D^2_{02})] \\
n_3 k_3 &= -\tfrac{1}{2\iota}\sqrt{\tfrac{2}{3}}(D^2_{0-2} - D^2_{02}) \\
m_1 k_1 &= \tfrac{1}{4\iota}[D^2_{-21} + D^2_{2-1} - D^2_{21} - D^2_{-2-1}] + \tfrac{1}{4\iota}\sqrt{\tfrac{2}{3}}(D^2_{01} + D^2_{0-1}) \\
m_2 k_2 &= \tfrac{1}{4\iota}[D^2_{-2-1} + D^2_{21} - D^2_{-21} - D^2_{2-1} + \sqrt{\tfrac{2}{3}}(D^2_{01} + D^2_{0-1})] \\
m_3 k_3 &= -\tfrac{1}{2\iota}\sqrt{\tfrac{2}{3}}(D^2_{01} + D^2_{0-1}) \\
n_1 k_2 &= -\tfrac{1}{4}[D^2_{-22} + D^2_{2-2} - D^2_{22} - D^2_{-2-2} - 2D^1_{00}] \\
n_2 k_1 &= -\tfrac{1}{4}[D^2_{-22} + D^2_{2-2} - D^2_{22} - D^2_{-2-2} + 2D^1_{00}] \\
k_1 m_2 &= \tfrac{1}{4}[D^2_{-2-1} + D^2_{2-1} - D^2_{21} - D^2_{-21}] - \tfrac{1}{2\sqrt{2}}(D^1_{01} - D^1_{0-1}) \\
k_2 m_1 &= \tfrac{1}{4}[D^2_{-2-1} + D^2_{2-1} - D^2_{21} - D^2_{-21}] + \tfrac{1}{2\sqrt{2}}(D^1_{01} - D^1_{0-1}) \\
m_1 n_2 &= \tfrac{\iota}{4}[D^2_{21} + D^2_{-2-1} - D^2_{2-1} - D^2_{-21}] + \tfrac{\iota}{2\sqrt{2}}(D^1_{01} + D^1_{0-1}) \\
m_2 n_1 &= \tfrac{\iota}{4}[D^2_{21} + D^2_{-2-1} - D^2_{2-1} - D^2_{-21}] - \tfrac{\iota}{2\sqrt{2}}(D^1_{01} + D^1_{0-1})
\end{aligned}
\tag{311}
$$

The different components of the elastic stress are derived next. First, we present a detailed expression for the normal stress components τ_e^{ii}:

$$\tau_e^{11} = \langle (L_m g_m^{11} + L_n g_n^{11} + L_k g_k^{11})(1+\mathcal{U})\rangle$$
$$= \langle \{\eta_{bc}[D_{22}^2 + D_{-2-2}^2 + D_{-22}^2 + D_{2-2}^2 - \sqrt{\tfrac{2}{3}}(D_{02}^2 + D_{0-2}^2)] + \eta_c[D_{-22}^2 + D_{2-2}^2 -$$
$$D_{22}^2 - D_{-2-2}^2 + 2D_{00}^2 + \sqrt{\tfrac{2}{3}}(D_{02}^2 + D_{0-2}^2)] + \eta_b[D_{-2-2}^2 - D_{22}^2 - D_{2-2}^2 + D_{-22}^2 +$$
$$\sqrt{\tfrac{2}{3}}(D_{02}^2 - D_{0-2}^2)]\}\{1+\mathcal{U}\}\rangle \tag{312}$$

where $\eta_{bc} = \frac{1}{2i}(\frac{r_b^2 - r_c^2}{r_b^2 + r_c^2})$, $\eta_b = \frac{1}{4i}(\frac{1-r_b^2}{1+r_b^2})$ and $\eta_c = \frac{1}{4i}(\frac{1-r_c^2}{1+r_c^2})$. $\mathcal{U}$ is the excluded volume potential given by Eq.(130). The constants r_L in the following expressions are given by $r_L = 8\pi^2/(2L+1)^2$

$$= \eta_{bc} r_2 (C_{2-2-2}(t) + C_{222}(t) + C_{22-2}(t) + C_{2-22}(t) - \sqrt{\tfrac{2}{3}}(C_{202}(t) + C_{20-2}(t))) +$$
$$\eta_c r_2 (C_{22-2}(t) + C_{2-22}(t) - C_{2-2-2}(t) - C_{222}(t) + 2C_{200}(t) + \sqrt{\tfrac{2}{3}}(C_{202}(t) +$$
$$C_{20-2}(t))) + \eta_b r_2 (C_{222}(t) - C_{2-2-2}(t) - C_{2-22}(t) + C_{22-2}(t) + \sqrt{\tfrac{2}{3}}(C_{20-2}(t) -$$
$$C_{202}(t))) + \eta_{bc} A_1(t)[\tfrac{2r_2}{7}(C_{22-2}(t) + C_{2-22}(t) + C_{2-2-2}(t) + C_{222}(t) + \sqrt{\tfrac{2}{3}}(C_{20-2}(t)$$
$$+ C_{202}(t))) + \tfrac{r_3}{2}(C_{3-2-2}(t) + C_{322}(t) - C_{32-2}(t) - C_{3-22}(t)) + \tfrac{3r_4}{14}(C_{42-2}(t)$$
$$+ C_{4-22}(t) + C_{4-2-2}(t) + C_{422}(t) - \tfrac{14}{9}\sqrt{\tfrac{2}{3}}(C_{40-2}(t) + C_{402}(t)))] + \eta_{bc} A_2(t)[\tfrac{4r_2}{7}$$
$$(C_{20-2}(t) + C_{202}(t) - \tfrac{1}{\sqrt{6}}(C_{22-2}(t) + C_{2-2-2}(t) + C_{222}(t) + C_{2-22}(t))) - \tfrac{r_3}{\sqrt{6}}$$
$$(C_{32-2}(t) - C_{322}(t) + C_{3-22}(t) - C_{3-2-2}(t)) + \tfrac{r_4}{7}\sqrt{\tfrac{3}{5}}(C_{402}(t) + C_{40-2}(t)) +$$
$$r_4\sqrt{\tfrac{3}{14}}(C_{442}(t) + C_{4-42}(t) + C_{44-2}(t) + C_{4-4-2}(t) + \sqrt{2.5}(C_{42-2}(t) + C_{4-2-2}(t) +$$
$$C_{422}(t) + C_{4-22}(t)))] + \eta_{bc} A_{12}(t)[\sqrt{\tfrac{2}{3}}\tfrac{2r_2}{7}(C_{2-22}(t) + C_{2-2-2}(t) - C_{22-2}(t) -$$
$$C_{222}(t)) + \tfrac{r_3}{\sqrt{5}}(C_{30-2}(t) - C_{302}(t) + \sqrt{\tfrac{5}{6}}(C_{3-22}(t) - C_{3-2-2}(t) + C_{322}(t) -$$
$$C_{32-2}(t))) + r_4\sqrt{\tfrac{3}{14}}(C_{44-2}(t) + C_{442}(t) - C_{4-4-2}(t) - C_{4-42}(t) + \tfrac{1}{\sqrt{7}}(C_{4-22}(t) +$$
$$C_{4-2-2}(t) - C_{42-2}(t) - C_{422}(t)))] + \eta_{bc} A_3(t)[-\sqrt{\tfrac{2}{3}}\tfrac{2r_0}{5}C_{000}(t) + \tfrac{4r_2}{7}(C_{2-20}(t)$$
$$+ C_{220}(t) + \sqrt{\tfrac{2}{3}}C_{200}(t)) + r_4\sqrt{\tfrac{3}{14}}(C_{42-4}(t) + C_{424}(t) + C_{4-2-4}(t) + C_{4-24}(t)$$
$$+ \sqrt{\tfrac{2}{35}}(C_{420}(t) + C_{4-20}(t)) - 0.8\tfrac{1}{\sqrt{7}}C_{400}(t) - \sqrt{\tfrac{8}{5}}(C_{40-4}(t) + C_{404}(t)))] + \eta_{bc} A_{23}(t)[$$
$$r_2\tfrac{\sqrt{6}}{7}(C_{212}(t) + C_{21-2}(t) + C_{2-12}(t) + C_{2-1-2}(t) + \tfrac{2}{3}(C_{212}(t) + C_{2-12}(t) +$$
$$C_{21-2}(t))] + C_{2-1-2}(t) + \tfrac{r_3}{2}\sqrt{\tfrac{3}{5}}(C_{3-1-2}(t) - C_{3-12}(t) + C_{312}(t) - C_{31-2}(t) + \sqrt{\tfrac{5}{3}}$$
$$(C_{332}(t) - C_{33-2}(t) + C_{3-3-2}(t) - C_{3-32}(t)) + \tfrac{2}{3}(C_{3-1-2}(t) - C_{3-12}(t) + C_{312}(t)$$

$$))-C_{31-2}(t)+r_4\tfrac{\sqrt{3}}{14}(C_{41-2}(t)+C_{412}(t)+C_{4-1-2}(t)+C_{4-12}(t)+\sqrt{7}(C_{432}(t)+$$
$$C_{43-2}(t)+C_{4-32}(t)+C_{4-3-2}(t))-2(C_{412}(t)+C_{41-2}(t)+C_{4-12}(t)+C_{4-1-2}(t)))]+$$
$$\eta_{bc}A_{13}(t)[r_2\tfrac{\sqrt{6}}{7}(C_{2-12}(t)-C_{21-2}(t)-C_{212}(t)+C_{2-1-2}(t)+\tfrac{2}{3}(C_{212}(t)-C_{2-12}(t)$$
$$+C_{21-2}(t)-C_{2-1-2}(t)))+\tfrac{r_3}{2}\sqrt{\tfrac{3}{5}}(C_{3-1-2}(t)-C_{3-12}(t)-C_{312}(t)+C_{31-2}(t)$$
$$+\sqrt{\tfrac{5}{3}}(C_{332}(t)-C_{33-2}(t)-C_{3-3-2}(t)+\tfrac{2}{3}(C_{312}(t)-C_{3-32}(t))-C_{31-2}(t)-$$
$$C_{3-1-2}(t)+C_{3-12}(t)))-r_4\tfrac{\sqrt{3}}{14}(-C_{41-2}(t)-C_{412}(t)+C_{4-1-2}(t)+C_{4-12}(t)+$$
$$\sqrt{7}(C_{432}(t)+C_{43-2}(t)-C_{4-32}(t)-C_{4-3-2}(t))-2(C_{412}(t)+C_{41-2}(t)-C_{4-12}(t)-$$
$$C_{4-1-2}(t)))]+\eta_{bc}B_{13}(t)[2r_2\tfrac{\sqrt{6}}{7}(C_{2-10}(t)-C_{210}(t)+\tfrac{2}{3}(C_{210}(t)-C_{2-10}(t))$$
$$)+\tfrac{r_4}{\sqrt{35}}(C_{430}(t)-C_{4-30}(t)+\sqrt{5/2}(C_{4-1-4}(t)-C_{414}(t)-C_{41-4}(t)+C_{4-14}(t)$$
$$)+\sqrt{\tfrac{35}{2}}(C_{43-4}(t)-C_{4-34}(t)-C_{4-3-4}(t)+C_{434}(t)))]+\eta_{bc}A_4(t)[\tfrac{4r_0}{5}C_{000}(t)+$$
$$\tfrac{8r_0}{7}(C_{200}(t)-\tfrac{1}{\sqrt{6}}(C_{220}(t)+C_{2-20}(t)))+\tfrac{2r_4}{35}(C_{400}(t)+\sqrt{\tfrac{35}{2}}(C_{40-4}(t)+C_{4-40}(t)$$
$$+C_{404}(t)+C_{440}(t))+\tfrac{35}{2}(C_{4-4-4}(t)+C_{44-4}(t)+C_{4-44}(t)+C_{444}(t))-\sqrt{\tfrac{5}{2}}$$
$$(C_{420}(t)+C_{4-20}(t)))]+B_{12}(t)[\tfrac{4r_2}{7}(C_{220}(t)-C_{2-20}(t))+r_4(C_{444}(t)-C_{4-4-4}(t)+$$
$$C_{44-4}(t)-C_{4-44}(t)+\tfrac{2}{\sqrt{70}}(C_{440}(t)-C_{4-40}(t))-\tfrac{1}{\sqrt{7}}(C_{42-4}(t)-C_{4-2-4}(t)+$$
$$C_{424}(t)-C_{4-24}(t)-\tfrac{1}{7}\sqrt{\tfrac{2}{5}}(C_{420}(t)-C_{4-20}(t)))]+2A_1(t)\eta_c[\tfrac{r_0}{5}C_{000}(t)+\tfrac{2r_2}{7}C_{200}(t)+$$
$$\tfrac{18r_4}{35}C_{400}(t)]+2A_2(t)\eta_c[-\tfrac{2r_2}{7}(C_{220}(t)+C_{2-20}(t))+\tfrac{r_4}{3}(C_{420}(t)+C_{4-20}(t))]+$$
$$2A_3(t)\eta_c[-\tfrac{2r_2}{7}(C_{202}(t)+C_{20-2}(t))+\tfrac{r_4}{3}(C_{402}(t)+C_{40-2}(t))]+2A_4(t)\eta_c[\tfrac{2r_2}{7}$$
$$(C_{22-2}(t)+C_{2-22}(t)+C_{222}(t)+C_{2-2-2}(t))+\tfrac{r_3}{2}(C_{322}(t)+C_{3-2-2}(t)-$$
$$C_{32-2}(t)-C_{3-22}(t))+\tfrac{3r_4}{14}(C_{422}(t)+C_{4-2-2}(t)+C_{42-2}(t)+C_{4-22}(t))]+$$
$$2A_{12}(t)\eta_c[-\tfrac{2r_2}{7}(C_{220}(t)-C_{2-20}(t))+\tfrac{r_4}{3}(C_{420}(t)-C_{4-20}(t))]+2B_{12}(t)\eta_c[\tfrac{2r_2}{7}$$
$$(C_{22-2}(t)-C_{2-22}(t)+C_{222}(t)-C_{2-2-2}(t))+\tfrac{r_3}{2}(C_{322}(t)-C_{3-2-2}(t)-C_{32-2}(t)+$$
$$C_{3-22}(t))+\tfrac{3r_4}{14}(C_{422}(t)-C_{4-2-2}(t)+C_{42-2}(t)-C_{4-22}(t))+2A_{23}(t)\eta_c[\tfrac{2r_2}{7}(C_{210}(t)$$
$$)+C_{2-10}(t)+r_4\sqrt{\tfrac{3}{14}}(C_{410}(t)+C_{4-10}(t))]+2A_{13}(t)\eta_c[\tfrac{2r_2}{7}(C_{210}(t)-C_{2-10}(t))$$
$$+r_4\sqrt{\tfrac{3}{14}}(C_{410}(t)-C_{4-10}(t))]+2B_{13}(t)\eta_c[\tfrac{2r_2}{7}(C_{2-12}(t)-C_{21-2}(t)+C_{2-1-2}(t)$$
$$-C_{212}(t))+\tfrac{r_3}{\sqrt{10}}(C_{3-12}(t)-C_{31-2}(t)-C_{3-1-2}(t)+C_{312}(t))+\tfrac{3r_4}{7\sqrt{2}}(C_{41-2}(t)-$$
$$C_{4-12}(t)-C_{4-1-2}(t)+C_{412}(t))]+\eta_cA_1(t)[\tfrac{2r_2}{7}(C_{22-2}(t)+C_{2-22}(t)+C_{2-2-2}(t)+$$
$$C_{222}(t)+\sqrt{\tfrac{2}{3}}(C_{20-2}(t)+C_{202}(t))]+\tfrac{r_3}{2}(C_{3-2-2}(t)+C_{322}(t)-C_{32-2}(t)-$$

$C_{3-22}(t)) + \frac{3r_4}{14}(C_{42-2}(t) + C_{4-22}(t) + C_{4-2-2}(t) + C_{422}(t) - \frac{14}{9}\sqrt{\frac{2}{3}}(C_{40-2}(t) +$
$C_{402}(t)))] + \eta_c A_2(t)[\frac{4r_2}{7}(C_{20-2}(t) + C_{202}(t) - \frac{1}{\sqrt{6}}(C_{22-2}(t) + C_{2-2-2}(t) +$
$C_{222}(t) + C_{2-22}(t))) - \frac{r_3}{\sqrt{6}}(C_{32-2}(t) - C_{322}(t) + C_{3-22}(t) - C_{3-2-2}(t)) + \frac{r_4}{7}\sqrt{\frac{3}{5}}($
$C_{402}(t) + C_{40-2}(t)) + r_4\sqrt{\frac{3}{14}}(C_{442}(t) + C_{4-42}(t) + C_{44-2}(t) + C_{4-4-2}(t) +$
$\sqrt{\frac{5}{2}}(C_{42-2}(t) + C_{4-2-2}(t) + C_{422}(t) + C_{4-22}(t)))] + \eta_c A_{12}(t)[\sqrt{\frac{2}{3}}\frac{2r_2}{7}(C_{2-22}(t)$
$+C_{2-2-2}(t) - C_{22-2}(t) - C_{222}(t)) + \frac{r_3}{\sqrt{5}}(C_{30-2}(t) - C_{302}(t) + \sqrt{\frac{5}{6}}(C_{3-22}(t)$
$-C_{3-2-2}(t) + C_{322}(t) - C_{32-2}(t))) + r_4\sqrt{\frac{3}{14}}(C_{44-2}(t) + C_{442}(t) - C_{4-4-2}(t)$
$-C_{4-42}(t) + \frac{1}{\sqrt{7}}(C_{4-22}(t) + C_{4-2-2}(t) - C_{42-2}(t) - C_{422}(t)))] + \eta_c A_3(t)[-\sqrt{\frac{2}{3}}\frac{2r_0}{5}$
$C_{000}(t) + \frac{4r_2}{7}(C_{2-20}(t) + C_{220}(t) + \sqrt{\frac{2}{3}}C_{200}(t)) + r_4\sqrt{\frac{3}{14}}(C_{42-4}(t) + C_{424}(t)$
$+C_{4-2-4}(t) + C_{4-24}(t) + \sqrt{\frac{2}{35}}(C_{420}(t) + C_{4-20}(t)) - 0.8\frac{1}{\sqrt{7}}C_{400}(t) - \sqrt{\frac{8}{5}}(C_{40-4}(t)$
$+C_{404}(t)))] + \eta_c A_{23}(t)[r_2\frac{\sqrt{6}}{7}(C_{212}(t) + C_{21-2}(t) + C_{2-12}(t) + C_{2-1-2}(t) + \frac{2}{3}$
$(C_{212}(t) + C_{2-12}(t) + C_{21-2}(t) + C_{2-1-2}(t))) + \frac{r_3}{2}\sqrt{\frac{3}{5}}(C_{3-1-2}(t) - C_{3-12}(t) +$
$C_{312}(t) - C_{31-2}(t) + \sqrt{\frac{5}{3}}(C_{332}(t) - C_{33-2}(t) + C_{3-3-2}(t) - C_{3-32}(t)) + \frac{2}{3}($
$C_{3-1-2}(t) - C_{3-12}(t) + C_{312}(t) - C_{31-2}(t))) + r_4\frac{\sqrt{3}}{14}(C_{41-2}(t) + C_{412}(t)$
$+C_{4-1-2}(t) + C_{4-12}(t) + \sqrt{7}(C_{432}(t) + C_{43-2}(t) + C_{4-32}(t) + C_{4-3-2}(t)) - 2($
$C_{412}(t) + C_{41-2}(t) + C_{4-12}(t) + C_{4-1-2}(t)))] + \eta_c A_{13}(t)[r_2\frac{\sqrt{6}}{7}(C_{2-12}(t) - C_{21-2}(t) -$
$C_{2-1-2}(t) + \frac{2}{3}(C_{212}(t) - C_{2-12}(t) + C_{21-2}(t) - C_{2-1-2}(t))) + \frac{r_3}{2}\sqrt{\frac{3}{5}}(C_{3-1-2}(t)$
$-C_{3-12}(t) - C_{312}(t) + C_{31-2}(t) + \sqrt{\frac{5}{3}}(C_{332}(t) - C_{33-2}(t) - C_{3-3-2}(t) + \frac{2}{3}(C_{312}(t) -$
$C_{3-32}(t)) - C_{31-2}(t) - C_{3-1-2}(t) + C_{3-12}(t))) - r_4\frac{\sqrt{3}}{14}(-C_{41-2}(t) - C_{412}(t) +$
$C_{4-1-2}(t) + C_{4-12}(t) + \sqrt{7}(C_{432}(t) + C_{43-2}(t) - C_{4-32}(t) - C_{4-3-2}(t)) - 2(C_{412}(t)$
$+C_{41-2}(t) - C_{4-12}(t) - C_{4-1-2}(t)))] + \eta_c B_{13}(t)[2r_2\frac{\sqrt{6}}{7}(C_{2-10}(t) - C_{210}(t) + \frac{2}{3}($
$C_{210}(t) - C_{2-10}(t))] + \frac{r_4}{\sqrt{35}}(C_{430}(t) - C_{4-30}(t) + \sqrt{5/2}(C_{4-1-4}(t) - C_{414}(t) -$
$C_{41-4}(t) + C_{4-14}(t)) + \sqrt{\frac{35}{2}}(C_{43-4}(t) - C_{4-34}(t) - C_{4-3-4}(t) + C_{434}(t)))] +$
$\eta_c A_4(t)[\frac{4r_0}{5}C_{000}(t) + \frac{8r_0}{7}(C_{200}(t) - \frac{1}{\sqrt{6}}(C_{220}(t) + C_{2-20}(t))) + \frac{2r_4}{35}(C_{400}(t) +$
$\sqrt{\frac{35}{2}}(C_{40-4}(t) + C_{4-40}(t) + C_{404}(t) + C_{440}(t)) + \frac{35}{2}(C_{4-4-4}(t) + C_{44-4}(t) +$
$C_{4-44}(t) + C_{444}(t)) - \sqrt{\frac{5}{2}}(C_{420}(t) + C_{4-20}(t)))] + \eta_c B_{12}(t)[\frac{4r_2}{7}(C_{220}(t) -$
$C_{2-20}(t)) + r_4(C_{444}(t) - C_{4-4-4}(t) + C_{44-4}(t) - C_{4-44}(t) + \frac{2}{\sqrt{70}}(C_{440}(t) -)C_{4-40}(t)$

$$) - \tfrac{1}{\sqrt{7}}(C_{42-4}(t) - C_{4-2-4}(t) + C_{424}(t) - C_{4-24}(t) - \tfrac{1}{7}\sqrt{\tfrac{2}{5}}(C_{420}(t) -$$
$$C_{4-20}(t)))] + \eta_b A_1(t)[\tfrac{2r_2}{7}(C_{2-22}(t) + C_{2-2-2}(t) + C_{222}(t) + \sqrt{\tfrac{2}{3}}(C_{20-2}(t) +$$
$$C_{202}(t))) + \tfrac{r_3}{2}(C_{3-2-2}(t) + C_{322}(t) - C_{32-2}(t) - C_{3-22}(t)) + \tfrac{3r_4}{14}(C_{42-2}(t) +$$
$$C_{4-22}(t) + C_{4-2-2}(t) + C_{422}(t) - \tfrac{14}{9}\sqrt{\tfrac{2}{3}}(C_{40-2}(t) + C_{402}(t)))] + \eta_b A_2(t)[\tfrac{4r_2}{7}$$
$$(C_{20-2}(t) + C_{202}(t) - \tfrac{1}{\sqrt{6}}(C_{22-2}(t) + C_{2-2-2}(t) + C_{222}(t) + C_{2-22}(t))) - \tfrac{r_3}{\sqrt{6}}$$
$$(C_{32-2}(t) - C_{322}(t) + C_{3-22}(t) - C_{3-2-2}(t)) + \tfrac{r_4}{7}\sqrt{\tfrac{3}{5}}(C_{402}(t) + C_{40-2}(t)) +$$
$$r_4\sqrt{\tfrac{3}{14}}(C_{442}(t) + C_{4-42}(t) + C_{44-2}(t) + C_{4-4-2}(t) + \sqrt{2.5}(C_{42-2}(t) + C_{4-2-2}(t) +$$
$$C_{422}(t) + C_{4-22}(t)))] + \eta_b A_{12}(t)[\sqrt{\tfrac{2}{3}}\tfrac{2r_2}{7}(C_{2-22}(t) + C_{2-2-2}(t) - C_{22-2}(t) -$$
$$C_{222}(t)) + \tfrac{r_3}{\sqrt{5}}(C_{30-2}(t) - C_{302}(t) + \sqrt{\tfrac{5}{6}}(C_{3-22}(t) - C_{3-2-2}(t) + C_{322}(t) - C_{32-2}(t)$$
$$)) + r_4\sqrt{\tfrac{3}{14}}(C_{44-2}(t) + C_{442}(t) - C_{4-4-2}(t) - C_{4-42}(t) + \tfrac{1}{\sqrt{7}}(C_{4-22}(t) + C_{4-2-2}(t) -$$
$$C_{42-2}(t) - C_{422}(t)))] + \eta_b A_3(t)[-\sqrt{\tfrac{2}{3}}\tfrac{2r_0}{5}C_{000}(t) + \tfrac{4r_2}{7}(C_{2-20}(t) + C_{220}(t) +$$
$$\sqrt{\tfrac{2}{3}}C_{200}(t)) + r_4\sqrt{\tfrac{3}{14}}(C_{42-4}(t) + C_{424}(t) + C_{4-2-4}(t) + C_{4-24}(t) + \sqrt{\tfrac{2}{35}}(C_{420}(t) +$$
$$C_{4-20}(t)) - 0.8\tfrac{1}{\sqrt{7}}C_{400}(t) - \sqrt{\tfrac{8}{5}}(C_{40-4}(t) + C_{404}(t)))] + \eta_b A_{23}(t)[r_2\tfrac{\sqrt{6}}{7}(C_{212}(t)$$
$$+ C_{21-2}(t) + C_{2-12}(t) + C_{2-1-2}(t) + \tfrac{2}{3}(C_{212}(t) + C_{2-12}(t) + C_{21-2}(t) + C_{2-1-2}(t)$$
$$)) + \tfrac{r_3}{2}\sqrt{\tfrac{3}{5}}(C_{3-1-2}(t) - C_{3-12}(t) + C_{312}(t) - C_{31-2}(t) + \sqrt{\tfrac{5}{3}}(C_{332}(t) - C_{33-2}(t) +$$
$$C_{3-3-2}(t) - C_{3-32}(t)) + \tfrac{2}{3}(C_{3-1-2}(t) - C_{3-12}(t) + C_{312}(t) - C_{31-2}(t))) +$$
$$r_4\tfrac{\sqrt{3}}{14}(C_{41-2}(t) + C_{412}(t) + C_{4-1-2}(t) + C_{4-12}(t) + \sqrt{7}(C_{432}(t) + C_{43-2}(t) +$$
$$C_{4-32}(t) + C_{4-3-2}(t)) - 2(C_{412}(t) + C_{41-2}(t) + C_{4-12}(t) + C_{4-1-2}(t)))] +$$
$$\eta_b A_{13}(t)[r_2\tfrac{\sqrt{6}}{7}(C_{2-12}(t) - C_{21-2}(t) - C_{212}(t) + C_{2-1-2}(t) + \tfrac{2}{3}(C_{212}(t) - C_{2-12}(t) +$$
$$C_{21-2}(t) - C_{2-1-2}(t))) + \tfrac{r_3}{2}\sqrt{\tfrac{3}{5}}(C_{3-1-2}(t) - C_{3-12}(t) - C_{312}(t) + C_{31-2}(t) +$$
$$\sqrt{\tfrac{5}{3}}(C_{332}(t) - C_{33-2}(t) - C_{3-3-2}(t) + \tfrac{2}{3}(C_{312}(t) - C_{3-32}(t)) - C_{31-2}(t) -$$
$$C_{3-1-2}(t) + C_{3-12}(t))) - r_4\tfrac{\sqrt{3}}{14}(-C_{41-2}(t) - C_{412}(t) + C_{4-1-2}(t) + C_{4-12}(t)$$
$$+ \sqrt{7}(C_{432}(t) + C_{43-2}(t) - C_{4-32}(t) - C_{4-3-2}(t)) - 2(C_{412}(t) + C_{41-2}(t) -$$
$$C_{4-12}(t) - C_{4-1-2}(t)))] + \eta_b B_{13}(t)[2r_2\tfrac{\sqrt{6}}{7}(C_{2-10}(t) - C_{210}(t) + \tfrac{2}{3}(C_{210}(t)$$
$$- C_{2-10}(t))) + \tfrac{r_4}{\sqrt{35}}(C_{430}(t) - C_{4-30}(t) + \sqrt{5/2}(C_{4-1-4}(t) - C_{414}(t) - C_{41-4}(t) +$$
$$C_{4-14}(t)) + \sqrt{\tfrac{35}{2}}(C_{43-4}(t) - C_{4-34}(t) - C_{4-3-4}(t) + C_{434}(t)))] + \eta_b A_4(t)[\tfrac{4r_0}{5}C_{000}(t)$$
$$+ \tfrac{8r_0}{7}(C_{200}(t) - \tfrac{1}{\sqrt{6}}(C_{220}(t) + C_{2-20}(t))) + \tfrac{2r_4}{35}(C_{400}(t) + \sqrt{\tfrac{35}{2}}(C_{40-4}(t) + C_{4-40}(t)$$

$$+C_{404}(t)+C_{440}(t))+\tfrac{35}{2}(C_{4-4-4}(t)+C_{44-4}(t)+C_{4-44}(t)+C_{444}(t))-\sqrt{\tfrac{5}{2}}($$
$$C_{420}(t)+C_{4-20}(t)))]+\eta_b B_{12}(t)[\tfrac{4r_2}{7}(C_{220}(t)-C_{2-20}(t))+r_4(C_{444}(t)-C_{4-4-4}(t)+$$
$$)C_{44-4}(t)-C_{4-44}(t)+\tfrac{2}{\sqrt{70}}(C_{440}(t)-C_{4-40}(t))-\tfrac{1}{\sqrt{7}}(C_{42-4}(t)-C_{4-2-4}(t)+$$
$$C_{424}(t)-C_{4-24}(t)-\tfrac{1}{7}\sqrt{\tfrac{2}{5}}(C_{420}(t)-C_{4-20}(t)))]$$

$$\tau_e^{22}=\langle(L_m g_m^{22}+L_n g_n^{22}+L_k g_k^{22})(1+\mathcal{U})\rangle$$
$$=\langle\{-\eta_{bc}[D_{22}^2+D_{-2-2}^2+D_{-22}^2+D_{2-2}^2+\sqrt{\tfrac{2}{3}}(D_{02}^2+D_{0-2}^2)]+\eta_c[D_{22}^2+D_{-2-2}^2-$$
$$D_{2-2}^2-D_{-22}^2+2D_{00}^2+\sqrt{\tfrac{2}{3}}(D_{02}^2+D_{0-2}^2)]+\eta_b[D_{22}^2-D_{-2-2}^2+D_{-22}^2-D_{2-2}^2+$$
$$\sqrt{\tfrac{2}{3}}(D_{02}^2-D_{0-2}^2)]\}\{1+\mathcal{U}\}\rangle \tag{313}$$
$$=-\eta_{bc}r_2(C_{2-2-2}(t)+C_{222}(t)+C_{22-2}(t)+C_{2-22}(t)+\sqrt{\tfrac{2}{3}}(C_{202}(t)+C_{20-2}(t)))+$$
$$\eta_c r_2(C_{222}(t)+C_{2-2-2}(t)-C_{22-2}(t)-C_{2-22}(t)+2C_{200}(t)+\sqrt{\tfrac{2}{3}}(C_{202}(t)+$$
$$C_{20-2}(t)))+\eta_b r_2(C_{2-2-2}(t)-C_{222}(t)+C_{22-2}(t)-C_{2-22}(t)+\sqrt{\tfrac{2}{3}}(C_{20-2}(t)-$$
$$C_{202}(t)))+\eta_{bc}A_1(t)[\tfrac{2r_2}{7}(C_{22-2}(t)+C_{2-22}(t)+C_{2-2-2}(t)+C_{222}(t)+\sqrt{\tfrac{2}{3}}(C_{20-2}(t)+$$
$$C_{202}(t)))+\tfrac{r_3}{2}(C_{3-2-2}(t)+C_{322}(t)-C_{32-2}(t)-C_{3-22}(t))+\tfrac{3r_4}{14}(C_{42-2}(t)+$$
$$C_{4-22}(t)+C_{4-2-2}(t)+C_{422}(t)-\tfrac{14}{9}\sqrt{\tfrac{2}{3}}(C_{40-2}(t)+C_{402}(t)))]+\eta_{bc}A_2(t)[\tfrac{4r_2}{7}$$
$$(C_{20-2}(t)+C_{202}(t)-\tfrac{1}{\sqrt{6}}(C_{22-2}(t)+C_{2-2-2}(t)+C_{222}(t)+C_{2-22}(t)))-\tfrac{r_3}{\sqrt{6}}$$
$$(C_{32-2}(t)-C_{322}(t)+C_{3-22}(t)-C_{3-2-2}(t))+\tfrac{r_4}{7}\sqrt{\tfrac{3}{5}}(C_{402}(t)+C_{40-2}(t))+r_4\sqrt{\tfrac{3}{14}}$$
$$(C_{442}(t)+C_{4-42}(t)+C_{44-2}(t)+C_{4-4-2}(t)+\sqrt{2.5}(C_{42-2}(t)+C_{4-2-2}(t)+$$
$$C_{422}(t)+C_{4-22}(t)))]+\eta_{bc}A_{12}(t)[\sqrt{\tfrac{2}{3}}\tfrac{2r_2}{7}(C_{2-22}(t)+C_{2-2-2}(t)-C_{22-2}(t)-$$
$$C_{222}(t))+\tfrac{r_3}{\sqrt{5}}(C_{30-2}(t)-C_{302}(t)+\sqrt{\tfrac{5}{6}}(C_{3-22}(t)-C_{3-2-2}(t)+C_{322}(t)$$
$$-C_{32-2}(t)))+r_4\sqrt{\tfrac{3}{14}}(C_{44-2}(t)+C_{442}(t)-C_{4-4-2}(t)-C_{4-42}(t)+\tfrac{1}{\sqrt{7}}(C_{4-22}(t)+$$
$$C_{4-2-2}(t)-C_{42-2}(t)-C_{422}(t)))]+\eta_{bc}A_3(t)[-\sqrt{\tfrac{2}{3}}\tfrac{2r_0}{5}C_{000}(t)+\tfrac{4r_2}{7}(C_{2-20}(t)+$$
$$C_{220}(t)+\sqrt{\tfrac{2}{3}}C_{200}(t))+r_4\sqrt{\tfrac{3}{14}}(C_{42-4}(t)+C_{424}(t)+C_{4-2-4}(t)+C_{4-24}(t)+$$
$$\sqrt{\tfrac{2}{35}}(C_{420}(t)+C_{4-20}(t))-0.8\tfrac{1}{\sqrt{7}}C_{400}(t)-\sqrt{\tfrac{8}{5}}(C_{40-4}(t)+C_{404}(t)))]+\eta_{bc}A_{23}(t)[r_2$$
$$\tfrac{\sqrt{6}}{7}(C_{212}(t)+C_{21-2}(t)+C_{2-12}(t)+C_{2-1-2}(t)+\tfrac{2}{3}(C_{212}(t)+C_{2-12}(t)+C_{21-2}(t)+$$
$$C_{2-1-2}(t)))+\tfrac{r_3}{2}\sqrt{\tfrac{3}{5}}(C_{3-1-2}(t)-C_{3-12}(t)+C_{312}(t)-C_{31-2}(t)+\sqrt{\tfrac{5}{3}}(C_{332}(t)$$

$$-C_{33-2}(t)+C_{3-3-2}(t)-C_{3-32}(t))+\tfrac{2}{3}(C_{3-1-2}(t)-C_{3-12}(t)+C_{312}(t)-$$
$$C_{31-2}(t)))+r_4\tfrac{\sqrt{3}}{14}(C_{41-2}(t)+C_{412}(t)+C_{4-1-2}(t)+C_{4-12}(t)+\sqrt{7}(C_{432}(t)$$
$$+C_{43-2}(t)+C_{4-32}(t)+C_{4-3-2}(t))-2(C_{412}(t)+C_{41-2}(t)+C_{4-12}(t)+C_{4-1-2}(t)$$
$$))]+\eta_{bc}A_{13}(t)[r_2\tfrac{\sqrt{6}}{7}(C_{2-12}(t)-C_{21-2}(t)-C_{212}(t)+C_{2-1-2}(t)+\tfrac{2}{3}(C_{212}(t)$$
$$-C_{2-12}(t)+C_{21-2}(t)-C_{2-1-2}(t)))+\tfrac{r_3}{2}\sqrt{\tfrac{3}{5}}(C_{3-1-2}(t)-C_{3-12}(t)-C_{312}(t)+$$
$$C_{31-2}(t)+\sqrt{\tfrac{5}{3}}(C_{332}(t)-C_{33-2}(t)-C_{3-3-2}(t)+\tfrac{2}{3}(C_{312}(t)-C_{3-32}(t))$$
$$-C_{31-2}(t)-C_{3-1-2}(t)+C_{3-12}(t)))-r_4\tfrac{\sqrt{3}}{14}(-C_{41-2}(t)-C_{412}(t)+C_{4-1-2}(t)+$$
$$C_{4-12}(t)+\sqrt{7}(C_{432}(t)+C_{43-2}(t)-C_{4-32}(t)-C_{4-3-2}(t))-2(C_{412}(t)+C_{41-2}(t)$$
$$-C_{4-12}(t)-C_{4-1-2}(t)))]+\eta_{bc}B_{13}(t)[2r_2\tfrac{\sqrt{6}}{7}(C_{2-10}(t)-C_{210}(t)+\tfrac{2}{3}(C_{210}(t)-$$
$$C_{2-10}(t)))+\tfrac{r_4}{\sqrt{35}}(C_{430}(t)-C_{4-30}(t)+\sqrt{5/2}(C_{4-1-4}(t)-C_{414}(t)-C_{41-4}(t)+$$
$$C_{4-14}(t))+\sqrt{\tfrac{35}{2}}(C_{43-4}(t)-C_{4-34}(t)-C_{4-3-4}(t)+C_{434}(t)))]+\eta_{bc}A_4(t)[\tfrac{4r_0}{5}C_{000}(t)$$
$$+\tfrac{8r_0}{7}(C_{200}(t)-\tfrac{1}{\sqrt{6}}(C_{220}(t)+C_{2-20}(t)))+\tfrac{2r_4}{35}(C_{400}(t)+\sqrt{\tfrac{35}{2}}(C_{40-4}(t)+C_{4-40}(t)+$$
$$C_{404}(t)+C_{440}(t))+\tfrac{35}{2}(C_{4-4-4}(t)+C_{44-4}(t)+C_{4-44}(t)+C_{444}(t))-\sqrt{\tfrac{5}{2}}($$
$$C_{420}(t)+C_{4-20}(t)))]+\eta_{bc}B_{12}(t)[\tfrac{4r_2}{7}(C_{220}(t)-C_{2-20}(t))+r_4(C_{444}(t)-C_{4-4-4}(t)+$$
$$C_{44-4}(t)-C_{4-44}(t)+\tfrac{2}{\sqrt{70}}(C_{440}(t)-C_{4-40}(t))-\tfrac{1}{\sqrt{7}}(C_{42-4}(t)-C_{4-2-4}(t)+$$
$$C_{424}(t)-C_{4-24}(t)-\tfrac{1}{7}\sqrt{\tfrac{2}{5}}(C_{420}(t)-C_{4-20}(t)))]+2A_1(t)\eta_c[\tfrac{r_0}{5}C_{000}(t)+\tfrac{2r_2}{7}$$
$$C_{200}(t)+\tfrac{18r_4}{35}C_{400}(t)]+2A_2(t)\eta_c[-\tfrac{2r_2}{7}(C_{220}(t)+C_{2-20}(t))+\tfrac{r_4}{3}(C_{420}(t)$$
$$+C_{4-20}(t))]+2A_3(t)\eta_c[-\tfrac{2r_2}{7}(C_{202}(t)+C_{20-2}(t))+\tfrac{r_4}{3}(C_{402}(t)+C_{40-2}(t))]$$
$$+2A_4(t)[\tfrac{2r_2}{7}(C_{22-2}(t)+C_{2-22}(t)+C_{222}(t)+C_{2-2-2}(t))+\tfrac{r_3}{2}(C_{322}(t)+C_{3-2-2}(t)-$$
$$C_{32-2}(t)-C_{3-22}(t))+\tfrac{3r_4}{14}(C_{422}(t)+C_{4-2-2}(t)+C_{42-2}(t)+C_{4-22}(t))]+$$
$$2A_{12}(t)\eta_c[-\tfrac{2r_2}{7}(C_{220}(t)-C_{2-20}(t))+\tfrac{r_4}{3}(C_{420}(t)-C_{4-20}(t))]+2B_{12}(t)\eta_c[\tfrac{2r_2}{7}($$
$$C_{22-2}(t)-C_{2-22}(t)+C_{222}(t)-C_{2-2-2}(t))+\tfrac{r_3}{2}(C_{322}(t)-C_{3-2-2}(t)-C_{32-2}(t)+$$
$$C_{3-22}(t))+\tfrac{3r_4}{14}(C_{422}(t)-C_{4-2-2}(t)+C_{42-2}(t)-C_{4-22}(t))+2A_{23}(t)[\tfrac{2r_2}{7}(C_{210}(t)+$$
$$C_{2-10}(t))+r_4\sqrt{\tfrac{3}{14}}(C_{410}(t)+C_{4-10}(t))]+2A_{13}(t)\eta_c[\tfrac{2r_2}{7}(C_{210}(t)-C_{2-10}(t))+$$
$$r_4\sqrt{\tfrac{3}{14}}(C_{410}(t)-C_{4-10}(t))]+2B_{13}(t)\eta_c[\tfrac{2r_2}{7}(C_{2-12}(t)-C_{21-2}(t)+C_{2-1-2}(t)-$$
$$C_{212}(t))+\tfrac{r_3}{\sqrt{10}}(C_{3-12}(t)-C_{31-2}(t)-C_{3-1-2}(t)+C_{312}(t))+\tfrac{3r_4}{7\sqrt{2}}(C_{41-2}(t)-$$
$$C_{4-12}(t)-C_{4-1-2}(t)+C_{412}(t))]\eta_cA_1(t)[\tfrac{2r_2}{7}(C_{22-2}(t)+C_{2-22}(t)+C_{2-2-2}(t)+$$

$C_{222}(t) + \sqrt{\frac{2}{3}}(C_{20-2}(t) + C_{202}(t))) + \frac{r_3}{2}(C_{3-2-2}(t) + C_{322}(t) - C_{32-2}(t) -$
$C_{3-22}(t)) + \frac{3r_4}{14}(C_{42-2}(t) + C_{4-22}(t) + C_{4-2-2}(t) + C_{422}(t) - \frac{14}{9}\sqrt{\frac{2}{3}}(C_{40-2}(t) +$
$C_{402}(t)))] + \eta_c A_2(t)[\frac{4r_2}{7}(C_{20-2}(t) + C_{202}(t) - \frac{1}{\sqrt{6}}(C_{22-2}(t) + C_{2-2-2}(t) +$
$C_{222}(t) + C_{2-22}(t))) - \frac{r_3}{\sqrt{6}}(C_{32-2}(t) - C_{322}(t) + C_{3-22}(t) - C_{3-2-2}(t))$
$+\frac{r_4}{7}\sqrt{\frac{3}{5}}(C_{402}(t)+C_{40-2}(t))+r_4\sqrt{\frac{3}{14}}(C_{442}(t)+C_{4-42}(t)+C_{44-2}(t)+C_{4-4-2}(t)$
$+\sqrt{2.5}(C_{42-2}(t)+C_{4-2-2}(t)+C_{422}(t)+C_{4-22}(t)))]+\eta_c A_{12}(t)[\sqrt{\frac{2}{3}}\frac{2r_2}{7}(C_{2-22}(t)$
$+C_{2-2-2}(t) - C_{22-2}(t) - C_{222}(t)) + \frac{r_3}{\sqrt{5}}(C_{30-2}(t) - C_{302}(t) + \sqrt{\frac{5}{6}}(C_{3-22}(t) -$
$C_{3-2-2}(t) + C_{322}(t) - C_{32-2}(t))) + r_4\sqrt{\frac{3}{14}}(C_{44-2}(t) + C_{442}(t) - C_{4-4-2}(t) -$
$C_{4-42}(t) + \frac{1}{\sqrt{7}}(C_{4-22}(t) + C_{4-2-2}(t) - C_{42-2}(t) - C_{422}(t)))] + \eta_c A_3(t)[-\sqrt{\frac{2}{3}}\frac{2r_0}{5}$
$C_{000}(t) + \frac{4r_2}{7}(C_{2-20}(t) + C_{220}(t) + \sqrt{\frac{2}{3}}C_{200}(t)) + r_4\sqrt{\frac{3}{14}}(C_{42-4}(t) + C_{424}(t) +$
$C_{4-2-4}(t)+C_{4-24}(t)+\sqrt{\frac{2}{35}}(C_{420}(t)+C_{4-20}(t))-0.8\frac{1}{\sqrt{7}}C_{400}(t)-\sqrt{\frac{8}{5}}(C_{40-4}(t) +$
$C_{404}(t)))]+\eta_c A_{23}(t)[r_2\frac{\sqrt{6}}{7}(C_{212}(t)+C_{21-2}(t)+C_{2-12}(t)+C_{2-1-2}(t)+\frac{2}{3}(C_{212}(t) +$
$C_{2-12}(t) + C_{21-2}(t) + C_{2-1-2}(t))) + \frac{r_3}{2}\sqrt{\frac{3}{5}}(C_{3-1-2}(t) - C_{3-12}(t) + C_{312}(t) -$
$C_{31-2}(t) + \sqrt{\frac{5}{3}}(C_{332}(t) - C_{33-2}(t) + C_{3-3-2}(t) - C_{3-32}(t)) + \frac{2}{3}(C_{3-1-2}(t) -$
$C_{3-12}(t)+C_{312}(t)-C_{31-2}(t)))+r_4\frac{\sqrt{3}}{14}(C_{41-2}(t)+C_{412}(t)+C_{4-1-2}(t)+C_{4-12}(t)$
$+\sqrt{7}(C_{432}(t) + C_{43-2}(t) + C_{4-32}(t) + C_{4-3-2}(t)) - 2(C_{412}(t) + C_{41-2}(t) +$
$C_{4-12}(t)+C_{4-1-2}(t)))]+\eta_c A_{13}(t)[r_2\frac{\sqrt{6}}{7}(C_{2-12}(t)-C_{21-2}(t)-C_{212}(t)+C_{2-1-2}(t)$
$+\frac{2}{3}(C_{212}(t) - C_{2-12}(t) + C_{21-2}(t) - C_{2-1-2}(t))) + \frac{r_3}{2}\sqrt{\frac{3}{5}}(C_{3-1-2}(t) - C_{3-12}(t)$
$-C_{312}(t)+C_{31-2}(t)+\sqrt{\frac{5}{3}}(C_{332}(t)-C_{33-2}(t)-C_{3-3-2}(t)+\frac{2}{3}(C_{312}(t)-C_{3-32}(t))-$
$C_{31-2}(t) - C_{3-1-2}(t) + C_{3-12}(t))) - r_4\frac{\sqrt{3}}{14}(-C_{41-2}(t) - C_{412}(t) + C_{4-1-2}(t) +$
$C_{4-12}(t)+\sqrt{7}(C_{432}(t)+C_{43-2}(t)-C_{4-32}(t)-C_{4-3-2}(t))-2(C_{412}(t)+C_{41-2}(t)$
$-C_{4-12}(t) - C_{4-1-2}(t)))] + \eta_c B_{13}(t)[2r_2\frac{\sqrt{6}}{7}(C_{2-10}(t) - C_{210}(t) + \frac{2}{3}(C_{210}(t) -$
$C_{2-10}(t))] + \frac{r_4}{\sqrt{35}}(C_{430}(t) - C_{4-30}(t) + \sqrt{5/2}(C_{4-1-4}(t) - C_{414}(t) - C_{41-4}(t)$
$+C_{4-14}(t))+\sqrt{\frac{35}{2}}(C_{43-4}(t)-C_{4-34}(t)-C_{4-3-4}(t)+C_{434}(t)))]+A_4(t)[\frac{4r_0}{5}C_{000}(t)$
$+\frac{8r_0}{7}(C_{200}(t)-\frac{1}{\sqrt{6}}(C_{220}(t)+C_{2-20}(t)))+\frac{2r_4}{35}(C_{400}(t)+\sqrt{\frac{35}{2}}(C_{40-4}(t)+C_{4-40}(t)+$
$C_{404}(t) + C_{440}(t)) + \frac{35}{2}(C_{4-4-4}(t) + C_{44-4}(t) + C_{4-44}(t) + C_{444}(t)) - \sqrt{\frac{5}{2}}($
$C_{420}(t)+C_{4-20}(t)))]+\eta_c B_{12}(t)[\frac{4r_2}{7}(C_{220}(t)-C_{2-20}(t))+r_4(C_{444}(t)-C_{4-4-4}(t)$

$$+C_{44-4}(t)-C_{4-44}(t)+\tfrac{2}{\sqrt{70}}(C_{440}(t)-C_{4-40}(t))-\tfrac{1}{\sqrt{7}}(C_{42-4}(t)-C_{4-2-4}(t)+$$
$$C_{424}(t)-C_{4-24}(t)-\tfrac{1}{7}\sqrt{\tfrac{2}{5}}(C_{420}(t)-C_{4-20}(t)))]+\eta_b A_1(t)[\tfrac{2r_2}{7}(C_{22-2}(t)+C_{2-22}(t)+$$
$$C_{2-2-2}(t)+C_{222}(t)+\sqrt{\tfrac{2}{3}}(C_{20-2}(t)+C_{202}(t)))+\tfrac{r_3}{2}(C_{3-2-2}(t)+C_{322}(t)-$$
$$C_{32-2}(t)-C_{3-22}(t))+\tfrac{3r_4}{14}(C_{42-2}(t)+C_{4-22}(t)+C_{4-2-2}(t)+C_{422}(t)-\tfrac{14}{9}\sqrt{\tfrac{2}{3}}($$
$$C_{40-2}(t)+C_{402}(t)))]+\eta_b A_2(t)[\tfrac{4r_2}{7}(C_{20-2}(t)+C_{202}(t)-\tfrac{1}{\sqrt{6}}(C_{22-2}(t)$$
$$+C_{2-2-2}(t)+C_{222}(t)+C_{2-22}(t)))-\tfrac{r_3}{\sqrt{6}}(C_{32-2}(t)-C_{322}(t)+C_{3-22}(t)$$
$$-C_{3-2-2}(t))+\tfrac{r_4}{7}\sqrt{\tfrac{3}{5}}(C_{402}(t)+C_{40-2}(t))+r_4\sqrt{\tfrac{3}{14}}(C_{442}(t)+C_{4-42}(t)+C_{44-2}(t)$$
$$+C_{4-4-2}(t)+\sqrt{2.5}(C_{42-2}(t)+C_{4-2-2}(t)+C_{422}(t)+C_{4-22}(t)))]+\eta_b A_{12}(t)[\sqrt{\tfrac{2}{3}}\tfrac{2r_2}{7}$$
$$(C_{2-22}(t)+C_{2-2-2}(t)-C_{22-2}(t)-C_{222}(t))+(C_{30-2}(t)-C_{302}(t)+\sqrt{\tfrac{5}{6}}(C_{3-22}(t)-$$
$$C_{3-2-2}(t)+C_{322}(t)-C_{32-2}(t)))+r_4\sqrt{\tfrac{3}{14}}(C_{44-2}(t)+C_{442}(t)-C_{4-4-2}(t)-$$
$$C_{4-42}(t)+\tfrac{1}{\sqrt{7}}(C_{4-22}(t)+C_{4-2-2}(t)-C_{42-2}(t)-C_{422}(t)))]+\eta_b A_3(t)[-\sqrt{\tfrac{2}{3}}\tfrac{2r_0}{5}$$
$$C_{000}(t)+\tfrac{4r_2}{7}(C_{2-20}(t)+C_{220}(t)+\sqrt{\tfrac{2}{3}}C_{200}(t))+r_4\sqrt{\tfrac{3}{14}}(C_{42-4}(t)+C_{424}(t)$$
$$+C_{4-2-4}(t)+C_{4-24}(t)+\sqrt{\tfrac{2}{35}}(C_{420}(t)+C_{4-20}(t))-0.8\tfrac{1}{\sqrt{7}}C_{400}(t)-\sqrt{\tfrac{8}{5}}(C_{40-4}(t)+$$
$$C_{404}(t)))]+\eta_b A_{23}(t)[r_2\tfrac{\sqrt{6}}{7}(C_{212}(t)+C_{21-2}(t)+C_{2-12}(t)+C_{2-1-2}(t)+\tfrac{2}{3}(C_{212}(t)$$
$$+C_{2-12}(t)+C_{21-2}(t)+C_{2-1-2}(t)))+\tfrac{r_3}{2}\sqrt{\tfrac{3}{5}}(C_{3-1-2}(t)-C_{3-12}(t)+C_{312}(t)-$$
$$C_{31-2}(t)+\sqrt{\tfrac{5}{3}}(C_{332}(t)-C_{33-2}(t)+C_{3-3-2}(t)-C_{3-32}(t))+\tfrac{2}{3}(C_{3-1-2}(t)-$$
$$C_{3-12}(t)+C_{312}(t)-C_{31-2}(t)))+r_4\tfrac{\sqrt{3}}{14}(C_{41-2}(t)+C_{412}(t)+C_{4-1-2}(t)+C_{4-12}(t)$$
$$+\sqrt{7}(C_{432}(t)+C_{43-2}(t)+C_{4-32}(t)+C_{4-3-2}(t))-2(C_{412}(t)+C_{41-2}(t)$$
$$+C_{4-12}(t)+C_{4-1-2}(t)))]+\eta_b A_{13}(t)[r_2\tfrac{\sqrt{6}}{7}(C_{2-12}(t)-C_{21-2}(t)-C_{212}(t)$$
$$+C_{2-1-2}(t)+\tfrac{2}{3}(C_{212}(t)-C_{2-12}(t)+C_{21-2}(t)-C_{2-1-2}(t)))+\tfrac{r_3}{2}\sqrt{\tfrac{3}{5}}(C_{3-1-2}(t)$$
$$-C_{3-12}(t)-C_{312}(t)+C_{31-2}(t)+\sqrt{\tfrac{5}{3}}(C_{332}(t)-C_{33-2}(t)-C_{3-3-2}(t)+\tfrac{2}{3}($$
$$C_{312}(t)-C_{3-32}(t))-C_{31-2}(t)-C_{3-1-2}(t)+C_{3-12}(t)))-r_4\tfrac{\sqrt{3}}{14}(C_{41-2}(t)-$$
$$C_{412}(t)+C_{4-1-2}(t)+C_{4-12}(t)+\sqrt{7}(C_{432}(t)+C_{43-2}(t)-C_{4-32}(t)-C_{4-3-2}(t))$$
$$-2(C_{412}(t)+C_{41-2}(t)-C_{4-12}(t)-C_{4-1-2}(t)))]+\eta_b B_{13}(t)[2r_2\tfrac{\sqrt{6}}{7}(C_{2-10}(t)-$$
$$C_{210}(t)+\tfrac{2}{3}(C_{210}(t)-C_{2-10}(t)))+\tfrac{r_4}{\sqrt{35}}(C_{430}(t)-C_{4-30}(t)+\sqrt{5/2}(C_{4-1-4}(t)-$$
$$C_{414}(t)-C_{41-4}(t)+C_{4-14}(t))+\sqrt{\tfrac{35}{2}}(C_{43-4}(t)-C_{4-34}(t)-C_{4-3-4}(t)+C_{434}(t)$$
$$))]+\eta_b A_4(t)[\tfrac{4r_0}{5}C_{000}(t)+\tfrac{8r_0}{7}(C_{200}(t)-\tfrac{1}{\sqrt{6}}(C_{220}(t)+C_{2-20}(t)))+\tfrac{2r_4}{35}(C_{400}(t)$$

$$+\sqrt{\tfrac{35}{2}}(C_{40-4}(t)+C_{4-40}(t)+C_{404}(t)+C_{440}(t))+\tfrac{35}{2}(C_{4-4-4}(t)+C_{44-4}(t)+$$
$$C_{4-44}(t)+C_{444}(t))-\sqrt{\tfrac{5}{2}}(C_{420}(t)+C_{4-20}(t)))]+\eta_b B_{12}(t)[\tfrac{4r_2}{7}(C_{220}(t)-$$
$$C_{2-20}(t))+r_4(C_{444}(t)-C_{4-4-4}(t)+C_{44-4}(t)-C_{4-44}(t)+\tfrac{2}{\sqrt{70}}(C_{440}(t)-$$
$$C_{4-40}(t))-\tfrac{1}{\sqrt{7}}(C_{42-4}(t)-C_{4-2-4}(t)+C_{424}(t)-C_{4-24}(t)-\tfrac{1}{7}\sqrt{\tfrac{2}{5}}(C_{420}(t)-$$
$$C_{4-20}(t)))]$$

$$\begin{aligned}\tau_e^{33} &= \langle(L_m g_m^{33}+L_n g_n^{33}+L_k g_k^{33})(1+\mathcal{U})\rangle \\ &= \langle\{-2(\eta_{bc}+\eta_c)\sqrt{\tfrac{2}{3}}(D_{02}^2+D_{0-2}^2)-2\eta_b\sqrt{\tfrac{2}{3}}(D_{02}^2-D_{0-2}^2)\}\{1+\mathcal{U}\}\rangle\end{aligned} \tag{314}$$

$$= -2(\eta_{bc}+\eta_c)r_2\sqrt{\tfrac{2}{3}}(C_{202}(t)+C_{20-2}(t))-2\eta_b r_2\sqrt{\tfrac{2}{3}}(C_{20-2}(t)-C_{202}(t))$$
$$-2\sqrt{\tfrac{2}{3}}(\eta_{bc}+\eta_c)\{A_1(t)[\tfrac{-2r_2}{7}(C_{202}(t)+C_{20-2}(t))+\tfrac{r_4}{3}(C_{402}(t)+C_{40-2}(t))]+$$
$$A_2(t)[\tfrac{2r_2}{7}(C_{222}(t)+C_{2-22}(t)+C_{22-2}(t)+C_{2-2-2}(t))+\tfrac{r_3}{2}(C_{3-22}(t)-C_{322}(t)+$$
$$C_{32-2}(t)-C_{3-2-2}(t))+\tfrac{3r_4}{14}(C_{4-22}(t)+C_{422}(t)+C_{42-2}(t)+C_{4-2-2}(t))]+$$
$$A_3(t)[\tfrac{2r_0}{5}C_{000}(t)-\tfrac{4r_2}{7}C_{200}(t)+\tfrac{6r_4}{35}(C_{400}(t)+\sqrt{\tfrac{35}{2}}(C_{404}(t)+C_{40-4}(t)))]+A_4(t)[$$
$$\tfrac{4r_2}{7}(C_{220}(t)+C_{2-20}(t))+r_4\sqrt{\tfrac{3}{14}}(C_{42-4}(t)+C_{4-24}(t)+C_{424}(t)+C_{4-2-4}(t)+$$
$$\tfrac{2}{\sqrt{70}}(C_{420}(t)+C_{4-20}(t)))]+A_{12}(t)[\tfrac{2r_2}{7}(C_{222}(t)-C_{2-22}(t)+C_{22-2}(t)-C_{2-2-2}(t))+$$
$$\tfrac{r_3}{2}(C_{32-2}(t)+C_{3-2-2}(t)-C_{3-22}(t)-C_{322}(t))+\tfrac{3r_4}{14}(C_{42-2}(t)+C_{422}(t)-C_{42-2}(t)$$
$$-C_{4-2-2}(t))]+A_{13}(t)[\tfrac{2r_2}{7}(C_{2-1-2}(t)+C_{2-12}(t)-C_{212}(t)-C_{21-2}(t))+\tfrac{r_3}{\sqrt{10}}($$
$$C_{31-2}(t)-C_{312}(t)+C_{3-12}(t)-C_{3-1-2}(t))+\tfrac{3r_4}{7\sqrt{2}}(C_{41-2}(t)+C_{412}(t)-C_{4-1-2}(t)$$
$$-C_{4-12}(t))]+A_{23}(t)[-\tfrac{2r_2}{7}(C_{212}(t)+C_{2-12}(t)+C_{21-2}(t)+C_{2-1-2}(t))+\tfrac{r_3}{\sqrt{10}}($$
$$C_{31-2}(t)+C_{3-12}(t)-C_{312}(t)-C_{3-1-2}(t))+\tfrac{3r_4}{7\sqrt{2}}(C_{412}(t)+C_{4-12}(t)+C_{41-2}(t)+$$
$$C_{4-1-2}(t))]+B_{12}(t)[\tfrac{4r_2}{7}(C_{220}(t)-C_{2-20}(t))+r_4\sqrt{\tfrac{3}{14}}(C_{42-4}(t)-C_{4-2-4}(t)+$$
$$C_{424}(t)-C_{4-24}(t)+\tfrac{2}{\sqrt{70}}(C_{420}(t)-C_{4-20}(t)))]+B_{13}(t)[\tfrac{4r_2}{7}(C_{2-10}(t)-C_{210}(t))$$
$$+\tfrac{2r_4}{7}\sqrt{\tfrac{3}{10}}(C_{410}(t)-C_{4-10}(t))]\}-2\sqrt{\tfrac{2}{3}}\eta_b\{A_1(t)[\tfrac{-2r_2}{7}(C_{202}(t)+C_{20-2}(t))+\tfrac{r_4}{3}($$
$$C_{402}(t)+C_{40-2}(t))]+A_2(t)[\tfrac{2r_2}{7}(C_{222}(t)+C_{2-22}(t)+C_{22-2}(t)+C_{2-2-2}(t))+\tfrac{r_3}{2}($$
$$C_{3-22}(t)-C_{322}(t)+C_{32-2}(t)-C_{3-2-2}(t))+\tfrac{3r_4}{14}(C_{4-22}(t)+C_{422}(t)+C_{42-2}(t)+$$
$$C_{4-2-2}(t))]+A_3(t)[\tfrac{2r_0}{5}C_{000}(t)-\tfrac{4r_2}{7}C_{200}(t)+\tfrac{6r_4}{35}(C_{400}(t)+\sqrt{\tfrac{35}{2}}(C_{404}(t)$$

$$+C_{40-4}(t)))] + A_4(t)[\tfrac{4r_2}{7}(C_{220}(t) + C_{2-20}(t)) + r_4\sqrt{\tfrac{3}{14}}(C_{42-4}(t) + C_{4-24}(t)+$$
$$C_{424}(t)+C_{4-2-4}(t)+\tfrac{2}{\sqrt{70}}(C_{420}(t)+C_{4-20}(t)))]+A_{12}(t)[\tfrac{2r_2}{7}(C_{222}(t)-C_{2-22}(t)+$$
$$C_{22-2}(t)-C_{2-2-2}(t))+\tfrac{r_3}{2}(C_{32-2}(t)+C_{3-2-2}(t)-C_{3-22}(t)-C_{322}(t))+(C_{42-2}(t)+$$
$$C_{422}(t) - C_{42-2}(t) - C_{4-2-2}(t))] + A_{13}(t)[\tfrac{2r_2}{7}(C_{2-1-2}(t) + C_{2-12}(t) - C_{212}(t)-$$
$$C_{21-2}(t)) + \tfrac{r_3}{\sqrt{10}}(C_{31-2}(t) - C_{312}(t) + C_{3-12}(t) - C_{3-1-2}(t)) + \tfrac{3r_4}{7\sqrt{2}}(C_{41-2}(t)+$$
$$C_{412}(t) - C_{4-1-2}(t) - C_{4-12}(t))] + A_{23}(t)[-\tfrac{2r_2}{7}(C_{212}(t) + C_{2-12}(t) + C_{21-2}(t)+$$
$$C_{2-1-2}(t)) + \tfrac{r_3}{\sqrt{10}}(C_{31-2}(t) + C_{3-12}(t) - C_{312}(t) - C_{3-1-2}(t)) + \tfrac{3r_4}{7\sqrt{2}}(C_{412}(t)+$$
$$C_{4-12}(t) + C_{41-2}(t) + C_{4-1-2}(t))] + B_{12}(t)[\tfrac{4r_2}{7}(C_{220}(t) - C_{2-20}(t)) + r_4\sqrt{\tfrac{3}{14}}($$
$$C_{42-4}(t)-C_{4-2-4}(t)+C_{424}(t)-C_{4-24}(t)+\tfrac{2}{\sqrt{70}}(C_{420}(t)-C_{4-20}(t)))]+B_{13}(t)[\tfrac{4r_2}{7}($$
$$C_{2-10}(t) - C_{210}(t)) + \tfrac{2r_4}{7}\sqrt{\tfrac{3}{10}}(C_{410}(t) - C_{4-10}(t))]\}$$

The elastic shear stress τ_e^{12} is given by:

$$\begin{aligned}\tau_e^{12} &= \langle(L_m g_m^{12} + L_n g_n^{12} + L_k g_k^{12})(1+\mathcal{U})\rangle \\ &= \langle\{-i\eta_{bc}(D^2_{-22} - D^2_{2-2} - D^2_{22} + D^2_{-2-2}) - i\eta_c(D^2_{-2-2} + D^2_{2-2} - D^2_{22} - D^2_{-22}) \\ &\quad -\eta_b(D^2_{-2-2} + D^2_{22} - D^2_{2-2} - D^2_{-22}) + \tfrac{1}{2}D^1_{00}\}\{1+\mathcal{U}\}\rangle \qquad (315)\end{aligned}$$

$$\begin{aligned}&= -i\eta_{bc}r_2(C_{22-2}(t)-C_{2-22}(t)-C_{2-2-2}(t)+C_{222}(t))-i\eta_c r_2(C_{222}(t)+C_{2-22}(t)- \\ &\quad C_{2-2-2}(t) - C_{22-2}(t)) - \eta_b r_2(C_{222}(t) - C_{2-2-2}(t) - C_{2-22}(t) + C_{22-2}(t))+ \\ &\quad \tfrac{r_1}{2}C_{100}(t) - i\eta_{bc}\{A_1(t)[\tfrac{2r_2}{7}(C_{22-2}(t) - C_{2-22}(t) - C_{2-2-2}(t) + C_{222}(t))+ \\ &\quad \tfrac{r_3}{2}(C_{3-22}(t) - C_{32-2}(t) - C_{3-2-2}(t) + C_{322}(t)) + \tfrac{3r_4}{14}(C_{42-2}(t) - C_{422}(t)- \\ &\quad C_{4-2-2}(t) + C_{422}(t))] + A_2(t)[\tfrac{r_3}{\sqrt{5}}(C_{302}(t) - C_{30-2}(t)) + r_4\sqrt{\tfrac{3}{14}}(C_{442}(t)+ \\ &\quad C_{44-2}(t) - C_{4-42}(t) - C_{4-4-2}(t))] + A_{12}(t)[-\tfrac{4r_2}{7}(C_{202}(t) + C_{20-2}(t)) - \tfrac{r_4}{7}\sqrt{\tfrac{3}{5}}(\\ &\quad C_{402}(t) + C_{40-2}(t) - \sqrt{\tfrac{35}{2}}(C_{442}(t) + C_{44-2}(t) + C_{4-42}(t) + C_{4-4-2}(t)))]+ \\ &\quad A_3(t)[\tfrac{4r_2}{7}(C_{220}(t) - C_{2-20}(t)) + \tfrac{r_4}{7}\sqrt{\tfrac{3}{5}}(C_{420}(t) - C_{4-20}(t) + \sqrt{\tfrac{35}{2}}(C_{42-4}(t) \\ &\quad -C_{4-2-4}(t)-C_{4-24}(t)+C_{424}(t)))]+A_{23}(t)[r_2\tfrac{\sqrt{6}}{7}(C_{212}(t)-C_{2-12}(t)-C_{2-1-2}(t) \\ &\quad +C_{21-2}(t)) + \tfrac{r_3}{2}\sqrt{35}(C_{312}(t) - C_{31-2}(t) + C_{3-12}(t) - C_{3-1-2}(t) + \sqrt{\tfrac{5}{3}}(C_{3-32}(t) \\ &\quad -C_{3-3-2}(t) - C_{33-2}(t) + C_{332}(t))) + r_4\tfrac{\sqrt{3}}{14}(C_{412}(t) + C_{41-2}(t) - C_{4-12}(t)\end{aligned}$$

$$-C_{4-1-2}(t)+\sqrt{7}(C_{43-2}(t)+C_{432}(t)-C_{4-32}(t)-C_{4-3-2}(t)))]+A_{13}(t)[-r_2\tfrac{\sqrt{6}}{7}$$
$$(C_{212}(t)+C_{2-12}(t)+C_{2-1-2}(t)+C_{21-2}(t))+\tfrac{r_3}{2}\sqrt{\tfrac{3}{5}}(C_{31-2}(t)-C_{312}(t)+$$
$$C_{3-12}(t)-C_{3-1-2}(t)+\sqrt{\tfrac{5}{3}}(C_{3-3-2}(t)-C_{3-32}(t)-C_{33-2}(t)+C_{332}(t)))$$
$$-r_4\tfrac{\sqrt{3}}{14}(C_{412}(t)+C_{41-2}(t)+C_{4-12}(t)+C_{4-1-2}(t)-\sqrt{7}(C_{43-2}(t)+C_{432}(t)+$$
$$C_{4-32}(t)+C_{4-3-2}(t)))]+A_4(t)[r_4(C_{44-4}(t)-C_{4-44}(t)-C_{4-4-4}(t)+C_{444}(t)+$$
$$\tfrac{2}{\sqrt{70}}(C_{440}(t)-C_{4-40}(t)))]+B_{12}(t)[-\tfrac{4r_0}{5}C_{000}(t)-\tfrac{8r_2}{7}C_{200}(t)+r_4($$
$$C_{44-4}(t)+C_{4-44}(t)+C_{4-4-4}(t)+C_{444}(t)+\tfrac{2}{\sqrt{70}}(C_{440}(t)-C_{40-4}(t)-C_{404}(t)+$$
$$C_{4-40}(t))-\tfrac{2}{35}C_{400}(t))]+B_{13}(t)[-2r_2\tfrac{\sqrt{6}}{7}(C_{210}(t)+C_{2-10}(t))-\tfrac{r_4}{7\sqrt{5}}(C_{410}(t)+$$
$$C_{4-10}(t)-\sqrt{7}(C_{430}(t)+C_{4-30}(t))-7\sqrt{\tfrac{5}{2}}(C_{434}(t)+C_{4-34}(t)+C_{43-4}(t)+$$
$$C_{4-3-4}(t))+\sqrt{\tfrac{35}{2}}(C_{414}(t)+C_{4-14}(t)+C_{41-4}(t)+C_{4-1-4}(t)))]\}-i\eta_c\{A_1(t)[\tfrac{2r_2}{7}$$
$$(C_{22-2}(t)-C_{2-22}(t)-C_{2-2-2}(t)+C_{222}(t))+\tfrac{r_3}{2}(C_{3-22}(t)-C_{32-2}(t)-$$
$$C_{3-2-2}(t)+C_{322}(t))+\tfrac{3r_4}{14}(C_{42-2}(t)-C_{422}(t)-C_{4-2-2}(t)+C_{422}(t))]+A_2(t)[\tfrac{r_3}{\sqrt{5}}$$
$$(C_{302}(t)-C_{30-2}(t))+r_4\sqrt{\tfrac{3}{14}}(C_{442}(t)+C_{44-2}(t)-C_{4-42}(t)-C_{4-4-2}(t))]+$$
$$A_{12}(t)[-\tfrac{4r_2}{7}(C_{202}(t)+C_{20-2}(t))-\tfrac{r_4}{7}\sqrt{\tfrac{3}{5}}(C_{402}(t)+C_{40-2}(t)-\sqrt{\tfrac{35}{2}}(C_{442}(t)+$$
$$C_{44-2}(t)+C_{4-42}(t)+C_{4-4-2}(t)))]+A_3(t)[\tfrac{4r_2}{7}(C_{220}(t)-C_{2-20}(t))+\tfrac{r_4}{7}\sqrt{\tfrac{3}{5}}($$
$$C_{420}(t)-C_{4-20}(t)+\sqrt{\tfrac{35}{2}}(C_{42-4}(t)-C_{4-2-4}(t)-C_{4-24}(t)+C_{424}(t)))]+$$
$$A_{23}(t)[r_2\tfrac{\sqrt{6}}{7}(C_{212}(t)-C_{2-12}(t)-C_{2-1-2}(t)+C_{21-2}(t))+\tfrac{r_3}{2}\sqrt{\tfrac{3}{5}}(C_{312}(t)-$$
$$C_{31-2}(t)+C_{3-12}(t)-C_{3-1-2}(t)+\sqrt{\tfrac{5}{3}}(C_{3-32}(t)-C_{3-3-2}(t)-C_{33-2}(t)+$$
$$C_{332}(t)))+r_4\tfrac{\sqrt{3}}{14}(C_{412}(t)+C_{41-2}(t)-C_{4-12}(t)-C_{4-1-2}(t)+\sqrt{7}(C_{43-2}(t)+$$
$$C_{432}(t)-C_{4-32}(t)-C_{4-3-2}(t)))]+A_{13}(t)[-r_2\tfrac{\sqrt{6}}{7}(C_{212}(t)+C_{2-12}(t)+$$
$$C_{2-1-2}(t)+C_{21-2}(t))+\tfrac{r_3}{2}\sqrt{35}(C_{31-2}(t)-C_{312}(t)+C_{3-12}(t)-C_{3-1-2}(t)+\sqrt{\tfrac{5}{3}}($$
$$C_{3-3-2}(t)-C_{3-32}(t)-C_{33-2}(t)+C_{332}(t)))-r_4\tfrac{\sqrt{3}}{14}(C_{412}(t)+C_{41-2}(t)+C_{4-12}(t)+$$
$$C_{4-1-2}(t)-\sqrt{7}(C_{43-2}(t)+C_{432}(t)+C_{4-32}(t)+C_{4-3-2}(t)))]+A_4(t)[r_4(C_{44-4}(t)-$$
$$C_{4-44}(t)-C_{4-4-4}(t)+C_{444}(t)+\tfrac{2}{\sqrt{70}}(C_{440}(t)-C_{4-40}(t)))]+B_{12}(t)[-\tfrac{4r_0}{5}C_{000}(t)-$$
$$\tfrac{8r_2}{7}C_{200}(t)+r_4(C_{44-4}(t)+C_{4-44}(t)+C_{4-4-4}(t)+C_{444}(t)+\tfrac{2}{\sqrt{70}}(C_{440}(t)-$$
$$C_{40-4}(t)-C_{404}(t)+C_{4-40}(t))-\tfrac{2}{35}C_{400}(t))]+B_{13}(t)[-2r_2\tfrac{\sqrt{6}}{7}(C_{210}(t)+$$
$$C_{2-10}(t))-\tfrac{r_4}{7\sqrt{5}}(C_{410}(t)+C_{4-10}(t)-\sqrt{7}(C_{430}(t)+C_{4-30}(t))-7\sqrt{\tfrac{5}{2}}(C_{434}(t)+$$

$C_{4-34}(t) + C_{43-4}(t) + C_{4-3-4}(t)) + \sqrt{\frac{35}{2}}(C_{414}(t) + C_{4-14}(t) + C_{41-4}(t) +$
$C_{4-1-4}(t)))]\} + -\eta_b\{A_1(t)[\frac{2r_2}{7}(C_{22-2}(t) - C_{2-22}(t) - C_{2-2-2}(t) + C_{222}(t)) +$
$\frac{r_3}{2}(C_{3-22}(t) - C_{32-2}(t) - C_{3-2-2}(t) + C_{322}(t)) + \frac{3r_4}{14}(C_{42-2}(t) - C_{422}(t) -$
$C_{4-2-2}(t) + C_{422}(t))] + A_2(t)[\frac{r_3}{\sqrt{5}}(C_{302}(t) - C_{30-2}(t)) + r_4\sqrt{\frac{3}{14}}(C_{442}(t) + C_{44-2}(t) -$
$C_{4-42}(t) - C_{4-4-2}(t))] + A_{12}(t)[-\frac{4r_2}{7}(C_{202}(t) + C_{20-2}(t)) - \frac{r_4}{7}\sqrt{\frac{3}{5}}(C_{402}(t) +$
$C_{40-2}(t) - \sqrt{\frac{35}{2}}(C_{442}(t) + C_{44-2}(t) + C_{4-42}(t) + C_{4-4-2}(t)))] + A_3(t)[\frac{4r_2}{7}$
$(C_{220}(t) - C_{2-20}(t)) + \frac{r_4}{7}\sqrt{\frac{3}{5}}(C_{420}(t) - C_{4-20}(t) + \sqrt{\frac{35}{2}}(C_{42-4}(t) - C_{4-2-4}(t)$
$-C_{4-24}(t) + C_{424}(t)))] + A_{23}(t)[r_2\frac{\sqrt{6}}{7}(C_{212}(t) - C_{2-12}(t) - C_{2-1-2}(t) + C_{21-2}(t))$
$+\frac{r_3}{2}\sqrt{\frac{3}{5}}(C_{312}(t) - C_{31-2}(t) + C_{3-12}(t) - C_{3-1-2}(t) + \sqrt{\frac{5}{3}}(C_{3-32}(t) - C_{3-3-2}(t) -$
$C_{33-2}(t) + C_{332}(t))) + (C_{412}(t) + C_{41-2}(t) - C_{4-12}(t) - C_{4-1-2}(t) + \sqrt{7}(C_{43-2}(t)$
$+C_{432}(t) - C_{4-32}(t) - C_{4-3-2}(t)))] + A_{13}(t)[-r_2\frac{\sqrt{6}}{7}(C_{212}(t) + C_{2-12}(t) +$
$C_{2-1-2}(t) + C_{21-2}(t)) + \frac{r_3}{2}\sqrt{35}(C_{31-2}(t) - C_{312}(t) + C_{3-12}(t) - C_{3-1-2}(t) +$
$\sqrt{\frac{5}{3}}(C_{3-3-2}(t) - C_{3-32}(t) - C_{33-2}(t) + C_{332}(t))) - r_4\frac{\sqrt{3}}{14}(C_{412}(t) + C_{41-2}(t) +$
$C_{4-12}(t) + C_{4-1-2}(t) - \sqrt{7}(C_{43-2}(t) + C_{432}(t) + C_{4-32}(t) + C_{4-3-2}(t)))] +$
$A_4(t)[r_4(C_{44-4}(t) - C_{4-44}(t) - C_{4-4-4}(t) + C_{444}(t) + \frac{2}{\sqrt{70}}(C_{440}(t) - C_{4-40}(t)))] +$
$B_{12}(t)[-\frac{4r_0}{5}C_{000}(t) - \frac{8r_2}{7}C_{200}(t) + r_4(C_{44-4}(t) + C_{4-44}(t) + C_{4-4-4}(t) + C_{444}(t) +$
$\frac{2}{\sqrt{70}}(C_{440}(t) - C_{40-4}(t) - C_{404}(t) + C_{4-40}(t)) - \frac{2}{35}C_{400}(t))] + B_{13}(t)[-2r_2$
$\frac{\sqrt{6}}{7}(C_{210}(t) + C_{2-10}(t)) - \frac{r_4}{7\sqrt{5}}(C_{410}(t) + C_{4-10}(t) - \sqrt{7}(C_{430}(t) + C_{4-30}(t)) - 7$
$\sqrt{\frac{5}{2}}(C_{434}(t) + C_{4-34}(t) + C_{43-4}(t) + C_{4-3-4}(t)) + \sqrt{\frac{35}{2}}(C_{414}(t) + C_{4-14}(t) +$
$C_{41-4}(t) + C_{4-1-4}(t)))]\} + A_1(t)(\frac{r_1}{5}C_{100}(t) + \frac{r_3}{10}C_{300}(t)) + A_2(t)\frac{r_3}{2\sqrt{5}}(C_{320}(t)$
$+C_{3-20}(t)) + A_3(t)\frac{r_3}{2\sqrt{5}}(C_{302}(t) + C_{30-2}(t)) + A_4(t)(\frac{r_2}{3}(C_{2-2-2}(t) - C_{2-22}(t) -$
$C_{22-2}(t) + C_{222}(t)) + \frac{r_3}{6}(C_{3-2-2}(t) + C_{3-22}(t) + C_{32-2}(t) + C_{322}(t))) + A_{12}(t)\frac{r_3}{2\sqrt{5}}($
$C_{320}(t) - C_{3-20}(t)) + A_{13}(t)(\frac{r_1\sqrt{3}}{10}(C_{110}(t) - C_{1-10}(t)) + \frac{r_2\sqrt{2}}{5}(C_{310}(t) - C_{3-10}(t))) +$
$A_{23}(t)(\frac{r_1\sqrt{3}}{10}(C_{110}(t) + C_{1-10}(t)) + \frac{r_2\sqrt{2}}{5}(C_{310}(t) + C_{3-10}(t))) + B_{12}(t)(\frac{r_2}{3}($
$C_{222}(t) - C_{2-2-2}(t) + C_{2-22}(t) - C_{22-2}(t)) + \frac{r_3}{6}(C_{322}(t) - C_{3-2-2}(t) + C_{32-2}(t) -$
$C_{3-22}(t))) + B_{13}(t)(\frac{r_2}{6}(C_{212}(t) + C_{2-12}(t) - C_{21-2}(t) - C_{2-1-2}(t)) + \frac{r_3}{3}\sqrt{\frac{2}{5}}(C_{312}(t)$
$-C_{3-12}(t) + C_{31-2}(t) - C_{3-1-2}(t)))$